CREEP BEHAVIOR OF OXIDE/OXIDE COMPOSITES WITH MONAZITE FIBER COATING AT 1100 °C IN AIR AND IN STEAM ENVIRONMENTS

THESIS

Tufan YELESER, First Lieutenant, TUAF

AFIT/GA/ENY/08-S01

DEPARTMENT OF THE AIR FORCE
AIR UNIVERSITY

AIR FORCE INSTITUTE OF TECHNOLOGY

Wright-Patterson Air Force Base, Ohio

APPROVED FOR PUBLIC RELEASE; DISTRIBUTION UNLIMITED.

The views expressed in this thesis are those of the author and do not reflect the official policy or position of the United States Air Force, Department of Defense, or the United States Government.

AFIT/GA/ENY/08-S01

CREEP BEHAVIOR OF OXIDE/OXIDE COMPOSITES WITH MONAZITE FIBER COATING AT 1100 °C IN AIR AND IN STEAM ENVIRONMENTS

THESIS

Presented to the Faculty

Department of Aeronautics and Astronautics

Graduate School of Engineering and Management

Air Force Institute of Technology

Air University

Air Education and Training Command

In Partial Fulfillment of the Requirements for the

Degree of Master of Science in Astronautical Engineering

Tufan YELESER, B.S.

First Lieutenant, TUAF

September 2008

APPROVED FOR PUBLIC RELEASE; DISTRIBUTION UNLIMITED.

AFIT/GA/ENY/08-S01

CREEP BEHAVIOR OF OXIDE/OXIDE COMPOSITES WITH MONAZITE FIBER COATING AT 1100 °C IN AIR AND IN STEAM ENVIRONMENTS

Tufan YELESER, B.S.

First Lieutenant, TUAF

Approved:

Dr. Marina B. Ruggles-Wrenn, (Chairman)	date
Dr. Geoff E. Fair (Member)	date
Maj. Eric Swenson (Member)	date

AFIT/GA/ENY/08-S01

Abstract

The creep behavior of six oxide-oxide ceramic-matrix composites (CMCs) was investigated at 1100 °C in laboratory air and in steam environments. The six CMC systems had an alumina (Al_2O_3) matrix reinforced with Nextel^{TM}610 fibers. The CMC systems C1, C2 and C3 were reinforced with 10 uni-directional fiber layers in a symmetric cross-ply $(0°/90°/0°/90°/0°)_s$ orientation. In the case of composites C2 and C3, monazite ($LaPO_4$) fiber coating was applied to the fibers. Composite C1 contained no fiber coating. In the case of composites C1 and C2, alumina matrix was infiltrated with monazite. The CMC systems C4, C5,and C6 were reinforced with 8 plies of fiber fabric woven in a balanced eight-harness satin weave (8HSW). In the case of composites C4 and C6, monazite ($LaPO_4$) fiber coating was applied to the fibers. Composite C5 contained no fiber coating. In the case of composite C6,alumina matrix was infiltrated with AlOCl. The tensile stress-strain behaviors of the six CMC systems were investigated,and the tensile properties measured at 1100 °C. Different methods used to apply the monazite coating to the uni-tape cross-ply composites, and the woven composites were the likely cause of reduced strength of the woven CMCs. Creep performance of all six CMC systems was noticeably degraded in steam. The presence of steam accelerated creep rates and significantly reduced creep lifetimes. In air, creep run-out, defined as 100 h at creep stress, was achieved for composites C4 and C6. In steam, creep run-out was not achieved. Results reveal that for a given fiber architecture and fiber coating method, the use of the monazite coating resulted in considerable improvement in creep resistance at 1100 °C in both air and steam environments. Composite microstructure, as well as damage and failure mechanisms were investigated.

Acknowledgements

To begin with I want to express my biggest appreciation to Dr. Ruggles-Wrenn for her exceptional guidance and support during this study. I would also like to thank lab technicians Chris Zickefoose, Barry Paige and Sean Miller for their help with lab equipment. Following that,I would like to thank,fellow student, Second Lt. Vipul Sharma for his friendship and assistance throughout this effort. Finally,I would like to thank my friends who have supported me sincerely,especially 1st Lt. Gokhan Altin for his support and help in my hardest days. Thank you all.

Tufan YELESER

Table of Contents

Page

Abstract iv

Acknowledgements v

List of Figures viii

List of Tables lxxvii

List of Symbols lxxviii

List of Abbreviations lxxix

I. Introduction 1

II. Background 4
- 2.1 Ceramic Matrix Composites (CMCs) 4
- 2.2 Matrix Materials 5
- 2.3 Ceramic Fibers 6
- 2.4 Fiber-Matrix Interface 8
- 2.5 Oxidation 10
- 2.6 Previous Work 12
- 2.7 Thesis Objective 13

III. Material and Test Specimen 14
- 3.1 Nextel^{TM}610 (N610) Fiber 14
- 3.2 Alumina (Al_2O_3) Matrix 15
- 3.3 Monazite Coating 16
- 3.4 Processing of Composites 1, 2, and 3 with Unidirectional Layers 17
- 3.5 Processing of Composites 4, 5, and 6 with Woven 0°/90° Layers 18
- 3.6 Composite Specifications 19
- 3.7 Specimen Geometry 20

IV. Experimental Arrangements and Test Procedures 22
- 4.1 Mechanical Testing Equipment 22
- 4.2 Environmental Testing Equipment 22
- 4.3 Microstructural Characterization 25
- 4.4 Test Procedures 29

Page

4.4.1 Testing Equipment - Calibration 29
4.4.2 Mechanical Testing - Preparation 29
4.4.3 Monotonic Tensile Test 31
4.4.4 Creep-Rupture Test 31
4.4.5 Microstructural Characterization 32

V. Results and Discussion 34
5.1 Thermal Expansion 34
5.2 Monotonic Tensile Tests 34
5.3 Creep-Rupture 41
5.4 Composite Microstructure 59
5.4.1 Composites C1 and C2 60
5.4.2 Composites C3 and C4 60
5.4.3 Composites C4 and C5 69
5.4.4 Composite C4 and Composite C6 72
5.4.5 Unusual Microstructural Features Observed in Composites C3, C4 and C6 78

VI. Conclusions and Recommendations 84
6.1 Conclusions 84
6.1.1 Tensile Stress-Strain Behavior and Properties of the Composites 84
6.1.2 Creep-Rupture Properties of the Composites . . 84
6.1.3 Creep Rate Properties of the Composites 86
6.1.4 Stress-Rupture Properties of the Composites . . 87
6.1.5 Retained Properties of the Composites 88
6.1.6 Microstructural evaluation of the Composites . 88
6.1.7 Composites C1 and C2 89
6.2 Recommendations 89

Appendix A. Additional SEM Micrographs 91

Appendix B. Additional Optical Micrographs 246

Bibliography 339

Vita 344

List of Figures

Figure		Page
2.1.	service temperatures of polymers, metals and ceramics [M7:5].	5
2.2.	Strength to weight ratio versus temperature range [43].	6
2.3.	Failure of a CMC as a function of interfacial bond [20, page 170].	9
2.4.	Typical stress strain curve for CMCs with weak interface [M20:10] [24, page 10].	9
2.5.	Schematics of the damage processes that enable damage tolerance in (a) conventional dense-matrix weak-interface CFCC and (b) porous matrix CFCC without fiber coatings [53].	10
2.6.	Schematic representation of oxidation progression through a matrix crack [49].	11
3.1.	Fine-grained Nextel^{TM}610 fiber [49].	16
3.2.	Schematic of slurry infiltration process [21].	17
3.3.	Schematic Representation of $(0°/90°/0°/90°/0°)_s$ Ply Lay-up. .	18
3.4.	Schematic of the set up of process for coating woven ceramic fibers with monazite using heterogeneous precipitation from solution precursors. From [12]	19
3.5.	Test specimen geometry	21
3.6.	Tabbed test specimen	21
4.1.	Mechanical testing station.	23
4.2.	NESLAB model HX-75 chiller.	24
4.3.	Close-up view of the MTS machine and the extensometer. . . .	24
4.4.	MTS Model 409.83B temperature controller.	26
4.5.	Susceptor assembly arrangement.	27
4.6.	Zeiss Discovery V12 optical microscope.	28
4.7.	FEI Scanning Electron Microscope (SEM).	28
4.8.	A typical test set-up.	30

Figure Page

4.9. A typical test setup. 31

4.10. SPI-Module Controller and Carbon Coater. 33

5.1. Tensile stress-strain curve for N^{TM}610/Al_2O_3-$LaPO_4$ composite with 0/90 unitape lay-up obtained at 1100 °C in laboratory air. 37

5.2. Tensile stress-strain curves for N^{TM}610/ $LaPO_4$/Al_2O_3-$LaPO_4$ composite with 0/90 unitape lay-up obtained at 1100 °C in laboratory air. 38

5.3. Tensile stress-strain curves for N^{TM}610/$LaPO_4$/Al_2O_3 composite (Composite 3) with 0/90 unitape lay-up and for N610/$LaPO_4$/Al_2O_3 woven composite (Composite 4) obtained at 1100 °C in laboratory air. All data are adjusted for $V_f = 0.39$. 39

5.4. Tensile stress-strain curves for N^{TM}610/$LaPO_4$/Al_2O_3 woven composite (Composite 4) and for N^{TM}610/Al_2O_3 woven composite (Composite 5) obtained at 1100 °C in laboratory air. All data are adjusted for $V_f = 0.39$. 40

5.5. Tensile stress-strain curves for N^{TM}610/$LaPO_4$/Al_2O_3 woven composite (Composite 4) and for N^{TM}610/$LaPO_4$/Al_2O_3-$LaPO_4$-AlOCl woven composite (Composite 6) obtained at 1100 °C in laboratory air. All data are adjusted for $V_f = 0.39$. 40

5.6. Creep strain vs time curves for N^{TM}610/Al_2O_3-$LaPO_4$ composite with 0/90 unitape lay-up obtained at 32 MPa at 1100 °C in laboratory air and in steam. 41

5.7. Creep strain vs time curve for N^{TM}610/ $LaPO_4$/Al_2O_3-$LaPO_4$ composite with 0/90 unitape lay-up obtained at 25 MPa at 1100 °C in steam. 43

5.8. Creep strain vs time curves for N^{TM}610/ $LaPO_4$/Al_2O_3 composite (C3) with 0/90 unitape lay-up obtained at 1100 °C in laboratory air and in steam:(a) time scale is adjusted to clearly show the creep curves obtained at 85 MPa (b) time scale is adjusted to clearly show the creep curves obtained at 110 and 120 MPa in steam. 44

Figure Page

5.9. Creep strain vs time curves for N^{TM}610/ $LaPO_4/Al_2O_3$ woven composite (C4) obtained at 1100 °C in laboratory air and in steam: (a) time scale is adjusted to clearly show all creep curves obtained in air (b) time scale is adjusted to clearly show the creep curves obtained at 48, 64 and 72 MPa in steam. 45

5.10. Creep strain vs time curves for N^{TM}610/Al_2O_3 woven composite (C5) obtained at 1100 °C in laboratory air and in steam. . . . 46

5.11. Creep strain vs time curves for N^{TM}610/ $LaPO_4/Al_2O_3$ woven composite (C4) and N^{TM}610/Al_2O_3 woven composite (C5) obtained at selected stress levels 1100 °C in laboratory air and in steam. Creep stress levels adjusted for $V_f = 0.39$. 47

5.12. Creep strain vs time curves for N^{TM}610/$LaPO_4/Al_2O_3$-AlOCl woven composite obtained at 1100 °C in laboratory air and in steam: (a) time scale is adjusted to clearly show all creep curves obtained at 32 MPa in air (b) time scale is adjusted to clearly show the creep curves obtained at 32 and 48 MPa in steam. . . 49

5.13. Creep strain vs time curves for for N^{TM}610/ $LaPO_4/Al_2O_3$ woven composite (C4) and for (C6) obtained at 1100 °C in laboratory air and in steam. Creep stress levels adjusted for $V_f = 0.39$. . . 50

5.14. Minimum creep rate as a function of applied stress for N^{TM}610/Al_2O_3-$LaPO_4$ composite with 0/90 unitape lay-up at 1100 °C in laboratory air and in steam. 51

5.15. Minimum creep rate as a function of applied stress for N^{TM}610/ $LaPO_4/Al_2O_3$-$LaPO_4$ composite with 0/90 unitape lay-up at 1100 °C in laboratory air and in steam. 51

5.16. Minimum creep rate as a function of applied stress for N^{TM}610/ $LaPO_4/Al_2O_3$ composite C3 with 0/90 unitape lay-up and for N610/ $LaPO_4/Al_2O_3$ woven composite C4 at 1100 °C in laboratory air and in steam. Creep stress levels adjusted for $V_f = 0.39$. 52

5.17. Minimum creep rate as a function of applied stress for N^{TM}610/ $LaPO_4/Al_2O_3$ woven composite C4 and for N610/Al_2O_3 woven composite C5 at 1100 °C in laboratory air and in steam. Creep stress levels adjusted for levels adjusted for $V_f = 0.39$. 53

5.18. Minimum creep rate as a function of applied stress for N^{TM}610/ $LaPO_4/Al_2O_3$ woven composite C4 and for N^{TM}610/$LaPO_4/Al_2O_3$-AlOCl woven composite C6 at 1100 °C in laboratory air and in steam. Creep stress levels adjusted for $V_f = 0.39$. 54

5.19. Creep stress vs time to rupture for N^{TM}610/ $LaPO_4/Al_2O_3$ composite C3 with 0/90 unitape lay-up and for N^{TM}610/ $LaPO_4/Al_2O_3$ woven composite C4 at 1100 °C in laboratory air and in steam. Creep stress levels adjusted for $V_f = 0.39$. 55

5.20. Creep stress vs time to rupture for N^{TM}610/ $LaPO_4/Al_2O_3$ woven composite C4 and for N^{TM}610/Al_2O_3 woven composite C5 at 1100 °C in laboratory air and in steam. Creep stress levels adjusted for $V_f = 0.39$. 56

5.21. Creep stress vs time to rupture for N^{TM}610/ $LaPO_4/Al_2O_3$ woven composite C4 and for N^{TM}610/$LaPO_4/Al_2O_3$-AlOCl woven composite C6 at 1100 °C in laboratory air and in steam. Creep stress levels adjusted for $V_f = 0.39$. 57

5.22. Effects of prior creep at 1100 °C in air on tensile stress-strain behavior of N^{TM}610/ $LaPO_4/Al_2O_3$ woven composite C4 at 1100 °C. 58

5.23. Effect of prior creep at 1100 °C in air on tensile stress-strain behavior of N^{TM}610/$LaPO_4/Al_2O_3$-AlOCl woven composite C6 at 1100 °C. 59

5.24. Fracture surface of C1 composite specimen tested in tension to failure at 1100 °C in laboratory air: (a) front view and (b) side view. 60

5.25. Fracture surface of C2 composite specimen tested in tension to failure at 1100 °C in laboratory air: (a) front view and (b) side view. 61

5.26. Fracture surface of C2 composite specimen tested in creep at 25 MPa at 1100 °C in laboratory air ($t_f = 40.1$ h): (a) front view and (b) side view. 61

5.27. Fracture surface of C3 composite specimen tested in tension to failure at 1100 °C in laboratory air: (a) front view and (b) side view. 61

Figure Page

5.28. Fracture surface of C4 composite specimen tested in tension to failure at 1100 °C in laboratory air: (a) front view and (b) side view. 62

5.29. Fracture surface of C3 composite specimen tested in creep at 85 MPa at 1100 °C in laboratory air (t_f = 16.2 h): (a) front view and (b) side view. 63

5.30. Fracture surface of C4 composite specimen tested in creep at 84.3 MPa at 1100 °C in laboratory air (t_f > 100 h): (a) front view and (b) side view 63

5.31. SEM micrographs of the fracture surface of C3 composite specimen tested in creep at 85 MPa at 1100 °C in laboratory air (t_f = 16.2 h). 64

5.32. SEM micrographs of the fracture surface of C4 composite specimen tested in creep at 84.3 MPa at 1100 °C in laboratory air (t_f > 100 h) 65

5.33. Fracture surface of C3 composite specimen tested in creep at 85 MPa at 1100 °C in steam (t_f = 8.18 h): (a) front view and (b) side view. 66

5.34. Fracture surface of C4 composite specimen tested in creep at 84.3 MPa at 1100 °C in steam (t_f = 2.24 h): (a) front view and (b) side view. 66

5.35. SEM micrographs of the fracture surface of C3 composite specimen tested in creep at 85 MPa at 1100 °C in steam (t_f = 8.18 h) 67

5.36. SEM micrographs of the fracture surface of C4 composite specimen tested in creep at 84.3 MPa at 1100 °C in steam (t_f = 2.24 h) 67

5.37. Fracture surface of C3 composite specimen tested in creep at 85 MPa at 1100 °C in steam (t_f = 8.18 h): (a) front view and (b) side view. 68

5.38. SEM micrographs of the fracture surface of C3 composite specimen tested in creep at 85 MPa at 1100 °C in steam (t_f = 8.18 h): 68

Figure Page

5.39. Fracture surface of C3 composite specimen tested in creep at 120 MPa at 1100 °C in steam (t_f = 0.03 h): (a) front view and (b) side view. 69

5.40. Fracture surface of C5 composite specimen tested in tension to failure at 1100 °C in laboratory air: (a) front view and (b) side view. 70

5.41. Fracture surface of C5 composite specimen tested in creep at 61 MPa at 1100 °C in laboratory air (t_f = 3.42 h): (a) front view and (b) side view. 70

5.42. Fracture surface of C4 composite specimen tested in creep at 37.5 MPa at 1100 °C in steam (t_f = 51.9 h): (a) front view and (b) side view. 71

5.43. Fracture surface of C5 composite specimen tested in creep at 30 MPa at 1100 °C in steam (t_f = 16.1 h): (a) front view and (b) side view. 71

5.44. SEM micrographs of the fracture surface of C4 composite specimen tested in creep at 32 MPa at 1100 °C in steam (t_f = 51.9 h 73

5.45. SEM micrographs of the fracture surface of C5 composite specimen tested in creep at 30 MPa at 1100 °C in steam (t_f = 16.1 h). 74

5.46. SEM micrographs of the fracture surface of C5 composite specimen tested in creep at 30 MPa at 1100 °C in steam (t_f = 16.1 h). 75

5.47. Fracture surface of C6 composite specimen tested in tension to failure at 1100 °C in laboratory air: (a) front view and (b) side view. 76

5.48. Fracture surface of C4 composite specimen tested in creep at 37.5 MPa at 1100 °C in laboratory air (t_f > 100 h): (a) front view and (b) side view 77

5.49. Fracture surface of C6 composite specimen tested in creep at 32 MPa at 1100 °C in laboratory air (t_f > 100 h): (a) front view and (b) side view. 77

Figure Page

5.50. SEM micrographs of the fracture surface of C4 composite specimen tested in creep at 37.5 MPa at 1100 °C in laboratory air (t_f > 100 h) 79

5.51. SEM micrographs of the fracture surface of C6 composite specimen tested in creep at 32 MPa at 1100 °C in air (tf > 100 h). 80

5.52. Fracture surface of C6 composite specimen tested in creep at 32 MPa at 1100 °C in steam (t_f = 3.47 h): (a) front view and (b) side view. 80

5.53. SEM micrographs of the fracture surface of C6 composite specimen tested in creep at 32 MPa at 1100 °C in steam (t_f = 3.47 h). 81

5.54. SEM micrographs of the fracture surfaces of C4-C6, respectively. 82

5.55. SEM micrograph of the fracture surface of specimen C6-1 showing unusual microstructural feature, i.e. structures resembling broken glass 83

A.1. Fracture surface of the N610/Al_2O_3-$LaPO_4$ specimen with 10ply 0°/90° uni-tape lay-up subjected to creep test at 32 MPa in steam at 1100 °C (t_f = 3.45h). 91

A.2. Fracture surface of the N610/Al_2O_3-$LaPO_4$ specimen with 10 ply 0°/90° uni-tape lay-up subjected to creep test at 32 MPa in steam at 1100 °C (t_f = 3.45h). 91

A.3. Fracture surface of the N610/Al_2O_3-$LaPO_4$ specimen with 10ply 0°/90° uni-tape lay-up subjected to creep test at 32 MPa in steam at 1100 °C (t_f = 3.45h). 92

A.4. Fracture surface of the N610/Al_2O_3-$LaPO_4$ specimen with 10ply 0°/90° uni-tape lay-up subjected to creep test at 32 MPa in steam at 1100 °C (t_f = 3.45h). 92

A.5. Fracture surface of the N610/Al_2O_3-$LaPO_4$ specimen with 10ply 0°/90° uni-tape lay-up subjected to creep test at 32 MPa in steam at 1100 °C (t_f=3.45h). 92

Figure Page

A.6. Fracture surface of the N610/Al_2O_3-$LaPO_4$ specimen with 10ply 0°/90° uni-tape lay-up subjected to creep test at 32 MPa in steam at 1100 °C (t_f = 3.45h). 93

A.7. Fracture surface of the N610/Al_2O_3-$LaPO_4$ specimen with 10ply 0°/90° uni-tape lay-up subjected to creep test at 32 MPa in steam at 1100 °C (t_f = 3.45h). 93

A.8. Fracture surface of the N610/Al_2O_3-$LaPO_4$ specimen with 10ply 0°/90° uni-tape lay-up subjected to creep test at 32 MPa in steam at 1100 °C (t_f = 3.45h). 93

A.9. Fracture surface of the N610/Al_2O_3-$LaPO_4$ specimen with 10ply 0°/90° uni-tape lay-up subjected to creep test at 32 MPa in steam at 1100 °C (t_f = 3.45h). 94

A.10. Fracture surface of the N610/Al_2O_3-$LaPO_4$ specimen with 10ply 0°/90° uni-tape lay-up subjected to creep test at 32 MPa in steam at 1100 °C (t_f = 3.45h). 94

A.11. Fracture surface of the N610/Al_2O_3-$LaPO_4$ specimen with 10ply 0°/90° uni-tape lay-up subjected to creep test at 32 MPa in steam at 1100 °C (t_f = 3.45h). 94

A.12. Fracture surface of the N610/Al_2O_3-$LaPO_4$ specimen with 10ply 0°/90° uni-tape lay-up subjected to creep test at 32 MPa in steam at 1100 °C (t_f = 3.45h). 95

A.13. Fracture surface of the N610/Al_2O_3-$LaPO_4$ specimen with 10ply 0°/90° uni-tape lay-up subjected to creep test at 32 MPa in steam at 1100 °C (t_f = 3.45h). 95

A.14. Fracture surface of the N610/Al_2O_3-$LaPO_4$ specimen with 10ply 0°/90° uni-tape lay-up subjected to creep test at 32 MPa in steam at 1100 °C (t_f = 3.45h). 95

A.15. Fracture surface of the N610/Al_2O_3-$LaPO_4$ specimen with 10ply 0°/90° uni-tape lay-up subjected to creep test at 32 MPa in steam at 1100 °C (t_f = 3.45h). 96

A.16. Fracture surface of the N610/Al_2O_3-$LaPO_4$ specimen with 10ply 0°/90° uni-tape lay-up subjected to creep test at 32 MPa in steam at 1100 °C (t_f = 3.45h). 96

Figure Page

A.17. Fracture surface of the N610/Al_2O_3-$LaPO_4$ specimen with 10ply 0°/90° uni-tape lay-up subjected to creep test at 32 MPa in steam at 1100 °C (t_f = 3.45h). 96

A.18. Fracture surface of the N610/Al_2O_3-$LaPO_4$ specimen with 10ply 0°/90° uni-tape lay-up subjected to creep test at 32 MPa in steam at 1100 °C (t_f = 3.45h). 97

A.19. Fracture surface of the N610/Al_2O_3-$LaPO_4$ specimen with 10ply 0°/90° uni-tape lay-up subjected to creep test at 32 MPa in steam at 1100 °C (t_f = 3.45h). 97

A.20. Fracture surface of the N610/Al_2O_3-$LaPO_4$ specimen with 10ply 0°/90° uni-tape lay-up subjected to creep test at 32 MPa in steam at 1100 °C (t_f = 3.45h). 97

A.21. Fracture surface of the N610/Al_2O_3-$LaPO_4$ specimen with 10ply 0°/90° uni-tape lay-up subjected to creep test at 32 MPa in steam at 1100 °C (t_f = 3.45h). 98

A.22. Fracture surface of the N610/Al_2O_3-$LaPO_4$ specimen with 10ply 0°/90° uni-tape lay-up subjected to creep test at 32 MPa in steam at 1100 °C (t_f = 3.45h). 98

A.23. Fracture surface of the N610/Al_2O_3-$LaPO_4$ specimen with 10ply 0°/90° uni-tape lay-up subjected to creep test at 32 MPa in steam at 1100 °C (t_f = 3.45h). 98

A.24. Fracture surface of the N610/Al_2O_3-$LaPO_4$ specimen with 10ply 0°/90° uni-tape lay-up subjected to creep test at 32 MPa in steam at 1100 °C (t_f = 3.45h). 99

A.25. Fracture surface of the N610/Al_2O_3-$LaPO_4$ specimen with 10ply 0°/90° uni-tape lay-up subjected to creep test at 32 MPa in steam at 1100 °C (t_f = 3.45h). 99

A.26. Fracture surface of the N610/Al_2O_3-$LaPO_4$ specimen with 10ply 0°/90° uni-tape lay-up subjected to creep test at 32 MPa in steam at 1100 °C (t_f = 3.45h). 99

A.27. Fracture surface of the N610/Al_2O_3-$LaPO_4$ specimen with 10ply 0°/90° uni-tape lay-up subjected to creep test at 32 MPa in steam at 1100 °C (t_f = 3.45h). 100

Figure Page

A.28. Fracture surface of the N610/Al_2O_3-$LaPO_4$ specimen with 10ply 0°/90° uni-tape lay-up subjected to creep test at 32 MPa in steam at 1100 °C (t_f = 3.45h). 100

A.29. Fracture surface of the N610/Al_2O_3-$LaPO_4$ specimen with 10ply 0°/90° uni-tape lay-up subjected to creep test at 32 MPa in steam at 1100 °C (t_f = 3.45h). 100

A.30. Fracture surface of the N610/Al_2O_3-$LaPO_4$ specimen with 10ply 0°/90° uni-tape lay-up subjected to creep test at 32 MPa in steam at 1100 °C (t_f = 3.45h). 101

A.31. Fracture surface of the N610/Al_2O_3-$LaPO_4$ specimen with 10ply 0°/90° uni-tape lay-up subjected to creep test at 32 MPa in steam at 1100 °C (t_f = 3.45h). 101

A.32. Fracture surface of the N610/Al_2O_3-$LaPO_4$ specimen with 10ply 0°/90° uni-tape lay-up subjected to creep test at 32 MPa in steam at 1100 °C (t_f = 3.45h). 101

A.33. Fracture surface of the N610/Al_2O_3-$LaPO_4$ specimen with 10ply 0°/90° uni-tape lay-up subjected to creep test at 32 MPa in steam at 1100 °C (t_f = 3.45h). 102

A.34. Fracture surface of the N610/Al_2O_3-$LaPO_4$ specimen with 10ply 0°/90° uni-tape lay-up subjected to creep test at 32 MPa in steam at 1100 °C (t_f = 3.45h). 102

A.35. Fracture surface of the N610/Al_2O_3-$LaPO_4$ specimen with 10ply 0°/90° uni-tape lay-up subjected to creep test at 32 MPa in steam at 1100 °C (t_f = 3.45h). 102

A.36. Fracture surface of the N610/Al_2O_3-$LaPO_4$ specimen with 10ply 0°/90° uni-tape lay-up subjected to creep test at 32 MPa in steam at 1100 °C (t_f = 3.45h). 103

A.37. Fracture surface of the N610/Al_2O_3-$LaPO_4$ specimen with 10ply 0°/90° uni-tape lay-up subjected to creep test at 32 MPa in steam at 1100 °C (t_f = 3.45h). 103

A.38. Fracture surface of the N610/Al_2O_3-$LaPO_4$ specimen with 10ply 0°/90° uni-tape lay-up subjected to creep test at 32 MPa in steam at 1100 °C (t_f = 3.45h). 103

A.39. Fracture surface of the N610/Al_2O_3-$LaPO_4$ specimen with 10ply 0°/90° uni-tape lay-up subjected to creep test at 32 MPa in steam at 1100 °C (t_f = 3.45h). 104

A.40. Fracture surface of the N610/Al_2O_3-$LaPO_4$ specimen with 10ply 0°/90° uni-tape lay-up subjected to creep test at 32 MPa in steam at 1100 °C (t_f = 3.45h). 104

A.41. Fracture surface of the N610/$LaPO_4$/Al_2O_3 specimen with 10ply 0°/90° uni-tape lay-up subjected to creep test at 85 MPa in air at 1100 °C (t_f = 16.23h). 104

A.42. Fracture surface of the N610/$LaPO_4$/Al_2O_3 specimen with 10ply 0°/90° uni-tape lay-up subjected to creep test at 85 MPa in air at 1100 °C (t_f = 16.23h). 105

A.43. Fracture surface of the N610/$LaPO_4$/Al_2O_3 specimen with 10ply 0°/90° uni-tape lay-up subjected to creep test at 85 MPa in air at 1100 °C (t_f = 16.23h). 105

A.44. Fracture surface of the N610/$LaPO_4$/Al_2O_3 specimen with 10ply 0°/90° uni-tape lay-up subjected to creep test at 85 MPa in air at 1100 °C (t_f = 16.23h). 105

A.45. Fracture surface of the N610/$LaPO_4$/Al_2O_3 specimen with 10ply 0°/90° uni-tape lay-up subjected to creep test at 85 MPa in air at 1100 °C (t_f = 16.23h). 106

A.46. Fracture surface of the N610/$LaPO_4$/Al_2O_3 specimen with 10ply 0°/90° uni-tape lay-up subjected to creep test at 85 MPa in air at 1100 °C (t_f = 16.23h). 106

A.47. Fracture surface of the N610/$LaPO_4$/Al_2O_3 specimen with 10ply 0°/90° uni-tape lay-up subjected to creep test at 85 MPa in air at 1100 °C (t_f = 16.23h). 106

A.48. Fracture surface of the N610/$LaPO_4$/Al_2O_3 specimen with 10ply 0°/90° uni-tape lay-up subjected to creep test at 85 MPa in air at 1100 °C (t_f = 16.23h). 107

A.49. Fracture surface of the N610/$LaPO_4$/Al_2O_3 specimen with 10ply 0°/90° uni-tape lay-up subjected to creep test at 85 MPa in air at 1100 °C (t_f = 16.23h). 107

Figure Page

A.50. Fracture surface of the N610/$LaPO_4$/Al_2O_3 specimen with 10ply 0°/90° uni-tape lay-up subjected to creep test at 85 MPa in air at 1100 °C (t_f = 16.23h). 107

A.51. Fracture surface of the N610/$LaPO_4$/Al_2O_3 specimen with 10ply 0°/90° uni-tape lay-up subjected to creep test at 85 MPa in air at 1100 °C (t_f = 16.23h). 108

A.52. Fracture surface of the N610/$LaPO_4$/Al_2O_3 specimen with 10ply 0°/90° uni-tape lay-up subjected to creep test at 85 MPa in air at 1100 °C (t_f = 16.23h). 108

A.53. Fracture surface of the N610/$LaPO_4$/Al_2O_3 specimen with 10ply 0°/90° uni-tape lay-up subjected to creep test at 85 MPa in air at 1100 °C (t_f = 16.23h). 108

A.54. Fracture surface of the N610/$LaPO_4$/Al_2O_3 specimen with 10ply 0°/90° uni-tape lay-up subjected to creep test at 85 MPa in air at 1100 °C (t_f = 16.23h). 109

A.55. Fracture surface of the N610/$LaPO_4$/Al_2O_3 specimen with 10ply 0°/90° uni-tape lay-up subjected to creep test at 85 MPa in air at 1100 °C (t_f = 16.23h). 109

A.56. Fracture surface of the N610/$LaPO_4$/Al_2O_3 specimen with 10ply 0°/90° uni-tape lay-up subjected to creep test at 85 MPa in air at 1100 °C (t_f = 16.23h). 109

A.57. Fracture surface of the N610/$LaPO_4$/Al_2O_3 specimen with 10ply 0°/90° uni-tape lay-up subjected to creep test at 85 MPa in air at 1100 °C (t_f = 16.23h). 110

A.58. Fracture surface of the N610/$LaPO_4$/Al_2O_3 specimen with 10ply 0°/90° uni-tape lay-up subjected to creep test at 85 MPa in air at 1100 °C (t_f = 16.23h). 110

A.59. Fracture surface of the N610/$LaPO_4$/Al_2O_3 specimen with 10ply 0°/90° uni-tape lay-up subjected to creep test at 85 MPa in air at 1100 °C (t_f = 16.23h). 110

A.60. Fracture surface of the N610/$LaPO_4$/Al_2O_3 specimen with 10ply 0°/90° uni-tape lay-up subjected to creep test at 85 MPa in air at 1100 °C (t_f = 16.23h). 111

Figure Page

A.61. Fracture surface of the N610/$LaPO_4$/Al_2O_3 specimen with 10ply 0°/90° uni-tape lay-up subjected to creep test at 85 MPa in air at 1100 °C (t_f = 16.23h). 111

A.62. Fracture surface of the N610/$LaPO_4$/Al_2O_3 specimen with 10ply 0°/90° uni-tape lay-up subjected to creep test at 85 MPa in air at 1100 °C (t_f = 16.23h). 111

A.63. Fracture surface of the N610/$LaPO_4$/Al_2O_3 specimen with 10ply 0°/90° uni-tape lay-up subjected to creep test at 120 MPa in steam at 1100 °C (t_f = 0.0313h). 112

A.64. Fracture surface of the N610/$LaPO_4$/Al_2O_3 specimen with 10ply 0°/90° uni-tape lay-up subjected to creep test at 120 MPa in steam at 1100 °C (t_f = 0.0313h). 112

A.65. Fracture surface of the N610/$LaPO_4$/Al_2O_3 specimen with 10ply 0°/90° uni-tape lay-up subjected to creep test at 120 MPa in steam at 1100 °C (t_f = 0.0313h). 112

A.66. Fracture surface of the N610/$LaPO_4$/Al_2O_3 specimen with 10ply 0°/90° uni-tape lay-up subjected to creep test at 120 MPa in steam at 1100 °C (t_f = 0.0313h). 113

A.67. Fracture surface of the N610/$LaPO_4$/Al_2O_3 specimen with 10ply 0°/90° uni-tape lay-up subjected to creep test at 120 MPa in steam at 1100 °C (t_f = 0.0313h). 113

A.68. Fracture surface of the N610/$LaPO_4$/Al_2O_3 specimen with 10ply 0°/90° uni-tape lay-up subjected to creep test at 120 MPa in steam at 1100 °C (t_f = 0.0313h). 113

A.69. Fracture surface of the N610/$LaPO_4$/Al_2O_3 specimen with 10ply 0°/90° uni-tape lay-up subjected to creep test at 120 MPa in steam at 1100 °C (t_f = 0.0313h). 114

A.70. Fracture surface of the N610/$LaPO_4$/Al_2O_3 specimen with 10ply 0°/90° uni-tape lay-up subjected to creep test at 120 MPa in steam at 1100 °C (t_f = 0.0313h). 114

A.71. Fracture surface of the N610/$LaPO_4$/Al_2O_3 specimen with 10ply 0°/90° uni-tape lay-up subjected to creep test at 120 MPa in steam at 1100 °C (t_f = 0.0313h). 114

A.72. Fracture surface of the N610/$LaPO_4$/Al_2O_3 specimen with 10ply 0°/90° uni-tape lay-up subjected to creep test at 120 MPa in steam at 1100 °C (t_f = 0.0313h). 115

A.73. Fracture surface of the N610/$LaPO_4$/Al_2O_3 specimen with 10ply 0°/90° uni-tape lay-up subjected to creep test at 120 MPa in air at 1100 °C (t_f = 0.748h). 115

A.74. Fracture surface of the N610/$LaPO_4$/Al_2O_3 specimen with 10ply 0°/90° uni-tape lay-up subjected to creep test at 120 MPa in air at 1100 °C (t_f = 0.748h). 115

A.75. Fracture surface of the N610/$LaPO_4$/Al_2O_3 specimen with 10ply 0°/90° uni-tape lay-up subjected to creep test at 120 MPa in air at 1100 °C (t_f = 0.748h). 116

A.76. Fracture surface of the N610/$LaPO_4$/Al_2O_3 specimen with 10ply 0°/90° uni-tape lay-up subjected to creep test at 120 MPa in air at 1100 °C (t_f = 0.748h). 116

A.77. Fracture surface of the N610/$LaPO_4$/Al_2O_3 specimen with 10ply 0°/90° uni-tape lay-up subjected to creep test at 120 MPa in air at 1100 °C (t_f = 0.748h). 116

A.78. Fracture surface of the N610/$LaPO_4$/Al_2O_3 specimen with 10ply 0°/90° uni-tape lay-up subjected to creep test at 120 MPa in air at 1100 °C (t_f = 0.748h). 117

A.79. Fracture surface of the N610/$LaPO_4$/Al_2O_3 specimen with 10ply 0°/90° uni-tape lay-up subjected to creep test at 120 MPa in air at 1100 °C (t_f = 0.748h). 117

A.80. Fracture surface of the N610/$LaPO_4$/Al_2O_3 specimen with 10ply 0°/90° uni-tape lay-up subjected to creep test at 120 MPa in air at 1100 °C (t_f = 0.748h). 117

A.81. Fracture surface of the N610/$LaPO_4$/Al_2O_3 specimen with 10ply 0°/90° uni-tape lay-up subjected to creep test at 120 MPa in air at 1100 °C (t_f = 0.748h). 118

A.82. Fracture surface of the N610/$LaPO_4$/Al_2O_3 specimen with 10ply 0°/90° uni-tape lay-up subjected to creep test at 120 MPa in air at 1100 °C (t_f = 0.748h). 118

Figure Page

A.83. Fracture surface of the N610/$LaPO_4$/Al_2O_3 specimen with 10ply 0°/90° uni-tape lay-up subjected to creep test at 120 MPa in air at 1100 °C (t_f = 0.748h). 118

A.84. Fracture surface of the N610/$LaPO_4$/Al_2O_3 specimen with 10ply 0°/90° uni-tape lay-up subjected to creep test at 120 MPa in air at 1100 °C (t_f = 0.748h). 119

A.85. Fracture surface of the N610/$LaPO_4$/Al_2O_3 specimen with 10ply 0°/90° uni-tape lay-up subjected to creep test at 120 MPa in air at 1100 °C (t_f = 0.748h). 119

A.86. Fracture surface of the N610/$LaPO_4$/Al_2O_3 specimen with 10ply 0°/90° uni-tape lay-up subjected to creep test at 120 MPa in air at 1100 °C (t_f = 0.748h). 119

A.87. Fracture surface of the N610/$LaPO_4$/Al_2O_3 specimen with 10ply 0°/90° uni-tape lay-up subjected to creep test at 120 MPa in air at 1100 °C (t_f = 0.748h). 120

A.88. Fracture surface of the N610/$LaPO_4$/Al_2O_3 specimen with 10ply 0°/90° uni-tape lay-up subjected to creep test at 120 MPa in air at 1100 °C (t_f = 0.748h). 120

A.89. Fracture surface of the N610/$LaPO_4$/Al_2O_3 specimen with 10ply 0°/90° uni-tape lay-up subjected to creep test at 120 MPa in air at 1100 °C (t_f = 0.748h). 120

A.90. Fracture surface of the N610/$LaPO_4$/Al_2O_3 specimen with 10ply 0°/90° uni-tape lay-up subjected to creep test at 120 MPa in air at 1100 °C (t_f = 0.748h). 121

A.91. Fracture surface of the N610/$LaPO_4$/Al_2O_3 specimen with 10ply 0°/90° uni-tape lay-up subjected to creep test at 120 MPa in air at 1100 °C (t_f = 0.748h). 121

A.92. Fracture surface of the N610/$LaPO_4$/Al_2O_3 specimen with 10ply 0°/90° uni-tape lay-up subjected to creep test at 120 MPa in air at 1100 °C (t_f = 0.748h). 121

A.93. Fracture surface of the N610/$LaPO_4$/Al_2O_3 specimen with 10ply 0°/90° uni-tape lay-up subjected to creep test at 120 MPa in air at 1100 °C (t_f = 0.748h). 122

Figure Page

A.94. Fracture surface of the N610/$LaPO_4$/Al_2O_3 specimen with 10ply 0°/90° uni-tape lay-up subjected to creep test at 120 MPa in air at 1100 °C (t_f = 0.748h). 122

A.95. Fracture surface of the N610/$LaPO_4$/Al_2O_3 specimen with 10ply 0°/90° uni-tape lay-up subjected to creep test at 120 MPa in air at 1100 °C (t_f = 0.748h). 122

A.96. Fracture surface of the N610/$LaPO_4$/Al_2O_3 specimen with 10ply 0°/90° uni-tape lay-up subjected to creep test at 120 MPa in air at 1100 °C (t_f = 0.748h). 123

A.97. Fracture surface of the N610/$LaPO_4$/Al_2O_3 specimen with 10ply 0°/90° uni-tape lay-up subjected to creep test at 120 MPa in air at 1100 °C (t_f = 0.748h). 123

A.98. Fracture surface of the N610/$LaPO_4$/Al_2O_3 specimen with 10ply 0°/90° uni-tape lay-up subjected to creep test at 120 MPa in air at 1100 °C (t_f = 0.748h). 123

A.99. Fracture surface of the N610/$LaPO_4$/Al_2O_3 specimen with 10ply 0°/90° uni-tape lay-up subjected to creep test at 120 MPa in air at 1100 °C (t_f = 0.748h). 124

A.100. Fracture surface of the N610/$LaPO_4$/Al_2O_3 specimen with 10ply 0°/90° uni-tape lay-up subjected to creep test at 120 MPa in air at 1100 °C (t_f = 0.748h). 124

A.101. Fracture surface of the N610/$LaPO_4$/Al_2O_3 specimen with 10ply 0°/90° uni-tape lay-up subjected to creep test at 120 MPa in air at 1100 °C (t_f = 0.748h). 124

A.102. Fracture surface of the N610/$LaPO_4$/Al_2O_3 specimen with 10ply 0°/90° uni-tape lay-up subjected to creep test at 120 MPa in air at 1100 °C (t_f = 0.748h). 125

A.103. Fracture surface of the N610/$LaPO_4$/Al_2O_3 specimen with 10ply 0°/90° uni-tape lay-up subjected to creep test at 120 MPa in air at 1100 °C (t_f = 0.748h). 125

A.104. Fracture surface of the N610/$LaPO_4$/Al_2O_3 specimen with 10ply 0°/90° uni-tape lay-up subjected to creep test at 120 MPa in air at 1100 °C (t_f = 0.748h). 125

A.105. Fracture surface of the N610/$LaPO_4$/Al_2O_3 specimen with 10ply 0°/90° uni-tape lay-up subjected to creep test at 120 MPa in air at 1100 °C (t_f = 0.748h). 126

A.106. Fracture surface of the N610/$LaPO_4$/Al_2O_3 specimen with 10ply 0°/90° uni-tape lay-up subjected to creep test at 120 MPa in air at 1100 °C (t_f = 0.748h). 126

A.107. Fracture surface of the N610/$LaPO_4$/Al_2O_3 specimen with 10ply 0°/90° uni-tape lay-up subjected to creep test at 120 MPa in air at 1100 °C (t_f = 0.748h). 126

A.108. Fracture surface of the N610/$LaPO_4$/Al_2O_3 specimen with 10ply 0°/90° uni-tape lay-up subjected to creep test at 85 MPa in steam at 1100 °C (t_f = 8.183h). 127

A.109. Fracture surface of the N610/$LaPO_4$/Al_2O_3 specimen with 10ply 0°/90° uni-tape lay-up subjected to creep test at 85 MPa in steam at 1100 °C (t_f = 8.183h). 127

A.110. Fracture surface of the N610/$LaPO_4$/Al_2O_3 specimen with 10ply 0°/90° uni-tape lay-up subjected to creep test at 85 MPa in steam at 1100 °C (t_f = 8.183h). 127

A.111. Fracture surface of the N610/$LaPO_4$/Al_2O_3 specimen with 10ply 0°/90° uni-tape lay-up subjected to creep test at 85 MPa in steam at 1100 °C (t_f = 8.183h). 128

A.112. Fracture surface of the N610/$LaPO_4$/Al_2O_3 specimen with 10ply 0°/90° uni-tape lay-up subjected to creep test at 85 MPa in steam at 1100 °C (t_f = 8.183h). 128

A.113. Fracture surface of the N610/$LaPO_4$/Al_2O_3 specimen with 10ply 0°/90° uni-tape lay-up subjected to creep test at 85 MPa in steam at 1100 °C (t_f = 8.183h). 128

A.114. Fracture surface of the N610/$LaPO_4$/Al_2O_3 specimen with 10ply 0°/90° uni-tape lay-up subjected to creep test at 85 MPa in steam at 1100 °C (t_f = 8.183h). 129

A.115. Fracture surface of the N610/$LaPO_4$/Al_2O_3 specimen with 10ply 0°/90° uni-tape lay-up subjected to creep test at 85 MPa in steam at 1100 °C (t_f = 8.183h). 129

A.116. Fracture surface of the N610/$LaPO_4$/Al_2O_3 specimen with 10ply 0°/90° uni-tape lay-up subjected to creep test at 85 MPa in steam at 1100 °C (t_f = 8.183h). 129

A.117. Fracture surface of the N610/$LaPO_4$/Al_2O_3 specimen with 10ply 0°/90° uni-tape lay-up subjected to creep test at 85 MPa in steam at 1100 °C (t_f = 8.183h). 130

A.118. Fracture surface of the N610/$LaPO_4$/Al_2O_3 specimen with 10ply 0°/90° uni-tape lay-up subjected to creep test at 85 MPa in steam at 1100 °C (t_f = 8.183h). 130

A.119. Fracture surface of the N610/$LaPO_4$/Al_2O_3 specimen with 10ply 0°/90° uni-tape lay-up subjected to creep test at 85 MPa in steam at 1100 °C (t_f = 8.183h). 130

A.120. Fracture surface of the N610/$LaPO_4$/Al_2O_3 specimen with 10ply 0°/90° uni-tape lay-up subjected to creep test at 85 MPa in steam at 1100 °C (t_f = 8.183h). 131

A.121. Fracture surface of the N610/$LaPO_4$/Al_2O_3 specimen with 10ply 0°/90° uni-tape lay-up subjected to creep test at 85 MPa in steam at 1100 °C (t_f = 8.183h). 131

A.122. Fracture surface of the N610/$LaPO_4$/Al_2O_3 specimen with 10ply 0°/90° uni-tape lay-up subjected to creep test at 85 MPa in steam at 1100 °C (t_f = 8.183h). 131

A.123. Fracture surface of the N610/$LaPO_4$/Al_2O_3 specimen with 10ply 0°/90° uni-tape lay-up subjected to creep test at 85 MPa in steam at 1100 °C (t_f = 8.183h). 132

A.124. Fracture surface of the N610/$LaPO_4$/Al_2O_3 specimen with 10ply 0°/90° uni-tape lay-up subjected to creep test at 85 MPa in steam at 1100 °C (t_f = 8.183h). 132

A.125. Fracture surface of the N610/$LaPO_4$/Al_2O_3 specimen with 10ply 0°/90° uni-tape lay-up subjected to creep test at 85 MPa in steam at 1100 °C (t_f = 8.183h). 132

A.126. Fracture surface of the N610/$LaPO_4$/Al_2O_3 specimen with 10ply 0°/90° uni-tape lay-up subjected to creep test at 85 MPa in steam at 1100 °C (t_f = 8.183h). 133

A.127. Fracture surface of the N610/$LaPO_4$/Al_2O_3 specimen with 10ply 0°/90° uni-tape lay-up subjected to creep test at 85 MPa in steam at 1100 °C (t_f = 8.183h). 133

A.128. Fracture surface of the N610/$LaPO_4$/Al_2O_3 specimen with 10ply 0°/90° uni-tape lay-up subjected to creep test at 85 MPa in steam at 1100 °C (t_f = 8.183h). 133

A.129. Fracture surface of the N610/$LaPO_4$/Al_2O_3 specimen with 10ply 0°/90° uni-tape lay-up subjected to creep test at 85 MPa in steam at 1100 °C (t_f = 8.183h). 134

A.130. Fracture surface of the N610/$LaPO_4$/Al_2O_3 specimen with 10ply 0°/90° uni-tape lay-up subjected to creep test at 85 MPa in steam at 1100 °C (t_f = 8.183h). 134

A.131. Fracture surface of the N610/$LaPO_4$/Al_2O_3 specimen with 10ply 0°/90° uni-tape lay-up subjected to creep test at 85 MPa in steam at 1100 °C (t_f = 8.183h). 134

A.132. Fracture surface of the N610/$LaPO_4$/Al_2O_3 specimen with 10ply 0°/90° uni-tape lay-up subjected to creep test at 85 MPa in steam at 1100 °C (t_f = 8.183h). 135

A.133. Fracture surface of the N610/$LaPO_4$/Al_2O_3 specimen with 10ply 0°/90° uni-tape lay-up subjected to creep test at 85 MPa in steam at 1100 °C (t_f = 8.183h). 135

A.134. Fracture surface of the N610/$LaPO_4$/Al_2O_3 specimen with 10ply 0°/90° uni-tape lay-up subjected to creep test at 85 MPa in steam at 1100 °C (t_f = 8.183h). 135

A.135. Fracture surface of the N610/$LaPO_4$/Al_2O_3 specimen with 10ply 0°/90° uni-tape lay-up subjected to creep test at 85 MPa in steam at 1100 °C (t_f = 8.183h). 136

A.136. Fracture surface of the N610/$LaPO_4$/Al_2O_3 specimen with 10ply 0°/90° uni-tape lay-up subjected to creep test at 85 MPa in steam at 1100 °C (t_f = 8.183h). 136

A.137. Fracture surface of the N610/$LaPO_4$/Al_2O_3 specimen with 10ply 0°/90° uni-tape lay-up subjected to creep test at 85 MPa in steam at 1100 °C (t_f = 8.183h). 136

A.138. Fracture surface of the N610/$LaPO_4$/Al_2O_3 specimen with 10ply 0°/90° uni-tape lay-up subjected to creep test at 85 MPa in steam at 1100 °C (t_f = 8.183h). 137

A.139. Fracture surface of the N610/$LaPO_4$/Al_2O_3 specimen with 10ply 0°/90° uni-tape lay-up subjected to creep test at 85 MPa in steam at 1100 °C (t_f = 8.183h). 137

A.140. Fracture surface of the N610/$LaPO_4$/Al_2O_3 specimen with 8ply HSW subjected to creep test at 32 MPa in air at 1100 °C (t_f = 100h). 137

A.141. Fracture surface of the N610/$LaPO_4$/Al_2O_3 specimen with 8ply HSW subjected to creep test at 32 MPa in air at 1100 °C (t_f = 100h). 138

A.142. Fracture surface of the N610/$LaPO_4$/Al_2O_3 specimen with 8ply HSW subjected to creep test at 32 MPa in air at 1100 °C (t_f = 100h). 138

A.143. Fracture surface of the N610/$LaPO_4$/Al_2O_3 specimen with 8ply HSW subjected to creep test at 32 MPa in air at 1100 °C (t_f = 100h). 138

A.144. Fracture surface of the N610/$LaPO_4$/Al_2O_3 specimen with 8ply HSW subjected to creep test at 32 MPa in air at 1100 °C (t_f = 100h). 139

A.145. Fracture surface of the N610/$LaPO_4$/Al_2O_3 specimen with 8ply HSW subjected to creep test at 32 MPa in air at 1100 °C (t_f = 100h). 139

A.146. Fracture surface of the N610/$LaPO_4$/Al_2O_3 specimen with 8ply HSW subjected to creep test at 32 MPa in air at 1100 °C (t_f = 100h). 139

A.147. Fracture surface of the N610/$LaPO_4$/Al_2O_3 specimen with 8ply HSW subjected to creep test at 32 MPa in air at 1100 °C (t_f = 100h). 140

A.148. Fracture surface of the N610/$LaPO_4$/Al_2O_3 specimen with 8ply HSW subjected to creep test at 32 MPa in air at 1100 °C (t_f = 100h). 140

A.149. Fracture surface of the N610/$LaPO_4$/Al_2O_3 specimen with 8ply HSW subjected to creep test at 32 MPa in air at 1100 °C (t_f = 100h). 140

A.150. Fracture surface of the N610/$LaPO_4$/Al_2O_3 specimen with 8ply HSW subjected to creep test at 32 MPa in air at 1100 °C (t_f = 100h). 141

A.151. Fracture surface of the N610/$LaPO_4$/Al_2O_3 specimen with 8ply HSW subjected to creep test at 32 MPa in air at 1100 °C (t_f = 100h). 141

A.152. Fracture surface of the N610/$LaPO_4$/Al_2O_3 specimen with 8ply HSW subjected to creep test at 32 MPa in air at 1100 °C (t_f = 100h). 141

A.153. Fracture surface of the N610/$LaPO_4$/Al_2O_3 specimen with 8ply HSW subjected to creep test at 32 MPa in air at 1100 °C (t_f = 100h). 142

A.154. Fracture surface of the N610/$LaPO_4$/Al_2O_3 specimen with 8ply HSW subjected to creep test at 32 MPa in air at 1100 °C (t_f = 100h). 142

A.155. Fracture surface of the N610/$LaPO_4$/Al_2O_3 specimen with 8ply HSW subjected to creep test at 32 MPa in air at 1100 °C (t_f = 100h). 142

A.156. Fracture surface of the N610/$LaPO_4$/Al_2O_3 specimen with 8ply HSW subjected to creep test at 32 MPa in air at 1100 °C (t_f = 100h). 143

A.157. Fracture surface of the N610/$LaPO_4$/Al_2O_3 specimen with 8ply HSW subjected to creep test at 32 MPa in air at 1100 °C (t_f = 100h). 143

A.158. Fracture surface of the N610/$LaPO_4$/Al_2O_3 specimen with 8ply HSW subjected to creep test at 32 MPa in air at 1100 °C (t_f = 100h). 143

A.159. Fracture surface of the N610/$LaPO_4$/Al_2O_3 specimen with 8ply HSW subjected to creep test at 32 MPa in air at 1100 °C (t_f = 100h). 144

A.160. Fracture surface of the N610/$LaPO_4$/Al_2O_3 specimen with 8ply HSW subjected to creep test at 32 MPa in air at 1100 °C (t_f = 100h). 144

A.161. Fracture surface of the N610/$LaPO_4$/Al_2O_3 specimen with 8ply HSW subjected to creep test at 32 MPa in air at 1100 °C (t_f = 100h). 144

A.162. Fracture surface of the N610/$LaPO_4$/Al_2O_3 specimen with 8ply HSW subjected to creep test at 32 MPa in air at 1100 °C (t_f = 100h). 145

A.163. Fracture surface of the N610/$LaPO_4$/Al_2O_3 specimen with 8ply HSW subjected to creep test at 32 MPa in air at 1100 °C (t_f = 100h). 145

A.164. Fracture surface of the N610/$LaPO_4$/Al_2O_3 specimen with 8ply HSW subjected to creep test at 32 MPa in air at 1100 °C (t_f = 100h). 145

A.165. Fracture surface of the N610/$LaPO_4$/Al_2O_3 specimen with 8ply HSW subjected to creep test at 32 MPa in air at 1100 °C (t_f = 100h). 146

A.166. Fracture surface of the N610/$LaPO_4$/Al_2O_3 specimen with 8ply HSW subjected to creep test at 32 MPa in air at 1100 °C (t_f = 100h). 146

A.167. Fracture surface of the N610/$LaPO_4$/Al_2O_3 specimen with 8ply HSW subjected to creep test at 32 MPa in air at 1100 °C (t_f = 100h). 146

A.168. Fracture surface of the N610/$LaPO_4$/Al_2O_3 specimen with 8ply HSW subjected to creep test at 32 MPa in air at 1100 °C (t_f = 100h). 147

A.169. Fracture surface of the N610/$LaPO_4$/Al_2O_3 specimen with 8ply HSW subjected to creep test at 32 MPa in air at 1100 °C (t_f = 100h). 147

A.170. Fracture surface of the N610/$LaPO_4$/Al_2O_3 specimen with 8ply HSW subjected to creep test at 32 MPa in air at 1100 °C (t_f = 100h). 147

Figure Page

A.171. Fracture surface of the N610/$LaPO_4$/Al_2O_3 specimen with 8ply HSW subjected to creep test at 32 MPa in air at 1100 °C (t_f = 100h). 148

A.172. Fracture surface of the N610/$LaPO_4$/Al_2O_3 specimen with 8ply HSW subjected to creep test at 32 MPa in steam at 1100 °C (t_f = 51.9h). 148

A.173. Fracture surface of the N610/$LaPO_4$/Al_2O_3 specimen with 8ply HSW subjected to creep test at 32 MPa in steam at 1100 °C (t_f = 51.9h). 148

A.174. Fracture surface of the N610/$LaPO_4$/Al_2O_3 specimen with 8ply HSW subjected to creep test at 32 MPa in steam at 1100 °C (t_f = 51.9h). 149

A.175. Fracture surface of the N610/$LaPO_4$/Al_2O_3 specimen with 8ply HSW subjected to creep test at 32 MPa in steam at 1100 °C (t_f = 51.9h). 149

A.176. Fracture surface of the N610/$LaPO_4$/Al_2O_3 specimen with 8ply HSW subjected to creep test at 32 MPa in steam at 1100 °C (t_f = 51.9h). 149

A.177. Fracture surface of the N610/$LaPO_4$/Al_2O_3 specimen with 8ply HSW subjected to creep test at 32 MPa in steam at 1100 °C (t_f = 51.9h). 150

A.178. Fracture surface of the N610/$LaPO_4$/Al_2O_3 specimen with 8ply HSW subjected to creep test at 32 MPa in steam at 1100 °C (t_f = 51.9h). 150

A.179. Fracture surface of the N610/$LaPO_4$/Al_2O_3 specimen with 8ply HSW subjected to creep test at 32 MPa in steam at 1100 °C (t_f = 51.9h). 150

A.180. Fracture surface of the N610/$LaPO_4$/Al_2O_3 specimen with 8ply HSW subjected to creep test at 32 MPa in steam at 1100 °C (t_f = 51.9h). 151

A.181. Fracture surface of the N610/$LaPO_4$/Al_2O_3 specimen with 8ply HSW subjected to creep test at 32 MPa in steam at 1100 °C (t_f = 51.9h). 151

A.182. Fracture surface of the N610/$LaPO_4$/Al_2O_3 specimen with 8ply HSW subjected to creep test at 32 MPa in steam at 1100 °C (t_f = 51.9h). 151

A.183. Fracture surface of the N610/$LaPO_4$/Al_2O_3 specimen with 8ply HSW subjected to creep test at 32 MPa in steam at 1100 °C (t_f = 51.9h). 152

A.184. Fracture surface of the N610/$LaPO_4$/Al_2O_3 specimen with 8ply HSW subjected to creep test at 32 MPa in steam at 1100 °C (t_f = 51.9h). 152

A.185. Fracture surface of the N610/$LaPO_4$/Al_2O_3 specimen with 8ply HSW subjected to creep test at 32 MPa in steam at 1100 °C (t_f = 51.9h). 152

A.186. Fracture surface of the N610/$LaPO_4$/Al_2O_3 specimen with 8ply HSW subjected to creep test at 32 MPa in steam at 1100 °C (t_f = 51.9h). 153

A.187. Fracture surface of the N610/$LaPO_4$/Al_2O_3 specimen with 8ply HSW subjected to creep test at 32 MPa in steam at 1100 °C (t_f = 51.9h). 153

A.188. Fracture surface of the N610/$LaPO_4$/Al_2O_3 specimen with 8ply HSW subjected to creep test at 32 MPa in steam at 1100 °C (t_f = 51.9h). 153

A.189. Fracture surface of the N610/$LaPO_4$/Al_2O_3 specimen with 8ply HSW subjected to creep test at 32 MPa in steam at 1100 °C (t_f = 51.9h). 154

A.190. Fracture surface of the N610/$LaPO_4$/Al_2O_3 specimen with 8ply HSW subjected to creep test at 72 MPa in air at 1100 °C (t_f = 100h). 154

A.191. Fracture surface of the N610/$LaPO_4$/Al_2O_3 specimen with 8ply HSW subjected to creep test at 72 MPa in air at 1100 °C (t_f = 100h). 154

A.192. Fracture surface of the N610/$LaPO_4$/Al_2O_3 specimen with 8ply HSW subjected to creep test at 72 MPa in air at 1100 °C (t_f = 100h). 155

A.193. Fracture surface of the N610/$LaPO_4$/Al_2O_3 specimen with 8ply HSW subjected to creep test at 72 MPa in air at 1100 °C (t_f = 100h). 155

A.194. Fracture surface of the N610/$LaPO_4$/Al_2O_3 specimen with 8ply HSW subjected to creep test at 72 MPa in air at 1100 °C (t_f = 100h). 155

A.195. Fracture surface of the N610/$LaPO_4$/Al_2O_3 specimen with 8ply HSW subjected to creep test at 72 MPa in air at 1100 °C (t_f = 100h). 156

A.196. Fracture surface of the N610/$LaPO_4$/Al_2O_3 specimen with 8ply HSW subjected to creep test at 72 MPa in air at 1100 °C (t_f = 100h). 156

A.197. Fracture surface of the N610/$LaPO_4$/Al_2O_3 specimen with 8ply HSW subjected to creep test at 72 MPa in air at 1100 °C (t_f = 100h). 156

A.198. Fracture surface of the N610/$LaPO_4$/Al_2O_3 specimen with 8ply HSW subjected to creep test at 72 MPa in air at 1100 °C (t_f = 100h). 157

A.199. Fracture surface of the N610/$LaPO_4$/Al_2O_3 specimen with 8ply HSW subjected to creep test at 72 MPa in air at 1100 °C (t_f = 100h). 157

A.200. Fracture surface of the N610/$LaPO_4$/Al_2O_3 specimen with 8ply HSW subjected to creep test at 72 MPa in air at 1100 °C (t_f = 100h). 157

A.201. Fracture surface of the N610/$LaPO_4$/Al_2O_3 specimen with 8ply HSW subjected to creep test at 72 MPa in air at 1100 °C (t_f = 100h). 158

A.202. Fracture surface of the N610/$LaPO_4$/Al_2O_3 specimen with 8ply HSW subjected to creep test at 72 MPa in air at 1100 °C (t_f = 100h). 158

A.203. Fracture surface of the N610/$LaPO_4$/Al_2O_3 specimen with 8ply HSW subjected to creep test at 72 MPa in air at 1100 °C (t_f = 100h). 158

A.204. Fracture surface of the N610/$LaPO_4$/Al_2O_3 specimen with 8ply HSW subjected to creep test at 72 MPa in air at 1100 °C (t_f = 100h). 159

A.205. Fracture surface of the N610/$LaPO_4$/Al_2O_3 specimen with 8ply HSW subjected to creep test at 72 MPa in air at 1100 °C (t_f = 100h). 159

A.206. Fracture surface of the N610/$LaPO_4$/Al_2O_3 specimen with 8ply HSW subjected to creep test at 72 MPa in air at 1100 °C (t_f = 100h). 159

A.207. Fracture surface of the N610/$LaPO_4$/Al_2O_3 specimen with 8ply HSW subjected to creep test at 72 MPa in air at 1100 °C (t_f = 100h). 160

A.208. Fracture surface of the N610/$LaPO_4$/Al_2O_3 specimen with 8ply HSW subjected to creep test at 72 MPa in air at 1100 °C (t_f = 100h). 160

A.209. Fracture surface of the N610/$LaPO_4$/Al_2O_3 specimen with 8ply HSW subjected to creep test at 72 MPa in air at 1100 °C (t_f = 100h). 160

A.210. Fracture surface of the N610/$LaPO_4$/Al_2O_3 specimen with 8ply HSW subjected to creep test at 72 MPa in air at 1100 °C (t_f = 100h). 161

A.211. Fracture surface of the N610/$LaPO_4$/Al_2O_3 specimen with 8ply HSW subjected to creep test at 72 MPa in air at 1100 °C (t_f = 100h). 161

A.212. Fracture surface of the N610/$LaPO_4$/Al_2O_3 specimen with 8ply HSW subjected to creep test at 72 MPa in air at 1100 °C (t_f = 100h). 161

A.213. Fracture surface of the N610/$LaPO_4$/Al_2O_3 specimen with 8ply HSW subjected to creep test at 72 MPa in air at 1100 °C (t_f = 100h). 162

A.214. Fracture surface of the N610/$LaPO_4$/Al_2O_3 specimen with 8ply HSW subjected to creep test at 72 MPa in air at 1100 °C (t_f = 100h). 162

A.215. Fracture surface of the N610/$LaPO_4$/Al_2O_3 specimen with 8ply HSW subjected to creep test at 72 MPa in air at 1100 °C (t_f = 100h). 162

A.216. Fracture surface of the N610/$LaPO_4$/Al_2O_3 specimen with 8ply HSW subjected to creep test at 72 MPa in air at 1100 °C (t_f = 100h). 163

A.217. Fracture surface of the N610/$LaPO_4$/Al_2O_3 specimen with 8ply HSW subjected to creep test at 72 MPa in air at 1100 °C (t_f = 100h). 163

A.218. Fracture surface of the N610/$LaPO_4$/Al_2O_3 specimen with 8ply HSW subjected to creep test at 72 MPa in air at 1100 °C (t_f = 100h). 163

A.219. Fracture surface of the N610/$LaPO_4$/Al_2O_3 specimen with 8ply HSW subjected to creep test at 72 MPa in air at 1100 °C (t_f = 100h). 164

A.220. Fracture surface of the N610/$LaPO_4$/Al_2O_3 specimen with 8ply HSW subjected to creep test at 72 MPa in air at 1100 °C (t_f = 100h). 164

A.221. Fracture surface of the N610/$LaPO_4$/Al_2O_3 specimen with 8ply HSW subjected to creep test at 72 MPa in air at 1100 °C (t_f = 100h). 164

A.222. Fracture surface of the N610/$LaPO_4$/Al_2O_3 specimen with 8ply HSW subjected to creep test at 72 MPa in air at 1100 °C (t_f = 100h). 165

A.223. Fracture surface of the N610/$LaPO_4$/Al_2O_3 specimen with 8ply HSW subjected to creep test at 72 MPa in air at 1100 °C (t_f = 100h). 165

A.224. Fracture surface of the N610/$LaPO_4$/Al_2O_3 specimen with 8ply HSW subjected to creep test at 72 MPa in steam at 1100 °C (t_f = 2.24h). 165

A.225. Fracture surface of the N610/$LaPO_4$/Al_2O_3 specimen with 8ply HSW subjected to creep test at 72 MPa in steam at 1100 °C (t_f = 2.24h). 166

A.226. Fracture surface of the N610/$LaPO_4$/Al_2O_3 specimen with 8ply HSW subjected to creep test at 72 MPa in steam at 1100 °C (t_f = 2.24h). 166

A.227. Fracture surface of the N610/$LaPO_4$/Al_2O_3 specimen with 8ply HSW subjected to creep test at 72 MPa in steam at 1100 °C (t_f = 2.24h). 166

A.228. Fracture surface of the N610/$LaPO_4$/Al_2O_3 specimen with 8ply HSW subjected to creep test at 72 MPa in steam at 1100 °C (t_f = 2.24h). 167

A.229. Fracture surface of the N610/$LaPO_4$/Al_2O_3 specimen with 8ply HSW subjected to creep test at 72 MPa in steam at 1100 °C (t_f = 2.24h). 167

A.230. Fracture surface of the N610/$LaPO_4$/Al_2O_3 specimen with 8ply HSW subjected to creep test at 72 MPa in steam at 1100 °C (t_f = 2.24h). 167

A.231. Fracture surface of the N610/$LaPO_4$/Al_2O_3 specimen with 8ply HSW subjected to creep test at 72 MPa in steam at 1100 °C (t_f = 2.24h). 168

A.232. Fracture surface of the N610/$LaPO_4$/Al_2O_3 specimen with 8ply HSW subjected to creep test at 72 MPa in steam at 1100 °C (t_f = 2.24h). 168

A.233. Fracture surface of the N610/$LaPO_4$/Al_2O_3 specimen with 8ply HSW subjected to creep test at 72 MPa in steam at 1100 °C (t_f = 2.24h). 168

A.234. Fracture surface of the N610/$LaPO_4$/Al_2O_3 specimen with 8ply HSW subjected to creep test at 72 MPa in steam at 1100 °C (t_f = 2.24h). 169

A.235. Fracture surface of the N610/$LaPO_4$/Al_2O_3 specimen with 8ply HSW subjected to creep test at 72 MPa in steam at 1100 °C (t_f = 2.24h). 169

A.236. Fracture surface of the N610/$LaPO_4$/Al_2O_3 specimen with 8ply HSW subjected to creep test at 72 MPa in steam at 1100 °C (t_f = 2.24h). 169

A.237. Fracture surface of the N610/$LaPO_4$/Al_2O_3 specimen with 8ply HSW subjected to creep test at 72 MPa in steam at 1100 °C (t_f = 2.24h). 170

A.238. Fracture surface of the N610/$LaPO_4$/Al_2O_3 specimen with 8ply HSW subjected to creep test at 72 MPa in steam at 1100 °C (t_f = 2.24h). 170

A.239. Fracture surface of the N610/$LaPO_4$/Al_2O_3 specimen with 8ply HSW subjected to creep test at 72 MPa in steam at 1100 °C (t_f = 2.24h). 170

A.240. Fracture surface of the N610/$LaPO_4$/Al_2O_3 specimen with 8ply HSW subjected to creep test at 72 MPa in steam at 1100 °C (t_f = 2.24h). 171

A.241. Fracture surface of the N610/$LaPO_4$/Al_2O_3 specimen with 8ply HSW subjected to creep test at 72 MPa in steam at 1100 °C (t_f = 2.24h). 171

A.242. Fracture surface of the N610/$LaPO_4$/Al_2O_3 specimen with 8ply HSW subjected to creep test at 72 MPa in steam at 1100 °C (t_f = 2.24h). 171

A.243. Fracture surface of the N610/$LaPO_4$/Al_2O_3 specimen with 8ply HSW subjected to creep test at 72 MPa in steam at 1100 °C (t_f = 2.24h). 172

A.244. Fracture surface of the N610/$LaPO_4$/Al_2O_3 specimen with 8ply HSW subjected to creep test at 72 MPa in steam at 1100 °C (t_f = 2.24h). 172

A.245. Fracture surface of the N610/$LaPO_4$/Al_2O_3 specimen with 8ply HSW subjected to creep test at 72 MPa in steam at 1100 °C (t_f = 2.24h). 172

A.246. Fracture surface of the N610/$LaPO_4$/Al_2O_3 specimen with 8ply HSW subjected to creep test at 72 MPa in steam at 1100 °C (t_f = 2.24h). 173

A.247. Fracture surface of the N610/$LaPO_4$/Al_2O_3 specimen with 8ply HSW subjected to creep test at 72 MPa in steam at 1100 °C (t_f = 2.24h). 173

A.248. Fracture surface of the N610/$LaPO_4$/Al_2O_3 specimen with 8ply HSW subjected to creep test at 72 MPa in steam at 1100 °C (t_f = 2.24h). 173

A.249. Fracture surface of the N610/$LaPO_4$/Al_2O_3 specimen with 8ply HSW subjected to creep test at 72 MPa in steam at 1100 °C (t_f = 2.24h). 174

A.250. Fracture surface of the N610/$LaPO_4$/Al_2O_3 specimen with 8ply HSW subjected to creep test at 72 MPa in steam at 1100 °C (t_f = 2.24h). 174

A.251. Fracture surface of the N610/$LaPO_4$/Al_2O_3 specimen with 8ply HSW subjected to creep test at 72 MPa in steam at 1100 °C (t_f = 2.24h). 174

A.252. Fracture surface of the N610/Al_2O_3 specimen with 8ply HSW subjected to creep test at 30 MPa in steam at 1100 °C (t_f = 16.1h). 175

A.253. Fracture surface of the N610/Al_2O_3 specimen with 8ply HSW subjected to creep test at 30 MPa in steam at 1100 °C (t_f = 16.1h). 175

A.254. Fracture surface of the N610/Al_2O_3 specimen with 8ply HSW subjected to creep test at 30 MPa in steam at 1100 °C (t_f = 16.1h). 175

A.255. Fracture surface of the N610/Al_2O_3 specimen with 8ply HSW subjected to creep test at 30 MPa in steam at 1100 °C (t_f = 16.1h). 176

A.256. Fracture surface of the N610/Al_2O_3 specimen with 8ply HSW subjected to creep test at 30 MPa in steam at 1100 °C (t_f = 16.1h). 176

A.257. Fracture surface of the N610/Al_2O_3 specimen with 8ply HSW subjected to creep test at 30 MPa in steam at 1100 °C (t_f = 16.1h). 176

A.258. Fracture surface of the N610/Al_2O_3 specimen with 8ply HSW subjected to creep test at 30 MPa in steam at 1100 °C (t_f = 16.1h). 177

A.259. Fracture surface of the N610/Al_2O_3 specimen with 8ply HSW subjected to creep test at 30 MPa in steam at 1100 °C (t_f = 16.1h). 177

A.260. Fracture surface of the N610/Al_2O_3 specimen with 8ply HSW subjected to creep test at 30 MPa in steam at 1100 °C (t_f = 16.1h). 177

A.261. Fracture surface of the N610/Al_2O_3 specimen with 8ply HSW subjected to creep test at 30 MPa in steam at 1100 °C (t_f = 16.1h). 178

A.262. Fracture surface of the N610/Al_2O_3 specimen with 8ply HSW subjected to creep test at 30 MPa in steam at 1100 °C (t_f = 16.1h). 178

A.263. Fracture surface of the N610/Al_2O_3 specimen with 8ply HSW subjected to creep test at 30 MPa in steam at 1100 °C (t_f = 16.1h). 178

A.264. Fracture surface of the N610/Al_2O_3 specimen with 8ply HSW subjected to creep test at 30 MPa in steam at 1100 °C (t_f = 16.1h). 179

A.265. Fracture surface of the N610/Al_2O_3 specimen with 8ply HSW subjected to creep test at 30 MPa in steam at 1100 °C (t_f = 16.1h). 179

A.266. Fracture surface of the N610/Al_2O_3 specimen with 8ply HSW subjected to creep test at 30 MPa in steam at 1100 °C (t_f = 16.1h). 179

A.267. Fracture surface of the N610/Al_2O_3 specimen with 8ply HSW subjected to creep test at 30 MPa in steam at 1100 °C (t_f = 16.1h). 180

A.268. Fracture surface of the N610/Al_2O_3 specimen with 8ply HSW subjected to creep test at 30 MPa in steam at 1100 °C (t_f = 16.1h). 180

A.269. Fracture surface of the N610/Al_2O_3 specimen with 8ply HSW subjected to creep test at 30 MPa in steam at 1100 °C (t_f = 16.1h). 180

A.270. Fracture surface of the N610/Al_2O_3 specimen with 8ply HSW subjected to creep test at 30 MPa in steam at 1100 °C (t_f = 16.1h). 181

A.271. Fracture surface of the N610/Al_2O_3 specimen with 8ply HSW subjected to creep test at 30 MPa in steam at 1100 °C (t_f = 16.1h). 181

A.272. Fracture surface of the N610/Al_2O_3 specimen with 8ply HSW subjected to creep test at 30 MPa in steam at 1100 °C (t_f = 16.1h). 181

A.273. Fracture surface of the N610/Al_2O_3 specimen with 8ply HSW subjected to creep test at 30 MPa in steam at 1100 °C (t_f = 16.1h). 182

A.274. Fracture surface of the N610/Al_2O_3 specimen with 8ply HSW subjected to creep test at 30 MPa in steam at 1100 °C (t_f = 16.1h). 182

A.275. Fracture surface of the N610/Al_2O_3 specimen with 8ply HSW subjected to creep test at 30 MPa in steam at 1100 °C (t_f = 16.1h). 182

A.276. Fracture surface of the N610/Al_2O_3 specimen with 8ply HSW subjected to creep test at 40.5 MPa in air at 1100 °C (t_f = 3.34h). 183

A.277. Fracture surface of the N610/Al_2O_3 specimen with 8ply HSW subjected to creep test at 40.5 MPa in air at 1100 °C (t_f = 3.34h). 183

A.278. Fracture surface of the N610/Al_2O_3 specimen with 8ply HSW subjected to creep test at 40.5 MPa in air at 1100 °C (t_f = 3.34h). 183

A.279. Fracture surface of the N610/Al_2O_3 specimen with 8ply HSW subjected to creep test at 40.5 MPa in air at 1100 °C (t_f = 3.34h). 184

A.280. Fracture surface of the N610/Al_2O_3 specimen with 8ply HSW subjected to creep test at 40.5 MPa in air at 1100 °C (t_f = 3.34h). 184

A.281. Fracture surface of the N610/Al_2O_3 specimen with 8ply HSW subjected to creep test at 40.5 MPa in air at 1100 °C (t_f = 3.34h). 184

A.282. Fracture surface of the N610/Al_2O_3 specimen with 8ply HSW subjected to creep test at 40.5 MPa in air at 1100 °C (t_f = 3.34h). 185

A.283. Fracture surface of the N610/Al_2O_3 specimen with 8ply HSW subjected to creep test at 40.5 MPa in air at 1100 °C (t_f = 3.34h). 185

A.284. Fracture surface of the N610/Al_2O_3 specimen with 8ply HSW subjected to creep test at 40.5 MPa in air at 1100 °C (t_f = 3.34h). 185

A.285. Fracture surface of the N610/Al_2O_3 specimen with 8ply HSW subjected to creep test at 40.5 MPa in air at 1100 °C (t_f = 3.34h). 186

A.286. Fracture surface of the N610/Al_2O_3 specimen with 8ply HSW subjected to creep test at 40.5 MPa in air at 1100 °C (t_f = 3.34h). 186

A.287. Fracture surface of the N610/Al_2O_3 specimen with 8ply HSW subjected to creep test at 40.5 MPa in air at 1100 °C (t_f = 3.34h). 186

A.288. Fracture surface of the N610/Al_2O_3 specimen with 8ply HSW subjected to creep test at 40.5 MPa in air at 1100 °C (t_f = 3.34h). 187

A.289. Fracture surface of the N610/Al_2O_3 specimen with 8ply HSW subjected to creep test at 40.5 MPa in air at 1100 °C (t_f = 3.34h). 187

A.290. Fracture surface of the N610/Al_2O_3 specimen with 8ply HSW subjected to creep test at 40.5 MPa in air at 1100 °C (t_f = 3.34h). 187

A.291. Fracture surface of the N610/Al_2O_3 specimen with 8ply HSW subjected to creep test at 40.5 MPa in air at 1100 °C (t_f = 3.34h). 188

A.292. Fracture surface of the N610/Al_2O_3 specimen with 8ply HSW subjected to creep test at 40.5 MPa in air at 1100 °C (t_f = 3.34h). 188

A.293. Fracture surface of the N610/Al_2O_3 specimen with 8ply HSW subjected to creep test at 40.5 MPa in air at 1100 °C (t_f = 3.34h). 188

A.294. Fracture surface of the N610/Al_2O_3 specimen with 8ply HSW subjected to creep test at 40.5 MPa in air at 1100 °C (t_f = 3.34h). 189

A.295. Fracture surface of the N610/Al_2O_3 specimen with 8ply HSW subjected to creep test at 40.5 MPa in air at 1100 °C (t_f = 3.34h). 189

A.296. Fracture surface of the N610/Al_2O_3 specimen with 8ply HSW subjected to creep test at 40.5 MPa in air at 1100 °C (t_f = 3.34h). 189

A.297. Fracture surface of the N610/Al_2O_3 specimen with 8ply HSW subjected to creep test at 40.5 MPa in air at 1100 °C (t_f = 3.34h). 190

A.298. Fracture surface of the N610/Al_2O_3 specimen with 8ply HSW subjected to creep test at 40.5 MPa in air at 1100 °C (t_f = 3.34h). 190

A.299. Fracture surface of the N610/Al_2O_3 specimen with 8ply HSW subjected to creep test at 40.5 MPa in air at 1100 °C (t_f = 3.34h). 190

A.300. Fracture surface of the N610/Al_2O_3 specimen with 8ply HSW subjected to creep test at 40.5 MPa in air at 1100 °C (t_f = 3.34h). 191

A.301. Fracture surface of the N610/Al_2O_3 specimen with 8ply HSW subjected to creep test at 40.5 MPa in air at 1100 °C (t_f = 3.34h). 191

A.302. Fracture surface of the N610/Al_2O_3 specimen with 8ply HSW subjected to creep test at 40.5 MPa in air at 1100 °C (t_f = 3.34h). 191

A.303. Fracture surface of the N610/Al_2O_3 specimen with 8ply HSW subjected to creep test at 40.5 MPa in air at 1100 °C (t_f = 3.34h). 192

A.304. Fracture surface of the N610/Al_2O_3 specimen with 8ply HSW subjected to creep test at 40.5 MPa in air at 1100 °C (t_f = 3.34h). 192

A.305. Fracture surface of the N610/Al_2O_3 specimen with 8ply HSW subjected to creep test at 40.5 MPa in air at 1100 °C (t_f = 3.34h). 192

A.306. Fracture surface of the N610/Al_2O_3 specimen with 8ply HSW subjected to creep test at 40.5 MPa in air at 1100 °C (t_f = 3.34h). 193

A.307. Fracture surface of the N610/Al_2O_3 specimen with 8ply HSW subjected to creep test at 40.5 MPa in air at 1100 °C (t_f = 3.34h). 193

A.308. Fracture surface of the N610/Al_2O_3 specimen with 8ply HSW subjected to creep test at 40.5 MPa in air at 1100 °C (t_f = 3.34h). 193

A.309. Fracture surface of the N610/Al_2O_3 specimen with 8ply HSW subjected to creep test at 40.5 MPa in air at 1100 °C (t_f = 3.34h). 194

A.310. Fracture surface of the N610/Al_2O_3 specimen with 8ply HSW subjected to creep test at 40.5 MPa in air at 1100 °C (t_f = 3.34h). 194

A.311. Fracture surface of the N610/Al_2O_3 specimen with 8ply HSW subjected to creep test at 40.5 MPa in air at 1100 °C (t_f = 3.34h). 194

A.312. Fracture surface of the N610/Al_2O_3 specimen with 8ply HSW subjected to creep test at 40.5 MPa in air at 1100 °C (t_f = 3.34h). 195

A.313. Fracture surface of the N610/Al_2O_3 specimen with 8ply HSW subjected to creep test at 40.5 MPa in air at 1100 °C (t_f = 3.34h). 195

A.314. Fracture surface of the N610/Al_2O_3 specimen with 8ply HSW subjected to creep test at 40.5 MPa in air at 1100 °C (t_f = 3.34h). 195

A.315. Fracture surface of the N610/Al_2O_3 specimen with 8ply HSW subjected to creep test at 40.5 MPa in air at 1100 °C (t_f = 3.34h). 196

A.316. Fracture surface of the N610/Al_2O_3 specimen with 8ply HSW subjected to creep test at 40.5 MPa in air at 1100 °C (t_f = 3.34h). 196

A.317. Fracture surface of the N610/Al_2O_3 specimen with 8ply HSW subjected to creep test at 40.5 MPa in air at 1100 °C (t_f = 3.34h). 196

A.318. Fracture surface of the N610/Al_2O_3 specimen with 8ply HSW subjected to creep test at 40.5 MPa in air at 1100 °C (t_f = 3.34h). 197

A.319. Fracture surface of the N610/Al_2O_3 specimen with 8ply HSW subjected to creep test at 40.5 MPa in air at 1100 °C (t_f = 3.34h). 197

A.320. Fracture surface of the N610/Al_2O_3 specimen with 8ply HSW subjected to creep test at 40.5 MPa in air at 1100 °C (t_f = 3.34h). 197

A.321. Fracture surface of the N610/Al_2O_3 specimen with 8ply HSW subjected to creep test at 40.5 MPa in air at 1100 °C (t_f = 3.34h). 198

A.322. Fracture surface of the N610/Al_2O_3 specimen with 8ply HSW subjected to creep test at 40.5 MPa in air at 1100 °C (t_f = 3.34h). 198

A.323. Fracture surface of the N610/Al_2O_3 specimen with 8ply HSW subjected to creep test at 40.5 MPa in air at 1100 °C (t_f = 3.34h). 198

A.324. Fracture surface of the N610/Al_2O_3 specimen with 8ply HSW subjected to creep test at 40.5 MPa in steam at 1100 °C (t_f = 0.01h). 199

A.325. Fracture surface of the N610/Al_2O_3 specimen with 8ply HSW subjected to creep test at 40.5 MPa in steam at 1100 °C (t_f = 0.01h). 199

A.326. Fracture surface of the N610/Al_2O_3 specimen with 8ply HSW subjected to creep test at 40.5 MPa in steam at 1100 °C (t_f = 0.01h). 199

A.327. Fracture surface of the N610/Al_2O_3 specimen with 8ply HSW subjected to creep test at 40.5 MPa in steam at 1100 °C (t_f = 0.01h). 200

A.328. Fracture surface of the N610/Al_2O_3 specimen with 8ply HSW subjected to creep test at 40.5 MPa in steam at 1100 °C (t_f = 0.01h). 200

A.329. Fracture surface of the N610/Al_2O_3 specimen with 8ply HSW subjected to creep test at 40.5 MPa in steam at 1100 °C (t_f = 0.01h). 200

A.330. Fracture surface of the N610/Al_2O_3 specimen with 8ply HSW subjected to creep test at 40.5 MPa in steam at 1100 °C (t_f = 0.01h). 201

A.331. Fracture surface of the N610/Al_2O_3 specimen with 8ply HSW subjected to creep test at 40.5 MPa in steam at 1100 °C (t_f = 0.01h). 201

A.332. Fracture surface of the N610/Al_2O_3 specimen with 8ply HSW subjected to creep test at 40.5 MPa in steam at 1100 °C (t_f = 0.01h). 201

A.333. Fracture surface of the N610/Al_2O_3 specimen with 8ply HSW subjected to creep test at 40.5 MPa in steam at 1100 °C (t_f = 0.01h). 202

A.334. Fracture surface of the N610/Al_2O_3 specimen with 8ply HSW subjected to creep test at 40.5 MPa in steam at 1100 °C (t_f = 0.01h). 202

A.335. Fracture surface of the N610/Al_2O_3 specimen with 8ply HSW subjected to creep test at 40.5 MPa in steam at 1100 °C (t_f = 0.01h). 202

A.336. Fracture surface of the N610/Al_2O_3 specimen with 8ply HSW subjected to creep test at 40.5 MPa in steam at 1100 °C (t_f = 0.01h). 203

A.337. Fracture surface of the N610/Al_2O_3 specimen with 8ply HSW subjected to creep test at 40.5 MPa in steam at 1100 °C (t_f = 0.01h). 203

A.338. Fracture surface of the N610/Al_2O_3 specimen with 8ply HSW subjected to creep test at 40.5 MPa in steam at 1100 °C (t_f = 0.01h). 203

A.339. Fracture surface of the N610/Al_2O_3 specimen with 8ply HSW subjected to creep test at 40.5 MPa in steam at 1100 °C (t_f = 0.01h). 204

A.340. Fracture surface of the N610/Al_2O_3 specimen with 8ply HSW subjected to creep test at 40.5 MPa in steam at 1100 °C (t_f = 0.01h). 204

A.341. Fracture surface of the N610/Al_2O_3 specimen with 8ply HSW subjected to creep test at 40.5 MPa in steam at 1100 °C (t_f = 0.01h). 204

A.342. Fracture surface of the N610/Al_2O_3 specimen with 8ply HSW subjected to creep test at 40.5 MPa in steam at 1100 °C (t_f = 0.01h). 205

A.343. Fracture surface of the N610/Al_2O_3 specimen with 8ply HSW subjected to creep test at 40.5 MPa in steam at 1100 °C (t_f = 0.01h). 205

A.344. Fracture surface of the N610/Al_2O_3 specimen with 8ply HSW subjected to creep test at 40.5 MPa in steam at 1100 °C (t_f = 0.01h). 205

A.345. Fracture surface of the N610/Al_2O_3 specimen with 8ply HSW subjected to creep test at 40.5 MPa in steam at 1100 °C (t_f = 0.01h). 206

A.346. Fracture surface of the N610/Al_2O_3 specimen with 8ply HSW subjected to creep test at 40.5 MPa in steam at 1100 °C (t_f = 0.01h). 206

A.347. Fracture surface of the N610/Al_2O_3 specimen with 8ply HSW subjected to creep test at 40.5 MPa in steam at 1100 °C (t_f = 0.01h). 206

A.348. Fracture surface of the N610/Al_2O_3 specimen with 8ply HSW subjected to creep test at 40.5 MPa in steam at 1100 °C (t_f = 0.01h). 207

A.349. Fracture surface of the N610/Al_2O_3 specimen with 8ply HSW subjected to creep test at 40.5 MPa in steam at 1100 °C (t_f = 0.01h). 207

A.350. Fracture surface of the N610/Al_2O_3 specimen with 8ply HSW subjected to creep test at 40.5 MPa in steam at 1100 °C (t_f = 0.01h). 207

A.351. Fracture surface of the N610/Al_2O_3 specimen with 8ply HSW subjected to creep test at 40.5 MPa in steam at 1100 °C (t_f = 0.01h). 208

A.352. Fracture surface of the N610/Al_2O_3 specimen with 8ply HSW subjected to creep test at 40.5 MPa in steam at 1100 °C (t_f = 0.01h). 208

A.353. Fracture surface of the N610/Al_2O_3 specimen with 8ply HSW subjected to creep test at 40.5 MPa in steam at 1100 °C (t_f = 0.01h). 208

A.354. Fracture surface of the N610/Al_2O_3 specimen with 8ply HSW subjected to creep test at 40.5 MPa in steam at 1100 °C (t_f = 0.01h). 209

A.355. Fracture surface of the N610/Al_2O_3 specimen with 8ply HSW subjected to creep test at 40.5 MPa in steam at 1100 °C (t_f = 0.01h). 209

A.356. Fracture surface of the N610/Al_2O_3 specimen with 8ply HSW subjected to creep test at 40.5 MPa in steam at 1100 °C (t_f = 0.01h). 209

A.357. Fracture surface of the N610/Al_2O_3 specimen with 8ply HSW subjected to creep test at 40.5 MPa in steam at 1100 °C (t_f = 0.01h). 210

A.358. Fracture surface of the N610/Al_2O_3 specimen with 8ply HSW subjected to creep test at 40.5 MPa in steam at 1100 °C (t_f = 0.01h). 210

A.359. Fracture surface of the N610/Al_2O_3 specimen with 8ply HSW subjected to creep test at 40.5 MPa in steam at 1100 °C (t_f = 0.01h). 210

A.360. Fracture surface of the N610/$LaPO_4$/Al_2O_3-$LaPO_4$-AlOCl specimen with 8ply HSW subjected to creep test at 32 MPa in air at 1100 °C (t_f = 100h). 211

A.361. Fracture surface of the N610/$LaPO_4$/Al_2O_3-$LaPO_4$-AlOCl specimen with 8ply HSW subjected to creep test at 32 MPa in air at 1100 °C (t_f = 100h). 211

A.362. Fracture surface of the N610/$LaPO_4$/Al_2O_3-$LaPO_4$-AlOCl specimen with 8ply HSW subjected to creep test at 32 MPa in air at 1100 °C (t_f = 100h). 211

A.363. Fracture surface of the N610/$LaPO_4$/Al_2O_3-$LaPO_4$-AlOCl specimen with 8ply HSW subjected to creep test at 32 MPa in air at 1100 °C (t_f = 100h). 212

A.364. Fracture surface of the N610/$LaPO_4$/Al_2O_3-$LaPO_4$-AlOCl specimen with 8ply HSW subjected to creep test at 32 MPa in air at 1100 °C (t_f = 100h). 212

A.365. Fracture surface of the N610/$LaPO_4$/Al_2O_3-$LaPO_4$-AlOCl specimen with 8ply HSW subjected to creep test at 32 MPa in air at 1100 °C (t_f = 100h). 212

A.366. Fracture surface of the N610/$LaPO_4$/Al_2O_3-$LaPO_4$-AlOCl specimen with 8ply HSW subjected to creep test at 32 MPa in air at 1100 °C (t_f = 100h). 213

A.367. Fracture surface of the N610/$LaPO_4$/Al_2O_3-$LaPO_4$-AlOCl specimen with 8ply HSW subjected to creep test at 32 MPa in air at 1100 °C (t_f = 100h). 213

A.368. Fracture surface of the N610/$LaPO_4$/Al_2O_3-$LaPO_4$-AlOCl specimen with 8ply HSW subjected to creep test at 32 MPa in air at 1100 °C (t_f = 100h). 213

A.369. Fracture surface of the N610/$LaPO_4$/Al_2O_3-$LaPO_4$-AlOCl specimen with 8ply HSW subjected to creep test at 32 MPa in air at 1100 °C (t_f = 100h). 214

A.370. Fracture surface of the N610/$LaPO_4$/Al_2O_3-$LaPO_4$-AlOCl specimen with 8ply HSW subjected to creep test at 32 MPa in air at 1100 °C (t_f = 100h). 214

A.371. Fracture surface of the N610/$LaPO_4$/Al_2O_3-$LaPO_4$-AlOCl specimen with 8ply HSW subjected to creep test at 32 MPa in air at 1100 °C (t_f = 100h). 214

A.372. Fracture surface of the N610/$LaPO_4$/Al_2O_3-$LaPO_4$-AlOCl specimen with 8ply HSW subjected to creep test at 32 MPa in air at 1100 °C (t_f = 100h). 215

A.373. Fracture surface of the N610/$LaPO_4$/Al_2O_3-$LaPO_4$-AlOCl specimen with 8ply HSW subjected to creep test at 32 MPa in air at 1100 °C (t_f = 100h). 215

A.374. Fracture surface of the N610/$LaPO_4$/Al_2O_3-$LaPO_4$-AlOCl specimen with 8ply HSW subjected to creep test at 32 MPa in air at 1100 °C (t_f = 100h). 215

A.375. Fracture surface of the N610/$LaPO_4$/Al_2O_3-$LaPO_4$-AlOCl specimen with 8ply HSW subjected to creep test at 32 MPa in air at 1100 °C (t_f = 100h). 216

A.376. Fracture surface of the N610/$LaPO_4$/Al_2O_3-$LaPO_4$-AlOCl specimen with 8ply HSW subjected to creep test at 32 MPa in air at 1100 °C (t_f = 100h). 216

A.377. Fracture surface of the N610/$LaPO_4$/Al_2O_3-$LaPO_4$-AlOCl specimen with 8ply HSW subjected to creep test at 32 MPa in air at 1100 °C (t_f = 100h). 216

A.378. Fracture surface of the N610/$LaPO_4$/Al_2O_3-$LaPO_4$-AlOCl specimen with 8ply HSW subjected to creep test at 32 MPa in air at 1100 °C (t_f = 100h). 217

A.379. Fracture surface of the N610/$LaPO_4$/Al_2O_3-$LaPO_4$-AlOCl specimen with 8ply HSW subjected to creep test at 32 MPa in air at 1100 °C (t_f = 100h). 217

A.380. Fracture surface of the N610/$LaPO_4$/Al_2O_3-$LaPO_4$-AlOCl specimen with 8ply HSW subjected to creep test at 32 MPa in air at 1100 °C (t_f = 100h). 217

A.381. Fracture surface of the N610/$LaPO_4$/Al_2O_3-$LaPO_4$-AlOCl specimen with 8ply HSW subjected to creep test at 32 MPa in air at 1100 °C (t_f = 100h). 218

A.382. Fracture surface of the N610/$LaPO_4$/Al_2O_3-$LaPO_4$-AlOCl specimen with 8ply HSW subjected to creep test at 32 MPa in air at 1100 °C (t_f = 100h). 218

A.383. Fracture surface of the N610/$LaPO_4$/Al_2O_3-$LaPO_4$-AlOCl specimen with 8ply HSW subjected to creep test at 32 MPa in air at 1100 °C (t_f = 100h). 218

A.384. Fracture surface of the N610/$LaPO_4$/Al_2O_3-$LaPO_4$-AlOCl specimen with 8ply HSW subjected to creep test at 32 MPa in air at 1100 °C (t_f = 100h). 219

A.385. Fracture surface of the N610/$LaPO_4$/Al_2O_3-$LaPO_4$-AlOCl specimen with 8ply HSW subjected to creep test at 32 MPa in air at 1100 °C (t_f = 100h). 219

A.386. Fracture surface of the N610/$LaPO_4$/Al_2O_3-$LaPO_4$-AlOCl specimen with 8ply HSW subjected to creep test at 32 MPa in air at 1100 °C (t_f = 100h). 219

A.387. Fracture surface of the N610/$LaPO_4$/Al_2O_3-$LaPO_4$-AlOCl specimen with 8ply HSW subjected to creep test at 32 MPa in air at 1100 °C (t_f = 100h). 220

A.388. Fracture surface of the N610/$LaPO_4$/Al_2O_3-$LaPO_4$-AlOCl specimen with 8ply HSW subjected to creep test at 32 MPa in air at 1100 °C (t_f = 100h). 220

A.389. Fracture surface of the N610/$LaPO_4$/Al_2O_3-$LaPO_4$-AlOCl specimen with 8ply HSW subjected to creep test at 32 MPa in air at 1100 °C (t_f = 100h). 220

A.390. Fracture surface of the N610/$LaPO_4$/Al_2O_3-$LaPO_4$-AlOCl specimen with 8ply HSW subjected to creep test at 32 MPa in air at 1100 °C (t_f = 100h). 221

Figure Page

A.391. Fracture surface of the N610/$LaPO_4$/Al_2O_3-$LaPO_4$-AlOCl specimen with 8ply HSW subjected to creep test at 32 MPa in air at 1100 °C (t_f = 100h). 221

A.392. Fracture surface of the N610/$LaPO_4$/Al_2O_3-$LaPO_4$-AlOCl specimen with 8ply HSW subjected to creep test at 32 MPa in air at 1100 °C (t_f = 100h). 221

A.393. Fracture surface of the N610/$LaPO_4$/Al_2O_3-$LaPO_4$-AlOCl specimen with 8ply HSW subjected to creep test at 32 MPa in air at 1100 °C (t_f = 100h). 222

A.394. Fracture surface of the N610/$LaPO_4$/Al_2O_3-$LaPO_4$-AlOCl specimen with 8ply HSW subjected to creep test at 32 MPa in air at 1100 °C (t_f = 100h). 222

A.395. Fracture surface of the N610/$LaPO_4$/Al_2O_3-$LaPO_4$-AlOCl specimen with 8ply HSW subjected to creep test at 32 MPa in air at 1100 °C (t_f = 100h). 222

A.396. Fracture surface of the N610/$LaPO_4$/Al_2O_3-$LaPO_4$-AlOCl specimen with 8ply HSW subjected to creep test at 32 MPa in air at 1100 °C (t_f = 100h). 223

A.397. Fracture surface of the N610/$LaPO_4$/Al_2O_3-$LaPO_4$-AlOCl specimen with 8ply HSW subjected to creep test at 32 MPa in air at 1100 °C (t_f = 100h). 223

A.398. Fracture surface of the N610/$LaPO_4$/Al_2O_3-$LaPO_4$-AlOCl specimen with 8ply HSW subjected to creep test at 32 MPa in air at 1100 °C (t_f = 100h). 223

A.399. Fracture surface of the N610/$LaPO_4$/Al_2O_3-$LaPO_4$-AlOCl specimen with 8ply HSW subjected to creep test at 32 MPa in steam at 1100 °C (t_f = 3.47h). 224

A.400. Fracture surface of the N610/$LaPO_4$/Al_2O_3-$LaPO_4$-AlOCl specimen with 8ply HSW subjected to creep test at 32 MPa in steam at 1100 °C (t_f = 3.47h). 224

A.401. Fracture surface of the N610/$LaPO_4$/Al_2O_3-$LaPO_4$-AlOCl specimen with 8ply HSW subjected to creep test at 32 MPa in steam at 1100 °C (t_f = 3.47h). 224

A.402. Fracture surface of the N610/$LaPO_4$/Al_2O_3-$LaPO_4$-AlOCl specimen with 8ply HSW subjected to creep test at 32 MPa in steam at 1100 °C (t_f = 3.47h). 225

A.403. Fracture surface of the N610/$LaPO_4$/Al_2O_3-$LaPO_4$-AlOCl specimen with 8ply HSW subjected to creep test at 32 MPa in steam at 1100 °C (t_f = 3.47h). 225

A.404. Fracture surface of the N610/$LaPO_4$/Al_2O_3-$LaPO_4$-AlOCl specimen with 8ply HSW subjected to creep test at 32 MPa in steam at 1100 °C (t_f = 3.47h). 225

A.405. Fracture surface of the N610/$LaPO_4$/Al_2O_3-$LaPO_4$-AlOCl specimen with 8ply HSW subjected to creep test at 32 MPa in steam at 1100 °C (t_f = 3.47h). 226

A.406. Fracture surface of the N610/$LaPO_4$/Al_2O_3-$LaPO_4$-AlOCl specimen with 8ply HSW subjected to creep test at 32 MPa in steam at 1100 °C (t_f = 3.47h). 226

A.407. Fracture surface of the N610/$LaPO_4$/Al_2O_3-$LaPO_4$-AlOCl specimen with 8ply HSW subjected to creep test at 32 MPa in steam at 1100 °C (t_f = 3.47h). 226

A.408. Fracture surface of the N610/$LaPO_4$/Al_2O_3-$LaPO_4$-AlOCl specimen with 8ply HSW subjected to creep test at 32 MPa in steam at 1100 °C (t_f = 3.47h). 227

A.409. Fracture surface of the N610/$LaPO_4$/Al_2O_3-$LaPO_4$-AlOCl specimen with 8ply HSW subjected to creep test at 32 MPa in steam at 1100 °C (t_f = 3.47h). 227

A.410. Fracture surface of the N610/$LaPO_4$/Al_2O_3-$LaPO_4$-AlOCl specimen with 8ply HSW subjected to creep test at 32 MPa in steam at 1100 °C (t_f = 3.47h). 227

A.411. Fracture surface of the N610/$LaPO_4$/Al_2O_3-$LaPO_4$-AlOCl specimen with 8ply HSW subjected to creep test at 32 MPa in steam at 1100 °C (t_f = 3.47h). 228

A.412. Fracture surface of the N610/$LaPO_4$/Al_2O_3-$LaPO_4$-AlOCl specimen with 8ply HSW subjected to creep test at 32 MPa in steam at 1100 °C (t_f = 3.47h). 228

A.413. Fracture surface of the N610/$LaPO_4$/Al_2O_3-$LaPO_4$-AlOCl specimen with 8ply HSW subjected to creep test at 32 MPa in steam at 1100 °C (t_f = 3.47h). 228

A.414. Fracture surface of the N610/$LaPO_4$/Al_2O_3-$LaPO_4$-AlOCl specimen with 8ply HSW subjected to creep test at 32 MPa in steam at 1100 °C (t_f = 3.47h). 229

A.415. Fracture surface of the N610/$LaPO_4$/Al_2O_3-$LaPO_4$-AlOCl specimen with 8ply HSW subjected to creep test at 32 MPa in steam at 1100 °C (t_f = 3.47h). 229

A.416. Fracture surface of the N610/$LaPO_4$/Al_2O_3-$LaPO_4$-AlOCl specimen with 8ply HSW subjected to creep test at 32 MPa in steam at 1100 °C (t_f = 3.47h). 229

A.417. Fracture surface of the N610/$LaPO_4$/Al_2O_3-$LaPO_4$-AlOCl specimen with 8ply HSW subjected to creep test at 32 MPa in steam at 1100 °C (t_f = 3.47h). 230

A.418. Fracture surface of the N610/$LaPO_4$/Al_2O_3-$LaPO_4$-AlOCl specimen with 8ply HSW subjected to creep test at 32 MPa in steam at 1100 °C (t_f = 3.47h). 230

A.419. Fracture surface of the N610/$LaPO_4$/Al_2O_3-$LaPO_4$-AlOCl specimen with 8ply HSW subjected to creep test at 32 MPa in steam at 1100 °C (t_f = 3.47h). 230

A.420. Fracture surface of the N610/$LaPO_4$/Al_2O_3-$LaPO_4$-AlOCl specimen with 8ply HSW subjected to creep test at 32 MPa in steam at 1100 °C (t_f = 3.47h). 231

A.421. Fracture surface of the N610/$LaPO_4$/Al_2O_3-$LaPO_4$-AlOCl specimen with 8ply HSW subjected to creep test at 32 MPa in steam at 1100 °C (t_f = 3.47h). 231

A.422. Fracture surface of the N610/$LaPO_4$/Al_2O_3-$LaPO_4$-AlOCl specimen with 8ply HSW subjected to creep test at 32 MPa in steam at 1100 °C (t_f = 3.47h). 231

A.423. Fracture surface of the N610/$LaPO_4$/Al_2O_3-$LaPO_4$-AlOCl specimen with 8ply HSW subjected to creep test at 32 MPa in steam at 1100 °C (t_f = 3.47h). 232

A.424. Fracture surface of the N610/$LaPO_4$/Al_2O_3-$LaPO_4$-AlOCl specimen with 8ply HSW subjected to creep test at 32 MPa in steam at 1100 °C (t_f = 3.47h). 232

A.425. Fracture surface of the N610/$LaPO_4$/Al_2O_3-$LaPO_4$-AlOCl specimen with 8ply HSW subjected to creep test at 32 MPa in steam at 1100 °C (t_f = 3.47h). 232

A.426. Fracture surface of the N610/$LaPO_4$/Al_2O_3-$LaPO_4$-AlOCl specimen with 8ply HSW subjected to creep test at 32 MPa in steam at 1100 °C (t_f = 3.47h). 233

A.427. Fracture surface of the N610/$LaPO_4$/Al_2O_3-$LaPO_4$-AlOCl specimen with 8ply HSW subjected to creep test at 32 MPa in steam at 1100 °C (t_f = 3.47h). 233

A.428. Fracture surface of the N610/$LaPO_4$/Al_2O_3-$LaPO_4$-AlOCl specimen with 8ply HSW subjected to creep test at 32 MPa in steam at 1100 °C (t_f = 3.47h). 233

A.429. Fracture surface of the N610/$LaPO_4$/Al_2O_3-$LaPO_4$-AlOCl specimen with 8ply HSW subjected to creep test at 32 MPa in steam at 1100 °C (t_f = 3.47h). 234

A.430. Fracture surface of the N610/$LaPO_4$/Al_2O_3-$LaPO_4$-AlOCl specimen with 8ply HSW subjected to creep test at 32 MPa in steam at 1100 °C (t_f = 3.47h). 234

A.431. Fracture surface of the N610/$LaPO_4$/Al_2O_3-$LaPO_4$-AlOCl specimen with 8ply HSW subjected to creep test at 32 MPa in steam at 1100 °C (t_f = 3.47h). 234

A.432. Fracture surface of the N610/$LaPO_4$/Al_2O_3-$LaPO_4$-AlOCl specimen with 8ply HSW subjected to creep test at 32 MPa in steam at 1100 °C (t_f = 3.47h). 235

A.433. Fracture surface of the N610/$LaPO_4$/Al_2O_3-$LaPO_4$-AlOCl specimen with 8ply HSW subjected to creep test at 32 MPa in steam at 1100 °C (t_f = 3.47h). 235

A.434. Fracture surface of the N610/$LaPO_4$/Al_2O_3-$LaPO_4$-AlOCl specimen with 8ply HSW subjected to creep test at 32 MPa in steam at 1100 °C (t_f = 3.47h). 235

A.435. Fracture surface of the N610/$LaPO_4$/Al_2O_3-$LaPO_4$-AlOCl specimen with 8ply HSW subjected to creep test at 32 MPa in steam at 1100 °C (t_f = 3.47h). 236

A.436. Fracture surface of the N610/$LaPO_4$/Al_2O_3-$LaPO_4$-AlOCl specimen with 8ply HSW subjected to creep test at 32 MPa in steam at 1100 °C (t_f = 3.47h). 236

A.437. Fracture surface of the N610/$LaPO_4$/Al_2O_3-$LaPO_4$-AlOCl specimen with 8ply HSW subjected to creep test at 32 MPa in steam at 1100 °C (t_f = 3.47h). 236

A.438. Fracture surface of the N610/$LaPO_4$/Al_2O_3-$LaPO_4$-AlOCl specimen with 8ply HSW subjected to creep test at 32 MPa in steam at 1100 °C (t_f = 3.47h). 237

A.439. Fracture surface of the N610/$LaPO_4$/Al_2O_3-$LaPO_4$-AlOCl specimen with 8ply HSW subjected to creep test at 32 MPa in steam at 1100 °C (t_f = 3.47h). 237

A.440. Fracture surface of the N610/$LaPO_4$/Al_2O_3-$LaPO_4$-AlOCl specimen with 8ply HSW subjected to creep test at 32 MPa in steam at 1100 °C (t_f = 3.47h). 237

A.441. Fracture surface of the N610/$LaPO_4$/Al_2O_3-$LaPO_4$-AlOCl specimen with 8ply HSW subjected to creep test at 32 MPa in steam at 1100 °C (t_f = 3.47h). 238

A.442. Fracture surface of the N610/$LaPO_4$/Al_2O_3-$LaPO_4$-AlOCl specimen with 8ply HSW subjected to creep test at 32 MPa in steam at 1100 °C (t_f = 3.47h). 238

A.443. Fracture surface of the N610/$LaPO_4$/Al_2O_3-$LaPO_4$-AlOCl specimen with 8ply HSW subjected to creep test at 48 MPa in steam at 1100 °C (t_f = 2.06h). 238

A.444. Fracture surface of the N610/$LaPO_4$/Al_2O_3-$LaPO_4$-AlOCl specimen with 8ply HSW subjected to creep test at 48 MPa in steam at 1100 °C (t_f = 2.06h). 239

A.445. Fracture surface of the N610/$LaPO_4$/Al_2O_3-$LaPO_4$-AlOCl specimen with 8ply HSW subjected to creep test at 48 MPa in steam at 1100 °C (t_f = 2.06h). 239

A.446. Fracture surface of the N610/$LaPO_4$/Al_2O_3-$LaPO_4$-AlOCl specimen with 8ply HSW subjected to creep test at 48 MPa in steam at 1100 °C (t_f = 2.06h). 239

A.447. Fracture surface of the N610/$LaPO_4$/Al_2O_3-$LaPO_4$-AlOCl specimen with 8ply HSW subjected to creep test at 48 MPa in steam at 1100 °C (t_f = 2.06h). 240

A.448. Fracture surface of the N610/$LaPO_4$/Al_2O_3-$LaPO_4$-AlOCl specimen with 8ply HSW subjected to creep test at 48 MPa in steam at 1100 °C (t_f = 2.06h). 240

A.449. Fracture surface of the N610/$LaPO_4$/Al_2O_3-$LaPO_4$-AlOCl specimen with 8ply HSW subjected to creep test at 48 MPa in steam at 1100 °C (t_f = 2.06h). 240

A.450. Fracture surface of the N610/$LaPO_4$/Al_2O_3-$LaPO_4$-AlOCl specimen with 8ply HSW subjected to creep test at 48 MPa in steam at 1100 °C (t_f = 2.06h). 241

A.451. Fracture surface of the N610/$LaPO_4$/Al_2O_3-$LaPO_4$-AlOCl specimen with 8ply HSW subjected to creep test at 48 MPa in steam at 1100 °C (t_f = 2.06h). 241

A.452. Fracture surface of the N610/$LaPO_4$/Al_2O_3-$LaPO_4$-AlOCl specimen with 8ply HSW subjected to creep test at 48 MPa in steam at 1100 °C (t_f = 2.06h). 241

A.453. Fracture surface of the N610/$LaPO_4$/Al_2O_3-$LaPO_4$-AlOCl specimen with 8ply HSW subjected to creep test at 48 MPa in steam at 1100 °C (t_f = 2.06h). 242

A.454. Fracture surface of the N610/$LaPO_4$/Al_2O_3-$LaPO_4$-AlOCl specimen with 8ply HSW subjected to creep test at 48 MPa in steam at 1100 °C (t_f = 2.06h). 242

A.455. Fracture surface of the N610/$LaPO_4$/Al_2O_3-$LaPO_4$-AlOCl specimen with 8ply HSW subjected to creep test at 48 MPa in steam at 1100 °C (t_f = 2.06h). 242

A.456. Fracture surface of the N610/$LaPO_4$/Al_2O_3-$LaPO_4$-AlOCl specimen with 8ply HSW subjected to creep test at 48 MPa in steam at 1100 °C (t_f = 2.06h). 243

A.457. Fracture surface of the N610/$LaPO_4$/Al_2O_3-$LaPO_4$-AlOCl specimen with 8ply HSW subjected to creep test at 48 MPa in steam at 1100 °C (t_f = 2.06h). 243

A.458. Fracture surface of the N610/$LaPO_4$/Al_2O_3-$LaPO_4$-AlOCl specimen with 8ply HSW subjected to creep test at 48 MPa in steam at 1100 °C (t_f = 2.06h). 243

A.459. Fracture surface of the N610/$LaPO_4$/Al_2O_3-$LaPO_4$-AlOCl specimen with 8ply HSW subjected to creep test at 48 MPa in steam at 1100 °C (t_f = 2.06h). 244

A.460. Fracture surface of the N610/$LaPO_4$/Al_2O_3-$LaPO_4$-AlOCl specimen with 8ply HSW subjected to creep test at 48 MPa in steam at 1100 °C (t_f = 2.06h). 244

A.461. Fracture surface of the N610/$LaPO_4$/Al_2O_3-$LaPO_4$-AlOCl specimen with 8ply HSW subjected to creep test at 48 MPa in steam at 1100 °C (t_f = 2.06h). 244

A.462. Fracture surface of the N610/$LaPO_4$/Al_2O_3-$LaPO_4$-AlOCl specimen with 8ply HSW subjected to creep test at 48 MPa in steam at 1100 °C (t_f = 2.06h). 245

A.463. Fracture surface of the N610/$LaPO_4$/Al_2O_3-$LaPO_4$-AlOCl specimen with 8ply HSW subjected to creep test at 48 MPa in steam at 1100 °C (t_f = 2.06h). 245

B.1. Side view of the virgin N610/Al_2O_3-$LaPO_4$ specimen with 10ply 0°/90° uni-tape lay-up. 246

B.2. Side view of the virgin N610/Al_2O_3-$LaPO_4$ specimen with 10ply 0°/90° uni-tape lay-up. 246

B.3. Side view of the virgin N610/Al_2O_3-$LaPO_4$ specimen with 10ply 0°/90° uni-tape lay-up. 247

B.4. Side view of the virgin N610/Al_2O_3-$LaPO_4$ specimen with 10ply 0°/90° uni-tape lay-up. 247

B.5. Fracture surface of the N610/Al_2O_3-$LaPO_4$ specimen with 10ply 0°/90° uni-tape lay-up subjected tension to failure in laboratory air at 1100 °C. 247

Figure Page

B.6. Fracture surface of the N610/Al_2O_3-$LaPO_4$ specimen with 10ply 0°/90° uni-tape lay-up subjected tension to failure in laboratory air at 1100 °C. 248

B.7. Fracture surface of the N610/Al_2O_3-$LaPO_4$ specimen with 10ply 0°/90° uni-tape lay-up subjected tension to failure in laboratory air at 1100 °C. 248

B.8. Fracture surface of the N610/Al_2O_3-$LaPO_4$ specimen with 10ply 0°/90° uni-tape lay-up subjected tension to failure in laboratory air at 1100 °C. 248

B.9. Fracture surface of the N610/Al_2O_3-$LaPO_4$ specimen with 10ply 0°/90° uni-tape lay-up subjected tension to failure in laboratory air at 1100 °C. 249

B.10. Fracture surface of the N610/Al_2O_3-$LaPO_4$ specimen with 10ply 0°/90° uni-tape lay-up subjected tension to failure in laboratory air at 1100 °C. 249

B.11. Fracture surface of the N610/Al_2O_3-$LaPO_4$ specimen with 10ply 0°/90° uni-tape lay-up subjected tension to failure in laboratory air at 1100 °C. 249

B.12. Fracture surface of the N610/Al_2O_3-$LaPO_4$ specimen with 10ply 0°/90° uni-tape lay-up subjected tension to failure in laboratory air at 1100 °C. 250

B.13. Fracture surface of the N610/Al_2O_3-$LaPO_4$ specimen with 10ply 0°/90° uni-tape lay-up subjected to creep test at 32 MPa in steam at 1100 °C (t_f = 3.45 h). 250

B.14. Fracture surface of the N610/Al_2O_3-$LaPO_4$ specimen with 10ply 0°/90° uni-tape lay-up subjected to creep test at 32 MPa in steam at 1100 °C (t_f = 3.45 h). 250

B.15. Fracture surface of the N610/Al_2O_3-$LaPO_4$ specimen with 10ply 0°/90° uni-tape lay-up subjected to creep test at 32 MPa in steam at 1100 °C (t_f = 3.45 h). 251

B.16. Fracture surface of the N610/Al_2O_3-$LaPO_4$ specimen with 10ply 0°/90° uni-tape lay-up subjected to creep test at 32 MPa in steam at 1100 °C (t_f = 3.45 h). 251

B.17. Fracture surface of the N610/Al_2O_3-$LaPO_4$ specimen with 10ply 0°/90° uni-tape lay-up subjected to creep test at 32 MPa in steam at 1100 °C (t_f = 3.45 h). 252

B.18. Fracture surface of the N610/Al_2O_3-$LaPO_4$ specimen with 10ply 0°/90° uni-tape lay-up subjected to creep test at 32 MPa in steam at 1100 °C (t_f = 3.45 h). 252

B.19. Side view of the virgin N610/$LaPO_4$/Al_2O_3-$LaPO_4$ specimen with 10ply 0°/90° uni-tape lay-up. 252

B.20. Side view of the virgin N610/$LaPO_4$/Al_2O_3-$LaPO_4$ specimen with 10ply 0°/90° uni-tape lay-up. 253

B.21. Side view of the virgin N610/$LaPO_4$/Al_2O_3-$LaPO_4$ specimen with 10ply 0°/90° uni-tape lay-up. 253

B.22. Side view of the virgin N610/$LaPO_4$/Al_2O_3-$LaPO_4$ specimen with 10ply 0°/90° uni-tape lay-up. 253

B.23. Side view of the virgin N610/$LaPO_4$/Al_2O_3-$LaPO_4$ specimen with 10ply 0°/90° uni-tape lay-up. 254

B.24. Side view of the virgin N610/$LaPO_4$/Al_2O_3-$LaPO_4$ specimen with 10ply 0°/90° uni-tape lay-up. 254

B.25. Fracture surface of the N610/$LaPO_4$/Al_2O_3-$LaPO_4$ specimen with 10ply 0°/90° uni-tape lay-up subjected tension to failure in laboratory air at 1100 °C. 254

B.26. Fracture surface of the N610/$LaPO_4$/Al_2O_3-$LaPO_4$ specimen with 10ply 0°/90° uni-tape lay-up subjected tension to failure in laboratory air at 1100 °C. 255

B.27. Fracture surface of the N610/$LaPO_4$/Al_2O_3-$LaPO_4$ specimen with 10ply 0°/90° uni-tape lay-up subjected tension to failure in laboratory air at 1100 °C. 255

B.28. Fracture surface of the N610/$LaPO_4$/Al_2O_3-$LaPO_4$ specimen with 10ply 0°/90° uni-tape lay-up subjected tension to failure in laboratory air at 1100 °C. 255

B.29. Fracture surface of the N610/$LaPO_4$/Al_2O_3-$LaPO_4$ specimen with 10ply 0°/90° uni-tape lay-up subjected tension to failure in laboratory air at 1100 °C. 256

Figure Page

B.30. Fracture surface of the N610/$LaPO_4$/Al_2O_3-$LaPO_4$ specimen with 10ply 0°/90° uni-tape lay-up subjected tension to failure in laboratory air at 1100 °C. 256

B.31. Fracture surface of the N610/$LaPO_4$/Al_2O_3-$LaPO_4$ specimen with 10ply 0°/90° uni-tape lay-up subjected tension to failure in laboratory air at 1100 °C. 256

B.32. Fracture surface of the N610/$LaPO_4$/Al_2O_3-$LaPO_4$ specimen with 10ply 0°/90° uni-tape lay-up subjected tension to failure in laboratory air at 1100 °C. 257

B.33. Fracture surface of the N610/$LaPO_4$/Al_2O_3-$LaPO_4$ specimen with 10ply 0°/90° uni-tape lay-up subjected tension to failure in laboratory air at 1100 °C. 257

B.34. Fracture surface of the N610/$LaPO_4$/Al_2O_3-$LaPO_4$ specimen with 10ply 0°/90° uni-tape lay-up subjected tension to failure in laboratory air at 1100 °C. 257

B.35. Fracture surface of the N610/$LaPO_4$/Al_2O_3-$LaPO_4$ specimen with 10ply 0°/90° uni-tape lay-up subjected tension to failure in laboratory air at 1100 °C. 258

B.36. Fracture surface of the N610/$LaPO_4$/Al_2O_3-$LaPO_4$ specimen with 10ply 0°/90° uni-tape lay-up subjected tension to failure in laboratory air at 1100 °C. 258

B.37. Fracture surface of the N610/$LaPO_4$/Al_2O_3-$LaPO_4$ specimen with 10ply 0°/90° uni-tape lay-up subjected tension to failure in laboratory air at 1100 °C. 258

B.38. Fracture surface of the N610/$LaPO_4$/Al_2O_3-$LaPO_4$ specimen with 10ply 0°/90° uni-tape lay-up subjected tension to failure in laboratory air at 1100 °C. 259

B.39. Fracture surface of the N610/Al_2O_3-$LaPO_4$ specimen with 10ply 0°/90° uni-tape lay-up subjected to creep test at 25 MPa in steam at 1100 °C (t_f = 40.1 h). 259

B.40. Fracture surface of the N610/Al_2O_3-$LaPO_4$ specimen with 10ply 0°/90° uni-tape lay-up subjected to creep test at 25 MPa in steam at 1100 °C (t_f = 40.1 h). 259

Figure Page

B.41. Fracture surface of the N610/Al_2O_3-$LaPO_4$ specimen with 10ply 0°/90° uni-tape lay-up subjected to creep test at 25 MPa in steam at 1100 °C (t_f = 40.1 h). 260

B.42. Fracture surface of the N610/Al_2O_3-$LaPO_4$ specimen with 10ply 0°/90° uni-tape lay-up subjected to creep test at 25 MPa in steam at 1100 °C (t_f = 40.1 h). 260

B.43. Fracture surface of the N610/Al_2O_3-$LaPO_4$ specimen with 10ply 0°/90° uni-tape lay-up subjected to creep test at 25 MPa in steam at 1100 °C (t_f = 40.1 h). 261

B.44. Fracture surface of the N610/Al_2O_3-$LaPO_4$ specimen with 10ply 0°/90° uni-tape lay-up subjected to creep test at 25 MPa in steam at 1100 °C (t_f = 40.1 h). 261

B.45. Side view of the virgin N610/$LaPO_4$/Al_2O_3 specimen with 10ply 0°/90° uni-tape lay-up. 261

B.46. Side view of the virgin N610/$LaPO_4$/Al_2O_3 specimen with 10ply 0°/90° uni-tape lay-up. 262

B.47. Side view of the virgin N610/$LaPO_4$/Al_2O_3 specimen with 10ply 0°/90° uni-tape lay-up. 262

B.48. Side view of the virgin N610/$LaPO_4$/Al_2O_3 specimen with 10ply 0°/90° uni-tape lay-up. 262

B.49. Side view of the virgin N610/$LaPO_4$/Al_2O_3 specimen with 10ply 0°/90° uni-tape lay-up. 263

B.50. Side view of the virgin N610/$LaPO_4$/Al_2O_3 specimen with 10ply 0°/90° uni-tape lay-up. 264

B.51. Fracture surface of the N610/$LaPO_4$/Al_2O_3 specimen with 10ply 0°/90° uni-tape lay-up subjected tension to failure in laboratory air at 1100 °C. 264

B.52. Fracture surface of the N610/$LaPO_4$/Al_2O_3 specimen with 10ply 0°/90° uni-tape lay-up subjected tension to failure in laboratory air at 1100 °C. 264

B.53. Fracture surface of the N610/$LaPO_4$/Al_2O_3 specimen with 10ply 0°/90° uni-tape lay-up subjected tension to failure in laboratory air at 1100 °C. 265

Figure Page

B.54. Fracture surface of the N610/$LaPO_4$/Al_2O_3 specimen with 10ply 0°/90° uni-tape lay-up subjected tension to failure in laboratory air at 1100 °C. 265

B.55. Fracture surface of the N610/$LaPO_4$/Al_2O_3 specimen with 10ply 0°/90° uni-tape lay-up subjected tension to failure in laboratory air at 1100 °C. 265

B.56. Fracture surface of the N610/$LaPO_4$/Al_2O_3 specimen with 10ply 0°/90° uni-tape lay-up subjected tension to failure in laboratory air at 1100 °C. 266

B.57. Fracture surface of the N610/$LaPO_4$/Al_2O_3 specimen with 10ply 0°/90° uni-tape lay-up subjected tension to failure in laboratory air at 1100 °C. 266

B.58. Fracture surface of the N610/$LaPO_4$/Al_2O_3 specimen with 10ply 0°/90° uni-tape lay-up subjected tension to failure in laboratory air at 1100 °C. 266

B.59. Fracture surface of the N610/$LaPO_4$/Al_2O_3 specimen with 10ply 0°/90° uni-tape lay-up subjected to creep test at 85 MPa in air at 1100 °C (t_f = 16.2 h). 267

B.60. Fracture surface of the N610/$LaPO_4$/Al_2O_3 specimen with 10ply 0°/90° uni-tape lay-up subjected to creep test at 85 MPa in air at 1100 °C (t_f = 16.2 h). 267

B.61. Fracture surface of the N610/$LaPO_4$/Al_2O_3 specimen with 10ply 0°/90° uni-tape lay-up subjected to creep test at 85 MPa in air at 1100 °C (t_f = 16.2 h). 268

B.62. Fracture surface of the N610/$LaPO_4$/Al_2O_3 specimen with 10ply 0°/90° uni-tape lay-up subjected to creep test at 85 MPa in air at 1100 °C (t_f = 16.2 h). 269

B.63. Fracture surface of the N610/$LaPO_4$/Al_2O_3 specimen with 10ply 0°/90° uni-tape lay-up subjected to creep test at 85 MPa in air at 1100 °C (t_f = 16.2 h). 269

B.64. Fracture surface of the N610/$LaPO_4$/Al_2O_3 specimen with 10ply 0°/90° uni-tape lay-up subjected to creep test at 85 MPa in air at 1100 °C (t_f = 16.2 h). 270

B.65. Fracture surface of the N610/$LaPO_4$/Al_2O_3 specimen with 10ply 0°/90° uni-tape lay-up subjected to creep test at 85 MPa in steam at 1100 °C (t_f = 8.18 h). 270

B.66. Fracture surface of the N610/$LaPO_4$/Al_2O_3 specimen with 10ply 0°/90° uni-tape lay-up subjected to creep test at 85 MPa in steam at 1100 °C (t_f = 8.18 h). 271

B.67. Fracture surface of the N610/$LaPO_4$/Al_2O_3 specimen with 10ply 0°/90° uni-tape lay-up subjected to creep test at 85 MPa in steam at 1100 °C (t_f = 8.18 h). 271

B.68. Fracture surface of the N610/$LaPO_4$/Al_2O_3 specimen with 10ply 0°/90° uni-tape lay-up subjected to creep test at 85 MPa in steam at 1100 °C (t_f = 8.18 h). 272

B.69. Fracture surface of the N610/$LaPO_4$/Al_2O_3 specimen with 10ply 0°/90° uni-tape lay-up subjected to creep test at 85 MPa in steam at 1100 °C (t_f = 8.18 h). 272

B.70. Fracture surface of the N610/$LaPO_4$/Al_2O_3 specimen with 10ply 0°/90° uni-tape lay-up subjected to creep test at 85 MPa in steam at 1100 °C (t_f = 8.18 h). 273

B.71. Fracture surface of the N610/$LaPO_4$/Al_2O_3 specimen with 10ply 0°/90° uni-tape lay-up subjected to creep test at 110 MPa in steam at 1100 °C (t_f = 0.35 h). 273

B.72. Fracture surface of the N610/$LaPO_4$/Al_2O_3 specimen with 10ply 0°/90° uni-tape lay-up subjected to creep test at 110 MPa in steam at 1100 °C (t_f = 0.35 h). 274

B.73. Fracture surface of the N610/$LaPO_4$/Al_2O_3 specimen with 10ply 0°/90° uni-tape lay-up subjected to creep test at 110 MPa in steam at 1100 °C (t_f = 0.35 h). 274

B.74. Fracture surface of the N610/$LaPO_4$/Al_2O_3 specimen with 10ply 0°/90° uni-tape lay-up subjected to creep test at 110 MPa in steam at 1100 °C (t_f = 0.35 h). 275

B.75. Fracture surface of the N610/$LaPO_4$/Al_2O_3 specimen with 10ply 0°/90° uni-tape lay-up subjected to creep test at 110 MPa in steam at 1100 °C (t_f = 0.35 h). 275

B.76. Fracture surface of the N610/$LaPO_4$/Al_2O_3 specimen with 10ply 0°/90° uni-tape lay-up subjected to creep test at 110 MPa in steam at 1100 °C (t_f = 0.35 h). 276

B.77. Fracture surface of the N610/$LaPO_4$/Al_2O_3 specimen with 10ply 0°/90° uni-tape lay-up subjected to creep test at 110 MPa in steam at 1100 °C (t_f = 0.35 h). 276

B.78. Fracture surface of the N610/$LaPO_4$/Al_2O_3 specimen with 10ply 0°/90° uni-tape lay-up subjected to creep test at 110 MPa in steam at 1100 °C (t_f = 0.35 h). 277

B.79. Fracture surface of the N610/$LaPO_4$/Al_2O_3 specimen with 10ply 0°/90° uni-tape lay-up subjected to creep test at 110 MPa in steam at 1100 °C (t_f = 0.35 h). 277

B.80. Fracture surface of the N610/$LaPO_4$/Al_2O_3 specimen with 10ply 0°/90° uni-tape lay-up subjected to creep test at 110 MPa in steam at 1100 °C (t_f = 0.35 h). 278

B.81. Fracture surface of the N610/$LaPO_4$/Al_2O_3 specimen with 10ply 0°/90° uni-tape lay-up subjected to creep test at 110 MPa in steam at 1100 °C (t_f = 0.35 h). 278

B.82. Fracture surface of the N610/$LaPO_4$/Al_2O_3 specimen with 10ply 0°/90° uni-tape lay-up subjected to creep test at 110 MPa in steam at 1100 °C (t_f = 0.35 h). 279

B.83. Fracture surface of the N610/$LaPO_4$/Al_2O_3 specimen with 10ply 0°/90° uni-tape lay-up subjected to creep test at 120 MPa in air at 1100 °C (t_f = 0.74 h). 279

B.84. Fracture surface of the N610/$LaPO_4$/Al_2O_3 specimen with 10ply 0°/90° uni-tape lay-up subjected to creep test at 120 MPa in air at 1100 °C (t_f = 0.74 h). 280

B.85. Fracture surface of the N610/$LaPO_4$/Al_2O_3 specimen with 10ply 0°/90° uni-tape lay-up subjected to creep test at 120 MPa in air at 1100 °C (t_f = 0.74 h). 280

B.86. Fracture surface of the N610/$LaPO_4$/Al_2O_3 specimen with 10ply 0°/90° uni-tape lay-up subjected to creep test at 120 MPa in air at 1100 °C (t_f = 0.74 h). 281

Figure Page

B.87. Fracture surface of the N610/$LaPO_4$/Al_2O_3 specimen with 10ply 0°/90° uni-tape lay-up subjected to creep test at 120 MPa in air at 1100 °C (t_f = 0.74 h). 281

B.88. Fracture surface of the N610/$LaPO_4$/Al_2O_3 specimen with 10ply 0°/90° uni-tape lay-up subjected to creep test at 120 MPa in air at 1100 °C (t_f = 0.74 h). 282

B.89. Fracture surface of the N610/$LaPO_4$/Al_2O_3 specimen with 10ply 0°/90° uni-tape lay-up subjected to creep test at 120 MPa in air at 1100 °C (t_f = 0.74 h). 282

B.90. Fracture surface of the N610/$LaPO_4$/Al_2O_3 specimen with 10ply 0°/90° uni-tape lay-up subjected to creep test at 120 MPa in air at 1100 °C (t_f = 0.74 h). 283

B.91. Fracture surface of the N610/$LaPO_4$/Al_2O_3 specimen with 10ply 0°/90° uni-tape lay-up subjected to creep test at 120 MPa in steam at 1100 °C (t_f = 0.03 h). 283

B.92. Fracture surface of the N610/$LaPO_4$/Al_2O_3 specimen with 10ply 0°/90° uni-tape lay-up subjected to creep test at 120 MPa in steam at 1100 °C (t_f = 0.03 h). 284

B.93. Fracture surface of the N610/$LaPO_4$/Al_2O_3 specimen with 10ply 0°/90° uni-tape lay-up subjected to creep test at 120 MPa in steam at 1100 °C (t_f = 0.03 h). 284

B.94. Fracture surface of the N610/$LaPO_4$/Al_2O_3 specimen with 10ply 0°/90° uni-tape lay-up subjected to creep test at 120 MPa in steam at 1100 °C (t_f = 0.03 h). 285

B.95. Fracture surface of the N610/$LaPO_4$/Al_2O_3 specimen with 10ply 0°/90° uni-tape lay-up subjected to creep test at 120 MPa in steam at 1100 °C (t_f = 0.03 h). 285

B.96. Fracture surface of the N610/$LaPO_4$/Al_2O_3 specimen with 10ply 0°/90° uni-tape lay-up subjected to creep test at 120 MPa in steam at 1100 °C (t_f = 0.03 h). 286

B.97. Fracture surface of the N610/$LaPO_4$/Al_2O_3 specimen with 8ply HSW subjected tension to failure in laboratory air at 1100 °C. 286

Figure Page

B.98. Fracture surface of the N610/$LaPO_4$/Al_2O_3 specimen with 8ply HSW subjected tension to failure in laboratory air at 1100 °C. 287

B.99. Fracture surface of the N610/$LaPO_4$/Al_2O_3 specimen with 8ply HSW subjected tension to failure in laboratory air at 1100 °C. 287

B.100. Fracture surface of the N610/$LaPO_4$/Al_2O_3 specimen with 8ply HSW subjected tension to failure in laboratory air at 1100 °C. 287

B.101. Fracture surface of the N610/$LaPO_4$/Al_2O_3 specimen with 8ply HSW subjected tension to failure in laboratory air at 1100 °C. 288

B.102. Fracture surface of the N610/$LaPO_4$/Al_2O_3 specimen with 8ply HSW subjected tension to failure in laboratory air at 1100 °C. 288

B.103. Fracture surface of the N610/$LaPO_4$/Al_2O_3 specimen with 8ply HSW subjected tension to failure in laboratory air at 1100 °C. 288

B.104. Fracture surface of the N610/$LaPO_4$/Al_2O_3 specimen with 8ply HSW subjected tension to failure in laboratory air at 1100 °C. 289

B.105. Fracture surface of the N610/$LaPO_4$/Al_2O_3 specimen with 8ply HSW subjected tension to failure in laboratory air at 1100 °C. 289

B.106. Fracture surface of the N610/$LaPO_4$/Al_2O_3 specimen with 8ply HSW subjected tension to failure in laboratory air at 1100 °C. 289

B.107. Fracture surface of the N610/$LaPO_4$/Al_2O_3 specimen with 8ply HSW subjected tension to failure in laboratory air at 1100 °C. 290

B.108. Fracture surface of the N610/$LaPO_4$/Al_2O_3 specimen with 8ply HSW subjected tension to failure in laboratory air at 1100 °C. 290

B.109. Fracture surface of the N610/$LaPO_4$/Al_2O_3 specimen with 8ply HSW subjected tension to failure in laboratory air at 1100 °C. 290

B.110. Fracture surface of the N610/$LaPO_4$/Al_2O_3 specimen with 8ply HSW subjected tension to failure in laboratory air at 1100 °C. 291

B.111. Fracture surface of the N610/$LaPO_4$/Al_2O_3 specimen with 8ply HSW subjected tension to failure in laboratory air at 1100 °C. 291

B.112. Fracture surface of the N610/$LaPO_4$/Al_2O_3 specimen with 8ply HSW subjected subjected to creep test at 32 MPa in air at 1100 °C ($t_f > 100$ h). 291

B.113. Fracture surface of the N610/$LaPO_4$/Al_2O_3 specimen with 8ply HSW subjected subjected to creep test at 32 MPa in air at 1100 °C ($t_f > 100$ h). 292

B.114. Fracture surface of the N610/$LaPO_4$/Al_2O_3 specimen with 8ply HSW subjected subjected to creep test at 32 MPa in air at 1100 °C ($t_f > 100$ h). 292

B.115. Fracture surface of the N610/$LaPO_4$/Al_2O_3 specimen with 8ply HSW subjected subjected to creep test at 32 MPa in air at 1100 °C ($t_f > 100$ h). 292

B.116. Fracture surface of the N610/$LaPO_4$/Al_2O_3 specimen with 8ply HSW subjected subjected to creep test at 32 MPa in air at 1100 °C ($t_f > 100$ h). 293

B.117. Fracture surface of the N610/$LaPO_4$/Al_2O_3 specimen with 8ply HSW subjected subjected to creep test at 32 MPa in air at 1100 °C ($t_f > 100$ h). 293

B.118. Fracture surface of the N610/$LaPO_4$/Al_2O_3 specimen with 8ply HSW subjected subjected to creep test at 32 MPa in steam at 1100 °C ($t_f = 51.9$ h). 293

B.119. Fracture surface of the N610/$LaPO_4$/Al_2O_3 specimen with 8ply HSW subjected subjected to creep test at 32 MPa in steam at 1100 °C ($t_f = 51.9$ h). 294

B.120. Fracture surface of the N610/$LaPO_4$/Al_2O_3 specimen with 8ply HSW subjected subjected to creep test at 32 MPa in steam at 1100 °C ($t_f = 51.9$ h). 294

B.121. Fracture surface of the N610/$LaPO_4$/Al_2O_3 specimen with 8ply HSW subjected subjected to creep test at 32 MPa in steam at 1100 °C ($t_f = 51.9$ h). 294

B.122. Fracture surface of the N610/$LaPO_4$/Al_2O_3 specimen with 8ply HSW subjected subjected to creep test at 32 MPa in steam at 1100 °C ($t_f = 51.9$ h). 295

B.123. Fracture surface of the N610/$LaPO_4$/Al_2O_3 specimen with 8ply HSW subjected subjected to creep test at 64 MPa in air at 1100 °C ($t_f > 100$ h). 295

Figure Page

B.124. Fracture surface of the N610/$LaPO_4$/Al_2O_3 specimen with 8ply HSW subjected subjected to creep test at 64 MPa in air at 1100 °C ($t_f > 100$ h). 295

B.125. Fracture surface of the N610/$LaPO_4$/Al_2O_3 specimen with 8ply HSW subjected subjected to creep test at 64 MPa in air at 1100 °C ($t_f > 100$ h). 296

B.126. Fracture surface of the N610/$LaPO_4$/Al_2O_3 specimen with 8ply HSW subjected subjected to creep test at 64 MPa in air at 1100 °C ($t_f > 100$ h). 296

B.127. Fracture surface of the N610/$LaPO_4$/Al_2O_3 specimen with 8ply HSW subjected subjected to creep test at 64 MPa in air at 1100 °C ($t_f > 100$ h). 296

B.128. Fracture surface of the N610/$LaPO_4$/Al_2O_3 specimen with 8ply HSW subjected subjected to creep test at 64 MPa in air at 1100 °C ($t_f > 100$ h). 297

B.129. Fracture surface of the N610/$LaPO_4$/Al_2O_3 specimen with 8ply HSW subjected subjected to creep test at 64 MPa in air at 1100 °C ($t_f > 100$ h). 297

B.130. Fracture surface of the N610/$LaPO_4$/Al_2O_3 specimen with 8ply HSW subjected subjected to creep test at 64 MPa in air at 1100 °C ($t_f > 100$ h). 297

B.131. Fracture surface of the N610/$LaPO_4$/Al_2O_3 specimen with 8ply HSW subjected subjected to creep test at 48 MPa in steam at 1100 °C ($t_f = 7.58$ h). 298

B.132. Fracture surface of the N610/$LaPO_4$/Al_2O_3 specimen with 8ply HSW subjected subjected to creep test at 48 MPa in steam at 1100 °C ($t_f = 7.58$ h). 298

B.133. Fracture surface of the N610/$LaPO_4$/Al_2O_3 specimen with 8ply HSW subjected subjected to creep test at 48 MPa in steam at 1100 °C ($t_f = 7.58$ h). 298

B.134. Fracture surface of the N610/$LaPO_4$/Al_2O_3 specimen with 8ply HSW subjected subjected to creep test at 48 MPa in steam at 1100 °C ($t_f = 7.58$ h). 299

B.135. Fracture surface of the N610/$LaPO_4$/Al_2O_3 specimen with 8ply HSW subjected subjected to creep test at 48 MPa in steam at 1100 °C (t_f = 7.58 h). 299

B.136. Fracture surface of the N610/$LaPO_4$/Al_2O_3 specimen with 8ply HSW subjected subjected to creep test at 48 MPa in steam at 1100 °C (t_f = 7.58 h). 299

B.137. Fracture surface of the N610/$LaPO_4$/Al_2O_3 specimen with 8ply HSW subjected subjected to creep test at 48 MPa in steam at 1100 °C (t_f = 7.58 h). 300

B.138. Fracture surface of the N610/$LaPO_4$/Al_2O_3 specimen with 8ply HSW subjected subjected to creep test at 48 MPa in steam at 1100 °C (t_f = 7.58 h). 300

B.139. Fracture surface of the N610/$LaPO_4$/Al_2O_3 specimen with 8ply HSW subjected subjected to creep test at 64 MPa in steam at 1100 °C (t_f = 2.38 h). 300

B.140. Fracture surface of the N610/$LaPO_4$/Al_2O_3 specimen with 8ply HSW subjected subjected to creep test at 64 MPa in steam at 1100 °C (t_f = 2.38 h). 301

B.141. Fracture surface of the N610/$LaPO_4$/Al_2O_3 specimen with 8ply HSW subjected subjected to creep test at 64 MPa in steam at 1100 °C (t_f = 2.38 h). 301

B.142. Fracture surface of the N610/$LaPO_4$/Al_2O_3 specimen with 8ply HSW subjected subjected to creep test at 64 MPa in steam at 1100 °C (t_f = 2.38 h). 301

B.143. Fracture surface of the N610/$LaPO_4$/Al_2O_3 specimen with 8ply HSW subjected subjected to creep test at 64 MPa in steam at 1100 °C (t_f = 2.38 h). 302

B.144. Fracture surface of the N610/$LaPO_4$/Al_2O_3 specimen with 8ply HSW subjected subjected to creep test at 64 MPa in steam at 1100 °C (t_f = 2.38 h). 302

B.145. Fracture surface of the N610/$LaPO_4$/Al_2O_3 specimen with 8ply HSW subjected subjected to creep test at 64 MPa in steam at 1100 °C (t_f = 2.38 h). 302

B.146. Fracture surface of the N610/$LaPO_4$/Al_2O_3 specimen with 8ply HSW subjected subjected to creep test at 64 MPa in steam at 1100 °C (t_f = 2.38 h). 303

B.147. Fracture surface of the N610/$LaPO_4$/Al_2O_3 specimen with 8ply HSW subjected subjected to creep test at 72 MPa in air at 1100 °C (t_f > 100 h). 303

B.148. Fracture surface of the N610/$LaPO_4$/Al_2O_3 specimen with 8ply HSW subjected subjected to creep test at 72 MPa in air at 1100 °C (t_f > 100 h). 303

B.149. Fracture surface of the N610/$LaPO_4$/Al_2O_3 specimen with 8ply HSW subjected subjected to creep test at 72 MPa in air at 1100 °C (t_f > 100 h). 304

B.150. Fracture surface of the N610/$LaPO_4$/Al_2O_3 specimen with 8ply HSW subjected subjected to creep test at 72 MPa in air at 1100 °C (t_f > 100 h). 304

B.151. Fracture surface of the N610/$LaPO_4$/Al_2O_3 specimen with 8ply HSW subjected subjected to creep test at 72 MPa in air at 1100 °C (t_f > 100 h). 304

B.152. Fracture surface of the N610/$LaPO_4$/Al_2O_3 specimen with 8ply HSW subjected subjected to creep test at 72 MPa in air at 1100 °C (t_f > 100 h). 305

B.153. Fracture surface of the N610/$LaPO_4$/Al_2O_3 specimen with 8ply HSW subjected subjected to creep test at 72 MPa in steam at 1100 °C (t_f = 2.24 h). 305

B.154. Fracture surface of the N610/$LaPO_4$/Al_2O_3 specimen with 8ply HSW subjected subjected to creep test at 72 MPa in steam at 1100 °C (t_f = 2.24 h). 305

B.155. Fracture surface of the N610/$LaPO_4$/Al_2O_3 specimen with 8ply HSW subjected subjected to creep test at 72 MPa in steam at 1100 °C (t_f = 2.24 h). 306

B.156. Fracture surface of the N610/$LaPO_4$/Al_2O_3 specimen with 8ply HSW subjected subjected to creep test at 72 MPa in steam at 1100 °C (t_f = 2.24 h). 306

Figure Page

B.157. Fracture surface of the N610/$LaPO_4$/Al_2O_3 specimen with 8ply HSW subjected subjected to creep test at 72 MPa in steam at 1100 °C (t_f = 2.24 h). 306

B.158. Fracture surface of the N610/$LaPO_4$/Al_2O_3 specimen with 8ply HSW subjected subjected to creep test at 72 MPa in steam at 1100 °C (t_f = 2.24 h). 307

B.159. Fracture surface of the N610/Al_2O_3 specimen with 8ply HSW subjected tension to failure in laboratory air at 1100 °C. 307

B.160. Fracture surface of the N610/Al_2O_3 specimen with 8ply HSW subjected tension to failure in laboratory air at 1100 °C. 307

B.161. Fracture surface of the N610/Al_2O_3 specimen with 8ply HSW subjected tension to failure in laboratory air at 1100 °C. 308

B.162. Fracture surface of the N610/Al_2O_3 specimen with 8ply HSW subjected tension to failure in laboratory air at 1100 °C. 308

B.163. Fracture surface of the N610/Al_2O_3 specimen with 8ply HSW subjected tension to failure in laboratory air at 1100 °C. 308

B.164. Fracture surface of the N610/Al_2O_3 specimen with 8ply HSW subjected tension to failure in laboratory air at 1100 °C. 309

B.165. Fracture surface of the N610/Al_2O_3 specimen with 8ply HSW subjected tension to failure in laboratory air at 1100 °C. 309

B.166. Fracture surface of the N610/Al_2O_3 specimen with 8ply HSW subjected tension to failure in laboratory air at 1100 °C. 309

B.167. Fracture surface of the N610/Al_2O_3 specimen with 8ply HSW subjected tension to failure in laboratory air at 1100 °C. 310

B.168. Fracture surface of the N610/Al_2O_3 specimen with 8ply HSW subjected tension to failure in laboratory air at 1100 °C. 310

B.169. Fracture surface of the N610/Al_2O_3 specimen with 8ply HSW subjected tension to failure in laboratory air at 1100 °C. 310

B.170. Fracture surface of the N610/Al_2O_3 specimen with 8ply HSW subjected tension to failure in laboratory air at 1100 °C. 311

B.171. Fracture surface of the N610/$LaPO_4$/Al_2O_3 specimen with 8ply HSW subjected subjected to creep test at 20 MPa in steam at 1100 °C (t_f = 3.53 h). 311

B.172. Fracture surface of the N610/$LaPO_4$/Al_2O_3 specimen with 8ply HSW subjected subjected to creep test at 20 MPa in steam at 1100 °C (t_f = 3.53 h). 311

B.173. Fracture surface of the N610/$LaPO_4$/Al_2O_3 specimen with 8ply HSW subjected subjected to creep test at 20 MPa in steam at 1100 °C (t_f = 3.53 h). 312

B.174. Fracture surface of the N610/$LaPO_4$/Al_2O_3 specimen with 8ply HSW subjected subjected to creep test at 20 MPa in steam at 1100 °C (t_f = 3.53 h). 312

B.175. Fracture surface of the N610/$LaPO_4$/Al_2O_3 specimen with 8ply HSW subjected subjected to creep test at 20 MPa in steam at 1100 °C (t_f = 3.53 h). 312

B.176. Fracture surface of the N610/$LaPO_4$/Al_2O_3 specimen with 8ply HSW subjected subjected to creep test at 20 MPa in steam at 1100 °C (t_f = 3.53 h). 313

B.177. Fracture surface of the N610/$LaPO_4$/Al_2O_3 specimen with 8ply HSW subjected subjected to creep test at 20 MPa in steam at 1100 °C (t_f = 3.53 h). 313

B.178. Fracture surface of the N610/$LaPO_4$/Al_2O_3 specimen with 8ply HSW subjected subjected to creep test at 20 MPa in steam at 1100 °C (t_f = 3.53 h). 313

B.179. Fracture surface of the N610/$LaPO_4$/Al_2O_3 specimen with 8ply HSW subjected subjected to creep test at 30 MPa in steam at 1100 °C (t_f = 16.1 h). 314

B.180. Fracture surface of the N610/$LaPO_4$/Al_2O_3 specimen with 8ply HSW subjected subjected to creep test at 30 MPa in steam at 1100 °C (t_f = 16.1 h). 314

B.181. Fracture surface of the N610/$LaPO_4$/Al_2O_3 specimen with 8ply HSW subjected subjected to creep test at 30 MPa in steam at 1100 °C (t_f = 16.1 h). 314

B.182. Fracture surface of the N610/$LaPO_4$/Al_2O_3 specimen with 8ply HSW subjected subjected to creep test at 30 MPa in steam at 1100 °C (t_f = 16.1 h). 315

B.183. Fracture surface of the N610/$LaPO_4$/Al_2O_3 specimen with 8ply HSW subjected subjected to creep test at 30 MPa in steam at 1100 °C (t_f = 16.1 h). 315

B.184. Fracture surface of the N610/$LaPO_4$/Al_2O_3 specimen with 8ply HSW subjected subjected to creep test at 30 MPa in steam at 1100 °C (t_f = 16.1 h). 315

B.185. Fracture surface of the N610/$LaPO_4$/Al_2O_3 specimen with 8ply HSW subjected subjected to creep test at 40.5 MPa in air at 1100 °C (t_f = 3.34 h). 316

B.186. Fracture surface of the N610/$LaPO_4$/Al_2O_3 specimen with 8ply HSW subjected subjected to creep test at 40.5 MPa in air at 1100 °C (t_f = 3.34 h). 316

B.187. Fracture surface of the N610/$LaPO_4$/Al_2O_3 specimen with 8ply HSW subjected subjected to creep test at 40.5 MPa in air at 1100 °C (t_f = 3.34 h). 316

B.188. Fracture surface of the N610/$LaPO_4$/Al_2O_3 specimen with 8ply HSW subjected subjected to creep test at 40.5 MPa in air at 1100 °C (t_f = 3.34 h). 317

B.189. Fracture surface of the N610/$LaPO_4$/Al_2O_3 specimen with 8ply HSW subjected subjected to creep test at 40.5 MPa in air at 1100 °C (t_f = 3.34 h). 317

B.190. Fracture surface of the N610/$LaPO_4$/Al_2O_3 specimen with 8ply HSW subjected subjected to creep test at 40.5 MPa in air at 1100 °C (t_f = 3.34 h). 317

B.191. Fracture surface of the N610/$LaPO_4$/Al_2O_3 specimen with 8ply HSW subjected subjected to creep test at 40.5 MPa in air at 1100 °C (t_f = 3.34 h). 318

B.192. Fracture surface of the N610/$LaPO_4$/Al_2O_3 specimen with 8ply HSW subjected subjected to creep test at 40.5 MPa in steam at 1100 °C (t_f = 0.01 h). 318

B.193. Fracture surface of the N610/$LaPO_4$/Al_2O_3 specimen with 8ply HSW subjected subjected to creep test at 40.5 MPa in steam at 1100 °C (t_f = 0.01 h). 319

B.194. Fracture surface of the N610/$LaPO_4$/Al_2O_3 specimen with 8ply HSW subjected subjected to creep test at 40.5 MPa in steam at 1100 °C (t_f = 0.01 h). 319

B.195. Fracture surface of the N610/$LaPO_4$/Al_2O_3 specimen with 8ply HSW subjected subjected to creep test at 40.5 MPa in steam at 1100 °C (t_f = 0.01 h). 319

B.196. Fracture surface of the N610/$LaPO_4$/Al_2O_3 specimen with 8ply HSW subjected subjected to creep test at 40.5 MPa in steam at 1100 °C (t_f = 0.01 h). 320

B.197. Fracture surface of the N610/$LaPO_4$/Al_2O_3 specimen with 8ply HSW subjected subjected to creep test at 40.5 MPa in steam at 1100 °C (t_f = 0.01 h). 320

B.198. Fracture surface of the N610/$LaPO_4$/Al_2O_3 specimen with 8ply HSW subjected subjected to creep test at 40.5 MPa in steam at 1100 °C (t_f = 0.01 h). 320

B.199. Fracture surface of the N610/$LaPO_4$/Al_2O_3 specimen with 8ply HSW subjected subjected to creep test at 40.5 MPa in steam at 1100 °C (t_f = 0.01 h). 321

B.200. Fracture surface of the N610/$LaPO_4$/Al_2O_3 specimen with 8ply HSW subjected subjected to creep test at 61 MPa in air at 1100 °C (t_f = 3.42 h). 321

B.201. Fracture surface of the N610/$LaPO_4$/Al_2O_3 specimen with 8ply HSW subjected subjected to creep test at 61 MPa in air at 1100 °C (t_f = 3.42 h). 321

B.202. Side view of the virgin N610/$LaPO_4$/Al_2O_3-AlOCl specimen with 8ply HSW. 322

B.203. Side view of the virgin N610/$LaPO_4$/Al_2O_3-AlOCl specimen with 8ply HSW. 322

B.204. Side view of the virgin N610/$LaPO_4$/Al_2O_3-AlOCl specimen with 8ply HSW. 322

Figure Page

B.205. Side view of the virgin N610/$LaPO_4$/Al_2O_3-AlOCl specimen with 8ply HSW. 323

B.206. Fracture surface of the N610/$LaPO_4$/Al_2O_3-AlOCl specimen with 8ply HSW subjected tension to failure in laboratory air at 1100 °C. 323

B.207. Fracture surface of the N610/$LaPO_4$/Al_2O_3-AlOCl specimen with 8ply HSW subjected tension to failure in laboratory air at 1100 °C. 323

B.208. Fracture surface of the N610/$LaPO_4$/Al_2O_3-AlOCl specimen with 8ply HSW subjected tension to failure in laboratory air at 1100 °C. 324

B.209. Fracture surface of the N610/$LaPO_4$/Al_2O_3-AlOCl specimen with 8ply HSW subjected tension to failure in laboratory air at 1100 °C. 324

B.210. Fracture surface of the N610/$LaPO_4$/Al_2O_3-AlOCl specimen with 8ply HSW subjected tension to failure in laboratory air at 1100 °C. 324

B.211. Fracture surface of the N610/$LaPO_4$/Al_2O_3-AlOCl specimen with 8ply HSW subjected tension to failure in laboratory air at 1100 °C. 325

B.212. Fracture surface of the N610/$LaPO_4$/Al_2O_3-AlOCl specimen with 8ply HSW subjected tension to failure in laboratory air at 1100 °C. 325

B.213. Fracture surface of the N610/$LaPO_4$/Al_2O_3-AlOCl specimen with 8ply HSW subjected tension to failure in laboratory air at 1100 °C. 325

B.214. Fracture surface of the N610/$LaPO_4$/Al_2O_3-AlOCl specimen with 8ply HSW subjected subjected to creep test at 32 MPa in air at 1100 °C ($t_f > 100$ h). 326

B.215. Fracture surface of the N610/$LaPO_4$/Al_2O_3-AlOCl specimen with 8ply HSW subjected subjected to creep test at 32 MPa in air at 1100 °C ($t_f > 100$ h). 326

B.216. Fracture surface of the N610/$LaPO_4$/Al_2O_3-AlOCl specimen with 8ply HSW subjected subjected to creep test at 32 MPa in air at 1100 °C ($t_f > 100$ h). 327

B.217. Fracture surface of the N610/$LaPO_4$/Al_2O_3-AlOCl specimen with 8ply HSW subjected subjected to creep test at 32 MPa in air at 1100 °C ($t_f > 100$ h). 328

B.218. Fracture surface of the N610/$LaPO_4$/Al_2O_3-AlOCl specimen with 8ply HSW subjected subjected to creep test at 32 MPa in air at 1100 °C ($t_f > 100$ h). 328

B.219. Fracture surface of the N610/$LaPO_4$/Al_2O_3-AlOCl specimen with 8ply HSW subjected subjected to creep test at 32 MPa in air at 1100 °C ($t_f > 100$ h). 329

B.220. Fracture surface of the N610/$LaPO_4$/Al_2O_3-AlOCl specimen with 8ply HSW subjected subjected to creep test at 32 MPa in air at 1100 °C ($t_f > 100$ h). 329

B.221. Fracture surface of the N610/$LaPO_4$/Al_2O_3-AlOCl specimen with 8ply HSW subjected subjected to creep test at 32 MPa in air at 1100 °C ($t_f > 100$ h). 330

B.222. Fracture surface of the N610/$LaPO_4$/Al_2O_3-AlOCl specimen with 8ply HSW subjected subjected to creep test at 32 MPa in air at 1100 °C ($t_f > 100$ h). 330

B.223. Fracture surface of the N610/$LaPO_4$/Al_2O_3-AlOCl specimen with 8ply HSW subjected subjected to creep test at 32 MPa in steam at 1100 °C ($t_f = 3.47$ h). 331

B.224. Fracture surface of the N610/$LaPO_4$/Al_2O_3-AlOCl specimen with 8ply HSW subjected subjected to creep test at 32 MPa in steam at 1100 °C ($t_f = 3.47$ h). 331

B.225. Fracture surface of the N610/$LaPO_4$/Al_2O_3-AlOCl specimen with 8ply HSW subjected subjected to creep test at 32 MPa in steam at 1100 °C ($t_f = 3.47$ h). 332

B.226. Fracture surface of the N610/$LaPO_4$/Al_2O_3-AlOCl specimen with 8ply HSW subjected subjected to creep test at 32 MPa in steam at 1100 °C ($t_f = 3.47$ h). 332

Figure Page

B.227. Fracture surface of the N610/$LaPO_4$/Al_2O_3-AlOCl specimen with 8ply HSW subjected subjected to creep test at 32 MPa in steam at 1100 °C (t_f = 3.47 h). 333

B.228. Fracture surface of the N610/$LaPO_4$/Al_2O_3-AlOCl specimen with 8ply HSW subjected subjected to creep test at 32 MPa in steam at 1100 °C (t_f = 3.47 h). 333

B.229. Fracture surface of the N610/$LaPO_4$/Al_2O_3-AlOCl specimen with 8ply HSW subjected subjected to creep test at 32 MPa in steam at 1100 °C (t_f = 3.47 h). 334

B.230. Fracture surface of the N610/$LaPO_4$/Al_2O_3-AlOCl specimen with 8ply HSW subjected subjected to creep test at 32 MPa in steam at 1100 °C (t_f = 3.47 h). 334

B.231. Fracture surface of the N610/$LaPO_4$/Al_2O_3-AlOCl specimen with 8ply HSW subjected subjected to creep test at 48 MPa in steam at 1100 °C (t_f = 2.06 h). 335

B.232. Fracture surface of the N610/$LaPO_4$/Al_2O_3-AlOCl specimen with 8ply HSW subjected subjected to creep test at 48 MPa in steam at 1100 °C (t_f = 2.06 h). 335

B.233. Fracture surface of the N610/$LaPO_4$/Al_2O_3-AlOCl specimen with 8ply HSW subjected subjected to creep test at 48 MPa in steam at 1100 °C (t_f = 2.06 h). 336

B.234. Fracture surface of the N610/$LaPO_4$/Al_2O_3-AlOCl specimen with 8ply HSW subjected subjected to creep test at 48 MPa in steam at 1100 °C (t_f = 2.06 h). 336

B.235. Fracture surface of the N610/$LaPO_4$/Al_2O_3-AlOCl specimen with 8ply HSW subjected subjected to creep test at 48 MPa in steam at 1100 °C (t_f = 2.06 h). 337

B.236. Fracture surface of the N610/$LaPO_4$/Al_2O_3-AlOCl specimen with 8ply HSW subjected subjected to creep test at 48 MPa in steam at 1100 °C (t_f = 2.06 h). 337

B.237. Fracture surface of the N610/$LaPO_4$/Al_2O_3-AlOCl specimen with 8ply HSW subjected subjected to creep test at 48 MPa in steam at 1100 °C (t_f = 2.06 h). 338

List of Tables

Table		Page
2.1.	Summary of key fiber properties and resulting CMC benefits. .	7
3.1.	Properties of Nextel^{TM}610 fibers	15
3.2.	Composite specifications.	20
5.1.	Test matrix.	35
5.2.	Summary of tensile properties for the six oxide-oxide composites obtained in displacement-controlled tensile tests conducted at 0.05 mm/s at 1100 °C in laboratory air.	36
5.3.	Summary of creep-rupture results for the six oxide-oxide composites at 1100 °C.	42
5.4.	Retained tensile properties of the N^{TM}610/$LaPO_4$/Al_2O_3 (8HSW) oxide-oxide composite subjected to prior tensile creep at 1100 °C in laboratory air. All data are adjusted for $V_f = 0.39$.	57

List of Symbols

Symbol		Page
%	Per cent	1
$\sim$	Approximately	2
°C	Centigrade Celsius	2
μm	Micrometer	4
$>$	Bigger Than	14
α	A form of Alumina	14
$\pm$	Plus-Minus	29
$\geq$	Equal or Greater	34
ε_{th}	Thermal Strain	34
Δ	Temperature Difference	34
mm	Milimeter	69

List of Abbreviations

Abbreviation		Page
CMC	Ceramic Matrix Composite	2
Al_2O_3	Alumina	2
™	Trade Mark	3
PMC	Polymer Matrix Composite	4
MMC	Metal Matrix Composite	4
UTS	Ultimate Tensile Strength	4
CFCC	Continuous Fiber Ceramic Composites	4
SiC	Silicon Carbide	5
Si_3N_4	Silicon Nitride	5
SiO_2	Silica	6
YAG	Yttrium Aluminum Garnet	7

CREEP BEHAVIOR OF OXIDE/OXIDE COMPOSITES WITH MONAZITE FIBER COATING AT 1100 °C IN AIR AND IN STEAM ENVIRONMENTS

I. Introduction

Development of new materials and our understanding of their properties have provided the basis for much technological advancement. Over the years,the single most important factor influencing cutting-edge developments in aerospace technology has been the application of new materials. Composite materials have been used for thousands of years, since when ancient Egyptians combined straw and clay to make a stronger brick. Composites made their appearance in the aviation industry when Boeing 707 was introduced in the 1950s. Fiberglass made up some two percent of the early Boeing 707 structure. Today, composites make up near 9% of the aircraft structural weight in the modern Boeing 777. It is expected that 50% of the material used on the 787 Dreamliner, scheduled for delivery in 2010, will be composites [50]. The Boeing 787 Dreamliner can be seen in Fig. 1.1.

Advances in aerospace technologies have raised the demand for structural materials that exhibit superior long-term mechanical properties and retained properties

under high temperature, high pressure, and severe environments [39]. Ceramic-matrix composites (CMCs), capable of maintaining excellent strength and fracture toughness at high temperatures, are attractive candidate materials for such applications. Furthermore, the lower densities of CMCs and their higher use temperatures, together with a reduced need for cooling air, allow for improved high-temperature performance when compared to conventional nickel-based superalloys [52]. It is envisioned that advanced reusable space launch vehicles will incorporate CMCs in critical propulsion components [43]. However, these applications require exposure to oxidizing environments. Therefore a better understanding of thermodynamic stability and oxidation resistance of CMCs are vital. CMCs can be divided into two groups as non-oxide and all-oxide composites. While non-oxide composite has at least one non-oxide phase, all-oxide (oxide-oxide) composite has phases all of which are inherently oxidized.

Non-oxide fiber/non-oxide matrix composites generally exhibit poor oxidation resistance [30, 41],particularly at intermediate temperatures (∼800 °C). The degradation involves oxidation of fibers, fiber coatings, and matrices and is typically accelerated by the presence of moisture [11, 14, 32]. Using a non-oxide fiber/oxide matrix or oxide fiber/non-oxide matrix composites generally does not substantially improve the high temperature oxidation resistance [15]. The need for environmentally stable composites motivated the development of CMCs based on environmentally stable oxide constituents [23, 26, 27, 31, 35, 36, 45, 46, 48]. Oxide/Oxide CMCs were developed to combat the environmental degradation. These materials use oxide based ceramics such as alumina (Al_2O_3) that have an inherent resistance to oxidation. While the oxide-oxide CMCs show improved oxidation resistance,their creep resistance and other aspects of performance are still below the levels required in aerospace applications. Active research into various ways to further improve performance of oxide-oxide CMCs at elevated temperatures in aggressive environments has taken place in recent years [12, 13, 26, 27, 35, 36, 48]. The use of various fiber coatings to promote environmental stability has been one aspect of such research efforts. Monazite coating is

one example. It provides a weak interface between the fiber and matrix and resists oxidation at elevated temperatures due to being inherently oxidized. Recent efforts [29, 40] investigated the effects of monazite fiber coating on tensile and compressive creep performance of the Nextel^{TM}610/alumina composite at elevated temperatures in laboratory air. Ruggles-Wrenn et al [29, page 3] reported that the addition of monazite improved the creep resistance of Nextel^{TM}610/alumina composite at elevated temperatures in air. The present study will investigate the effects of monazite coating on creep performance of six different variants of the Nextel^{TM}610/alumina material system at 1100 °C in air and in steam environments.

II. Background

2.1 Ceramic Matrix Composites (CMCs)

Composite materials are often classified according to the characteristics of the matrix material, i.e. polymer matrix composites (PMCs), metal matrix composites (MMCs), ceramic matrix composites (CMCs). The term "ceramic" applies to a wide range of materials. Ceramics are typically inorganic and non-metallic materials, which consist of a combination of metallic and non-metallic elements with a crystalline structure [1]. Ceramics generally exhibit high strength, hardness, and excellent heat resistance. The high-temperature strength of ceramics makes them particularly attractive to the aerospace design community. The maximum service temperatures of polymers, metals and ceramics [20, page 5] are shown in Fig. 2.1. Ceramics are the only class of material that can be reliably used at temperatures above 1100 °C.

Despite the many attractive properties of ceramics,the use of this class of materials in load-bearing components has been limited due to inherent brittleness and low thermal shock tolerance until last several decades [37]. Most metallic alloys exhibit significant deformation in tension prior to failure. Ceramics, on the other hand, exhibit elastic behavior until the stress level reaches the ultimate tensile strength (UTS). Catastrophic tensile failure in monolithic ceramics initiates at small defects formed during processing. Minimization of such defects may improve performance, but thermal shock and cyclic loading can exacerbate any existing flaws in the structure [41, page 9]. CMCs,introduced in the late 1970s, were developed specifically to combat the brittle behavior of monolithic ceramics.

Ceramic matrix composites are designed to minimize the drawbacks of monolithic ceramics. Continuous fiber ceramic composites (CFCCs) consist of a ceramic matrix reinforced with high aspect-ratio ceramic fibers (typical fiber diameter 10 μm). Ceramic matrix composites are designed to combine the high temperature resistance of ceramics with higher fracture toughness. Energy dissipating phenomena such as fiber matrix debonding, crack deflection, fiber bridging and fiber pullout inherent in CMCs significantly raise the damage tolerance of the material [20, page 8]. Compared

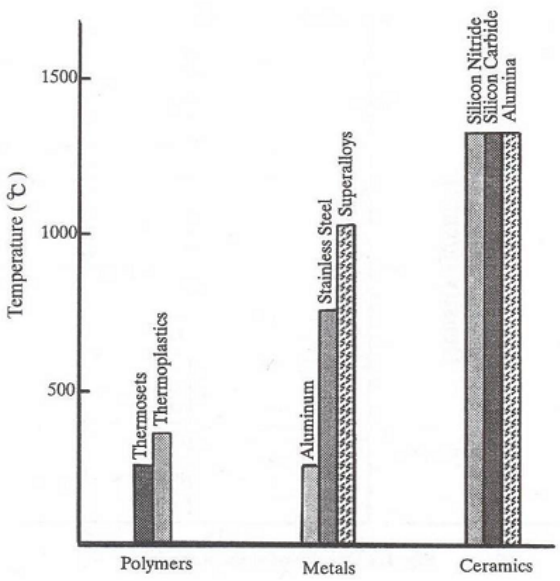

Figure 2.1: service temperatures of polymers, metals and ceramics [M7:5].

to monolithic ceramics, CFCCs exhibit reduced brittleness and decreased susceptibility to both flaws and thermal shock, while maintaining excellent properties at high temperatures [42]. This permits the use of CMCs in applications where monolithic ceramics cannot be employed. Fig. 2.2 shows general trends of strength to weight ratio versus temperature for various types of materials, including CMCs [43].

2.2 Matrix Materials

Ceramic matrix materials possess the ability to withstand very high temperatures. Ceramics are made up of one or more metals combined with a nonmetal such as oxygen, carbon, nitrogen, or boron. They are generally stoichiometric, i.e. they have a fixed ratio of cations to anions. Some examples of ceramic matrix materials are alumina (Al_2O_3), silicon carbide (SiC), and silicon nitride (Si_3N_4).

Ceramic matrix materials can be non-oxide or oxide ceramics. Common non-oxide ceramic matrix materials are silicon carbide, silicon nitride,and titanium diboride. Oxide ceramic matrix materials include alumina or zirconia. Oxide ceramics

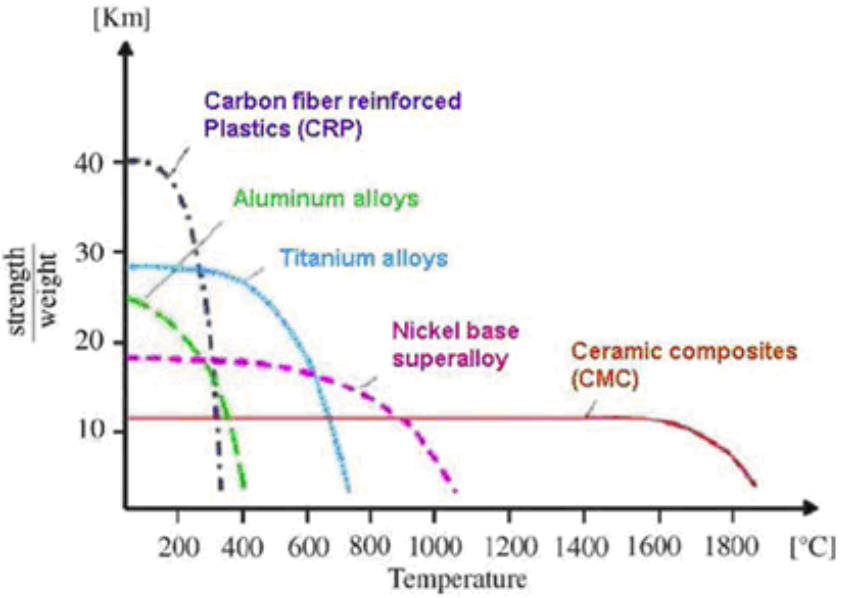

Figure 2.2: Strength to weight ratio versus temperature range [43].

are inherently oxidation resistant, whereas non-oxide ceramics rely on a layer of silica (SiO_2) to prevent oxidation.

2.3 Ceramic Fibers

Ceramic fibers exhibit high fracture toughness,high strength and high elastic modulus, along with high temperature resistant capability. With these excellent properties, ceramic fibers are useful as reinforcements in high-temperature structural composites. Ceramic fibers are categorized on the basis of fiber size. Typically,ceramic fibers are produced as (1) multifiber tows consisting of 100-1000 smaller (5-15 μm) diameter fibers or (2) larger monofilaments (50-100 μm in diameter). Monofilament fibers are used mainly in metal matrix composites. Smaller diameter fiber tows are used in CMCs, where the use of small-diameter fibers causes a reduction in scale of microstructural defects associated with the fibers [7, page 15].

Ceramic fibers can be non-oxide or oxide fibers. Non-oxide fibers generally contain silicon carbide (SiC). Examples of SiC based fibers include Nicalon, Tyranno and Sylramic [51]. Other non-oxide fibers contain silicon nitride, boron carbide, and

Table 2.1: Summary of key fiber properties and resulting CMC benefits. From DiCarlo et al [10].

Fiber Property	**CMC Benefit**
· High Modulus	· Improves CMC stiffness and reduces matrix stresses.
· High As-Produced Strength	· Improves CMC toughness and ultimate strength.
· High Thermomechanical Stability	· Improves CMC as-fabricated strength, CMC strength retention and creep resistance during service.
· High Oxidative Stability	· Improves CMC service life in oxidizing environments.
· Small Diameter	· Improves matrix strength and facilitates fabrication of thin and complex-shaped CMCs.
· Low Density	· Improves CMC specific properties for weight-sensitive applications and reduces stresses in CMC rotating components.
· Low Cost	· Reduces CMC cost and improves CMC commercial viability.

boron nitride [21, page 49]. Oxide fibers are mostly alumina-based (Al_2O_3), but may contain small amounts of SiO_2. Some examples of oxide fibers are the Nextel^{TM}610, 650, and 720 fibers developed by 3M or yttrium-aluminum garnet (YAG) fibers developed by General Atomics [51]. Oxide fibers are inherently oxidation resistant.

The key properties needed in a continuous ceramic fiber for use as reinforcement in high temperature continuous-fiber ceramic matrix composite, along with the benefit gained from each property are summarized in Table 2.1 from DiCarlo et al [10].

2.4 Fiber-Matrix Interface

The increased toughness in CMCs is derived from the interaction between the fiber and the matrix at the fiber/matrix interface. The failure of a typical CMC evolves in several stages. During initial applied loading, fibers and matrix share the stress based on their respective elastic moduli and volume fractions. The matrix, which typically has numerous pores and flaws, fails first. A network of microcracks develops in the matrix. Matrix microcracks eventually coalesce into larger cracks that will propagate through the matrix and toward the fibers. In order to maintain structural integrity of the fibers, cracks must be deflected around the fibers and not allowed to propagate through the fiber. A weak fiber/matrix interface allows fiber-matrix debonding and crack deflection followed by crack bridging, fiber fracture and finally fiber pullout [20, page 169]. Crack deflection is the energy dissipating event that provides for a delayed failure and higher toughness in CMCs (Fig. 2.3). A schematic of the CMC failure as a function of the interfacial bond is shown in Fig. 2.4. The interface between fiber and matrix is critical to achieving the flaw tolerance, which distinguishes CMCs from monolithic ceramics [47].

In the earliest ceramic composites, weak fiber/matrix interfacial layers were formed by the degradation of the fiber. The weak interfacial layer protected the fiber by deflecting matrix cracks through fiber-matrix debonding and sliding, thereby reducing the stress concentration on the fiber [19]. Ceramic matrix composites that rely on a weak interface for crack deflection can be characterized by their stress strain curve (see Fig. 2.4). Initially, when the matrix and fibers share the load, the stress-strain curve is linear. The slope of the curve starts to decrease as microcracks form in the matrix. As the matrix cracks grow and begin to coalesce, a distinctive knee is seen in the stress-strain curve. At this stage,cracks propagate through the thickness of the material and all load is transferred to the fibers. Now, the material response is dominated by failure of individual fibers and subsequent load transfer to other fibers until the material fails.

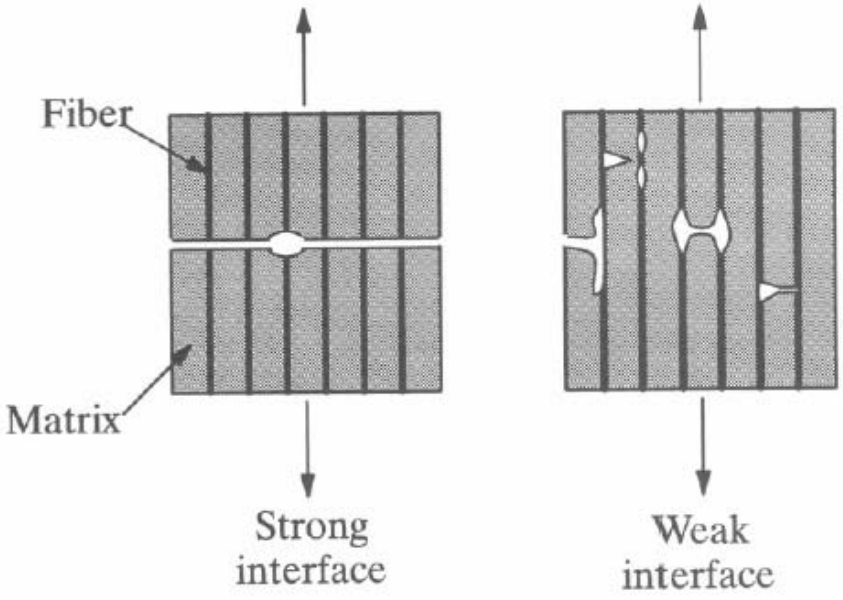

Figure 2.3: Failure of a CMC as a function of interfacial bond [20, page 170].

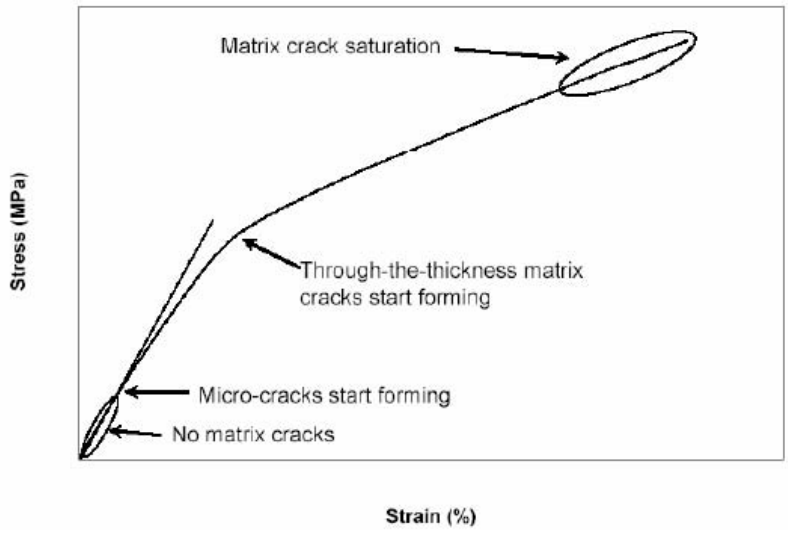

Figure 2.4: Typical stress strain curve for CMCs with weak interface [M20:10] [24, page 10].

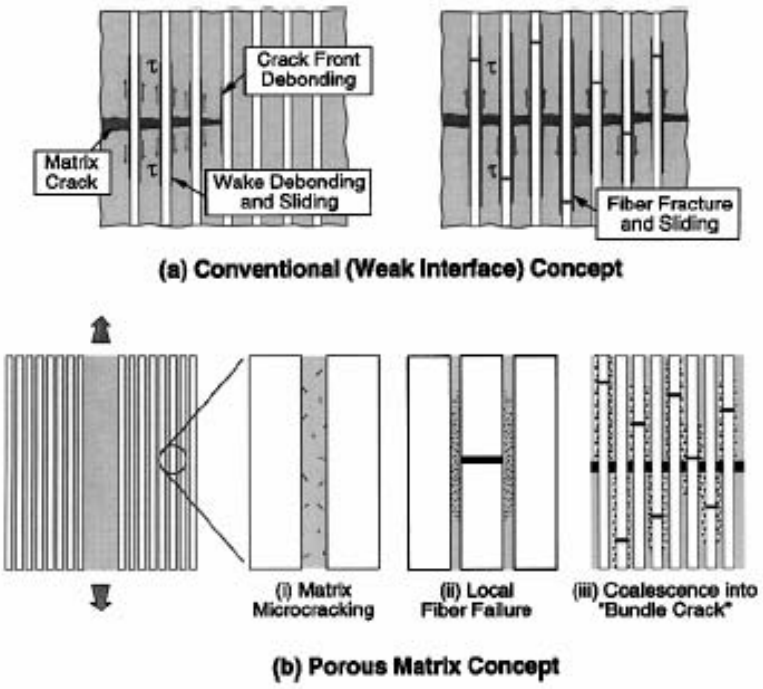

Figure 2.5: Schematics of the damage processes that enable damage tolerance in (a) conventional dense-matrix weak-interface CFCC and (b) porous matrix CFCC without fiber coatings [53].

More recently, another method of achieving damage tolerance has been developed and used in CMCs. The approach involves using a weak porous matrix [23, page 37]. The porosity and strength of the matrix must be controlled to be low enough to enable crack deflection, yet high enough to maintain adequate off-axis and interlaminar strength properties [25]. The different damage processes that enable damage tolerance in CMCs with a weak interface and in CMCs with a porous matrix are schematically shown in Fig. 2.5 [53].

2.5 Oxidation

Environmental degradation of CMCs is the biggest limiting factor for use of CMCs in high temperature applications. Oxidation is of particular concern in composites containing carbon, where at elevated temperatures carbon is with time completely dissipated in the form of carbon monoxide or carbon dioxide. Such composites

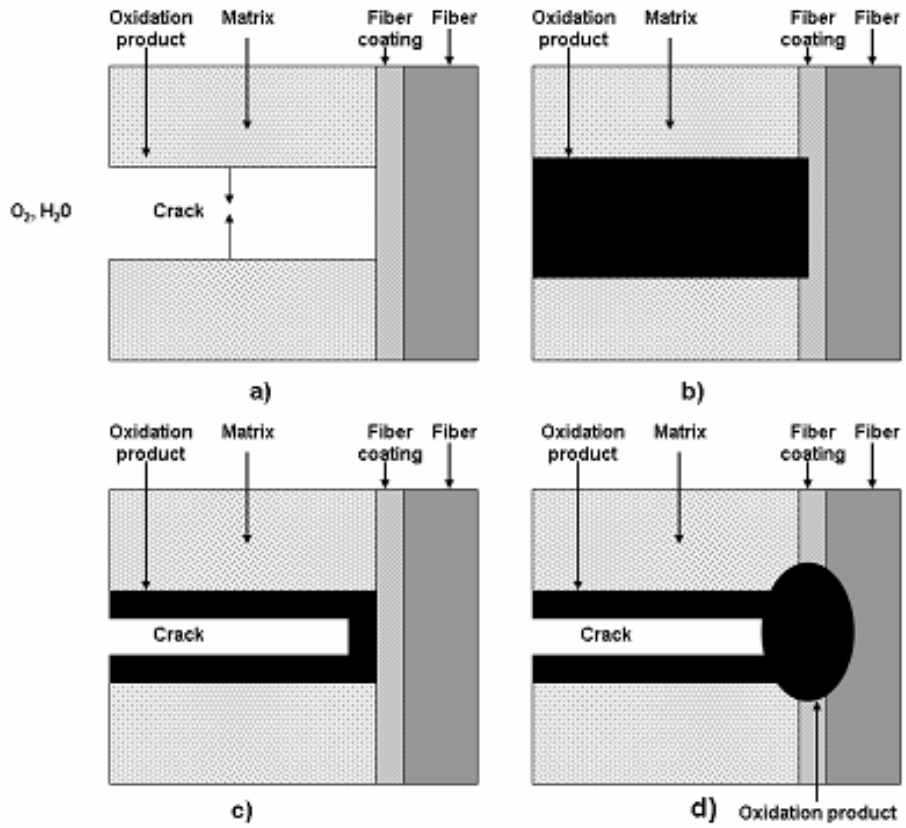

Figure 2.6: Schematic representation of oxidation progression through a matrix crack [49].

include carbon/carbon (C/C), carbon/silicon carbide (C/SiC), and silicon carbide/silicon carbide (SiC/SiC). These composites exhibit excellent high temperature strength, but readily oxidize at high temperatures. In C/SiC composites, matrix cracks form during the cool-down stage of processing due to a thermal mismatch between the fiber and matrix. These cracks represent pathways for oxygen to enter the composite and attack the fibers. Some SiC/SiC composites use a pyrolytic carbon fiber coating to allow fiber/matrix interface debonding. In this case, the matrix will crack allowing oxygen to attack the carbon coating [44, page 24]. Fig. 2.6 gives a schematic representation of the progression of oxidation of a coated fiber through a matrix crack.

Oxidants, such as oxygen and water vapor, diffuse through an open matrix crack, oxidizing the sides of the crack and fiber coating (Fig. 2.6a). The oxidation

product fills the crack area, reducing its width, as shown in Fig. 2.6b. In some cases the crack can become sealed by oxidation products before the coating is oxidized, thus preventing significant damage to the fiber/coating/matrix interface (Fig. 2.6c). In other cases, the coating is breached by oxidation prior to the crack sealing and oxygen diffuses through the oxidation product of the fiber coating and continues to oxidize the fiber, as shown in Fig. 2.6d [49].

The oxide/oxide ceramic composites were developed specifically to combat oxidation at elevated temperatures. Two microstructural design philosophies have been used in developing oxide/oxide CMCs. The first method employs a weak fiber/matrix interface concept and requires stable oxide fiber coatings to create the weak interface between the fiber and a dense matrix. The second method accepts formation of a strong interface, and employs a matrix with fine, uniformly distributed porosity to enable crack deflection [Mu27:2077] [49, page 2077]. The first method requires oxide interfacial coatings, such as monazite, which not only provide the weak fiber/matrix interface, but are also oxidation resistant and chemically stable with the composite constituents. The composites investigated in this effort explore the effects of monazite fiber coating on creep performance of a Nextel^{TM}610/alumina material system at 1100 °C in air and in steam.

2.6 Previous Work

Morgan and Marshall have first demonstrated the usefulness of monazite for promoting crack deflection in 1995. Since then, numerous studies considered the effects of monazite fiber coating on performance of CMCs. Chawla et al evaluated performance of a CMC consisting of an alumina matrix reinforced with monazite-coated Saphikon (single crystal α-alumina) fibers [6]. and demonstrated that monazite coating was effective in creating a weak interfacial bond between monazite and alumina. Several studies explored the use of monazite coated Nextel^{TM}610 fiber in an aluminosilicate matrix. Cazzato et al [5] showed that while the monazite fiber coating produced a weak interface, it also caused a decrease in tensile strength and in strain to fail-

ure. This was attributed to the fiber coating technique and fiber bridging caused by clumped tows of coated fibers. Investigations have also been performed on monazite coated Nextel^{TM}fiber tows, in an effort to determine the effect of various monazite precursors on fiber strength [3].

Most of the recent research has focused on unidirectional composites, although several studies evaluated the effectiveness of monazite as a weak interface material in 2-D laminated composites. Keller et al [18] investigated the effectiveness of monazite coatings in Nextel^{TM}610/alumina composites after long-term exposure at 1100 °C and 1200 °C. Coated fiber samples exhibited better tensile strength retention after 1000 h at 1200 °C when compared to the control (uncoated fiber) material. Ruggles-Wrenn et al [29] reported that the use of monazite coating in a Nextel^{TM}610/alumina porous-matrix CMC resulted in improved tensile creep resistance at 900 °C.

2.7 Thesis Objective

The objective of this thesis is to characterize the tensile creep behavior of six variants of the Nextel^{TM}610/Monazite/Alumina composite at 1100 °C in air and in steam. The different variants of the material system include composites with different fiber architectures: composite with a 0°/90° unitape lay-up and a composite reinforced with woven 0°/90° fiber layers. The present study also considers composites manufactured using different techniques to apply monazite fiber coating. In addition, composites with (1) alumina matrix, (2) alumina matrix infiltrated with monazite ($LaPO_4$) precursor, and (3) alumina matrix infiltrated with AlOCl precursor are investigated. Because creep was shown to be considerably more damaging than cyclic loading to porous-matrix oxide-oxide CMCs [16, 28], creep-rupture testing is ideally suited to evaluate the environmental durability of these materials.

III. Material and Test Specimen

Six oxide-oxide composites were investigated in this study. All composites consisted of a porous alumina (Al_2O_3) matrix reinforced with Nextel^{TM}610 fibers. Composites 1, 2, and 3 consisted of ten unidirectional plies in a symmetric cross-ply $(0°/90°/0°/90°/0°)_s$ orientation. Composites 4, 5, and 6 were consisted of eight $0°/90°$ layers woven in an 8 harness satin weave (8HSW). In the case of composites 2, 3, 4, and 6, monazite ($LaPO_4$) fiber coating was applied to the fibers. Composites 1 and 5 contained no fiber coating. In the case of composites 1 and 2, alumina matrix was infiltrated with a monazite ($LaPO_4$) precursor. Alumina matrix of composite 6 was infiltrated with a AlOCl precursor.

This chapter will discuss fiber, matrix and interphase materials used in all six composites, describe composite processing,and conclude with the details of geometry and preparation of test specimens.

3.1 Nextel^{TM}610 (N610) Fiber

The six composites investigated in this study employed the N610 ceramic fibers as reinforcement. The N610 fiber was developed by the 3M Corporation in the 1990's for load-bearing applications. While most commercially available fibers contain silica or other non-crystalline phases, Nextel^{TM}610 is $> 99\%$ poly-crystalline α-alumina (Al_2O_3) and contains no glassy phases. Because Nextel^{TM}610 fiber does not contain amorphous phases, which can become viscous at elevated temperatures, it exhibits fairly good creep resistance as well as high retained strength at elevated temperatures [38]. The average grain size in the Nextel^{TM}610 fiber is about 0.1 μm. While it has the highest strength among the other Nextel^{TM}fibers at room temperature, due to being single-phased the strength of the fiber decreases rapidly at elevated temperatures. This is attributed to the grain growth mechanism. This fully crystalline fiber consisting of nearly pure α - Al_2O_3 is chemical stable which leads to environmental stability in corrosive atmospheres. Typical properties of the Nextel^{TM}610 fiber as

Table 3.1: Properties of Nextel^{TM}610 fibers

Chemical Composition	**Wt. (%)**
Al_2O_3	> 99
SiO_2	0.2-0.3
Fe_2O_3	0.4-0.7
Average Grain Size (μm)	0.1
Filament Diameter (μm)	10-12
Density (g/cm^3)	3.88
Tensile Elastic Modulus (GPa)	373
Tensile Strength (MPa)	3100

reported by the manufacturer are given in Table 3.1 and Fig. 3.1, from Johnson et al [49], shows a uniform, high density microstructure of the Nextel^{TM}610 fiber.

3.2 Alumina (Al_2O_3) Matrix

Alumina was the matrix material in all six composites investigated in this study. Alumina has only one stable form, α-alumina. Alumina is an oxide of aluminum, and is therefore oxidation resistant. The tensile strength of crystalline alumina is ∼300 MPa, tensile modulus is ∼380 GPa, and its coefficient of thermal expansion is 8.8 $\times$ 10^{-6} /°C [22]. (At temperatures below 200 °C and above 800 °C, alumina has a friction coefficient of 0.40 [38, page 115]. Low friction coefficient of the matrix reduces friction between matrix and fibers promoting fiber pull-out and graceful failure.) The sintering temperature for alumina is 1400 °C, but shrinkage can occur at temperatures near 1100 °C [38, page 112]. The six composites studied in this effort were processed at 1200 °C. As a result matrix shrinkage and microcracking occur during processing that are typical for oxide-oxide CMCs which require high processing temperatures.

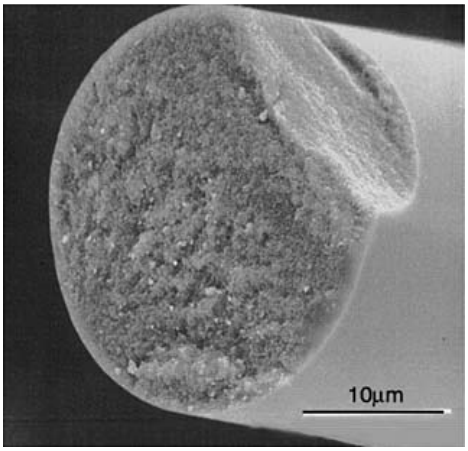

Figure 3.1: Fine-grained Nextel^{TM}610 fiber [49].

3.3 Monazite Coating

Monazite ($LaPO_4$) fiber coating was used in four of the six composites investigated in this study. In order to retain the oxidation resistance inherent in an oxide/oxide composite, oxide fiber coatings must be used. Among many oxidation-resistant fiber coatings investigated over the past 20 years, monazite ($LaPO_4$) is the most promising. In early efforts, monazite fiber coatings degraded strength of the Nextel^{TM}610 fibers. However, recently the coating composition was found that did not cause degradation of strength of the fibers after sintering [4,8]. Monazite is refractory, thermochemically stable with refractory oxides like alumina [33, 34], bonds weakly to other oxides [17], and was demonstrated to be machineable [9]. Furthermore, because monazite is an oxide, it is stable in air and water-containing environments. Monazite has a melting point is over 2000 °C, a thermal expansion coefficient of 9.6 $\times$ 10^{-6}/ °C,which is very similar that of Al_2O_3, and a density of 5.13 g/cc. Monazite can be applied as coating to fibers or formed in-situ between fiber and matrix during processing.

For composites 1, 2, and 3, the Nextel^{TM}610 fibers were coated with monazite using a sol-gel dip coating technique. This method employs low processing temperatures, which reduces fabrication cost as well the potential for coating degradation and interaction of the fiber and coating during processing [6]. For composites 4 and

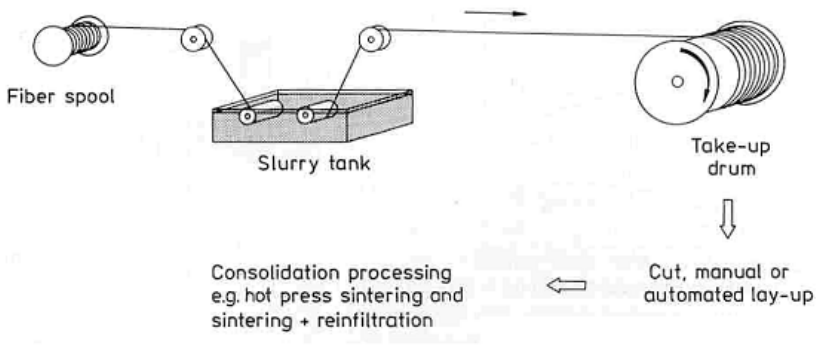

Figure 3.2: Schematic of slurry infiltration process [21].

6, the Nextel^{TM}610 fiber woven (8HSW) layers were coated with monazite using the precipitation technique developed at the Materials and Manufacturing Directorate of the Air Force Research Lab, AFRL/RXLN located on Wright-Patterson Air Force Base, Ohio [12, 13].

3.4 Processing of Composites 1, 2, and 3 with Unidirectional Layers

Composites 1, 2, and 3 consisted of unidirectional layers in 0°/90° cross-ply lay-up. For composites 2 and 3, the Nextel^{TM}610 fiber to be coated was first desized at 1100 °C, then coated with $LaPO_4$ using a sol-gel technique with a 20 g/l sol at 1100 °C. Coating speed was approximately 0.05 m/s. The coated fiber was spooled onto a take-up wheel. No sizing was applied over the coating.

Two matrix slurries were prepared. The slurry prepared for the uncoated fiber composite 1 consisted of 15 vol.% alumina powder (AKP-53, Sumitomo Corp.) and 85 vol.% alumina sol (aluminum nitrate + deoionized water + citric acid + ethylene glycol). The slurry for the coated fiber composites 2 and 3 consisted of 12.5 vol.% alumina powder and 87.5 vol.% sol. The fibers prepared for composites 1, 2, and 3 were drawn through their respective slurries and wound onto a drum, forming a tape. The slurry infiltration process is schematically depicted in Fig. 3.2.

The wound tape was cut and stacked in $(0°/90°/0°/90°/0°)_s$ orientation (an 10-layer symmetric cross-ply orientation), schematically shown in Fig. 3.3. The com-

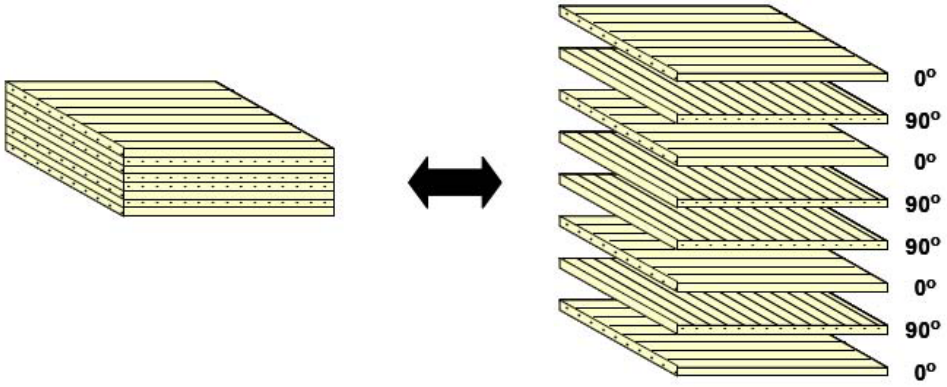

Figure 3.3: Schematic Representation of $(0°/90°/0°/90°/0°)_s$ Ply Lay-up.

posite stack was sealed in a vacuum bag and placed in an autoclave. The sample was evacuated, then heated to approximately 85 °C and held at this temperature for 1 h under 100 psig. The sample was removed from an autoclave after it had cooled and allowed to air-dry overnight. Finally,the sample was heat treated at 1200 °C in a box furnace for 5 h in air.

3.5 Processing of Composites 4, 5, and 6 with Woven 0°/90° Layers

Composites 4, 5, and 6 consisted of woven (8HSW) 0°/ 90° layers. For composites 4 and 6, the woven fiber layers were coated with monazite using the precipitation technique developed at AFRL/RXLN. The detailed description of this technique is given in [12]. A brief description of this process is given below.

The process for coating woven ceramic fibers with monazite, schematically shown in Fig. 3.4, includes several steps. First the woven fiber cloth is placed in a vessel filled with two chilled precursor solutions: (1) lanthanum citrate and (2) phosphoric acid. These precursor solutions react very slowly at low temperature. To saturate the cloth with the chilled precursor solutions, the vessel containing the mixed solutions and cloth is placed in an ultrasonic bath for 15 s. Then the cloth saturated with mixed precursor solutions is submerged in a vessel containing warm de-ionized water at 90 °C. This step increases the reaction rate between lanthanum citrate and

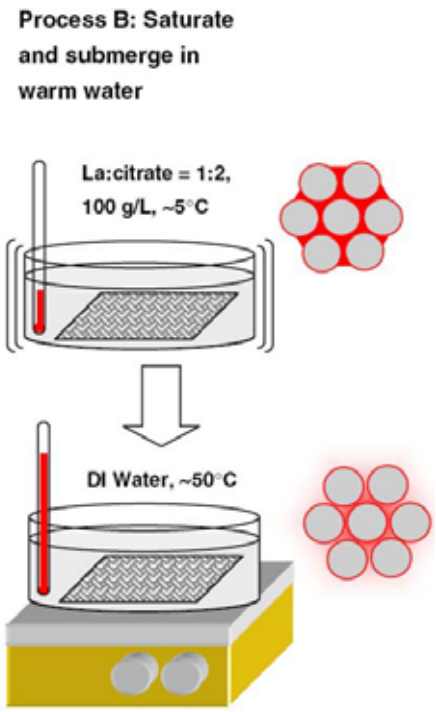

Figure 3.4: Schematic of the set up of process for coating woven ceramic fibers with monazite using heterogeneous precipitation from solution precursors. From [12]

.

phosphoric acid. As a result hydrated $LaPO_4$ (i.e. $LaPO_4 \ xH_2O$) is rapidly precipitated onto the fiber surfaces. The fiber cloth is removed after 5 min. in the warm water bath and rinsed in de-ionized water to remove any remaining dissolved chemicals. Next,the cloth is dried for 15 min. at 100 °C in air and then placed in a tube furnace at 600 °C for 5 min. in air. When this process is repeated multiple times (5 times), a thicker coating is produced with excellent coverage of fibers in tightly packed regions, such as tow crossovers in the woven fabric.

3.6 Composite Specifications

Six different composites were studied. Composites 1, 2, and 3 consisted of ten unidirectional plies in a symmetric cross-ply $(0°/90°/0°/90°/0°)_s$ orientation. Composites 4, 5, and 6 were consisted of eight $0°/90°$ layers woven in an 8 harness satin weave (8HSW). Composites 2, 3, 4, and 6 contained monazite ($LaPO_4$) fiber coating. There was no fiber coating in Composites 1 and 5. Composites 1 and 2 had

Table 3.2: Composite specifications.

Material	**Designation**	**Fiber Architecture**	**Fiber Volume Fraction (%)**	**Density (g/cc)**
Nextel610/Al2O3-LaPO4	C1	$[(0°/90°)_2]_s$	41.4	3.31
Nextel610/ LaPO4/Al2O3-LaPO4	C2	$[(0°/90°)_2]_s$	31.5	2.71
Nextel610/LaPO4/ Al2O3	C3	$[(0°/90°)_2]_s$	39	3
Nextel610/LaPO4/ Al2O3	C4	8HSW	33.3	3.18
Nextel610/Al2O3	C5	8HSW	38.8	3.22
Nextel610/LaPO4/ Al2O3-AlOCl	C6	8HSW	35.5	3.26

alumina matrix infiltrated with a monazite ($LaPO_4$) precursor. Composite 6 had alumina matrix infiltrated with a AlOCl precursor. Composites 3, 4, and 5 had alumina matrix.

Composite specifications are given in Table 3.2. Tensile specimens were cut from all composite panels. Note that in this document, composites will be referred to as C1, C2, C3, C4, C5, and C6. Specimen numbers used in this report also contain reference to the composite number. For example, specimen number C4-1 refers to specimen 1 for composite C4.

3.7 Specimen Geometry

Test specimens were cut from the composite panels using an abrasive water-jet machine to specifications in Fig. 3.5. Waterjet machining uses a computer-controlled nozzle that sprays water mixed with garnet particles at high pressures to precision-cut various materials. To reduce fraying at the top edges of the specimens - except some panels which had plastic sheets glued on them - a thin aluminum sheet was placed over the panels during cutting. After machining, the specimens were cleaned to remove any debris from the waterjet process. Specimens were placed in an ultrasonic bath for 15 min., then soaked in alcohol for 20 min. and lastly dried in an oven for 1 h

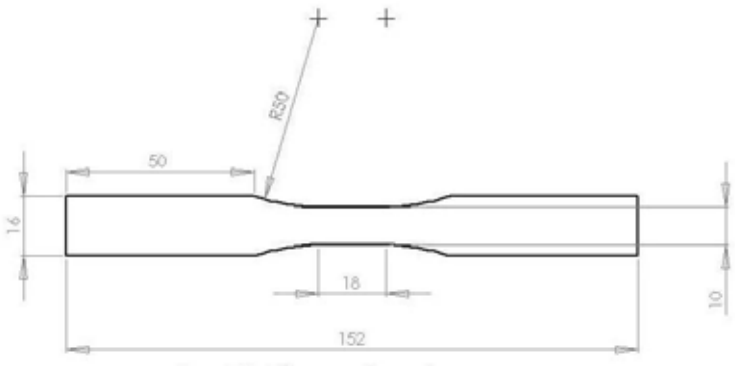

Figure 3.5: Test specimen geometry

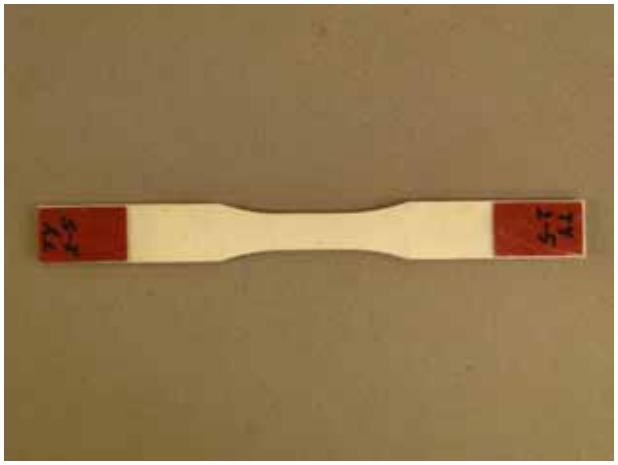

Figure 3.6: Tabbed test specimen

at 250 °C. Fiberglass tabs were attached to the grip sections of the specimens with M-Bond 200 adhesive. The tabs protected the surface of the specimen from the rough, surfalloy grips. Specimen with tabs is shown in Fig. 3.6.

IV. Experimental Arrangements and Test Procedures

This chapter will introduce the mechanical testing equipment and will discuss the testing and microstructural analyzing procedures.

4.1 Mechanical Testing Equipment

Mechanical testing was conducted on a MTS Systems Corporation model 810 Material Test System servo-hydraulic machine with the load capacity of 25 kN (5.5 kip). MTS Series 647 hydraulic wedge grips with a Surfalloy surfaces were used to grip the test specimen. A grip pressure in the 4-8 MPa range was used in all tests. Specific value of the grip pressure was selected based on the maximum load level expected in a particular test. The grips were water cooled with a Neslab model HX-75 chiller (shown in Fig. 4.2), which ensured that 15 °C cooling water was circulated through the grips during all tests. An MTS Test Star II controller was used for data acquisition and test control. MTS System Software and Multipurpose Testware (MPT) were used to program and execute the various tests. Fig. 4.1 shows the overall mechanical testing station set-up

An MTS Force Transducer (Model 661.19E-04), with a 25 kN maximum capacity, was used for force measurement. Strain measurement was accomplished with a uniaxial, air-cooled, high-temperature, low contact force MTS Extensometer (Model 632.53E-14) with the 12.5 mm gage length. In all elevated temperature tests,the extensometer was equipped with 6-inch alumina contact rods and protected by a heat shield to maintain the unit temperatures within the manufacturers recommended range. Displacement measurement was accomplished with an LVDT internal to the MTS servo-hydraulic machine. Fig. 4.3 shows a close-up view of the MTS machine and the extensometer set-up.

4.2 Environmental Testing Equipment

To maintain the elevated temperature and environment needed for testing, the mechanical testing station was equipped with a resistance-heated furnace, temper-

Figure 4.1: Mechanical testing station.

Figure 4.2: NESLAB model HX-75 chiller.

Figure 4.3: Close-up view of the MTS machine and the extensometer.

ature controllers and a steam generator. A compact, two-zone AMTECO Hot-Rail Furnace System controlled by a MTS Model 409.83B temperature controller (shown in Fig. 4.4) was used in all tests. Each half of the furnace was fitted with a non-contacting R-type thermocouple, which provided temperature reading to the controller.

Temperature was controlled in the following manner. Temperature set-point information was transmitted from the TestStar II to the temperature controller which applied a PID control algorithm to the furnace elements with a feedback loop from the control thermocouples. The temperature controller also transmitted the temperature measurements back to the TestStar II for temperature data recording if desired. It should be noted that this temperature was not the temperature of the specimen, but rather the ambient temperature near the specimen in the furnace.

An AMTECO HRFS-STMGEN Steam Generation System was employed to provide continuous steam environment for testing in steam. Deionized water was supplied from a one gallon water reservoir connected to the pump of the Steam Generation System. An alumina susceptor (a tube with end caps), which fits inside the furnace was used for testing in steam. The ends of the specimen pass through slots in the susceptor and the specimen gage section is located inside the susceptor. Steam is introduced into the susceptor through a ceramic feeding tube, fitted through an opening in the back wall of the susceptor. Steam was supplied in a continuous stream with a slightly positive pressure, expelling the dry air and creating a 100% steam environment inside the susceptor. The front wall of the susceptor had two elongated openings for the extensometer rods. The susceptor was not used in tests conducted in air environment. Fig. 4.5 shows the susceptor assembled around a specimen in the MTS machine with one of the furnace halves removed.

4.3 Microstructural Characterization

The A Zeiss Discovery V12 optical microscope with was used to examine the fracture surface of each specimen at magnifications of up to 100X. The optical micro-

Figure 4.4: MTS Model 409.83B temperature controller.

Figure 4.5: Susceptor assembly arrangement.

scope was equipped with a Zeiss AxioCam HRc digital camera and Axiovision version 4.4 software. This system allowed digital images to be recorded and later used to compare the fracture surfaces of different specimens. The optical microscope system is shown in Fig. 4.6.

An FEI Quanta 200 HV Scanning Electron Microscope (SEM) was used for microstructural characterization of the fracture surfaces at magnifications of up to 20,000X. Unlike the optical microscope the scanning electron microscope does not use reflected light to characterize the specimen. Instead, the SEM bombards the specimen with an electron beam and uses special detectors to capture secondary or back-scatter electrons emitted back from the specimen. An SEM can be used on bulk size specimens. The only limitation is the size of the specimen chamber and stage. An SEM is an excellent tool for examining the topography of the fracture surfaces. Fig. 4.7 shows the SEM system.

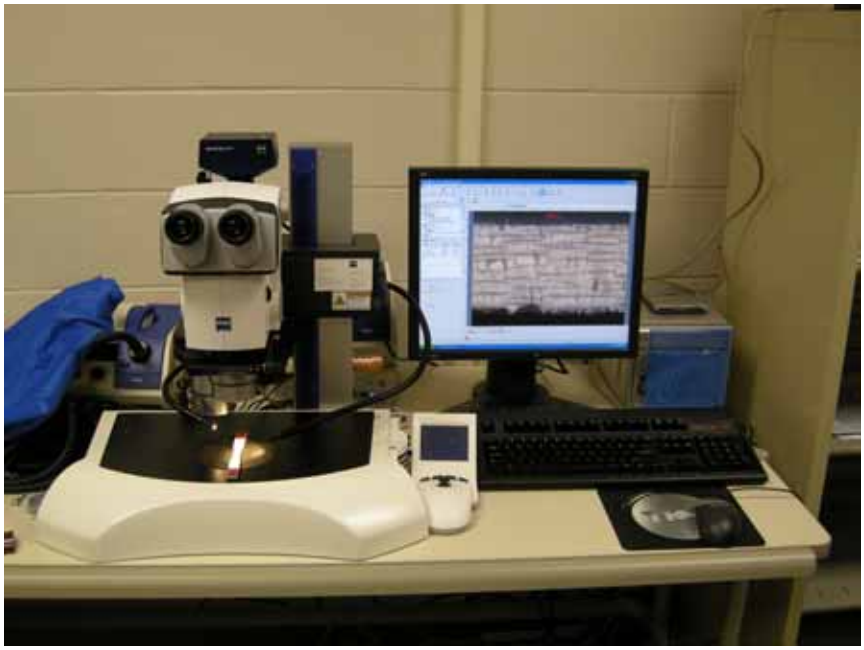

Figure 4.6: Zeiss Discovery V12 optical microscope.

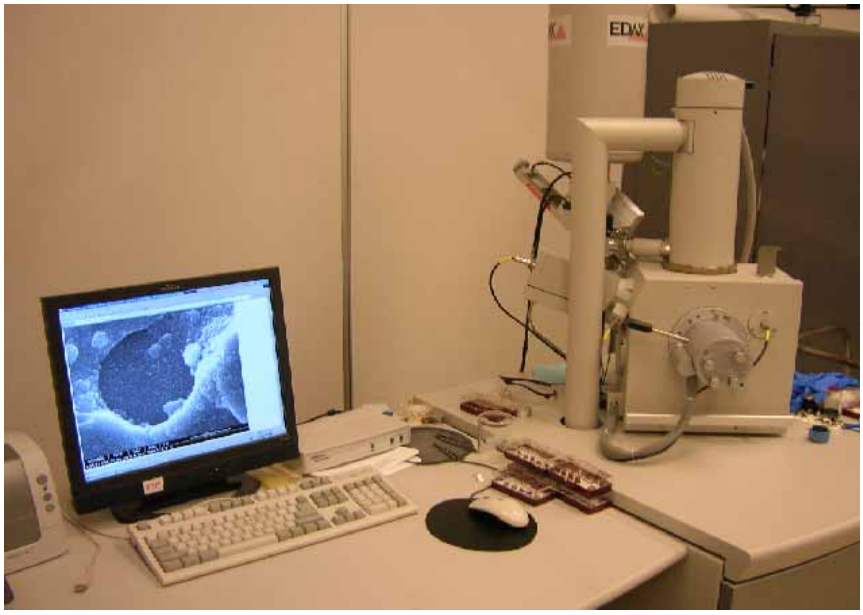

Figure 4.7: FEI Scanning Electron Microscope (SEM).

4.4 Test Procedures

4.4.1 Testing Equipment - Calibration. Before testing, various components of the mechanical testing equipment had to be calibrated. The load cell and extensometer were calibrated by MTS and AFIT technicians. Likewise,grip alignment was verified and/or adjusted by AFIT technicians. The MTS controller was tuned in displacement (stroke) and force control modes. To tune the controller in displacement control, no specimen had to be installed in the machine. A cyclic command with a square waveform was employed. The gains of the controller were adjusted to achieve a close agreement between command and feedback signals. To tune the force control, a CMC specimen was loaded into the machine.

The furnace temperature controllers were calibrated to maintain the desired test temperature of the specimen. One specimen was fitted with two R-type thermocouples. The specimen was mounted into the MTS machine as it would be in a typical experiment. The furnace temperature was slowly raised until the specimen temperature reached the desired test temperature (1100 °C). This temperature was held for 8 h to demonstrate that the temperature controllers could maintain stable temperatures within ± 5 °C of the nominal temperature. For the tests conducted in steam, temperature calibration was repeated using the susceptor and the test set-up designed for testing in steam.

4.4.2 Mechanical Testing - Preparation. Before testing, the servo-hydraulic machine was warmed up to ensure that the hydraulic fluid was at operating temperature and that the gains for the controller determined in tuning would be accurate. To warm up the testing machine,the MTS function generator was programmed to cycle the actuator in displacement control mode for at least 15 min. A saw tooth waveform with an amplitude of ± 0.1 inch was used.

While the hydraulics were warming up, the specimen test section width and thickness were measured with a Mitutoyo Corporation Digital Micrometer (model NTD12-6 C). Based on these measurements the cross-sectional area of the specimen

Figure 4.8: A typical test set-up.

gage section was calculated, which was then used to determine the required loads for the MPT procedure using the following equation:

$$Load = Stress \times Area \tag{4.1}$$

Next,the specimen was placed in the grips. The top grip was closed while in displacement control and the load cell was auto-zeroed. Control was switched to force mode and the bottom grip was closed. For testing in steam, the susceptor was closed around the specimen and the oven was pulled forward into position making sure that the steam feeding tube was inserted into the opening in the back of the susceptor. The extensometer was mounted on the specimen. Then the oven was closed around the specimen and clearances for the extensometer rods were checked. The water chiller was turned on and the cooling water temperature set to 15 °C. The water lines for each grip were opened fully and the air cooling line for the extensometer was opened to 30 psi. A typical test set-up is shown in Fig. 4.8.

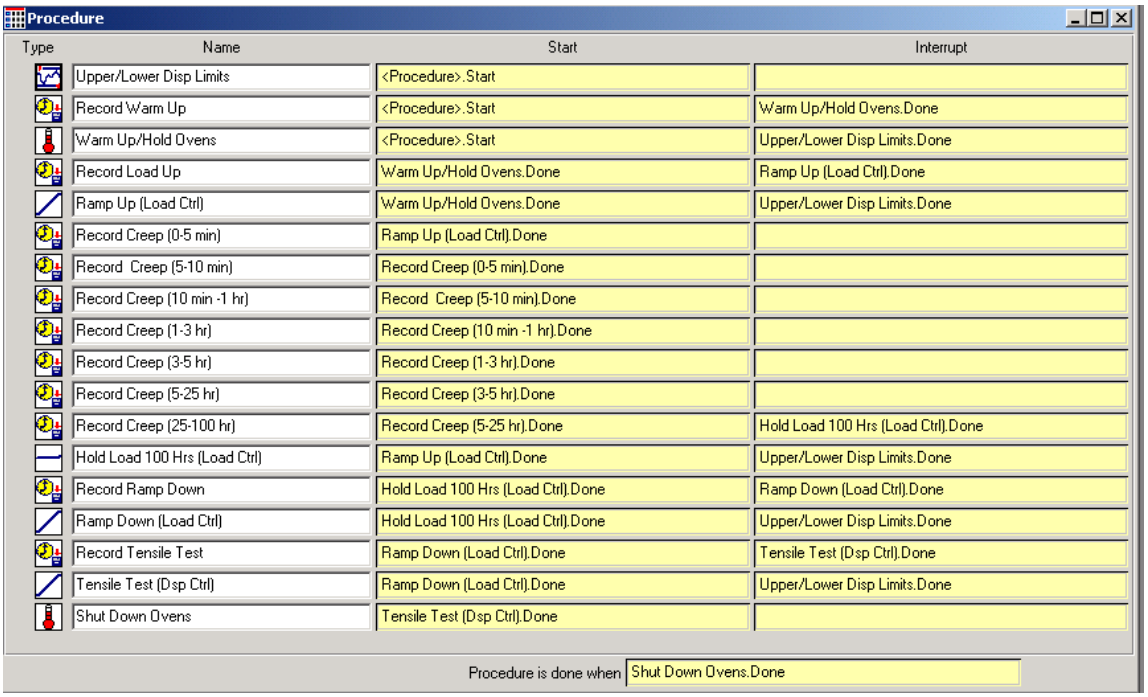

Figure 4.9: A typical test setup.

Next,the MPT software was used to program the test procedure. A sample creep-rupture test procedure can be seen in Fig. 4.9. Lastly, the test procedure was started and heating of the specimen began. If steam was used, the steam generator was turned on right after the start of the test. In all tests, the furnace temperature was ramped to 900 °C in 15 min. Then, the furnace temperature was ramped more slowly (10-15 min) to the desired set point for the test. Lastly, the specimen was allowed to thermally stabilize for 20 min. prior to applying the mechanical loading.

4.4.3 Monotonic Tensile Test. All monotonic tensile tests to failure were conducted at 1100 °C in laboratory air. These tests were conducted in displacement control at a constant rate of 0.05 mm/s. Load, strain, displacement,and time were measured and recorded every 0.05 s for the duration of the test, which was approximately 10 s.

4.4.4 Creep-Rupture Test. Creep-rupture tests were conducted in load control in accordance with the procedure in ASTM standard C 1337 at 1100 °C in lab-

oratory air and in steam environments. In all creep tests,the specimens were loaded to the creep stress level at the stress rate of 15 MPa/s. Creep run-out was defined as 100 h at a given creep stress. Load, strain, displacement and time were measured and recorded. In each test, data were recorded during both loading to the creep stress level and the actual creep period. Thus,both total strain and creep strain could be calculated and examined. Specimens that achieved run-out in creep tests were subjected to tensile tests to failure at 1100 °C in order to evaluate the retained tensile strength and modulus. The tensile tests were conducted in displacement control in a manner described above.

4.4.5 Microstructural Characterization. Post-test microstructure was first examined with the optical microscope. Digital pictures of each half of the failed specimens were taken for documentation. After observations by the optical microscope, the specimens were prepared for examination with the SEM. One half of the failed specimen was chosen and the fracture surface was cut off with a Sherline Model 5410 diamond saw. The cut was made $\sim$2 mm behind the damage zone of the specimen. The fracture surface was then mounted onto a 12.4 mm SEM specimen stage with carbon paint.

Non-conductive materials like the alumina found in the six composites used in this study tend to build up a charge when bombarded by the electron beam of the SEM. This leads to distortion of the image and, if severe enough, can lead to damage of the specimen. To address this problem, SEM specimens were coated with a thin layer of a conductive material. Carbon coating was used in this research. An SPI Supplies SPI-Module Control and Carbon Coater, shown in Fig. 4.10, were used to coat the specimens.

Figure 4.10: SPI-Module Controller and Carbon Coater.

V. Results and Discussion

This chapter will report the experimental results obtained during the course of this research. The section will begin with a discussion of thermal properties of the six oxide/oxide composite material systems. Results of the monotonic tensile tests,creep rupture tests and tensile tests conducted for retained properties will be presented . Finally Microstructure of the composites will be discussed.

The tests carried out during this study are summarized in Table 5.1, where composite, specimen number, test type and test environment are given together with the maximum stress level for each test.

5.1 Thermal Expansion

In each test, the strain data were collected as the specimen was heated to test temperature of 1100 °C. Then the coefficient of linear thermal expansion was calculated for each specimen with a curve fit to the linear portion of the strain-temperature curve, for temperatures $\geq$ 400 °C, as shown in [2]. The linear portion of the $\varepsilon_{th}-T$ curve was assumed to behave according to the linear relationship

$$\varepsilon_{th} = \alpha \times \Delta T \tag{5.1}$$

where ε_{th} is the thermal strain, α is the coefficient of linear thermal expansion, and ΔT is the temperature change from room temperature, taken as 23 °C. Similar values of thermal expansion coefficients were obtained in tests conducted in air and in steam. Coefficients of linear thermal expansion obtained in this effort are included in Table 5.1.

5.2 Monotonic Tensile Tests

Monotonic tensile tests to failure were conducted on specimens from each composite. All tensile tests were conducted at 1100 °C in laboratory air in displacement control at a constant rate of 0.05 mm/s. Results of the tensile tests are summarized in

Table 5.1: Test matrix.

Composite	Specimen Number	Environment	Test Type	Maximum Stress(MPa)	Coefficient of Thermal Expansion $\times 10^{-6}$ (1/°C)
N610/Al_2O_3-$LaPO_4$ (0/90 unitape lay-up)	C1-1	Air	Tension to failure	38.0	7.97
	C1-5	Air	Creep-rupture	32.0	8.84
	C1-2	Steam	Creep-rupture	32.0	8.12
N610/$LaPO_4$/Al_2O_3-$LaPO_4$ (0/90 unitape lay-up)	C2-1	Air	Tension to failure	36.7	7.41
	C2-3	Air	Tension to failure	35.9	7.33
	C2-5	Air	Tension to failure	30.1	8.80
	C2-4	Air	Creep-rupture	25	8.97
	C2-2	Steam	Creep-rupture	25	9.18
N610/$LaPO_4$/Al_2O_3 (0/90 unitape lay-up)	C3-3	Air	Tension to failure	213	7.74
	C3-1	Air	Creep-rupture	85.0	7.07
	C3-4	Air	Creep-rupture	120	7.13
	C3-6	Steam	Creep-rupture	85.0	9.14
	C3-5	Steam	Creep-rupture	110	8.65
	C3-2	Steam	Creep-rupture	120	9.53
N610/$LaPO_4$/Al_2O_3 (8HSW)	C4-1	Air	Tension to failure	67.6	7.39
	C4-5	Air	Tension to failure	84.9	7.01
	C4-6*	Air	Tension to failure	91.2	7.34
	C4-2	Air	Creep-rupture	32.0	7.01
	C4-7	Air	Creep-rupture	64.0	7.58
	C4-11	Air	Creep-rupture	72.0	6.91
	C4-3	Steam	Creep-rupture	32	7.58
	C4-4	Steam	Creep-rupture	48	7.80
	C4-8	Steam	Creep-rupture	64	7.58
	C4-10	Steam	Creep-rupture	72	8.52
N610/Al_2O_3 (8HSW)	C5-3	Air	Tension to failure	79.2	6.84
	C5-4	Air	Tension to failure	77.2	7.79
	C5-11	Air	Creep-rupture	40.5	7.90
	C5-9	Air	Creep-rupture	61.0	7.79
	C5-7	Steam	Creep-rupture	20.0	7.98
	C5-8	Steam	Creep-rupture	30.0	7.71
	C5-6	Steam	Creep-rupture	40.5	7.99
	C5-5	Steam	Creep-rupture	61.0	8.04
N610/$LaPO_4$/Al_2O_3-AlOCl (8HSW)	C6-4	Air	Tension to failure	74.9	7.14
	C6-1	Air	Creep-rupture	32.0	8.55
	C6-3	Steam	Creep-rupture	32.0	9.14
	C6-5	Steam	Creep-rupture	48.0	8.67

* Adjusted for V_f=0.39

Table 5.2: Summary of tensile properties for the six oxide-oxide composites obtained in displacement-controlled tensile tests conducted at 0.05 mm/s at 1100 °C in laboratory air.

Composite	Specimen	Elastic Modulus (GPa)	UTS(MPa)	Failure Strain (%)
N610/Al_2O_3-$LaPO_4$ (0/90 unitape lay-up)	C1-1	108(101[a])	38.0(35.7[a])	0.04
N610/ $LaPO_4$/Al_2O_3-$LaPO_4$ (0/90 unitape lay-up)	C2-1	108(134[a])	36.7(45.4[a])	0.03
	C2-3	104(129[a])	35.9(44.4[a])	0.04
	C2-5	108(134[a])	30.1(37.3[a])	0.03
N610/$LaPO_4$/Al_2O_3 (0/90 unitape lay-up)	C3-3	73.0	213	0.34
N610/$LaPO_4$/Al_2O_3 (8HSW)	C4-1	81.5(95.5[a])	67.6(79.2[a])	0.09
	C4-5	91.6(107[a])	84.9(99.4[a])	0.09
	C4-6*	94.1(110[a])	91.2(107[a])	0.12
N610/Al_2O_3 (8HSW)	C5-3	99.2	79.2	0.07
	C5-4	97.9	77.2	0.08
N610/$LaPO_4$/Al_2O_3-AlOCl (8HSW)	C6-4	80.6(88.5[a])	74.9(82.3[a])	0.07

* Test conducted in stress control with the stress rate of 15 MPa/s.
[a] Adjusted for V_f=0.39

Table 5.2, where elastic modulus, ultimate tensile strength (UTS) and failure strain are presented for specimens cut from each composite. To facilitate comparison of results obtained for different composites, all data are adjusted for $V_f = 0.39$. Specimen C4-6 was designated for creep testing and was therefore tested in stress control. However, specimen C4-6 failed before the desired creep stress level was reached. The results of the stress-controlled tensile loading of specimen C4-6 to failure are reported in Table 5.1.

Note that the N^{TM}610/Al_2O_3-$LaPO_4$ (composite C1) and the N610/ $LaPO_4$/Al_2O_3-$LaPO_4$ (composite C2) produced lower UTS values than composites C3, C4, C5, and C6. This is attributed to a considerable curvature noticed in panels of composites C1 and C2. Any such curvature (warp) in a tensile specimen is translated into bending stress when gripped. Thus,instead of a uniaxial tension, the specimen would be sub-

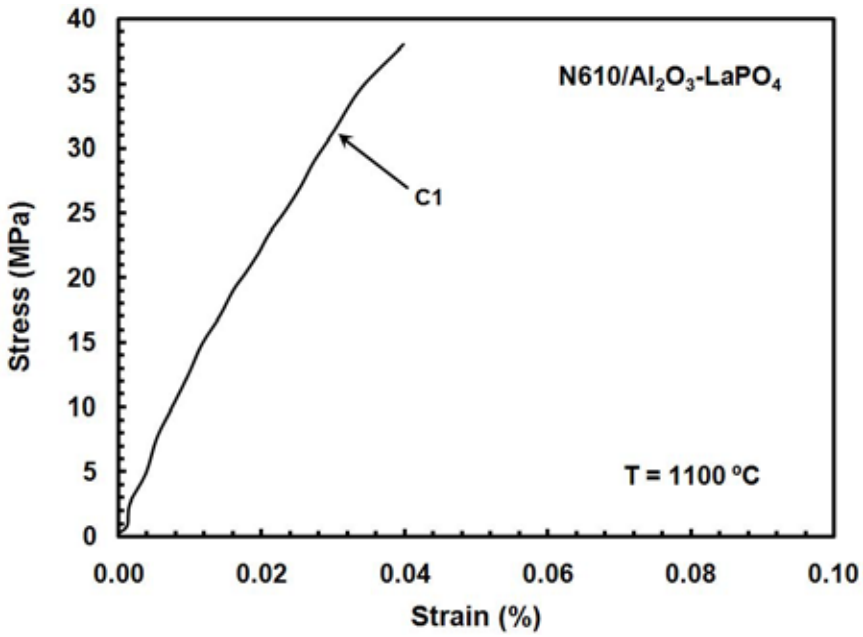

Figure 5.1: Tensile stress-strain curve for $N^{TM}610/Al_2O_3$-$LaPO_4$ composite with 0/90 unitape lay-up obtained at 1100 °C in laboratory air.

ject to combined tension and bending. Note that specimens of composites C1 and C2 also failed in the "shoulder" region, and not in the gage "shoulder" region, and not in the gage section. The curvature in specimens of composites C1 and C2 is likely the cause of early failures and low UTS values, as well as of failures outside the gauge section. In view of these considerations, the strength values obtained for composites C1 and C2 are not reliable.

Tensile stress-strain curves obtained for composites C1 and C2 at 1100 °C are shown in Fig.s 5.1 and 5.2, respectively.

To facilitate comparison between tensile stress-strain behaviors and tensile properties obtained for different composites, tensile stress-strain curves obtained for composites C3 and C4 are plotted together in Fig. 5.3. Likewise,tensile stress-strain curves obtained for composites C4 and C5 and those obtained for composites C4 and C6 are presented together in Fig.s 5.4 and 5.5, respectively. As seen in Figs. 5.3-5.5, the stress-strain curves produced by composites C3-C6 are nearly linear to failure. Yet results in Table 5.2 and in Fig.s 5.1-5.5 show that composite C3 exhibits consid-

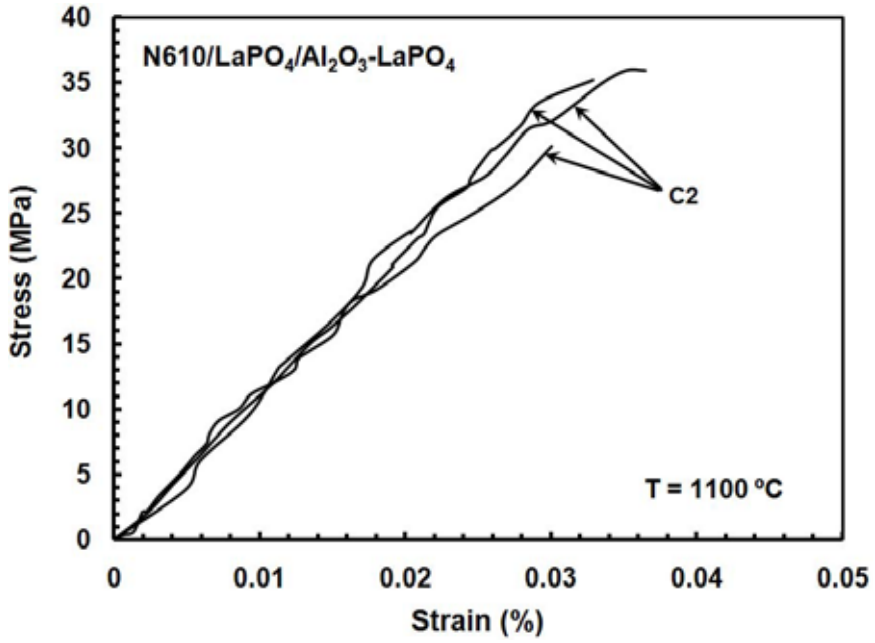

Figure 5.2: Tensile stress-strain curves for N^{TM}610/ $LaPO_4/Al_2O_3$-$LaPO_4$ composite with 0/90 unitape lay-up obtained at 1100 °C in laboratory air.

erably higher UTS than composites C4, C5 and C6. Conversely, elastic modulus of composite C3 is lower than that of composites C4-C6.

Consider tensile properties produced by composites C3 and C4 that have the same constituents, but different fiber architecture. The tensile strength of composite C3 is ∼2 times that of composite C4. However, it is unlikely that a woven composite would exhibit such significantly lower UTS values than the composite consisting of unidirectional layers in 0°/90° cross-ply lay-up. In fact, the opposite trend would be expected. Recall that in addition to having different fiber architectures, composites 3 and 4 had different processing condition. Therefore different methods used to coat the individual fibers in composite C3 and the woven fiber fabric in composite C4 are likely behind the much reduced tensile strength of the woven composite C4. Fair et al [13] reported that the loss of tensile strength of the woven cloth of Nextel^{TM}610 fibers due to coating with monazite by means of precipitation coating method was limited to 30%. Results of the present study reveal a much greater loss of tensile strength that may be attributable to the coating method. Because only a very limited number of

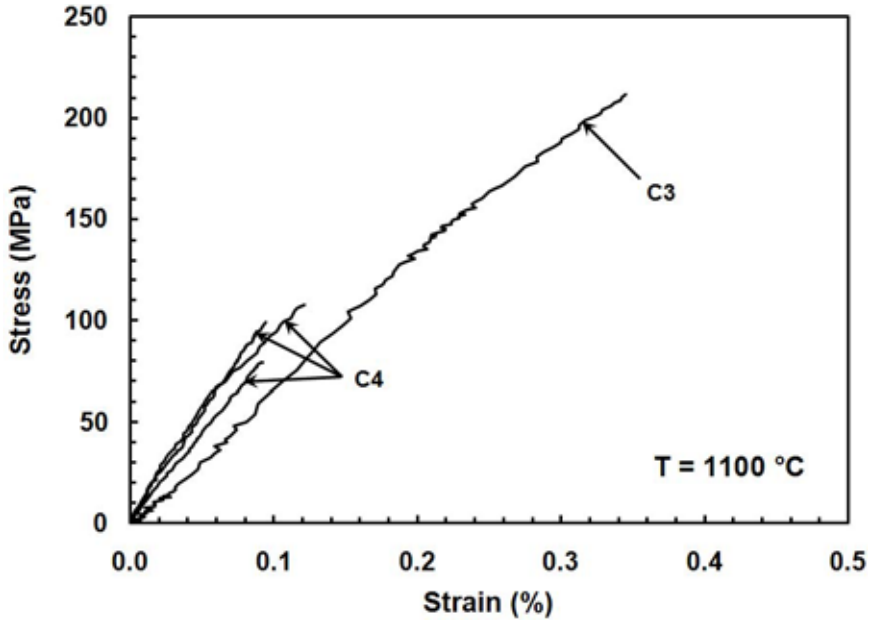

Figure 5.3: Tensile stress-strain curves for N^{TM}610/$LaPO_4$/Al_2O_3 composite (Composite 3) with 0/90 unitape lay-up and for N610/$LaPO_4$/Al_2O_3 woven composite (Composite 4) obtained at 1100 °C in laboratory air. All data are adjusted for V_f = 0.39.

specimens were available for testing, a larger number of specimens representing each of the composites C3 and C4 needs to be tested before a definitive conclusion can be reached regarding effects of coating method on tensile strength of the monazite-containing composite.

To assess the effect of monazite fiber coating on tensile properties of the woven composite, we compare results obtained for the monazite-containing composite C4 and the uncoated-fiber composite C5. Results in Table 5.2 and in Fig. 5.4 demonstrate that the addition of the monazite fiber coating results in 22% improvement in tensile strength and in 6% improvement in elastic modulus. To assess the effect of infiltration of the alumina matrix with AlOCl precursor on tensile properties of the woven composite, we compare results obtained for the composites C4 and C6. Results in Table 5.2 and in Fig. 5.5 show that the infiltration of the alumina matrix with AlOCl precursor result in near 15% decrease in elastic modulus and near 14% loss of tensile strength.

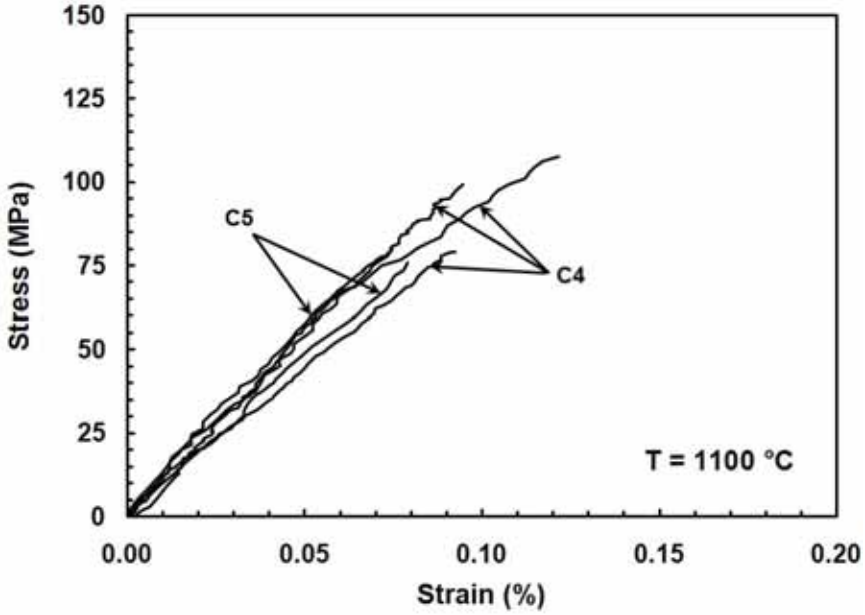

Figure 5.4: Tensile stress-strain curves for N^{TM}610/$LaPO_4$/Al_2O_3 woven composite (Composite 4) and for N^{TM}610/Al_2O_3 woven composite (Composite 5) obtained at 1100 °C in laboratory air. All data are adjusted for $V_f = 0.39$.

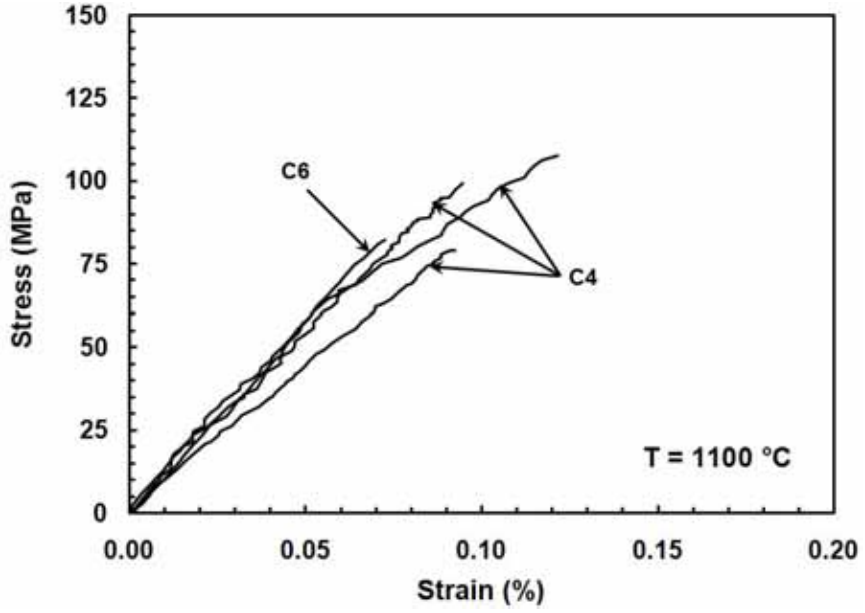

Figure 5.5: Tensile stress-strain curves for N^{TM}610/$LaPO_4$/Al_2O_3 woven composite (Composite 4) and for N^{TM}610/$LaPO_4$/Al_2O_3-$LaPO_4$-AlOCl woven composite (Composite 6) obtained at 1100 °C in laboratory air. All data are adjusted for $V_f = 0.39$.

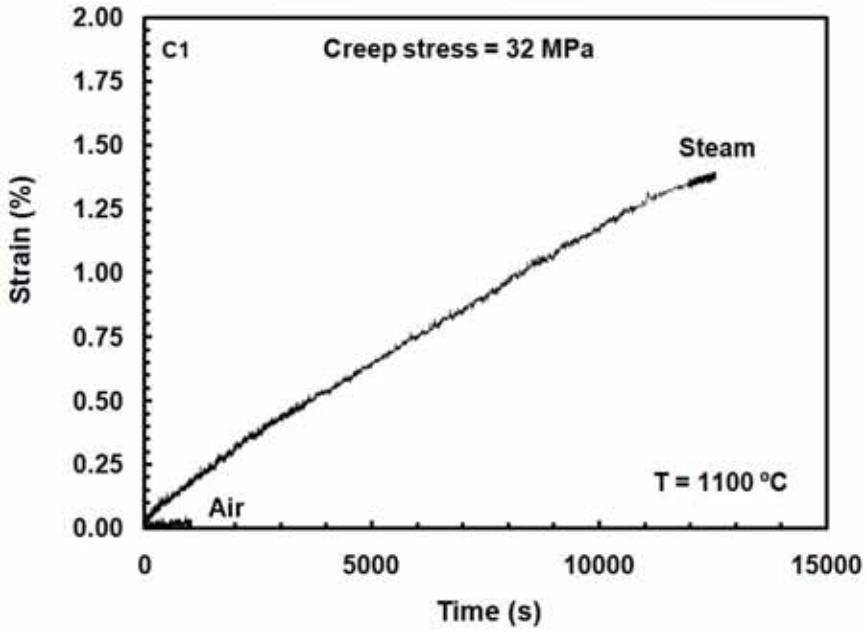

Figure 5.6: Creep strain vs time curves for N^{TM}610/Al_2O_3-$LaPO_4$ composite with 0/90 unitape lay-up obtained at 32 MPa at 1100 °C in laboratory air and in steam.

5.3 Creep-Rupture

Creep-rupture tests at various stress levels were conducted at 1100 °C in air and in steam on specimens from each composite. In all tests creep run-out was set to 100 h. Results of the creep-rupture tests are summarized in Table 5.3, where test environment, creep stress level, creep strain accumulation and time to rupture are presented for specimens cut from each composite. As the untested specimens of composites C1 and C2 were noticeably warped, only tests at creep stress levels of 32 and 25 MPa could be performed for composites C1 and C2, respectively. Attempts to perform creep tests at higher stress levels were unsuccessful. The test specimens failed before reaching the creep stress level. Failures of C1 and C2 specimens at fairly low stress levels are attributed to the curvature observed in the composite panels and, consequently, in the untested specimens. While results obtained for these two composites are presented in Table 5.3 and in Fig.s 5.6 and 5.7, they cannot be considered reliable or conclusive.

Table 5.3: Summary of creep-rupture results for the six oxide-oxide composites at 1100 °C.

Composite	Specimen	Environment	Creep Stress (MPa)	Creep Strain (%)	Time to Rupture (h)
N610/Al_2O_3- $LaPO_4$ (0/90 unitape lay-up)	C1-5	Air	32	0.02	0.028
	C1-2	Steam	32	1.35	3.45
N610/ $LaPO_4$/Al_2O_3- $LaPO_4$ (0/90 unitape lay-up)	C2-4	Air	25	0.01	0.01
	C2-2	Steam	25	1.78	40.1
N610/$LaPO_4$/Al_2O_3 (0/90 unitape lay-up)	C3-1	Air	85	3.07	16.2
	C3-4	Air	120	1.08	0.74
	C3-6	Steam	85	3.58	8.18
	C3-5	Steam	110	0.90	0.35
	C3-2	Steam	120	0.91	0.03
N610/$LaPO_4$/Al_2O_3 (8HSW)	C4-2	Air	32(37.5[a])	0.04	>100
	C4-7	Air	64(74.9[a])	0.17	>100
	C4-11	Air	72(84.3[a])	0.72	>100
	C4-3	Steam	32(37.5[a])	2.30	51.9
	C4-4	Steam	48(56.2[a])	1.92	7.58
	C4-8	Steam	64(74.9[a])	1.44	2.38
	C4-10	Steam	72(84.3[a])	2.35	2.24
N610/Al_2O_3 (8HSW)	C5-11[b]	Air	40.5	0.02	3.34
	C5-9	Air	61	0.06	3.42
	C5-7	Steam	20	0.08	3.53
	C5-8	Steam	30	0.06	16.1
	C5-6	Steam	40.5	0.02	0.01
N610/$LaPO_4$/Al_2O_3- AlOCl (8HSW)	C6-1	Air	32(35.2[a])	0.49	>100
	C6-3	Steam	32(35.2[a])	2.85	3.47
	C6-5	Steam	48(52.7[a])	2.68	2.06

[a] Adjusted for V_f=0.39

[b] Test interrupted due to equipment failure.

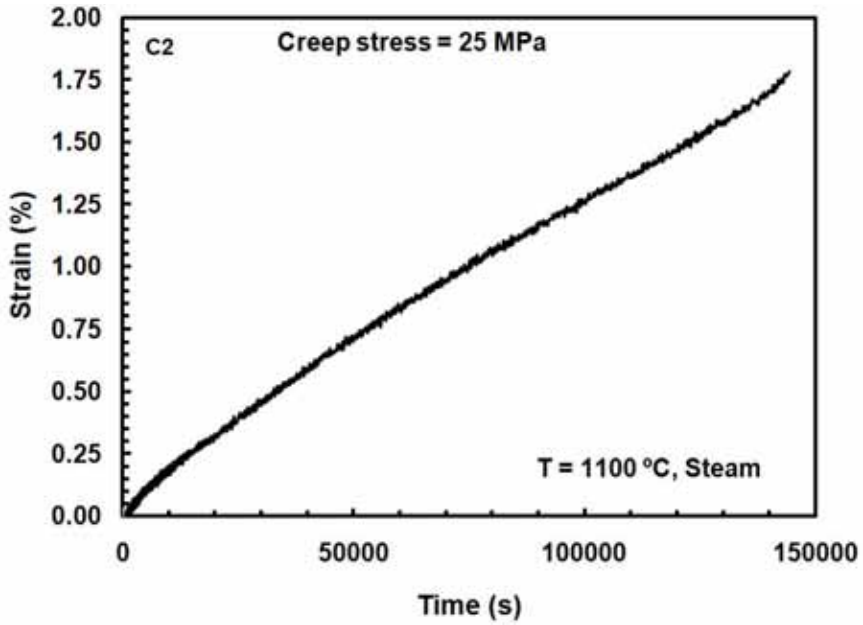

Figure 5.7: Creep strain vs time curve for N^{TM}610/ $LaPO_4/Al_2O_3$-$LaPO_4$ composite with 0/90 unitape lay-up obtained at 25 MPa at 1100 °C in steam.

Creep strain vs time curves for composite C3 obtained in air and in steam are shown in Fig. 5.8.

Primary and secondary creep regimes, but no tertiary creep regime, are observed in all tests. Creep test conducted at 110 MPa in steam represents an exception. In this test tertiary creep (albeit minimal) was observed. Note that creep run-out was not achieved in any of the tests. In both air and steam creep strain accumulation decreased as the applied stress increased. Creep strains produced at 85 MPa are an order of magnitude higher than the failure strain obtained in the tension test. Creep strains produced at the two higher stress levels were approximately three times the failure strain obtained in tension tests. Fig. 5.8 shows that test environment has little effect on the appearance of the creep curves obtained for the C3 composite. For a given creep stress, creep curves and creep strains obtained in air are comparable to those produced in steam.

Creep vs time curves obtained for composite C4 in air and in steam are presented in Fig. 5.9. Results in Table 5.3 and Fig. 5.9 show that creep run-out is achieved in

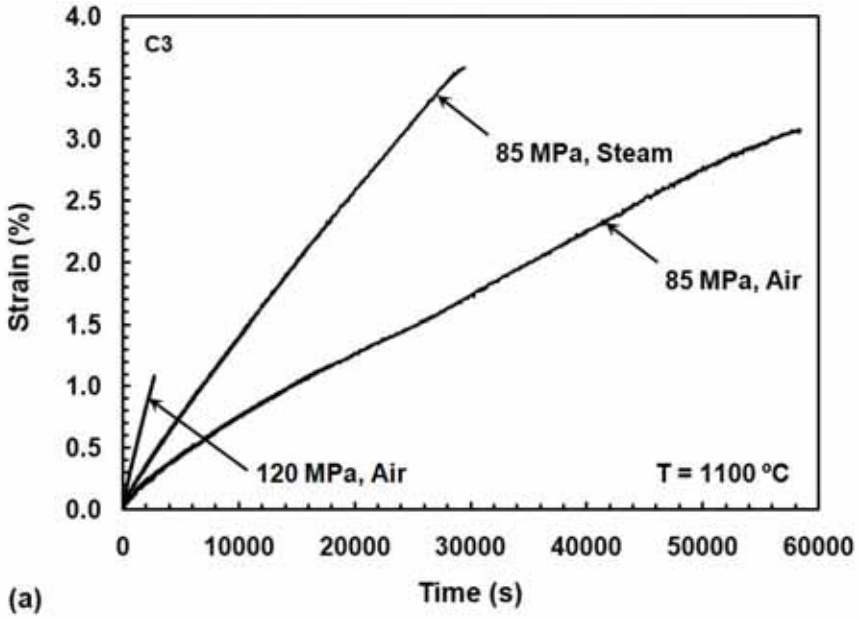

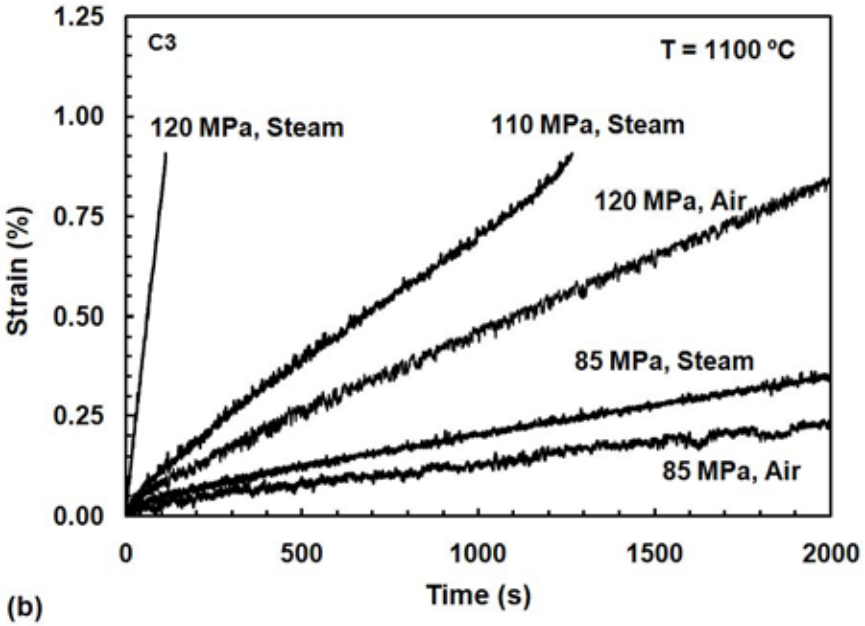

Figure 5.8: Creep strain vs time curves for N^{TM}610/ $LaPO_4/Al_2O_3$ composite (C3) with 0/90 unitape lay-up obtained at 1100 °C in laboratory air and in steam:(a) time scale is adjusted to clearly show the creep curves obtained at 85 MPa (b) time scale is adjusted to clearly show the creep curves obtained at 110 and 120 MPa in steam.

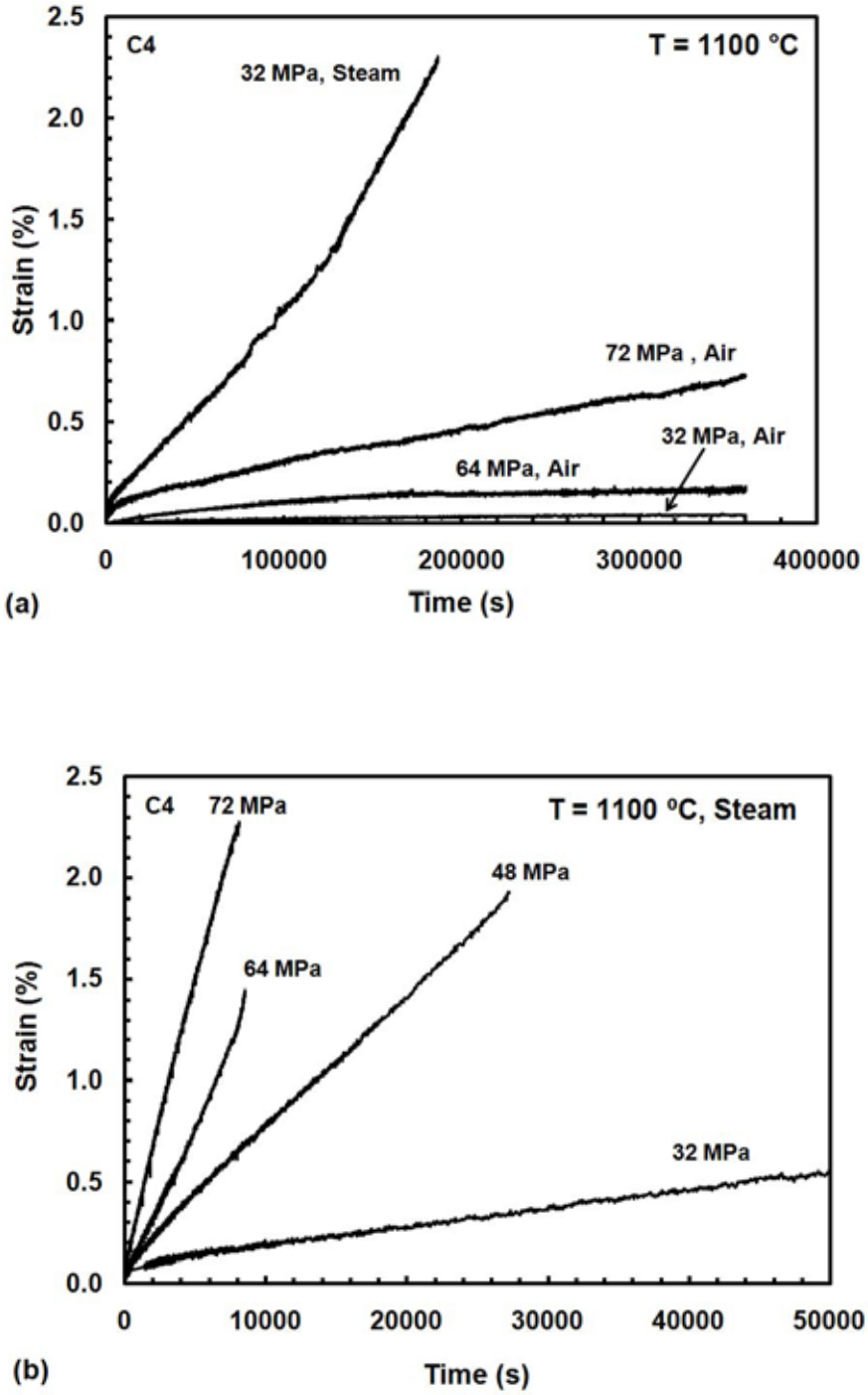

Figure 5.9: Creep strain vs time curves for $N^{TM}610/ LaPO_4/Al_2O_3$ woven composite (C4) obtained at 1100 °C in laboratory air and in steam: (a) time scale is adjusted to clearly show all creep curves obtained in air (b) time scale is adjusted to clearly show the creep curves obtained at 48, 64 and 72 MPa in steam.

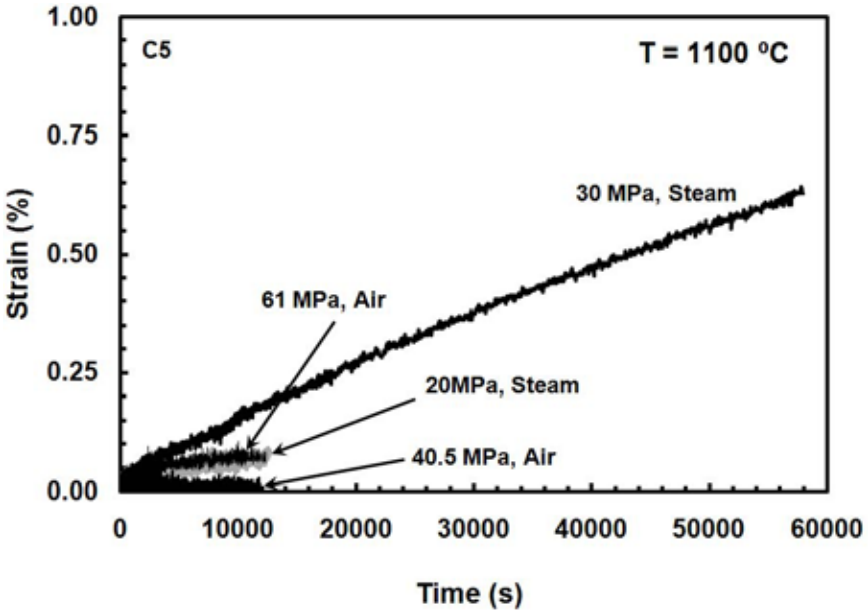

Figure 5.10: Creep strain vs time curves for $N^{TM}610/Al_2O_3$ woven composite (C5) obtained at 1100 °C in laboratory air and in steam.

all tests conducted in air. While creep strain accumulation increased with increasing applied stress, all creep strains accumulated in air were $\leq 0.72\%$. It is seen that creep strains produced at 64 and 72 MPa in air exceed the failure strain obtained in the tension test. Conversely, creep strain accumulated at 32 MPa is less than half the failure strain obtained in the tension test. The presence of steam has little effect on the appearance of the creep curves for the C4 composites. However, creep strains produced in steam are considerably higher (in some cases an order of magnitude higher) than those obtained in air for a given creep stress. Note that in steam creep-run-out was not achieved. The longest creep lifetime in steam was 51.9 h.

Creep curves obtained for C5 composite are shown in Fig. 5.10. Note that all specimens tested in air produced short lifetimes. Yet the creep curves produced in these tests suggest low creep rates consistent with longer lifetimes. Note that creep test conducted at 61 MPa in air was interrupted due to equipment malfunction. The specimen failed during the equipment shutdown. It is possible that a considerably longer lifetime could be achieved at 61 MPa in air. Likewise the test conducted at 40.5 MPa in air appears to have failed prematurely. The creep curve produced at 40.5 MPa

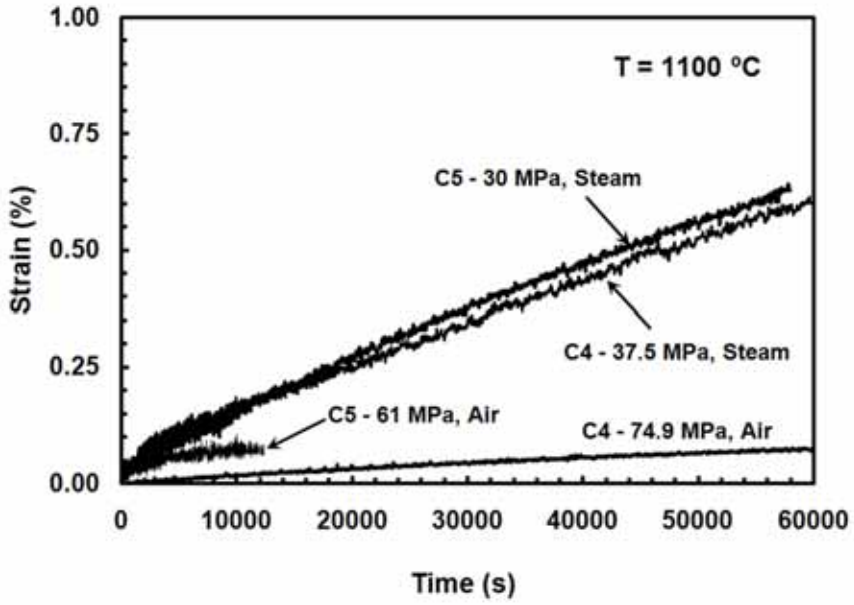

Figure 5.11: Creep strain vs time curves for N^{TM}610/ $LaPO_4/Al_2O_3$ woven composite (C4) and N^{TM}610/Al_2O_3 woven composite (C5) obtained at selected stress levels 1100 °C in laboratory air and in steam. Creep stress levels adjusted for $V_f = 0.39$.

in air is indicative of low strain rate and shows minimal creep strain accumulation. Note that specimen tested at 40.5 in air showed some limited delamination as well as curvature prior to testing. It is possible that creep run-out could be achieved at 40.5 MPa in air provided the specimen without defects could be tested. Unfortunately only a very limited number of specimens of composite C5 were available and several of them exhibited curvature before testing. It is believed that the specimen curvature is also the cause of a short lifetime produced at 20 MPa in steam. It is likely that a specimen without the initial curvature would produce a longer lifetime at 20 MPa in steam. To facilitate comparison between creep performance of composites C4 and C5, selected creep curves produced by both composites are shown in together in Fig. 5.11.

Results in Fig. 5.11 suggest that the addition of monazite in composite C4 has beneficial effects on creep performance in both air and steam environments. The creep curve produced by composite C4 at 74.9 MPa in air lies below the creep curve

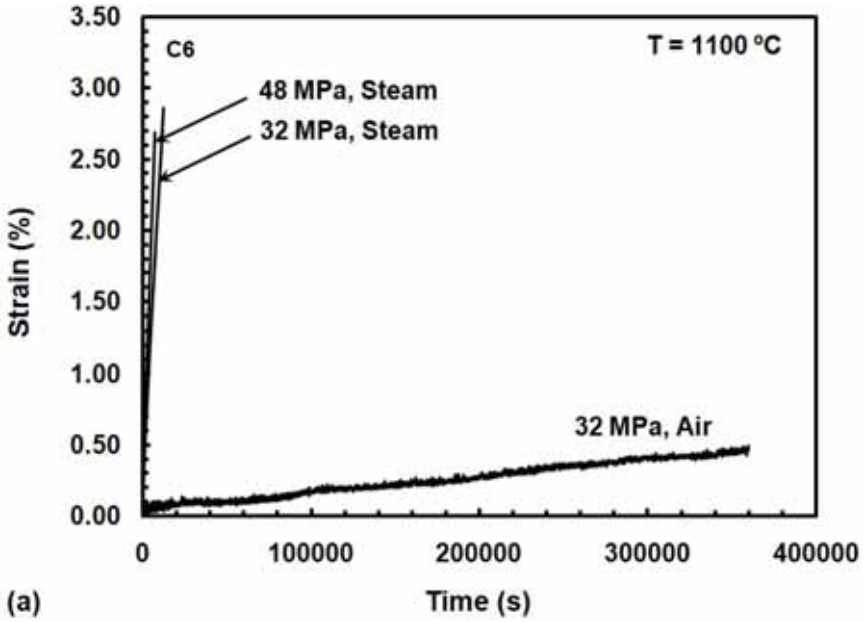

produced by composite C5 at a lower stress of 61 MPa in air, indicating lower creep strain accumulation in a given time. Likewise, the creep curve produced by composite C4 at 37.5 MPa in steam lies below the creep curve produced by composite C5 at a lower stress of 30 MPa in steam, a indicating somewhat lower creep rate for composite C4. The lifetime produced by the monazite-containing composite C4 at 37.5 MPa in steam is at least 3 times that produced by the uncoated fiber composite C5 at a lower stress of 30 MPa in steam.

Creep vs time curves obtained for composite C6 are shown in Fig. 5.12. It is seen that primary and secondary creep regimes are observed in all tests. Tertiary creep was not observed. In air, creep run-out was achieved at 32 MPa. Creep strain accumulated during 100 h at 32 MPa in air was 0.49%. Test environment had negligible effect on the form of creep curves produced by composite C6. Creep curves obtained in steam are qualitatively similar to those obtained in air. However, the presence of steam had a dramatic effect on creep strains. Creep strains accumulated at 32 and 48 MPa in steam approached an appreciable 3%. Moreover, in steam creep run-out was not achieved. Even at the low stress of 32 MPa composite C6 survived only 3.47 h in steam. This represents a near 97% reduction in creep lifetime due to steam.

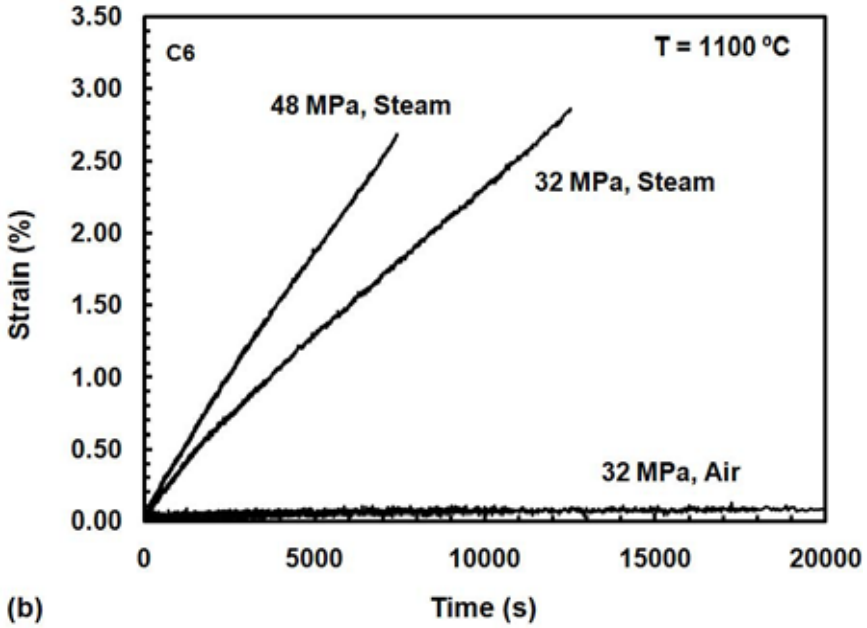

Figure 5.12: Creep strain vs time curves for N^{TM}610/$LaPO_4$/Al_2O_3-AlOCl woven composite obtained at 1100 °C in laboratory air and in steam: (a) time scale is adjusted to clearly show all creep curves obtained at 32 MPa in air (b) time scale is adjusted to clearly show the creep curves obtained at 32 and 48 MPa in steam.

To assess the effects of AlOCl infiltration of the alumina matrix on creep performance of the composite, results produced by composite C6 are compared to those produced by composite C4 in Fig. 5.13. It appears that infiltration of the alumina matrix with the AlOCl precursor did not result in improved creep performance. On the contrary, the creep curve produced by the composite C6 with the infiltrated matrix at 32 MPa (35.2 MPa for $V_f = 0.39$) lies not only above the creep curve produced by composite C4 with the uninfiltrated alumina matrix at 32 MPa (37.5 MPa for $V_f = 0.39$) in air (which is indistinguishable from the x-axis in Fig. 5.13, but also above the creep curve produced by composite C4 at that stress level in steam. Creep curves produced by the C6 composite at 32 MPa (37.5 MPa for $V_f = 0.39$) and at 48 MPa (52.7 MPa for $V_f = 0.39$) in steam also fall considerably above the creep curve produced by composite C4 at 48 MPa (56.2 MPa for $V_f = 0.39$) in steam.

Minimum creep rate was reached in all tests. Creep rate as a function of applied stress for composites C1 and C2 is presented in Fig.s 5.14 and 5.15, respectively. It

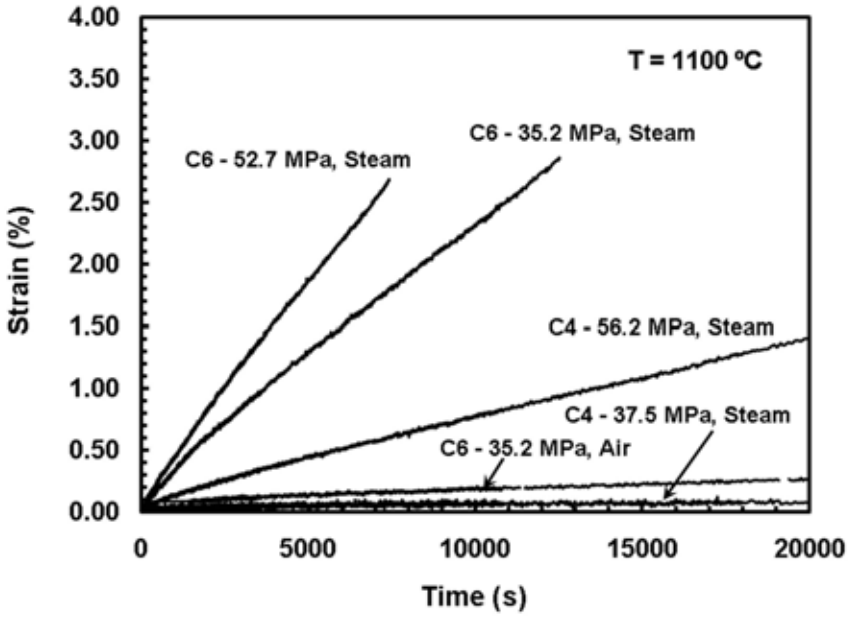

Figure 5.13: Creep strain vs time curves for for N^{TM}610/ $LaPO_4/Al_2O_3$ woven composite (C4) and for (C6) obtained at 1100 °C in laboratory air and in steam. Creep stress levels adjusted for $V_f = 0.39$.

is recognized that the results obtained for these two composites are likely biased due to the initial curvature present in the untested specimens. The results for composites C1 and C2 are included for completeness.

Minimum creep rate as a function of applied stress for composites C3 and C4 is presented in Fig. 5.16. In air, secondary creep rate for the C3 composite is almost two order of magnitude higher than that for the C4 composite at same stress level. Supporting this result, the woven composite C4 achieved a run-out at the adjusted stress level of 85 MPa (adjusted for $V_f = 0.39$), the unitape cross-ply composite C3 survived only 16.2 h at 85 MPa. In steam the secondary creep rates of the woven composite C4 can be slightly higher than those of the unitape cross-ply composite C3. This can be seen when comparing the creep strain rates produced by composites C3 and C4 at 85 MPa (adjusted for $V_f = 0.39$). It is seen that the creep strain rate of composite C4 is slightly higher than that produced by composite C3. The creep lifetimes produced by the two composites at 85 MPa (adjusted for $V_f = 0.39$) follow

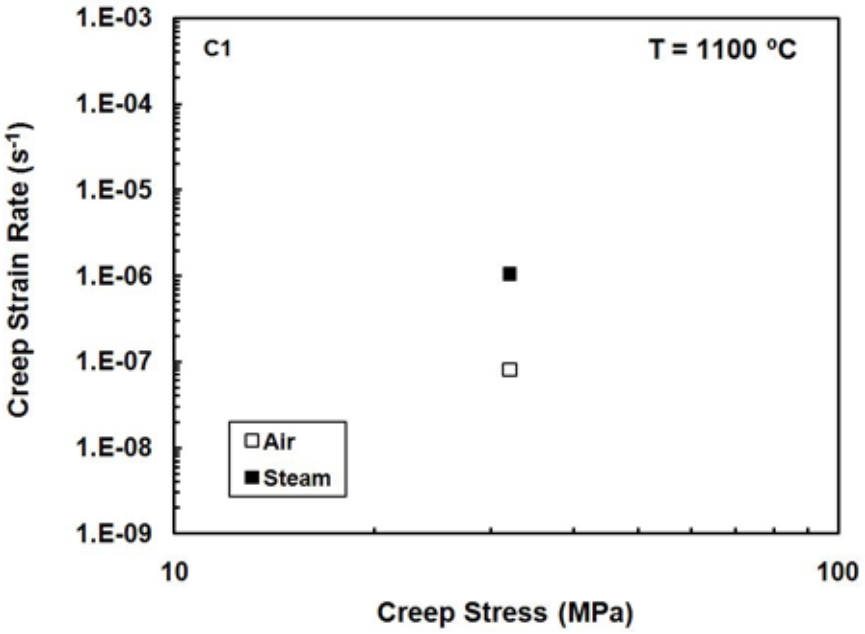

Figure 5.14: Minimum creep rate as a function of applied stress for N^{TM}610/Al_2O_3-$LaPO_4$ composite with 0/90 unitape lay-up at 1100 °C in laboratory air and in steam.

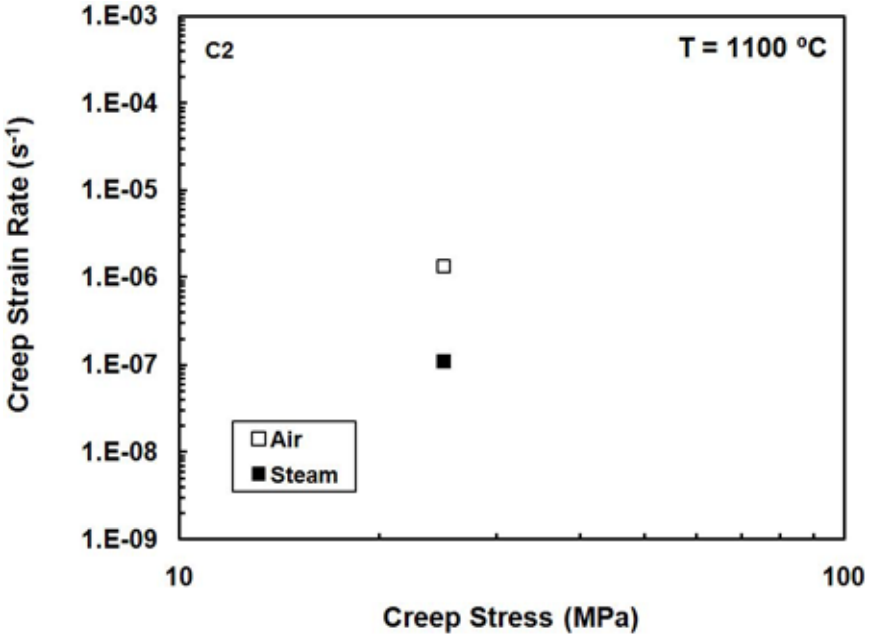

Figure 5.15: Minimum creep rate as a function of applied stress for N^{TM}610/ $LaPO_4$/Al_2O_3-$LaPO_4$ composite with 0/90 unitape lay-up at 1100 °C in laboratory air and in steam.

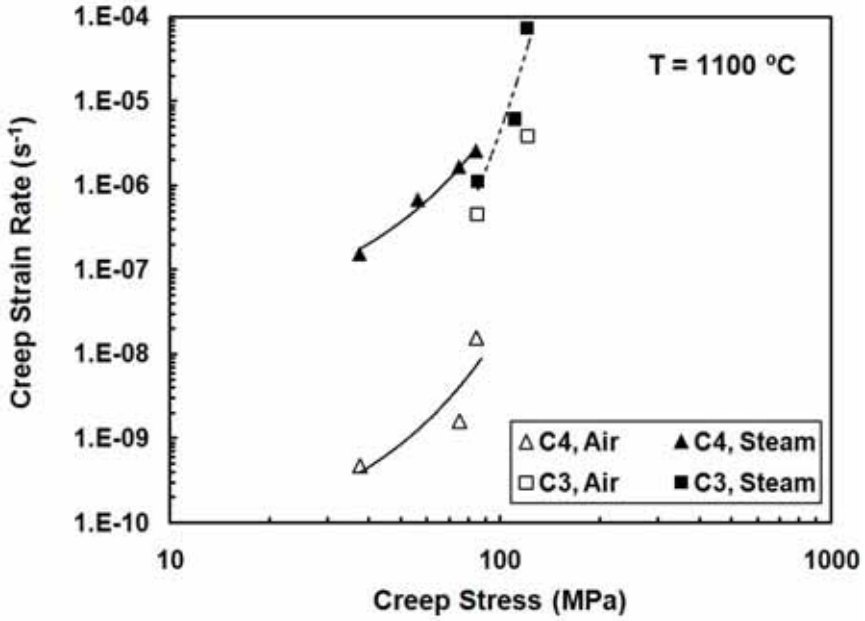

Figure 5.16: Minimum creep rate as a function of applied stress for N^{TM}610/ $LaPO_4/Al_2O_3$ composite C3 with 0/90 unitape lay-up and for N610/ $LaPO_4/Al_2O_3$ woven composite C4 at 1100 °C in laboratory air and in steam. Creep stress levels adjusted for $V_f = 0.39$.

a similar trend. While composite C3 survived 8.18 h, composite C4 failed after only 2.24 h at 85 MPa (adjusted for $V_f = 0.39$) in steam.

Minimum creep rate as a function of applied stress for composites C4 and C5 is presented in Fig. 5.17. In air, secondary creep rates for the C5 composite are almost one magnitude higher than those of the C4 composite. For example, at 32 MPa (37.5 MPa when adjusted for $V_f = 0.39$) the creep rate of the monazite-containing composite C4 was 4.77×10^{-10} s^{-1}, while the uncoated fiber composite C5 produced a creep rate of 4.68×10^{-9} s^{-1} at 40.5 MPa. The addition of monazite appears to improve secondary creep rates in air. In steam, the creep rate produced by the monazite-containing composite C4 at 32 MPa (37.5 MPa when adjusted for $V_f = 0.39$) was almost one magnitude lower than that produced by composite C5 at 40.5 MPa. In a similar trend, while the composite C4 survived 51.9 h at 32 MPa (37.5 MPa when adjusted for $V_f = 0.39$) in steam, the composite C5 with uncoated fiber structure survived only 36 s at 40.5 MPa in steam. Considerably longer creep lifetime exhibited

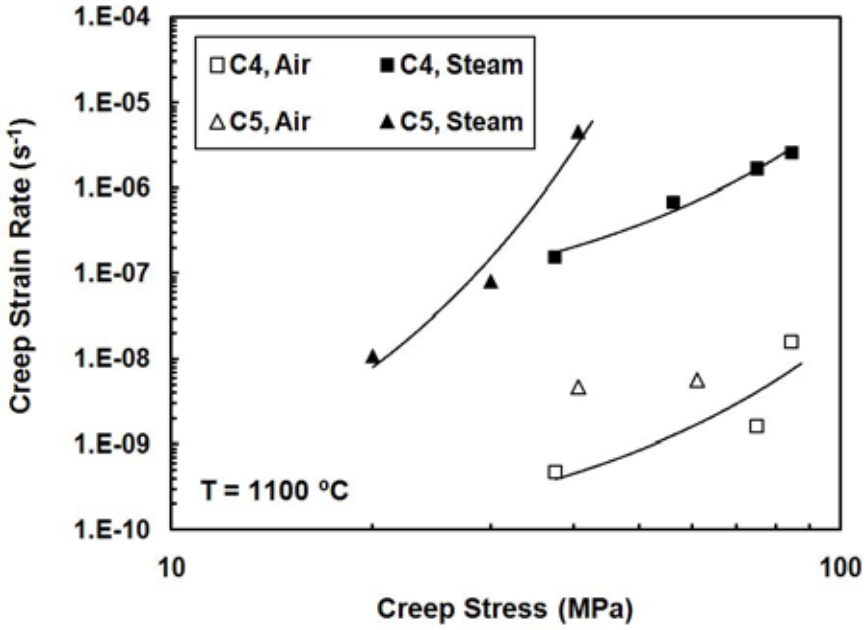

Figure 5.17: Minimum creep rate as a function of applied stress for N^{TM}610/ $LaPO_4/Al_2O_3$ woven composite C4 and for N610/Al_2O_3 woven composite C5 at 1100 °C in laboratory air and in steam. Creep stress levels adjusted for levels adjusted for $V_f = 0.39$.

by composite C4 suggests that the addition of monazite has beneficial effects on creep lifetime in steam environment.

Minimum creep rate as a function of applied stress for composites C4 and C6 is presented in Fig. 5.18. In air, secondary creep rate for the composite C6 is almost one magnitude higher than that of the composite C4 at similar stress level. However, both specimens achieved run out. In the same manner, in steam secondary creep rates of the composite C6 with the AlOCl infiltrated matrix are approximately an order or magnitude higher than those of the C4 composite with an uninfiltrated alumina matrix. For example the creep rate of the monazite-containing C4 at 32 MPa (37.5 MPa when adjusted for $V_f = 0.39$) was almost one magnitude lower than that produced by composite C6 at 32 MPa (35.2 MPa when adjusted for $V_f = 0.39$). Supporting this result,specimen from composite C4 survived 51.9 h while the specimen from composite C6 survived 3.47 h, in steam. For the specimen from composite C4 tested at 48 MPa (56.2 MPa when adjusted for $V_f = 0.39$)in steam, secondary creep

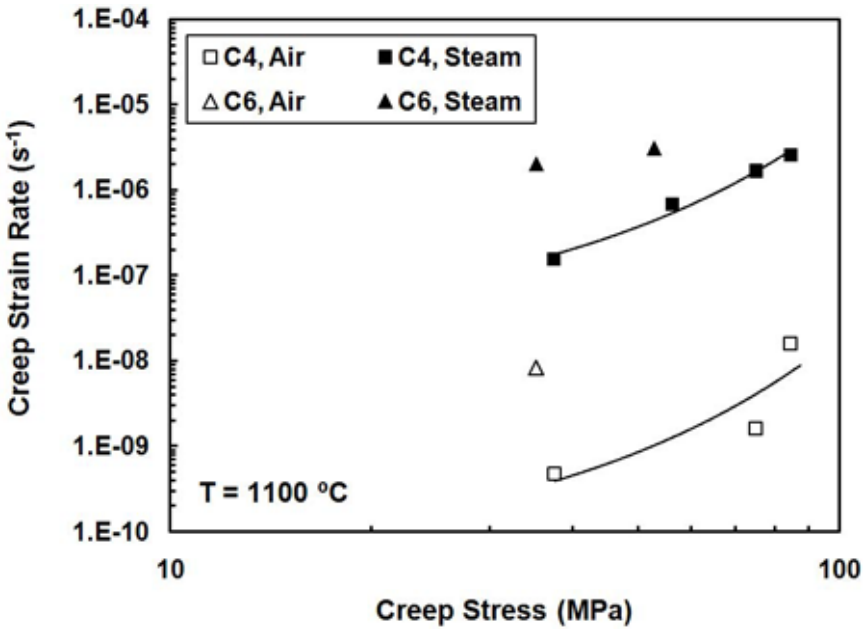

Figure 5.18: Minimum creep rate as a function of applied stress for N^{TM}610/ $LaPO_4/Al_2O_3$ woven composite C4 and for N^{TM}610/$LaPO_4/Al_2O_3$-AlOCl woven composite C6 at 1100 °C in laboratory air and in steam. Creep stress levels adjusted for $V_f = 0.39$.

strain rate was almost five times lower than the specimen from composite C6 tested at 48 MPa (52.7 MPa when adjusted for $V_f = 0.39$)in steam. In this case creep lifetimes are more comparable. Specimen from composite C4 survived 7.58 h while the specimen from composite C6 survived 2.06 h. It seems that matrix infiltration with AlOCl degraded the creep rate and creep life performance of the material.

Stress-rupture behaviors of composites C3 and C4 are summarized in Fig. 5.19. It is seen that creep life of both composites decreases with applied stress. The precipitation method of coating fiber fabric in Composite 4 did not appear to have a detrimental effect on creep lifetimes in air. On the contrary, at 84.3 MPa (adjusted for $V_f = 0.39$) the woven composite C4 achieved creep run-out, while the unitape cross-ply composite C3 failed after 16.2 h at 85 MPa. The presence of steam degraded the creep lifetimes of both composites. For the unitape cross-ply composite C3, reduction in creep lifetime due to steam was ∼50% at the lowest stress of 85 MPa. At the highest stress level of 120 MPa, the creep lifetime was reduced by at least an

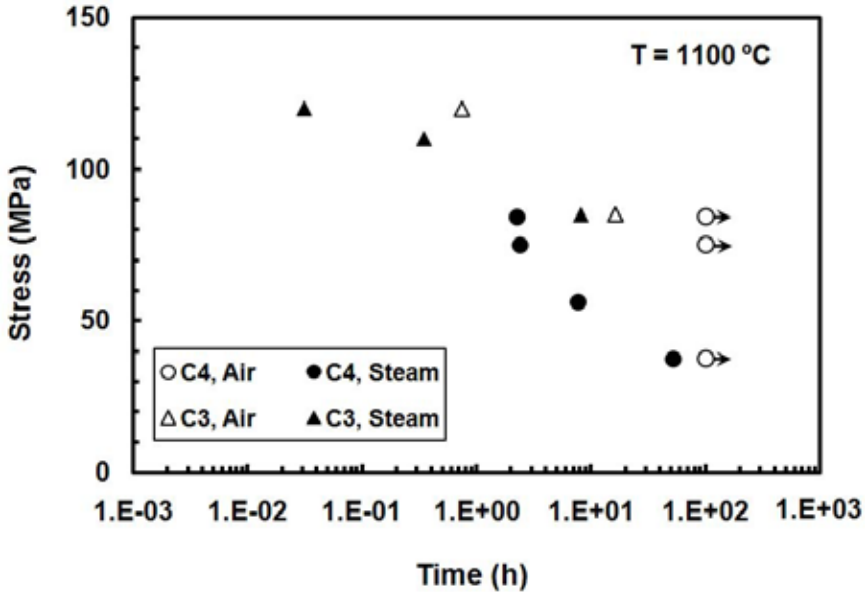

Figure 5.19: Creep stress vs time to rupture for N^{TM}610/ $LaPO_4/Al_2O_3$ composite C3 with 0/90 unitape lay-up and for N^{TM}610/ $LaPO_4/Al_2O_3$ woven composite C4 at 1100 °C in laboratory air and in steam. Creep stress levels adjusted for $V_f = 0.39$.

order of magnitude in the presence of steam. In the case of the woven composite C4, the reduction in creep lifetime due to steam was ∼50% at 37.5 MPa (adjusted for $V_f = 0.39$) and over 90% at stress level 56.2 MPa (adjusted for $V_f = 0.39$).

Stress-rupture behaviors of composites C5 and C4 are summarized in Fig. 5.20. As mentioned earlier in this chapter, specimen of composite C5 tested at 61 MPa in air failed prematurely due to equipment malfunction. It is possible that a longer creep lifetime may have been achieved in this test. A short creep lifetime of the C5 specimen tested at 40.5 MPa in air also may be due to some limited delamination as well as curvature observed in the specimen prior to testing. The short creep lifetime of the C5 specimen tested at 20 MPa in steam is also likely caused by curvature present in the specimen prior to testing. A more reliable assessment of the effects of monazite on creep lifetime can be made by comparing the results produced by the monazite-containing composite C4 at 37.5 MPa (adjusted for $V_f = 0.39$) in steam and those obtained for the uncoated fiber composite C5 at 30 MPa in steam. In this case the addition of monazite significantly improves creep lifetime in steam, with

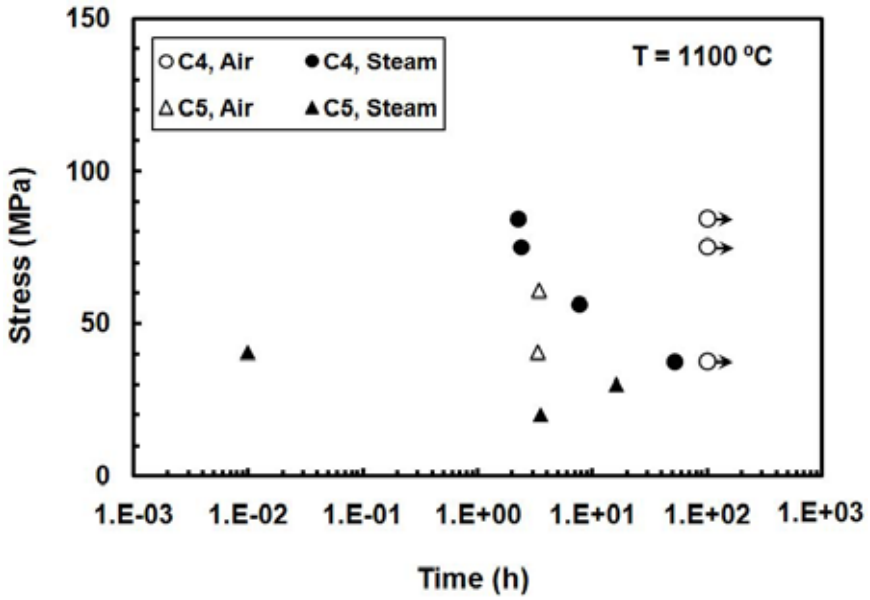

Figure 5.20: Creep stress vs time to rupture for N^{TM}610/ $LaPO_4/Al_2O_3$ woven composite C4 and for N^{TM}610/Al_2O_3 woven composite C5 at 1100 °C in laboratory air and in steam. Creep stress levels adjusted for $V_f = 0.39$.

creep lifetime of composite C4 being at over 3 times that of composite C5. The effect of matrix infiltration with the AlOCl precursor on creep-rupture behavior of the N^{TM}610/ $LaPO_4/Al_2O_3$ material system can be evaluated by examining the creep stress vs time to rupture curves for composites C4 and C6 presented in Fig. 5.21. In air both composites achieved creep run-out at the lowest stress levels. In steam, creep lifetime of each composites decreases with applied stress. However, the reduction in creep life due to steam appears to be much more pronounced in the case of composite C6 with the AlOCl-infiltrated matrix. For composite C4 the reduction in creep life due to steam at 37.5 MPa (adjusted for $V_f = 0.39$) was ∼50%, while for composite C6 the reduction in creep life due to steam at 35.2 MPa (adjusted for $V_f = 0.39$) was ∼97%.

Retained strength and modulus of the specimens that achieved run-out are summarized in Table 5.4. Stress-strain curves obtained for composite C4 and composite C6 specimens subjected to prior creep are shown in Fig.s 5.22 and 5.23, respectively. Stress-strain curves for the as-processed materials are included for comparison.

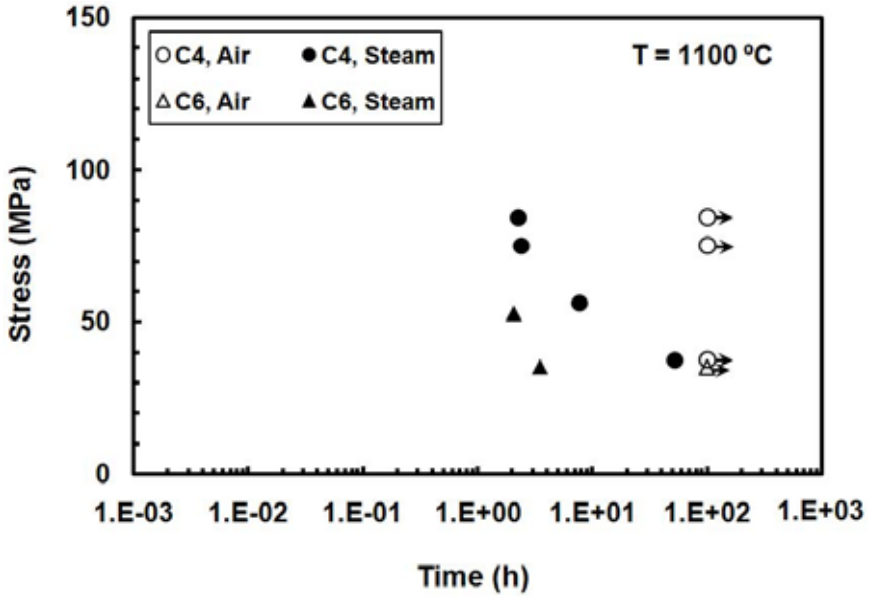

Figure 5.21: Creep stress vs time to rupture for N^{TM}610/ $LaPO_4/Al_2O_3$ woven composite C4 and for N^{TM}610/$LaPO_4/Al_2O_3$-AlOCl woven composite C6 at 1100 °C in laboratory air and in steam. Creep stress levels adjusted for $V_f = 0.39$.

Table 5.4: Retained tensile properties of the N^{TM}610/$LaPO_4/Al_2O_3$ (8HSW) oxide-oxide composite subjected to prior tensile creep at 1100 °C in laboratory air. All data are adjusted for $V_f = 0.39$.

Composite	**Specimen**	**Creep Stress(MPa)**	**Retained Strength (MPa)**	**Retained Modulus (GPa)**	**Failure Strain(%)**
Nextel610/$LaPO_4$/ Al_2O_3	C4-2	37.5	112	103	0.12
	C4-7	74.9	139	105	0.12
	C4-11	84.3	134	71.9	0.16
Nextel610/$LaPO_4$/ Al_2O_3-AlOCl	C6-1	35.2	82.9	90.0	0.07

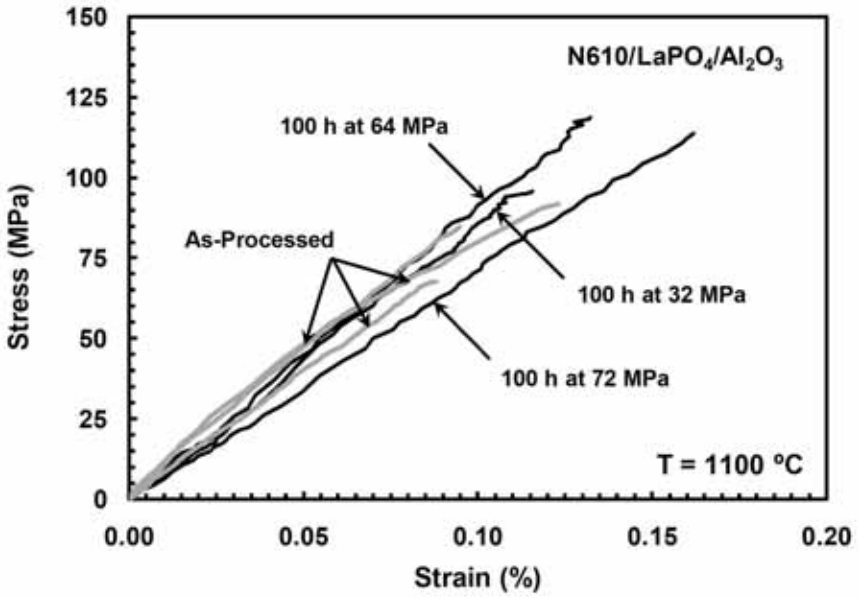

Figure 5.22: Effects of prior creep at 1100 °C in air on tensile stress-strain behavior of N^{TM}610/ $LaPO_4/Al_2O_3$ woven composite C4 at 1100 °C.

The composite C4 specimen subjected to 100 h of prior creep at 32 MPa (equivalent to 37.5 MPa for $V_f = 0.39$) in air showed a 17% increase in tensile strength, Loss in elastic modulus was less than 1%. After 100 h of prior creep in air at 64 MPa (equivalent to 74.9 MPa for $V_f = 0.39$), the tensile strength of the C4 composite is increased by 45.5% and the elastic modulus is increased by 1%. After 100 h of prior creep in air at 72 MPa (equivalent to 84.3 MPa for $V_f = 0.39$), the tensile strength of the C4 composite is increased by 40.3%, but the elastic modulus is reduced by 30.8%. Failure strains of the pre-crept specimens are somewhat larger than those obtained for the as-processed material, which is consistent with the higher strength values and similar or lower modulus values exhibited by the pre-crept specimens. Results in Fig. 5.22 reveal that the stress-strain behavior of the composite C4 is not significantly affected by prior creep. The stress-strain curves produced by the pre-crept specimens are nearly linear to failure as are the stress-strain curves produced by the as-processed material.

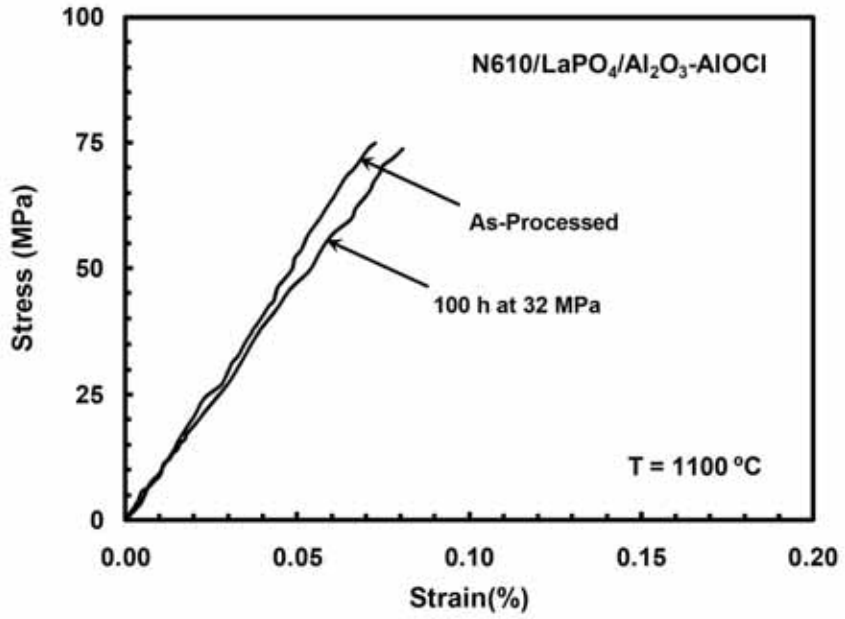

Figure 5.23: Effect of prior creep at 1100 °C in air on tensile stress-strain behavior of N^{TM}610/$LaPO_4$/Al_2O_3-AlOCl woven composite C6 at 1100 °C.

As evidenced by the results in Table 5.4 and in Fig. 5.23, the strength and modulus of composite C6 appear to be little affected to prior creep in air. After 100 h of prior creep at 32 MPa (equivalent to 35.2 MPa for $V_f = 0.39$) in air, the strength increased by less than 1% and the modulus increased by less than 2%.

5.4 Composite Microstructure

Microstructural investigation was conducted in order to explore damage and degradation mechanisms behind mechanical performance. Composite microstructure and fracture surfaces of all specimens examined using optical microscope. Further understanding of the influence of elevated temperature and oxidizing environment on microstructure of the composites is gained by examining the SEM images. To facilitate comparison of results obtained for different composites, all data are adjusted for V_f = 0.39

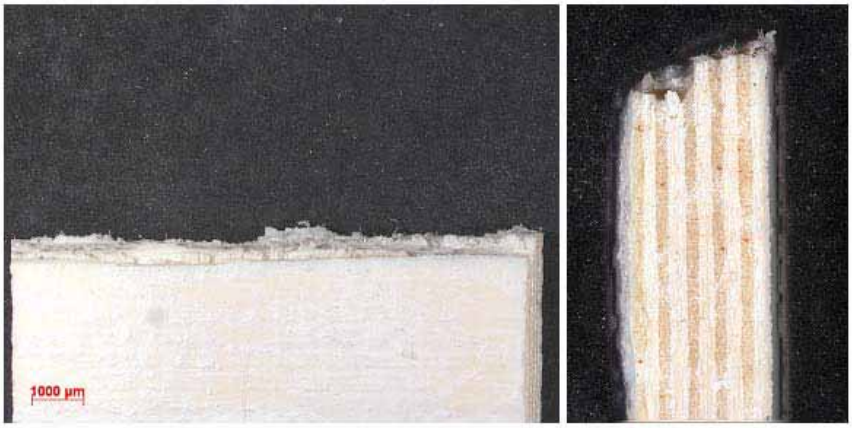

Figure 5.24: Fracture surface of C1 composite specimen tested in tension to failure at 1100 °C in laboratory air: (a) front view and (b) side view.

5.4.1 Composites C1 and C2. Optical images of the specimens tested in air and in steam of the composites C1 and C2 can be seen in Fig.s 5.24, 5.25, 5.26. All specimens exhibited largely planar fracture surfaces devoid of fiber pull out. Damage zones were very short. Even the specimen C2-2 which survived for 40.1 h at 25 MPa in steam had damage zone less than 1 *mm* in length. Planar fracture surfaces may be attributed to the reduced matrix porosity and subsequent matrix densification due to additional sintering. As mentioned earlier, because the untested specimen of composites C1 and C2 were bent the results obtained for composites C1 and C2 are not conclusive. The discussion of microstructure of composites C1 and C2 is offered here for completeness.

5.4.2 Composites C3 and C4. Optical micrographs of C3 and C4 specimens subjected to monotonic tensile tests can be seen in Fig.s 5.27, 5.28. Specimen C3-3 exhibited brushy failure surface with discernable fiber pull out. Damage zone reached 10 *mm* in length. However specimen C4-5 produced a predominantly planar fracture surface. Hardly any fiber pull out was visible. The damage zone of the specimen C4-5 was noticeably shorter than that of C3-3 and is limited to 2 *mm* in length. Both specimens exhibited multiple fracture planes which suggest that a single crack front did not cause the failure.

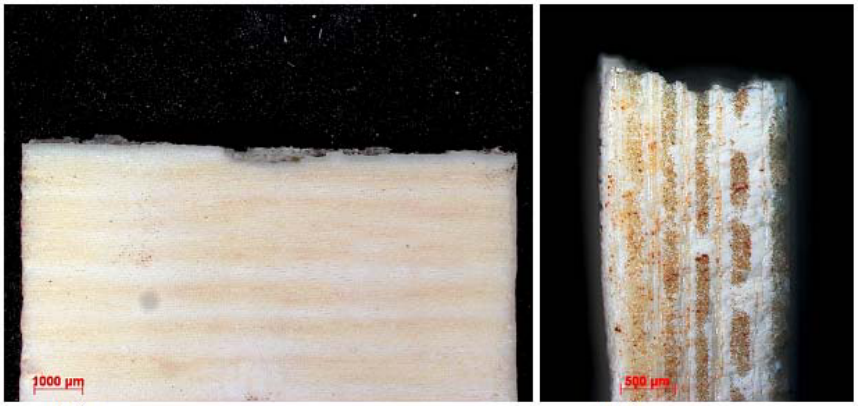

Figure 5.25: Fracture surface of C2 composite specimen tested in tension to failure at 1100 °C in laboratory air: (a) front view and (b) side view.

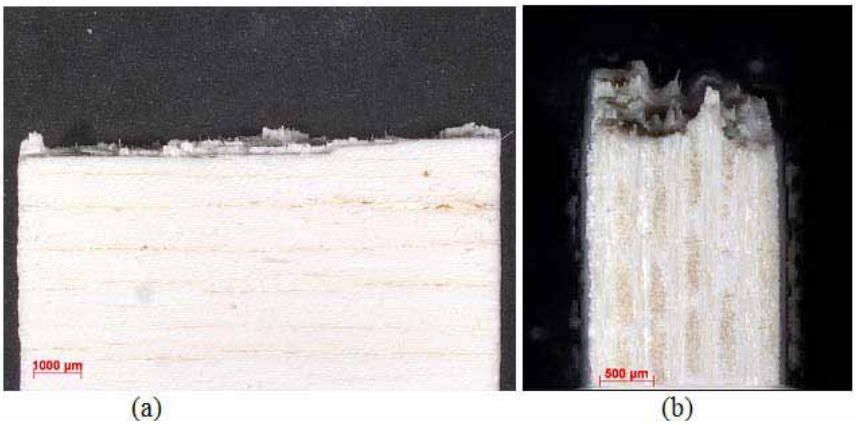

Figure 5.26: Fracture surface of C2 composite specimen tested in creep at 25 MPa at 1100 °C in laboratory air (t_f = 40.1 h): (a) front view and (b) side view.

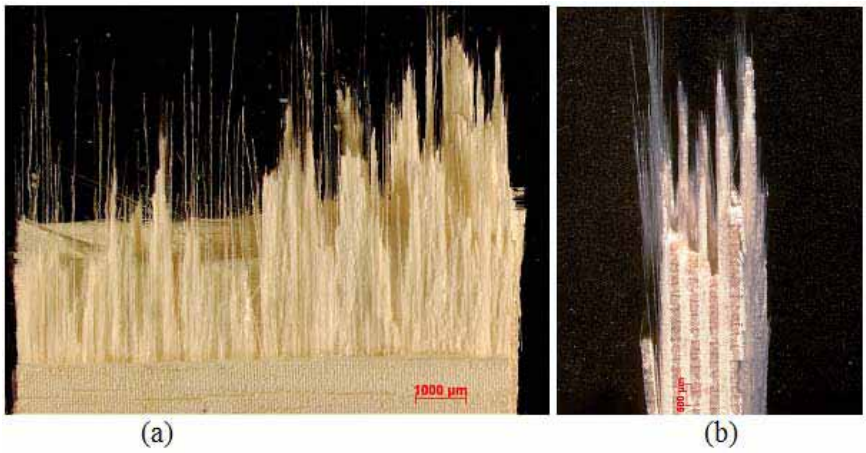

Figure 5.27: Fracture surface of C3 composite specimen tested in tension to failure at 1100 °C in laboratory air: (a) front view and (b) side view.

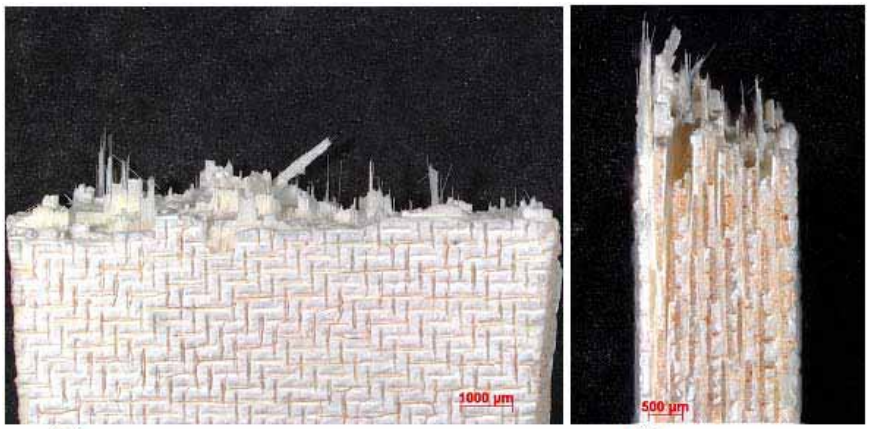

Figure 5.28: Fracture surface of C4 composite specimen tested in tension to failure at 1100 °C in laboratory air: (a) front view and (b) side view.

In all creep tests specimens of composite C3 produced brushy fracture surfaces (see Fig.s 5.27, 5.29, 5.33, 5.37, 5.39). However, this was not the case for composite C4. Fracture surfaces of composite C4 were predominantly planar with very limited amount of fiber pull out. As seen in Fig.s 5.30, 5.34, 5.48, 5.42, the damage zones were limited to 3 mm. It is instructive to compare the fracture surfaces produced by specimen C3-1 tested in creep at 85 MPa in air (see Fig. 5.29) and specimen C4-11 tested at in creep at 84.3 MPa (see Fig. 5.30). Specimen C3-1 exhibited a somewhat more brushy fracture surface with limited fiber pull out, while specimen C4-11 showed a nearly planar fracture surface. The damage zone of specimen C3-1 was nearly three times longer than that of the specimen C4-11. Note that specimen C3-1, which survived only 16.2 h at creep stress, produced a considerably shorter lifetime than specimen C4-11, which achieved creep run-out of 100 h. Uncoordinated fiber failures for both 0° and 90° fibers as well as nearly planar fracture regions can be seen in SEM image of specimen C3-1 in Fig. 5.31a. Fig. 5.32a shows that specimen C4-11 produced a predominantly planar fracture surface. It can be seen from the image in Fig. 5.31b that in the case of specimen C3-1 the amount of matrix attached to the fibers is less than that observed for specimen C4-11 (Fig. 5.32d). This may be attributed to the differences in processes used to apply monazite coating to the

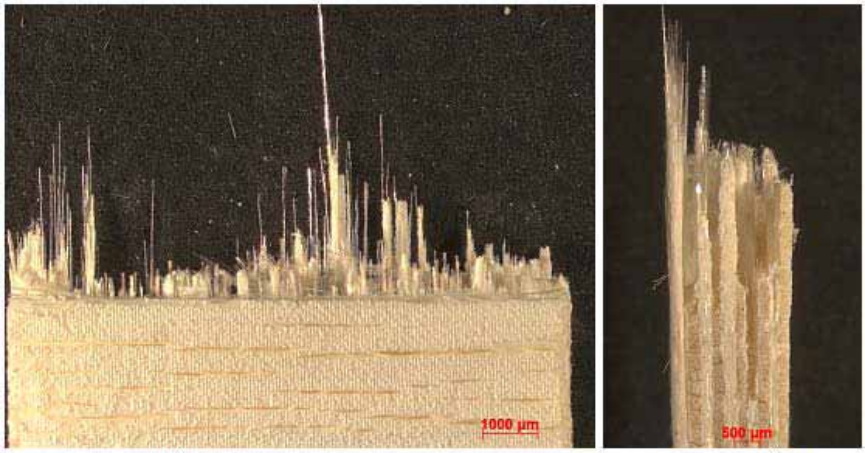

Figure 5.29: Fracture surface of C3 composite specimen tested in creep at 85 MPa at 1100 °C in laboratory air (t_f = 16.2 h): (a) front view and (b) side view.

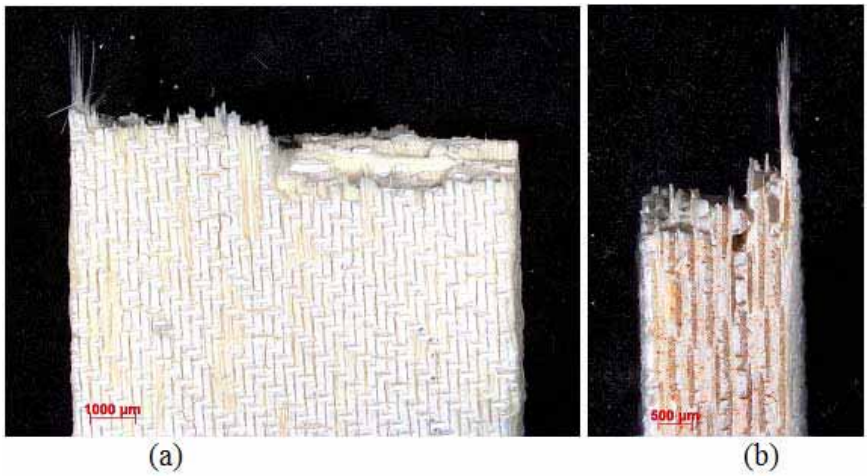

Figure 5.30: Fracture surface of C4 composite specimen tested in creep at 84.3 MPa at 1100 °C in laboratory air ($t_f > 100$ h): (a) front view and (b) side view

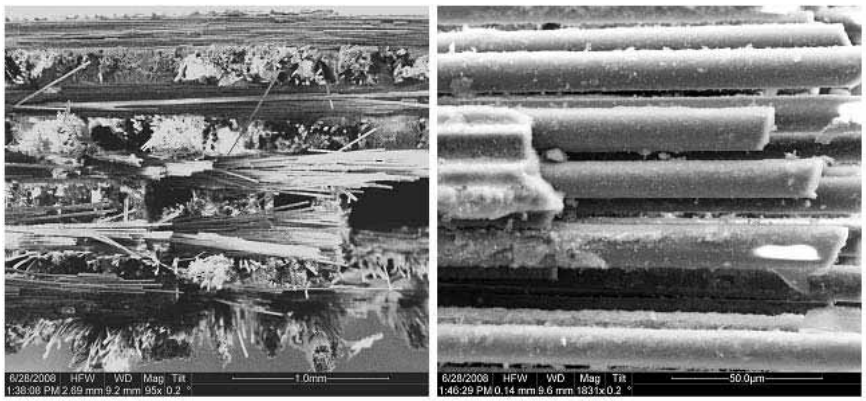

Figure 5.31: SEM micrographs of the fracture surface of C3 composite specimen tested in creep at 85 MPa at 1100 °C in laboratory air (t_f = 16.2 h).

fibers of composites C3 and C4. Like other specimens of composite C4, specimen C4-11 exhibited large matrix-rich areas (Fig.s 5.32c, 5.36b-c, 5.50c), which were not observed in composite C3 and are unlikely to improve composite performance. It is possible that such proliferation of matrix-rich areas as that observed in composite C4 could be avoided with careful composite processing. The findings were similar for the same stress levels in steam environment. Fig. 5.33 shows that specimen C3-6, tested at 85 MPa in steam, shows brushy fracture surface along with planar regions. Fracture surface was more complex and longer than C3-1 which was expected due to harsh environment. In the same manner Fig. 5.34 shows that specimen C4-10 exhibited longer damage zone and fiber bundles than the specimen C4-11 which can be attributed to steam environment. However also C4-10 exhibited less fiber pull out and more planar fracture surface than specimen C3-6. SEM images of both specimens supports the observations made by optical micrographs (see Fig.s 5.35, 5.36). Images for both specimens showed that matrix kept its shape after fiber pull out. This can be seen more apparently from Fig. 5.36b of specimen C4-10 where matrix formed troughs existed. This may be an indication of reduced matrix porosity and subsequent matrix densification due to additional sintering which can severely affect crack deflection capability of the composite.

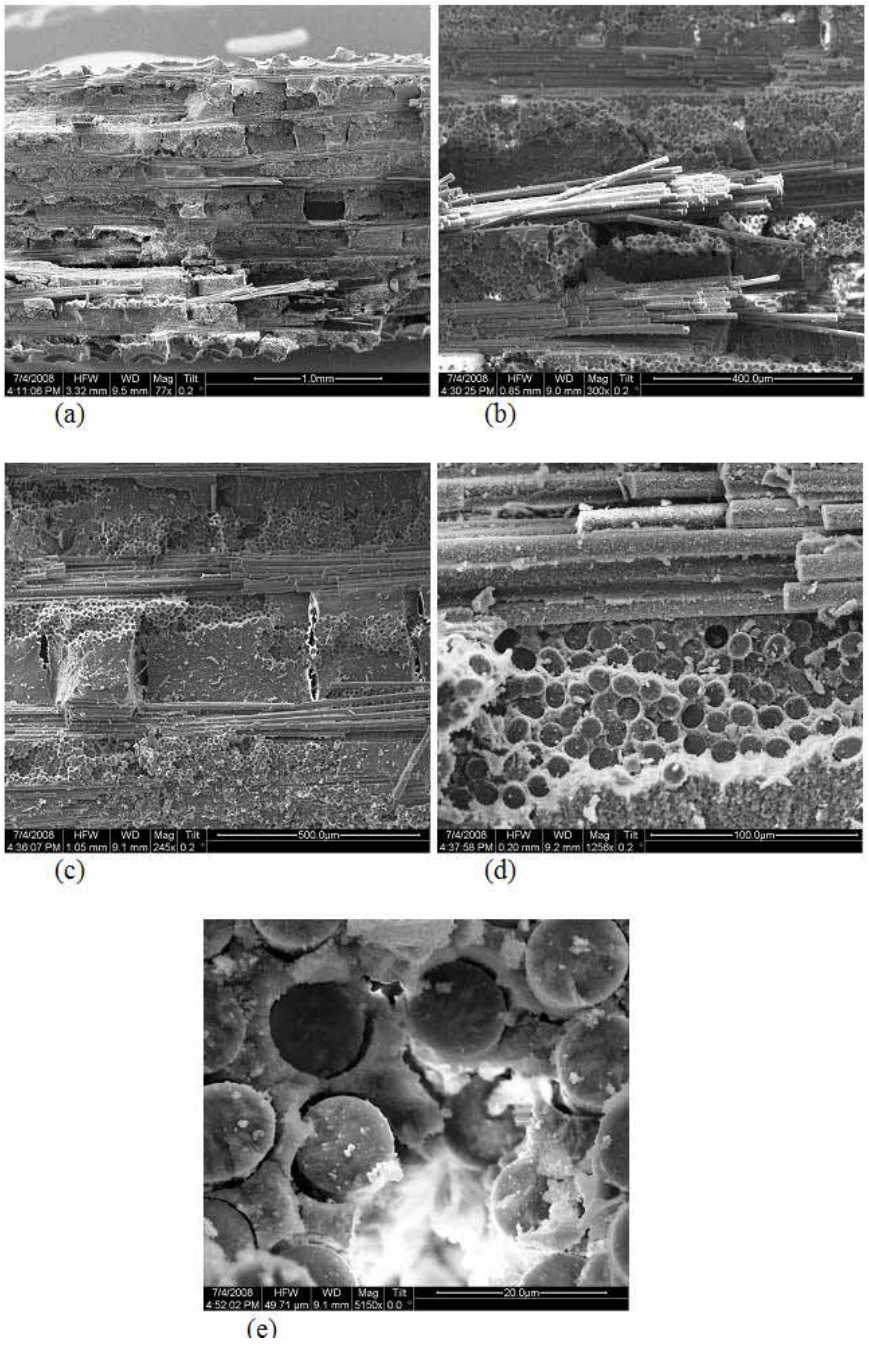

Figure 5.32: SEM micrographs of the fracture surface of C4 composite specimen tested in creep at 84.3 MPa at 1100 °C in laboratory air ($t_f > 100$ h)

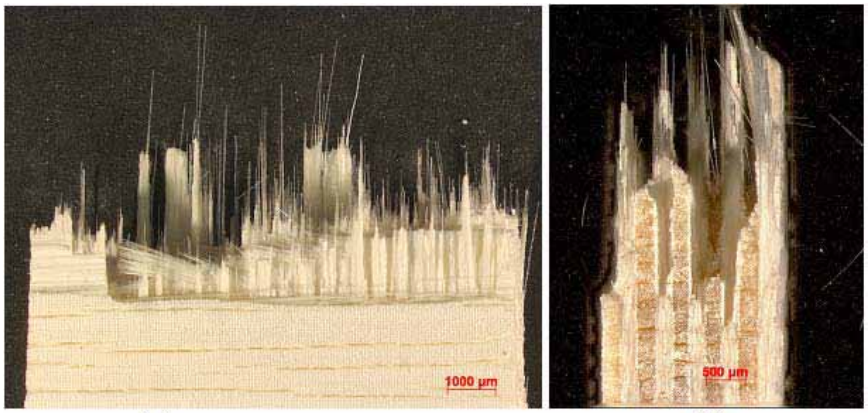

Figure 5.33: Fracture surface of C3 composite specimen tested in creep at 85 MPa at 1100 °C in steam (t_f = 8.18 h): (a) front view and (b) side view.

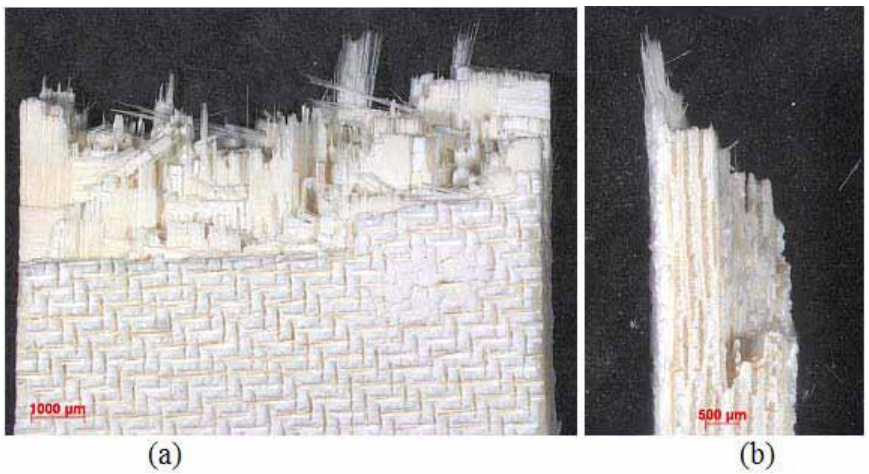

Figure 5.34: Fracture surface of C4 composite specimen tested in creep at 84.3 MPa at 1100 °C in steam (t_f = 2.24 h): (a) front view and (b) side view.

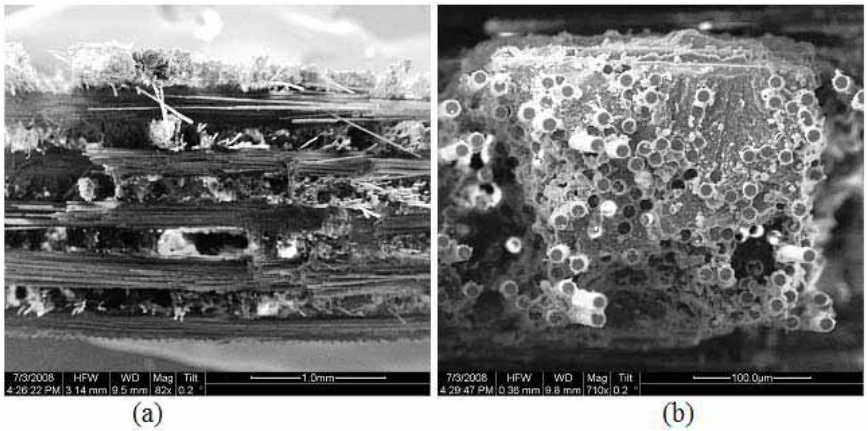

Figure 5.35: SEM micrographs of the fracture surface of C3 composite specimen tested in creep at 85 MPa at 1100 °C in steam ($t_f = 8.18$ h)

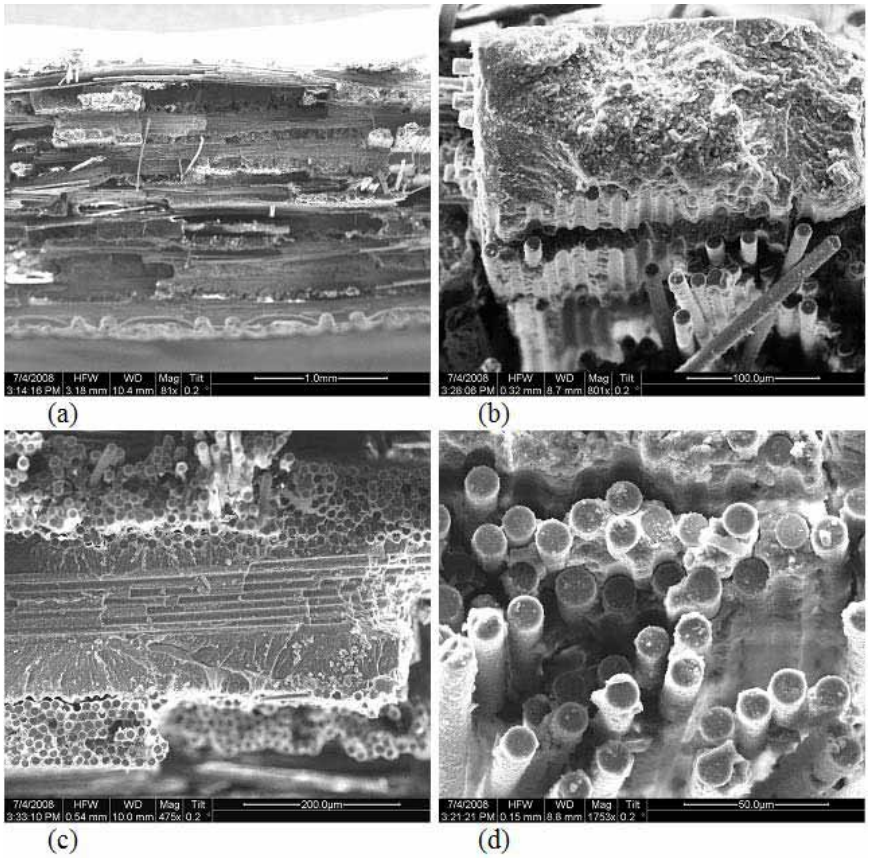

Figure 5.36: SEM micrographs of the fracture surface of C4 composite specimen tested in creep at 84.3 MPa at 1100 °C in steam ($t_f = 2.24$ h)

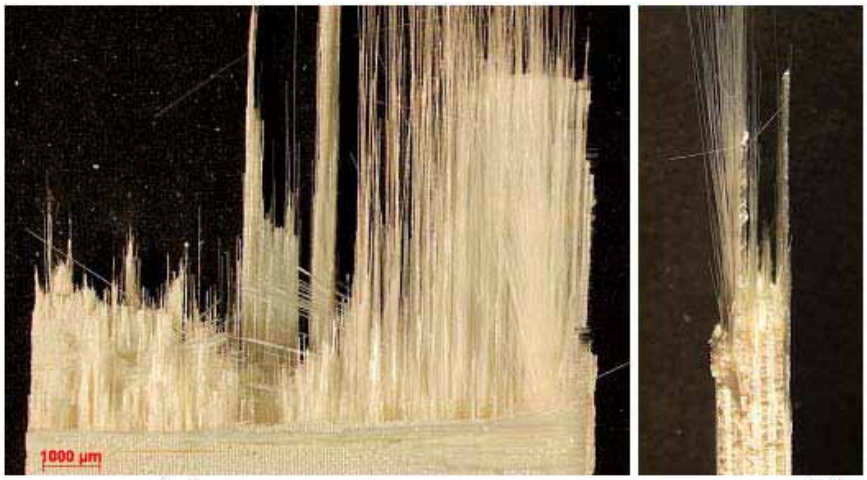

Figure 5.37: Fracture surface of C3 composite specimen tested in creep at 85 MPa at 1100 °C in steam (t_f = 8.18 h): (a) front view and (b) side view.

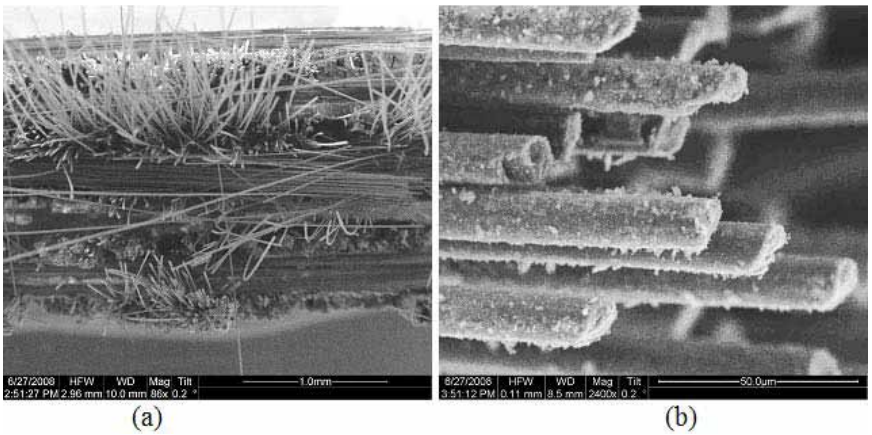

Figure 5.38: SEM micrographs of the fracture surface of C3 composite specimen tested in creep at 85 MPa at 1100 °C in steam (t_f = 8.18 h):

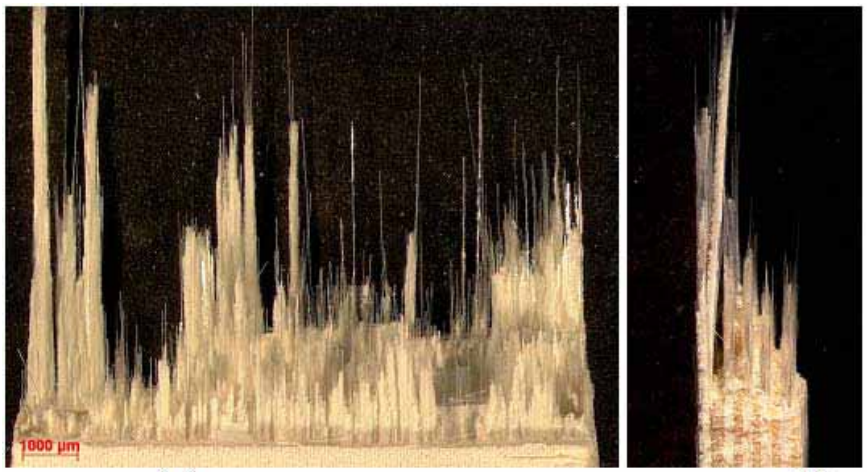

Figure 5.39: Fracture surface of C3 composite specimen tested in creep at 120 MPa at 1100 °C in steam (t_f = 0.03 h): (a) front view and (b) side view.

5.4.3 Composites C4 and C5. As mentioned earlier both composites had woven fiber fabric and Al_2O_3 matrix. Composite C4 had monazite fiber coating while composite C5 had no fiber coating and relied on porous matrix for crack deflection. Fig. 5.28 and Fig. 5.40 shows that specimens from both composite exhibited predominantly planar fracture surfaces in monotonic tensile tests. However specimen C4-5 exhibited relatively longer damage zone and had more fiber bundles in the fracture surface.

Optical micrographs of C4-11 tested at 84.3 MPa in air and C5-9 tested at 60.1 MPa in air can be seen in Fig.s 5.30 and 5.41 , respectively. Both specimens exhibit predominantly planar fracture surfaces. Specimen C4-11 exhibited very limited fiber pull out and had longer damage zone, up to 1.5 *mm* in length. It is noteworthy that specimen C4-11 was subjected a higher stress level.

Optical micrographs of C4-3 tested at 37.5 MPa in steam and C5-8 tested at 30 MPa in steam can be seen in Fig.s 5.42 and 5.43 , respectively. Both specimens, again, exhibited predominantly planar fracture surfaces. Specimen C4-3 showed some limited randomly spread fiber pull out. Specimen C4-3 had slightly longer damage zone than specimen C5-8 had.

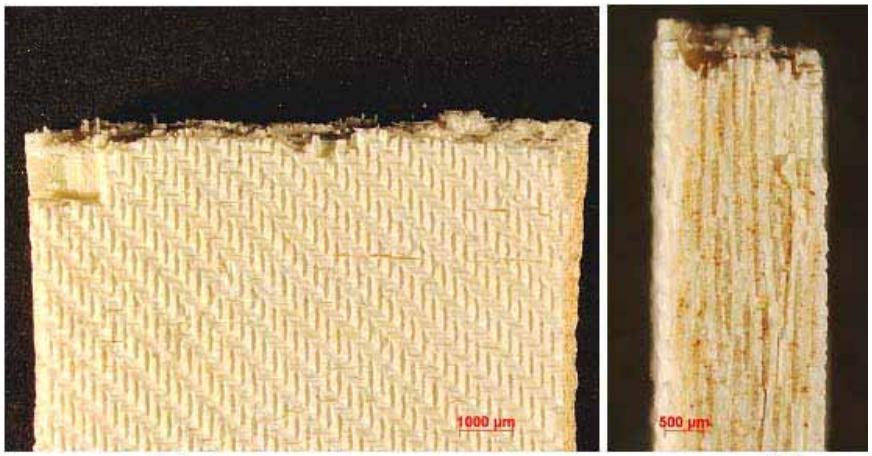

Figure 5.40: Fracture surface of C5 composite specimen tested in tension to failure at 1100 °C in laboratory air: (a) front view and (b) side view.

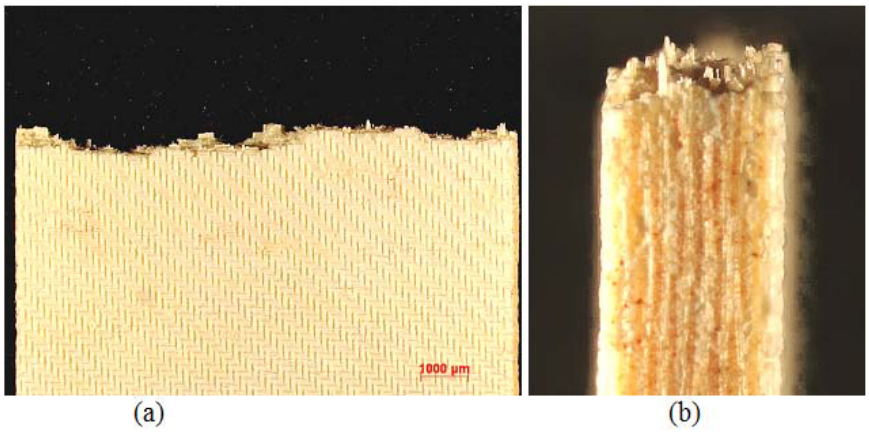

Figure 5.41: Fracture surface of C5 composite specimen tested in creep at 61 MPa at 1100 °C in laboratory air (t_f = 3.42 h): (a) front view and (b) side view.

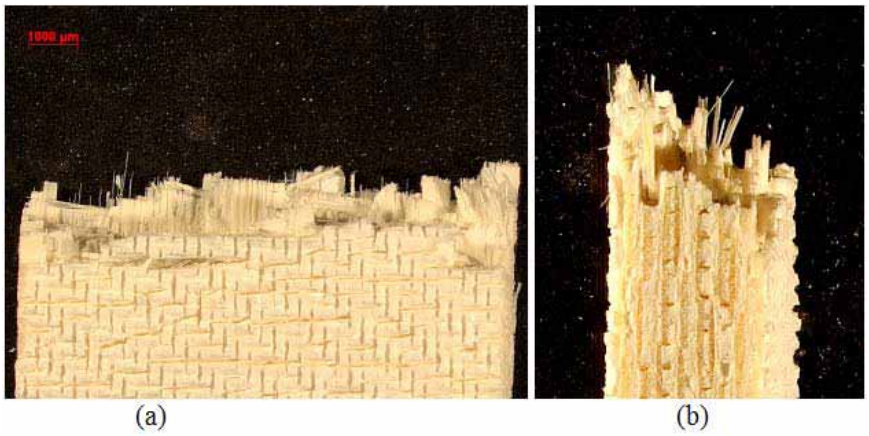

Figure 5.42: Fracture surface of C4 composite specimen tested in creep at 37.5 MPa at 1100 °C in steam (t_f = 51.9 h): (a) front view and (b) side view.

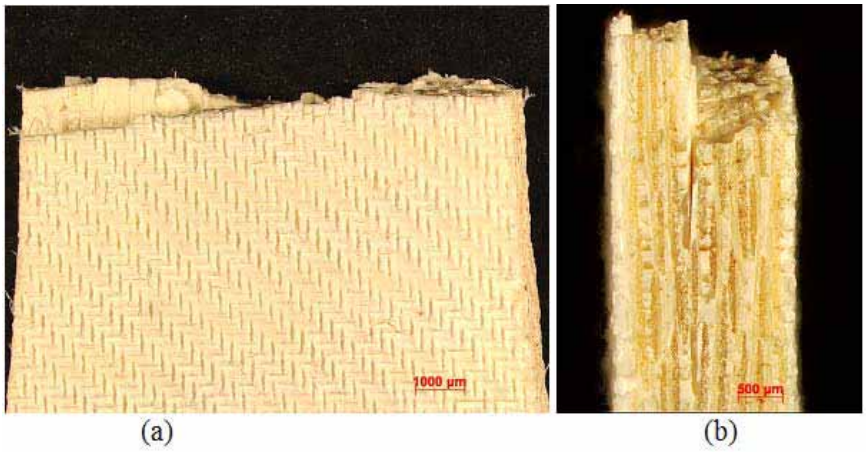

Figure 5.43: Fracture surface of C5 composite specimen tested in creep at 30 MPa at 1100 °C in steam (t_f = 16.1 h): (a) front view and (b) side view.

SEM micrographs of both specimen are presented in Fig.s 5.44, 5.45 respectively. Fig.s 5.44a and 5.45a supports the observations of having dominantly planar surfaces for both specimens. From Fig.s 5.44c and 5.46a-c it can be seen that more amount of matrix attached to the specimen C5-8 than specimen C4-3. It is noteworthy that C4-3 subjected to 25% higher stress than C5-8 and lasted 300% longer in steam environment. This may be attributed to the presence of monazite coating for composite C4. For both specimens it is observed that matrix kept its shape following debonding. This can be seen more apparently from Fig. 5.44d at where troughs can be distinctively seen. These findings might be caused by reduced porosity of matrix due to additional sintering of the matrix at elevated temperature. This phenomena degraded the flaw tolerance of both composites, especially composite C5 which relied on porous matrix for crack deflection.

Entire SEM micrographs of two composites exhibited large matrix chunks accompanied with microcracks up to 0.3 *mm* in length. Although microcracks are almost unavoidable due to present processing methods, having large matrix rich areas can be addressed to misprocessing. This defect might have degraded the composites' performance. In Fig.s 5.45d and 5.46b matrix void and fiber bridging features can be seen for composite C5,respectively. Matrix void is believed to be originated from accumulation of pores in the processing which results in decreased finely distribution of porosity. Fiber bridging is supposedly resulted from closed fiber packets not allowing adequate matrix distribution during the processing. Since inadequate matrix exists between these closed packed fibers, a crack directly penetrates through all fibers without deflection by the porous matrix.

5.4.4 Composite C4 and Composite C6. Composites C4 and C6 had woven fiber fabric and same coating process. Composite C6 had an additional AlOCl matrix infiltration. Fig.s 5.28 and 5.47 show that specimen C6-4 subjected to monotonic tensile test exhibited relatively more planar fracture surface than specimen C4-5. There was no fiber pull out nor significant damage zone throughout the fracture surface.

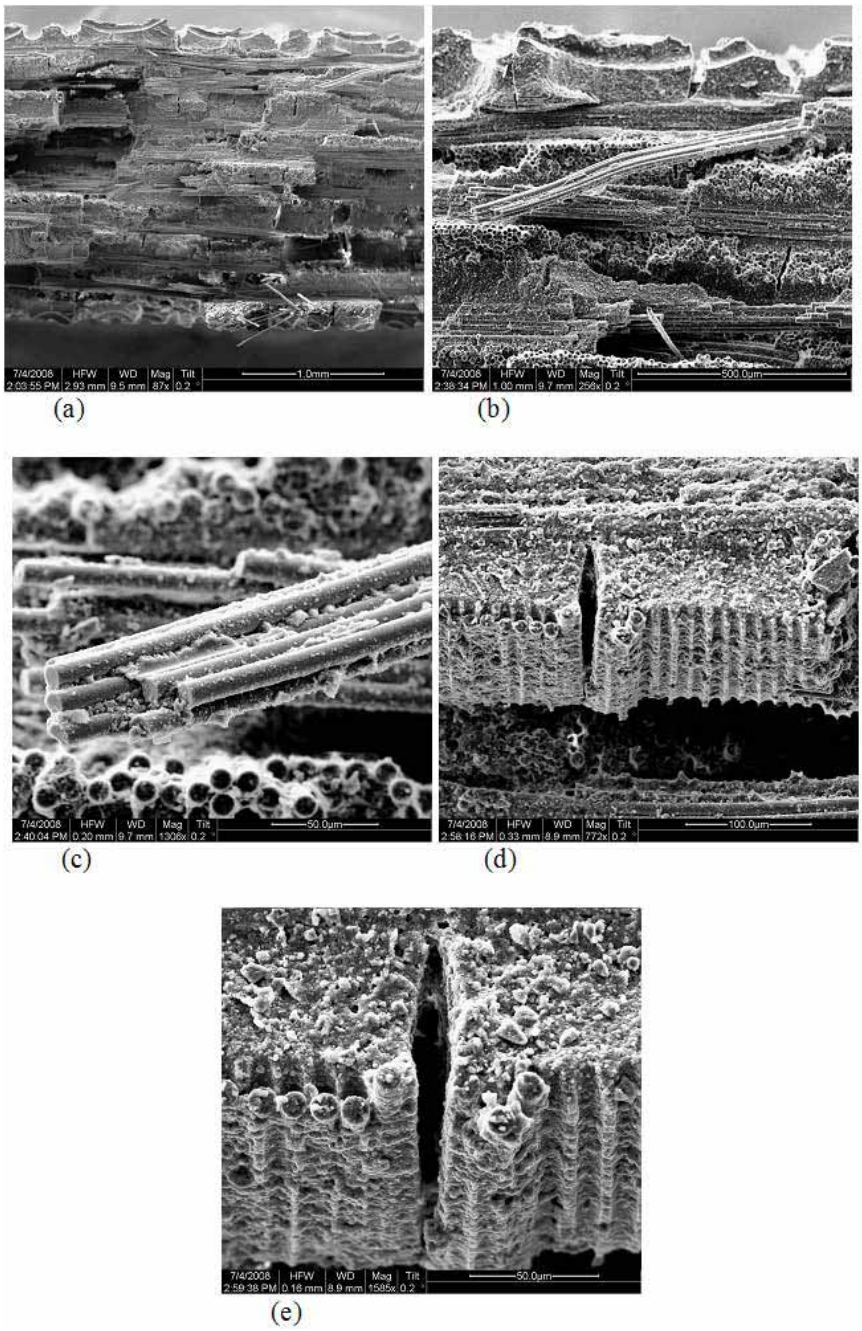

Figure 5.44: SEM micrographs of the fracture surface of C4 composite specimen tested in creep at 32 MPa at 1100 °C in steam (t_f = 51.9 h

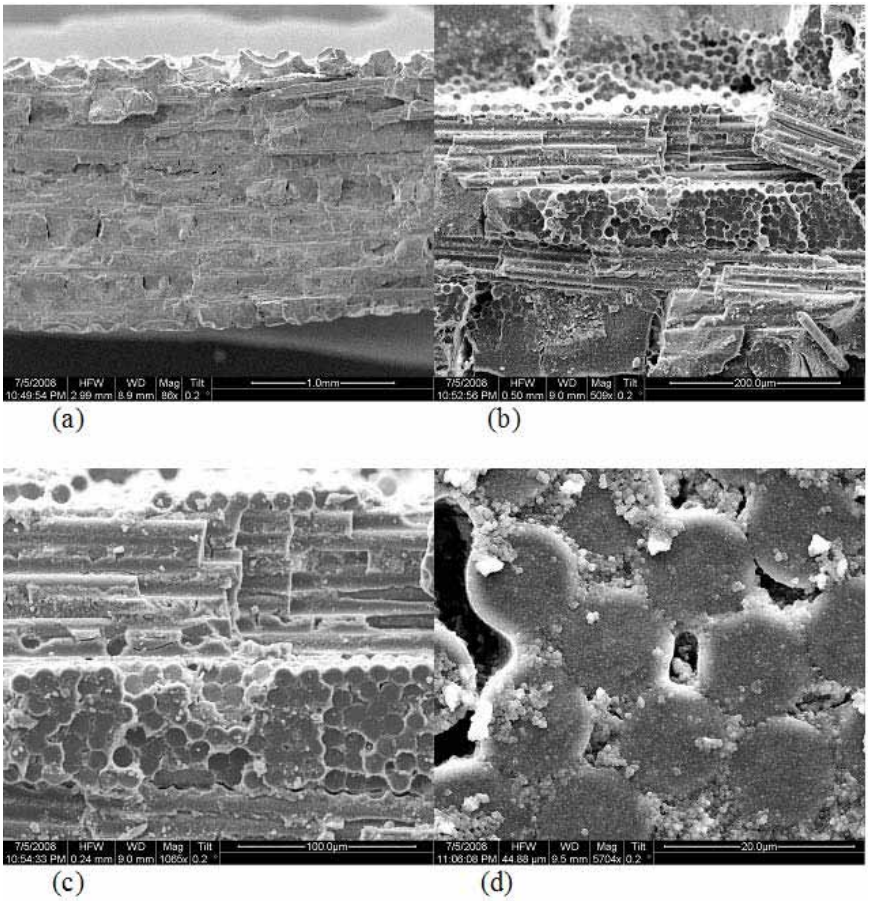

Figure 5.45: SEM micrographs of the fracture surface of C5 composite specimen tested in creep at 30 MPa at 1100 °C in steam (t_f = 16.1 h).

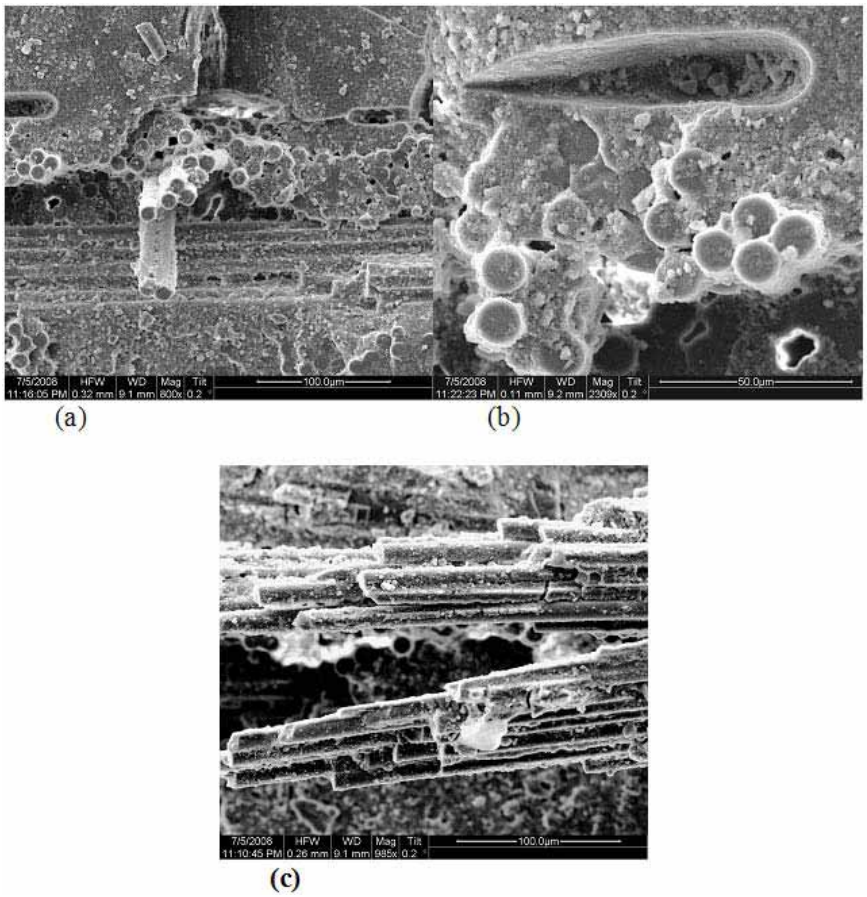

Figure 5.46: SEM micrographs of the fracture surface of C5 composite specimen tested in creep at 30 MPa at 1100 °C in steam (t_f = 16.1 h).

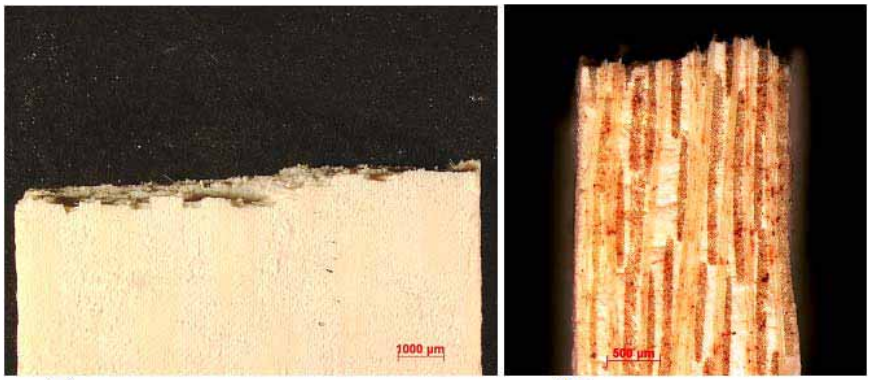

Figure 5.47: Fracture surface of C6 composite specimen tested in tension to failure at 1100 °C in laboratory air: (a) front view and (b) side view.

Optical micrographs of specimens C4-2 and C6-1 tested in air at stress levels of 37.5 MPa and 35.2 MPa, respectively are presented in Fig.s 5.48 and 5.49. It is noteworthy that both specimens achieved run out. Both specimens had similar fracture surface characteristics compared to their tensile test fracture surfaces. This observation is in consistent with achieving full retained tensile strength for both specimens. Both specimens had hardly any fibrous failure. Specimen C6-1 exhibited mostly planar fracture surface with damage zone up to 1 mm in length. However, as aforementioned, specimen C4-5 had longer damage zone (up to 2 mm in length). Absence of single plane of fracture suggests that no single crack caused the specimens to fail.

SEM micrographs of specimens C4-2 and C6-1 are presented in Fig.s 5.50 and 5.51. From these magnified images it can be easily seen that coordinated fiber failure is dominant fracture characteristic for both fracture surfaces. Fig.s 5.50a and 5.51a show that both specimens had large matrix rich areas with microcracks up to 0.5 mm in length. This was more apparent for specimen C4-2. Both specimens had similar amount of matrix attached to the fibers which was expected due to the same fiber coating process and very similar stress levels that were used in laboratory air. In Fig. 5.51d of specimen C6-1 it can be seen that a matrix chunk was fractured and lost integrity with fibers. The troughs on the matrix may be an indication of reduced porosity and subsequent matrix densification due to additional sintering. This feature

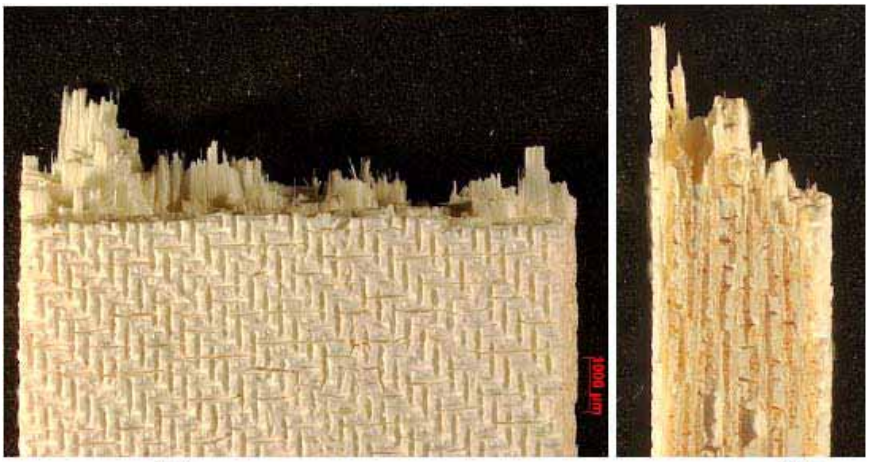

Figure 5.48: Fracture surface of C4 composite specimen tested in creep at 37.5 MPa at 1100 °C in laboratory air ($t_f > 100$ h): (a) front view and (b) side view

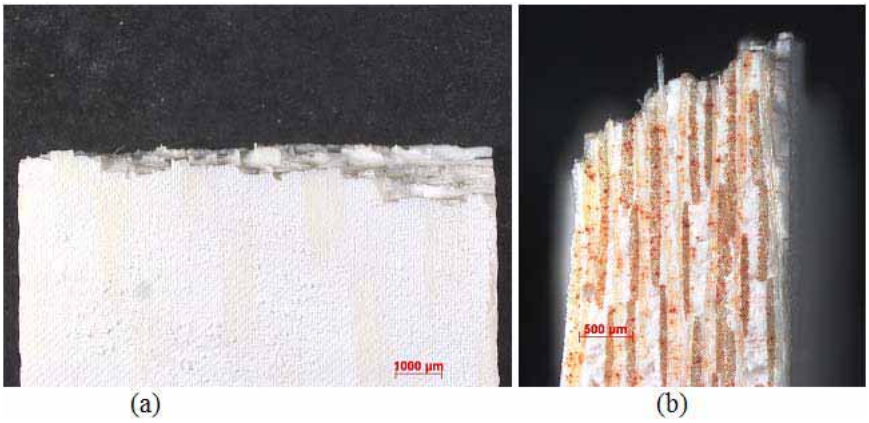

Figure 5.49: Fracture surface of C6 composite specimen tested in creep at 32 MPa at 1100 °C in laboratory air ($t_f > 100$ h): (a) front view and (b) side view.

was more apparent for the specimen C6-1 which can be attributed to the additional AlOCl infiltration. However crack deflection mechanism worked for the specimens and both of them achieved run out.

Fig.s 5.42 and 5.52 show the optical micrographs of specimens C4-3 and C6-3 tested in steam at 37.5 MPa and 35.2 MPa, respectively. Both specimens exhibited mostly planar fracture surfaces. Specimen C6-3 exhibited no visible fiber pull out.However specimen C4-3 had some limited number of visible pull out. It is noteworthy that specimen C4-3 survived almost 52 h while specimen C6-3 survived for only 3.5 h in. The specimen C4-3 had also slightly longer damage zone than specimen C6-3 which may be attributed to higher creep time under steam environment.

The SEM micrographs related to specimens C4-3 and C6-3 are presented in Fig.s 5.44 and 5.53, respectively. Consistent with other specimens from composites C4, C5 and C6, these specimens also exhibited large matrix rich areas with cracks on them up to 0.4 *mm* in length. Overall view of Fig.s 5.44a and 5.53a were consistent with optical micrographs. Along with apparent troughs on matrix for both specimens, fibers in specimen C4-3 had less amount of matrix attached on them than the fibers of specimen C6-3 had.(see Fig.s 5.44d and 5.53c) This may be attributed to the composite C6 being infiltrated with AlOCl. The infiltration might have caused additional sintering in steam environment which could trigger additional matrix sintering and consequently increased matrix adherence to the fibers. This finding supports significant decrease in lifetime of composite C6 in steam environment.

5.4.5 Unusual Microstructural Features Observed in Composites C3, C4 and C6. There were two unexpected microstructural feature that were observed under SEM:

(i) Micrographs of fracture surfaces produced by composites C3, C4 and C6 (shown in Fig. 5.54a-c, respectively) reveal fibers of other than round cross-section. It is possible that the fibers were deformed and assumed the elliptical cross-

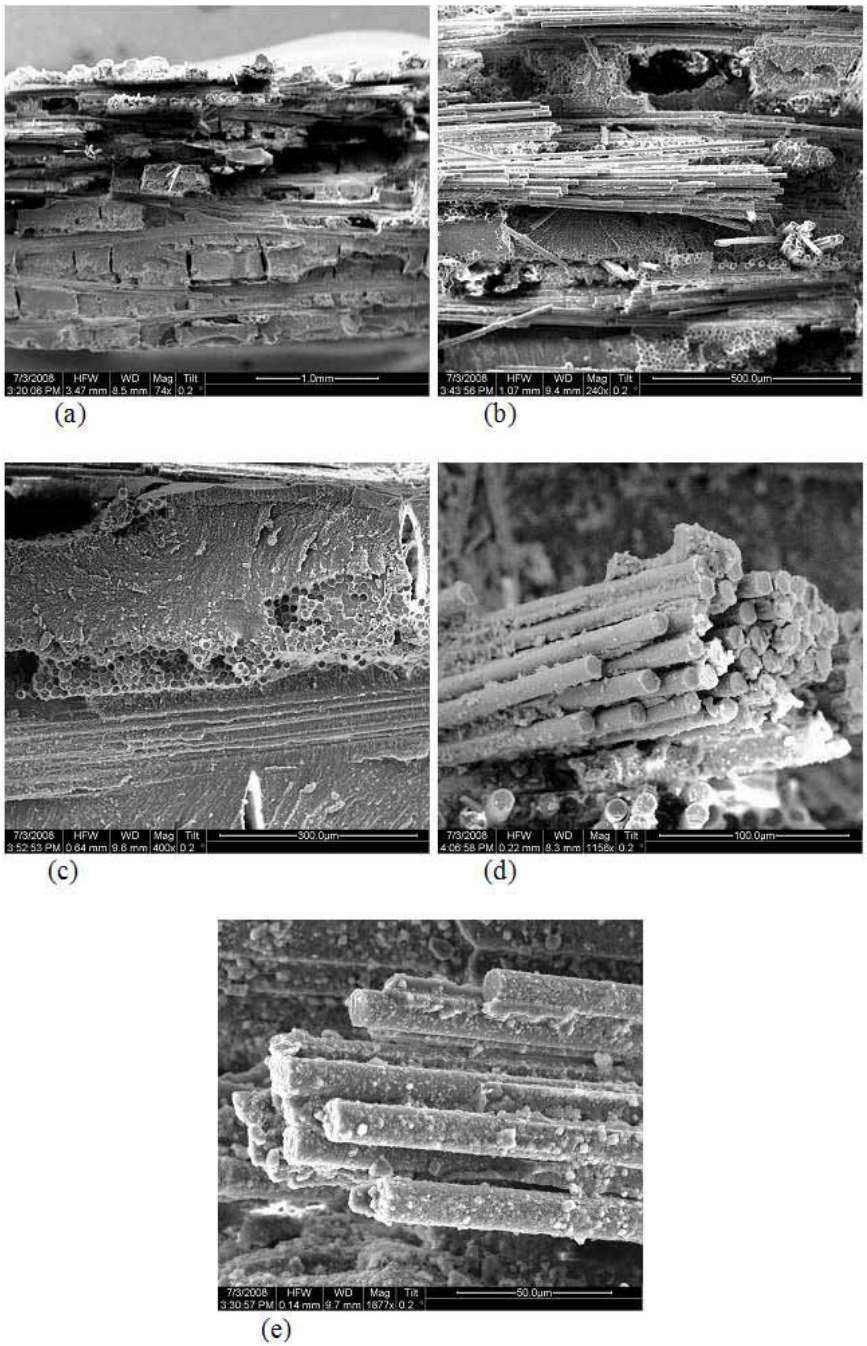

Figure 5.50: SEM micrographs of the fracture surface of C4 composite specimen tested in creep at 37.5 MPa at 1100 °C in laboratory air ($t_f > 100$ h)

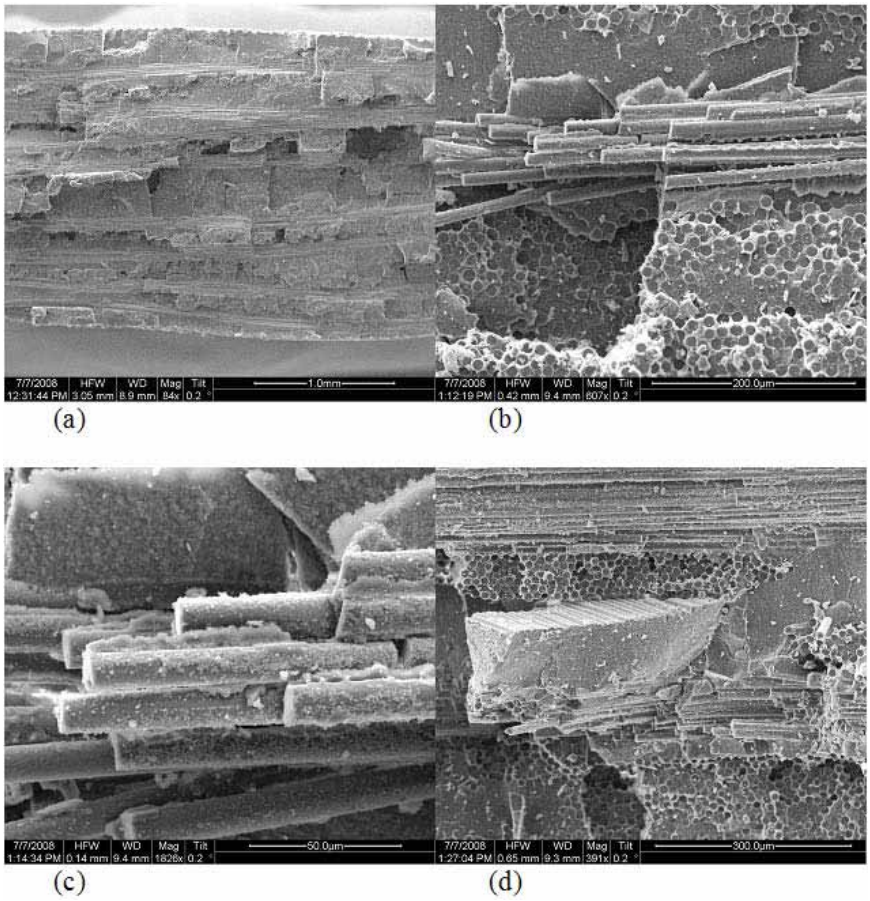

Figure 5.51: SEM micrographs of the fracture surface of C6 composite specimen tested in creep at 32 MPa at 1100 °C in air (tf > 100 h).

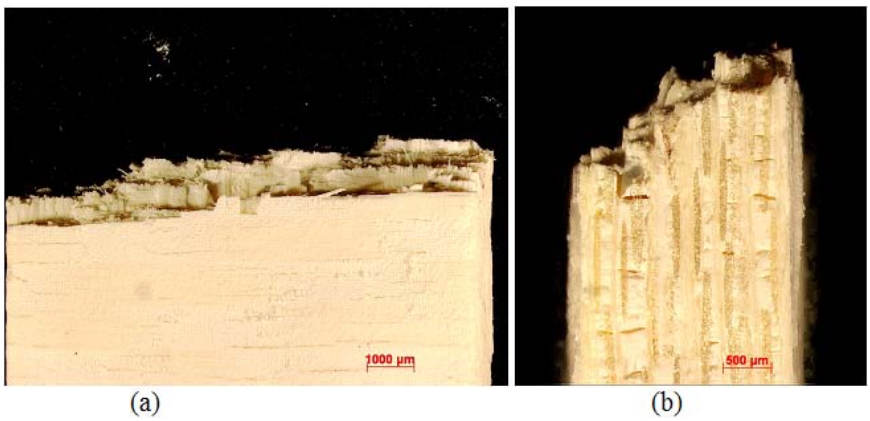

Figure 5.52: Fracture surface of C6 composite specimen tested in creep at 32 MPa at 1100 °C in steam (t_f = 3.47 h): (a) front view and (b) side view.

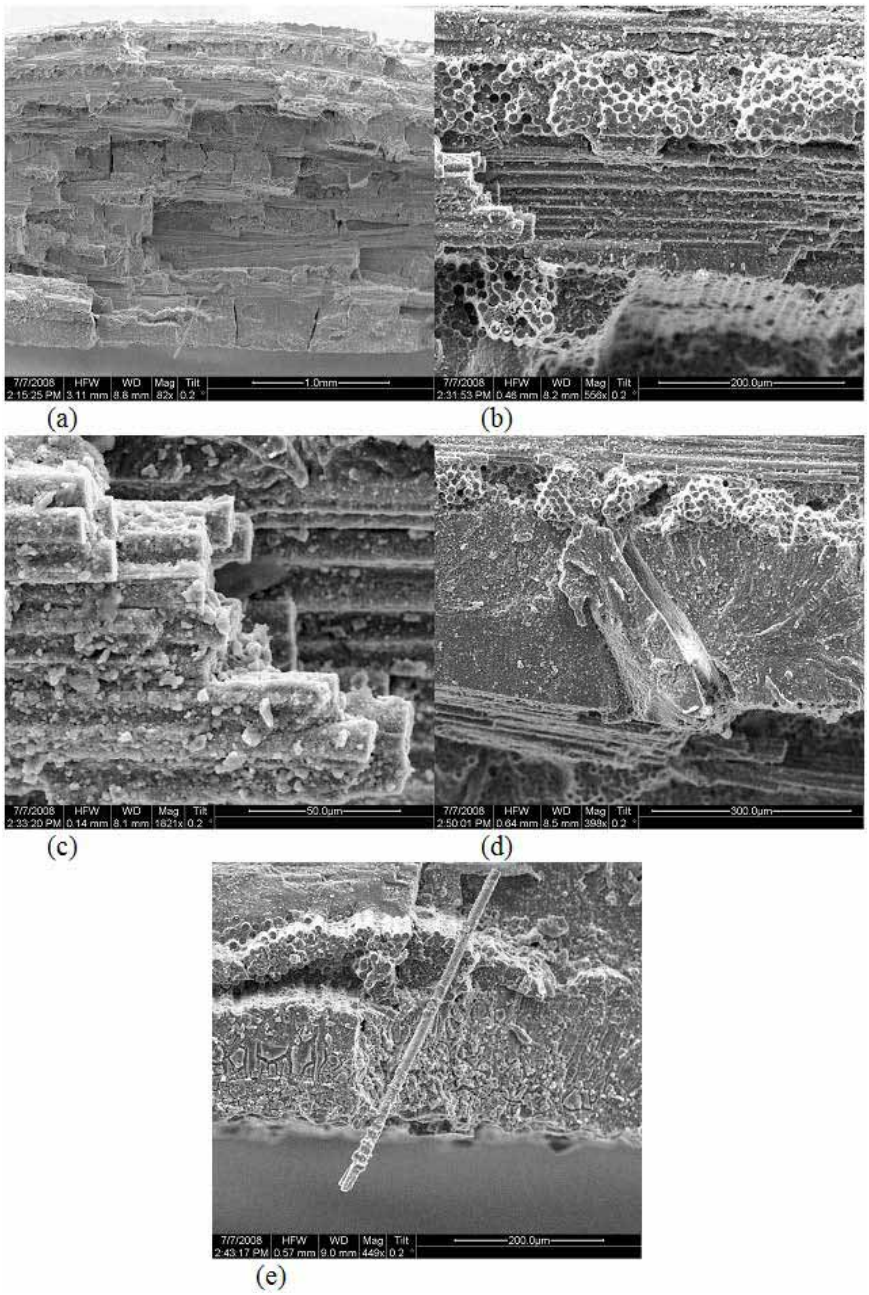

Figure 5.53: SEM micrographs of the fracture surface of C6 composite specimen tested in creep at 32 MPa at 1100 °C in steam (t_f = 3.47 h).

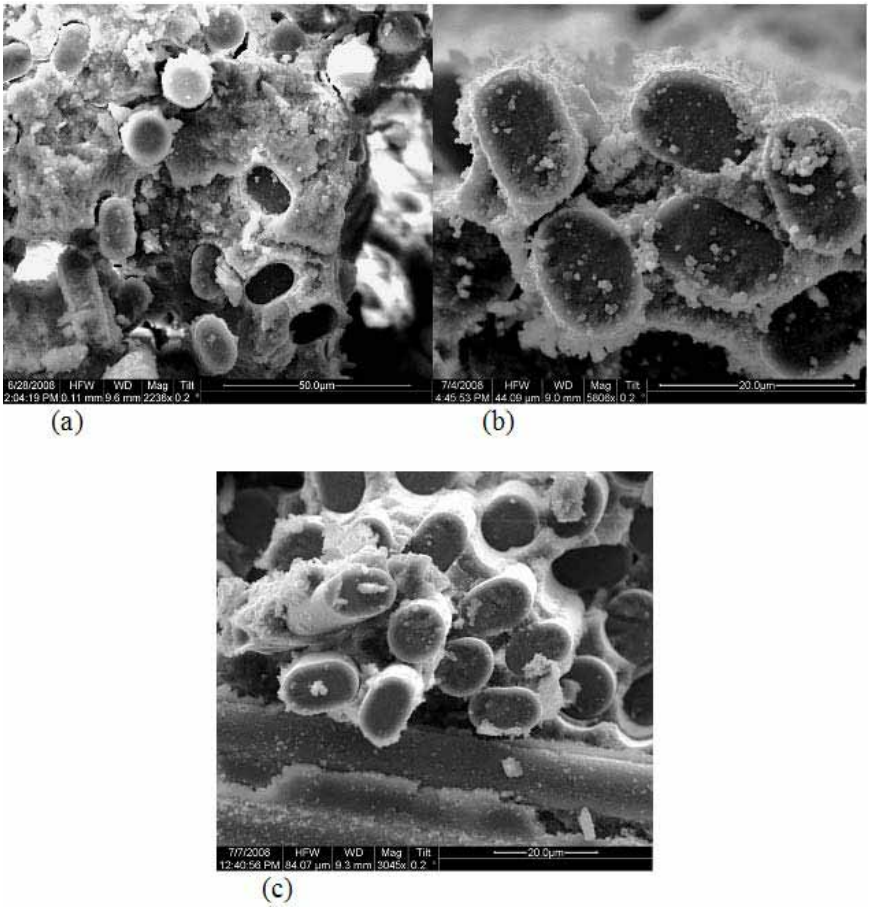

Figure 5.54: SEM micrographs of the fracture surfaces of C4-C6, respectively.

section during processing. The effect of such change in fiber shape on composite performance is not clear at present.

(ii) A unique feature observed in specimen C6-3 is presented in Fig. 5.55. Structures shaped like broken glass were not observed in the other specimens of composite C6. The nature of this microstructural feature is not clear.

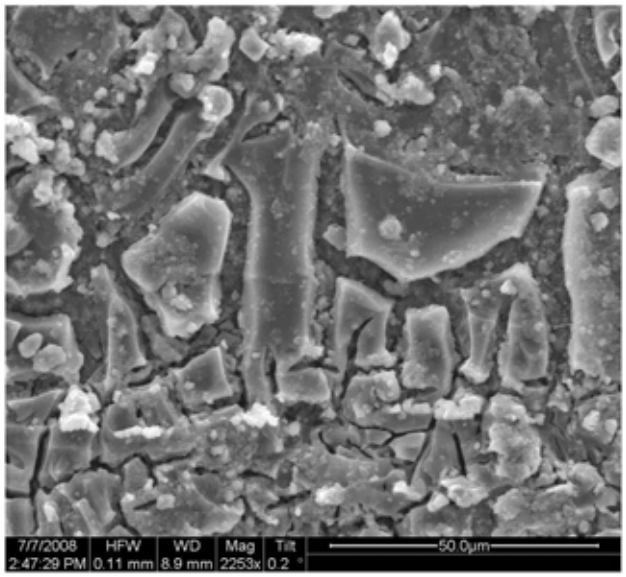

Figure 5.55: SEM micrograph of the fracture surface of specimen C6-1 showing unusual microstructural feature, i.e. structures resembling broken glass

VI. Conclusions and Recommendations

6.1 Conclusions

To facilitate comparison of results obtained for different composites, all data are adjusted for $V_f = 0.39$.

6.1.1 Tensile Stress-Strain Behavior and Properties of the Composites. Monotonic tensile tests to failure were conducted on specimens from each composite. All tensile tests were conducted at 1100 °C in laboratory air in displacement control at a constant rate of 0.05 mm/s. Results show that composite C3 exhibits considerably higher UTS than composites C4, C5 and C6. Conversely, elastic modulus of composite C3 is lower than that of composites C4-C6. The tensile strength of composite C3 was more than 2 times that of composites C4 and C5. Different methods used to coat the fibers in composite C3 and the woven fiber fabric in composite C4 is believed to be the reason for such mechanical behavior. Precipitation method, used for coating the woven fiber fabric, was reported to have a degrading effect on the strength of the fibers [12, 13]. Fair et al [12, 13] observed the loss of fiber strength of up to 30%. However, the results in this study reveal that the strength of composite C4 was reduced by more than 30% compared to the strength of composite C3.

The addition of the monazite fibercoating to composite C4 resulted in 22% improvement in tensile strength and in 6% improvement in elastic modulus compared to the uncoated-fiber composite C5.

The infiltration of the alumina matrix with AlOCl precursor in composite C6 resulted in almost 15% decrease in elastic modulus and in 14% loss of tensile strength compared to the composite C4 with uninfiltrated Al_2O_3 matrix.

6.1.2 Creep-Rupture Properties of the Composites. Creep-rupture tests at various stress levels were conducted at 1100 °C in air and in steam environment on specimens from each composite. All specimens from composite C3 that were subjected to creep in air and in steam exhibited primary and secondary creep regime.

Only specimen C3-5 which was tested at 110 MPa in steam exhibited tertiary creep regime. Both in air and in steam creep strain accumulation decreased as the applied stress increased. Creep strains produced at 85 MPa were an order of magnitude higher than the failure strain obtained in the tension test. Creep strains produced at the two higher stress levels were approximately three times the failure strain obtained in tension tests. Test environment has little effect on the appearance of the creep curves obtained for the C3 composite. For a given creep stress, creep curves and creep strains obtained in air are comparable to those produced in steam.

In composite C4 creep strain accumulation increased with increasing applied stress, whereas all creep strains accumulated in air were $\leq 0.72\%$. Creep strains produced at 64 and 84.3 MPa in air exceed the failure strain obtained in the tension test. Conversely, creep strain accumulated at 32 MPa is less than half the failure strain obtained in the tension test. The presence of steam had little effect on the appearance of the creep curves for the C4 composites. However, creep strains produced in steam are considerably higher (in some cases an order of magnitude higher) than those obtained in air for a given creep stress. No creep-run-out was achieved in steam.

All specimens from composite C5 tested in air, produced short lifetimes. However low creep rates, especially with specimens that were subjected to creep test at 40.5 and 61 MPa in air, are consistent with longer lifetimes. It is noteworthy that specimen tested at 61 MPa in air failed due to equipment failure and the specimen tested at 40.5 MPa in air showed some limited delamination as well as curvature prior to testing. It is possible that considerably longer lifetimes could be achieved at those stress levels in air in the absence of defects and equipment malfunction. It is believed that the specimen curvature is also the cause of a short lifetime produced at 20 MPa in steam. It is likely that a specimen without the initial curvature would produce a longer lifetime at 20 MPa in steam.

The addition of monazite in composite C4 had beneficial effects on creep performance in both air and steam environments. Both in air and in steam specimens

from composite C4 exhibited significantly lower creep strain accumulations in a given time compared to the specimens from composite C5, tested at lower stress levels. The lifetime produced by the monazite-containing composite C4 at 37.5 MPa in steam was at least 3 times that produced by the uncoated fiber composite C5 at a lower stress of 30 MPa in steam.

Only the primary and secondary creep regimes are observed in all creep tests conducted in composite C6. Creep strain accumulated during 100 h at 32 MPa in air was 0.49%. Test environment had negligible effect on the form of creep curves produced by composite C6. Creep curves obtained in steam are qualitatively similar to those obtained in air. However, the presence of steam had a dramatic effect on creep strains. Creep strains accumulated at 32 and 48 MPa in steam approached to an appreciable 3%. Moreover, in steam creep run-out was not achieved.

It appears that infiltration of the alumina matrix with the AlOCl precursor degraded creep performance. As an example the creep curve produced by the composite C6 with the infiltrated matrix at 35.2 MPa lied not only above the creep curve produced by composite C4 with the uninfiltrated alumina matrix at 37.5 MPa in air but also above the creep curve produced by composite C4 at that stress level in steam.

6.1.3 Creep Rate Properties of the Composites. Minimum creep rate was reached in all tests. In air, secondary creep rate for the C3 composite is almost two order of magnitude higher than that for the C4 composite. It is likely that in air monazite fiber coating technique by precipitation did not have a degrading effect on the creep rates of composite C4. In steam the secondary creep rate of the woven composite C4 can be slightly higher than that of the unitape cross-ply composite C3. These results are consistent with creep lifetimes of the compared specimens.

Both in air and in steam, secondary creep rates of the composite C4 are approximately one order of magnitude lower than those of the composite C5. The addition of monazite appears to have improving effect on creep rates in both environments.

In air, secondary creep rate for the composite C6 is almost one magnitude higher than that of the composite C4 at similar stress level. However, both specimens achieved run out. In the same manner, in steam secondary creep rates of the composite C6 with the AlOCl infiltrated matrix are approximately an order or magnitude higher than those of the C4 composite with an uninfiltrated alumina matrix. It seems that matrix infiltration with AlOCl degraded the creep rate and creep life performance of the material.

6.1.4 Stress-Rupture Properties of the Composites. It is seen that creep life of both composites C3 and C4 decreased with applied stress. The precipitation method of coating fiber fabric in Composite 4 did not appear to have a detrimental effect on creep lifetimes in air. At 84.3 MPa the woven composite C4 achieved creep run-out, while the unitape cross-ply composite C3 failed after 16.2 h at 85 MPa. The presence of steam degraded the creep lifetimes of both composites. For the unitape cross-ply composite C3, reduction in creep lifetime due to steam was $\sim 50\%$ at the lowest stress of 85 MPa. At the highest stress level of 120 MPa, the creep lifetime was reduced by at least an order of magnitude in the presence of steam. In the case of the woven composite C4, the reduction in creep lifetime due to steam was $\sim 50\%$ at 37.5 MPa and over 90% at stress level of 56.2 MPa.

In the presence of several bent and a delaminated specimen from composite C5, a more reliable assessment of the effects of monazite on creep lifetime can be made by comparing the results produced by the monazite-containing composite C4 at 37.5 MPa in steam and those obtained for the uncoated fiber composite C5 at 30 MPa in steam. In this case the addition of monazite significantly improves creep lifetime in steam, with creep lifetime of composite C4 being over 3 times that of composite C5.

In air both composites C4 and C6 achieved creep run-out at the lowest stress levels. In steam, creep lifetime of each composite decreased with applied stress. For composite C4 the reduction in creep life due to steam at 37.5 MPa was $\sim 50\%$, while

for composite C6 with AlOCl infiltrated matrix, the reduction in creep life due to steam at 35.2 MPa was $\sim$ 97%.

6.1.5 Retained Properties of the Composites. The specimens from composite C4 tested at stress levels 37.5 MPa, 74.9 MPa and 84.3 MPa in air achieved run out. This results suggests that this composite may qualify as a candidate for high temperature applications below 78% UTS in air. All three specimens retained more than 100 % tensile strength and somewhat lower elastic modulus. These results are consistent with larger failure strains produced in pre-creep tensile tests compared to failure strains produced in as-processed specimens' tensile tests. The stress-strain behavior of the composite C4 was not significantly affected by prior creep. Having almost identical optical micrograph features in fracture surfaces and stress strain curves for pre-crept and as-processed specimens support these results.

The strength and modulus of composite C6 appear to be little affected to prior creep in air. After 100 h of prior creep at 35.2 MPa in air, which is almost 47% UTS, the tensile strength increased by less than 1% and the modulus increased by less than 2%.

6.1.6 Microstructural evaluation of the Composites. Except composite C3, all composites investigated in this study produced predominantly planar fracture surfaces. Damage zone were less than 1 mm in length for most specimens. Hardly any fibrous failures were observed. The SEM images showed that composites C4, C5 and C6 produced extensive areas of coordinated fiber failure. These findings may be attributed to the reduced porosity of the matrix and subsequent matrix densification due to additional sintering, but other mechanisms may also be operating. Moreover large matrix rich areas were apparent in these composites which are believed to compromise the performance of the composites. These noticeable matrix layers were likely formed during processing of the materials.

Composite C3 exhibited brushy failure regions along with some planar fracture areas. In some cases damage zone were greater than 10 mm in length. Fiber pull out was apparent in all C3 specimens tested. The SEM micrographs also showed significant amount of uncoordinated fiber failure along with some regions of near planar fracture. The fibrous fracture indicative of crack deflection and graceful failure of composite C3 is attributed to the monazite coating of the fibers, which provided the weak interface between matrix and fibers.

6.1.7 Composites C1 and C2. As mentioned earlier, the untested specimens of composites C1 and C2 were severely bent. Thus in all tests conducted, specimens were subjected to combined tension and bending instead of tension alone. Note that specimens of Composites C1 and C2 did not fail in the gage section. The curvature present in untested specimens of Composites C1 and C2 is likely the cause of early failures and low UTS values, as well as of failure locations outside the gauge section.

Creep tests at stress levels of 32 and 25 MPa were performed for composites C1 and C2, respectively. Attempts to perform creep tests at higher stress levels were unsuccessful because the test specimens failed before reaching the creep stress level. Failures of C1 and C2 specimens at fairly low stress levels are, again, attributed to the curvature observed in the composite panels and, consequently, in the untested specimens. The results of monotonic tensile and creep tests conducted with the specimens from composites C1 and C2 presented in this study cannot be considered definite due to the curvature of the as-processed composite panels. Discussion related these composites is offered for completeness only.

6.2 Recommendations

All composites investigated in this study had limited numbers of specimens. In the absence of additional specimens, repeated tests for validating the data obtained from the tests conducted in this effort could not be performed. In future work more specimens from similar composites should be tested. As mentioned earlier composite

panels C1 and C2 were bent. Additional panels of composites C1 and C2 are needed to obtain reliable data for these materials. In composites C4, C5 and C6 large matrix-rich areas were observed. In most fracture surfaces these areas appeared as thick matrix layers. The microstructural analysis along with results obtained from tests, suggest that proliferation of the extended matrix-rich areas may have compromised performance of the composites. This problem could be addressed by imposing stricter control on processing of composites C4, C5 and C6.

Appendix A. Additional SEM Micrographs

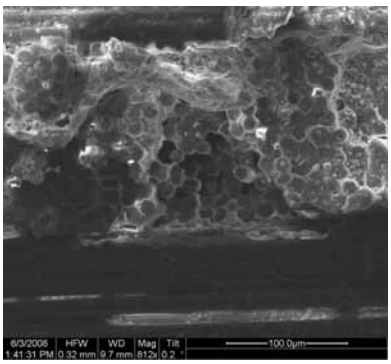

Figure A.1: Fracture surface of the N610/Al_2O_3-$LaPO_4$ specimen with 10ply 0°/90° uni-tape lay-up subjected to creep test at 32 MPa in steam at 1100 °C (t_f = 3.45h).

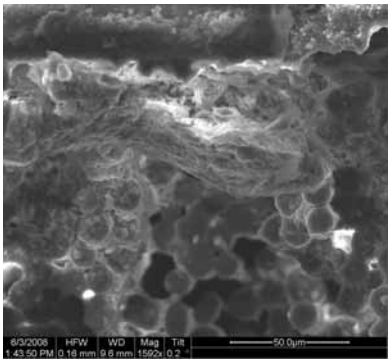

Figure A.2: Fracture surface of the N610/Al_2O_3-$LaPO_4$ specimen with 10 ply 0°/90° uni-tape lay-up subjected to creep test at 32 MPa in steam at 1100 °C (t_f = 3.45h).

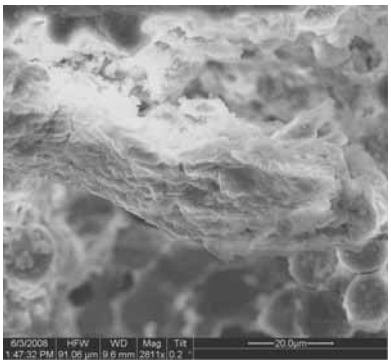

Figure A.3: Fracture surface of the N610/Al_2O_3-$LaPO_4$ specimen with 10ply 0°/90° uni-tape lay-up subjected to creep test at 32 MPa in steam at 1100 °C (t_f = 3.45h).

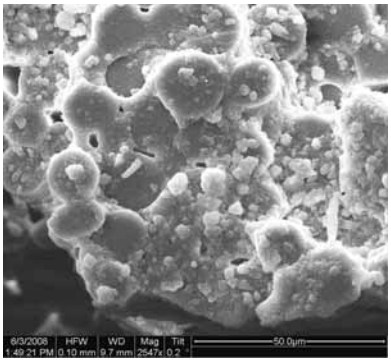

Figure A.4: Fracture surface of the N610/Al_2O_3-$LaPO_4$ specimen with 10ply 0°/90° uni-tape lay-up subjected to creep test at 32 MPa in steam at 1100 °C (t_f = 3.45h).

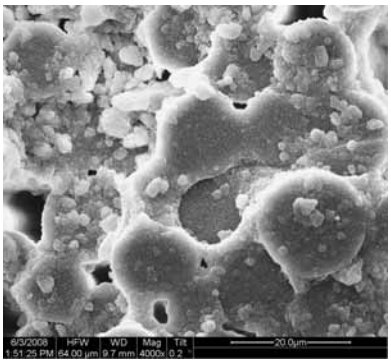

Figure A.5: Fracture surface of the N610/Al_2O_3-$LaPO_4$ specimen with 10ply 0°/90° uni-tape lay-up subjected to creep test at 32 MPa in steam at 1100 °C (t_f=3.45h).

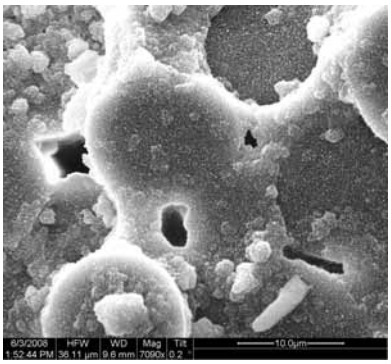

Figure A.6: Fracture surface of the N610/Al_2O_3-$LaPO_4$ specimen with 10ply 0°/90° uni-tape lay-up subjected to creep test at 32 MPa in steam at 1100 °C (t_f = 3.45h).

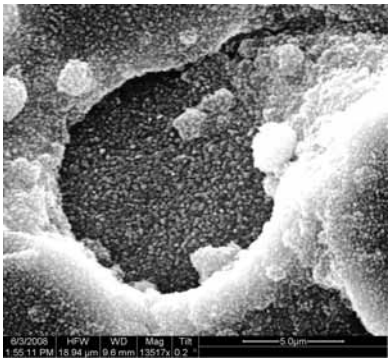

Figure A.7: Fracture surface of the N610/Al_2O_3-$LaPO_4$ specimen with 10ply 0°/90° uni-tape lay-up subjected to creep test at 32 MPa in steam at 1100 °C (t_f = 3.45h).

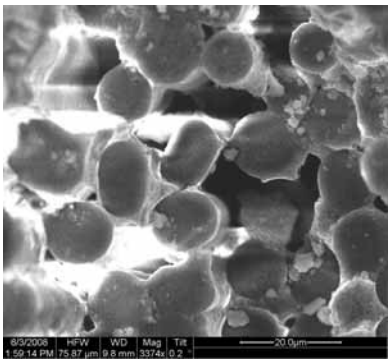

Figure A.8: Fracture surface of the N610/Al_2O_3-$LaPO_4$ specimen with 10ply 0°/90° uni-tape lay-up subjected to creep test at 32 MPa in steam at 1100 °C (t_f = 3.45h).

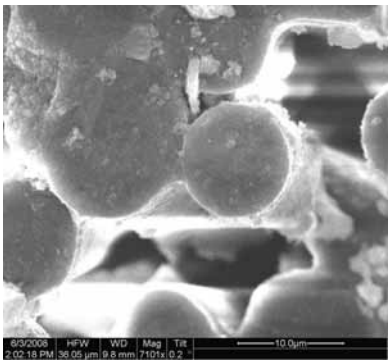

Figure A.9: Fracture surface of the N610/Al_2O_3-$LaPO_4$ specimen with 10ply 0°/90° uni-tape lay-up subjected to creep test at 32 MPa in steam at 1100 °C (t_f = 3.45h).

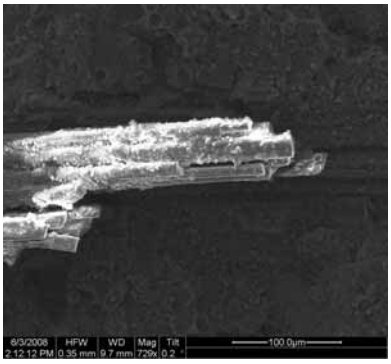

Figure A.10: Fracture surface of the N610/Al_2O_3-$LaPO_4$ specimen with 10ply 0°/90° uni-tape lay-up subjected to creep test at 32 MPa in steam at 1100 °C (t_f = 3.45h).

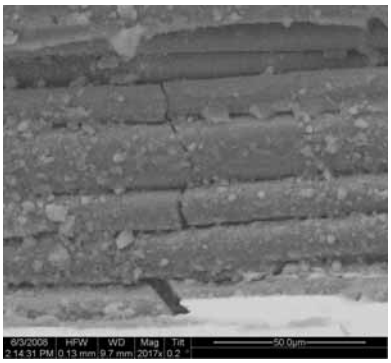

Figure A.11: Fracture surface of the N610/Al_2O_3-$LaPO_4$ specimen with 10ply 0°/90° uni-tape lay-up subjected to creep test at 32 MPa in steam at 1100 °C (t_f = 3.45h).

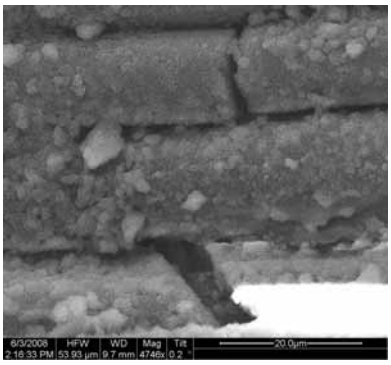

Figure A.12: Fracture surface of the N610/Al_2O_3-$LaPO_4$ specimen with 10ply 0°/90° uni-tape lay-up subjected to creep test at 32 MPa in steam at 1100 °C (t_f = 3.45h).

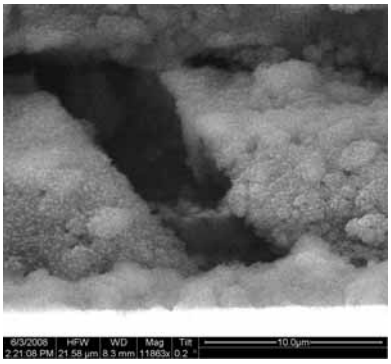

Figure A.13: Fracture surface of the N610/Al_2O_3-$LaPO_4$ specimen with 10ply 0°/90° uni-tape lay-up subjected to creep test at 32 MPa in steam at 1100 °C (t_f = 3.45h).

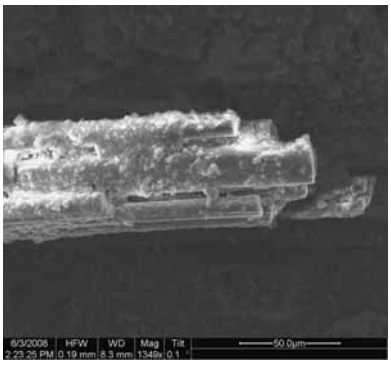

Figure A.14: Fracture surface of the N610/Al_2O_3-$LaPO_4$ specimen with 10ply 0°/90° uni-tape lay-up subjected to creep test at 32 MPa in steam at 1100 °C (t_f = 3.45h).

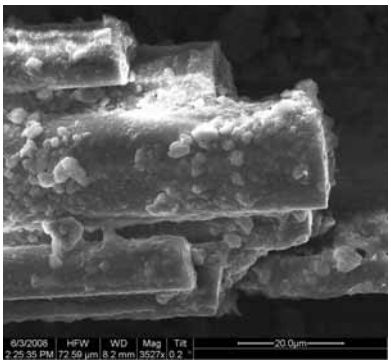

Figure A.15: Fracture surface of the N610/Al_2O_3-$LaPO_4$ specimen with 10ply 0°/90° uni-tape lay-up subjected to creep test at 32 MPa in steam at 1100 °C (t_f = 3.45h).

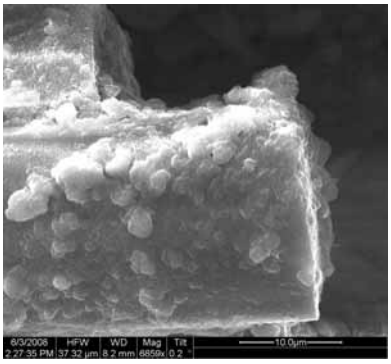

Figure A.16: Fracture surface of the N610/Al_2O_3-$LaPO_4$ specimen with 10ply 0°/90° uni-tape lay-up subjected to creep test at 32 MPa in steam at 1100 °C (t_f = 3.45h).

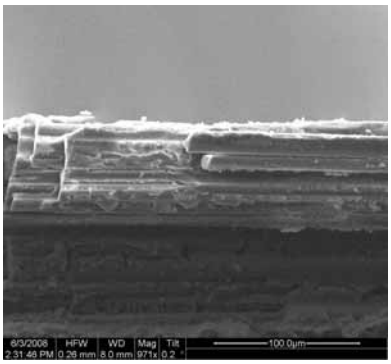

Figure A.17: Fracture surface of the N610/Al_2O_3-$LaPO_4$ specimen with 10ply 0°/90° uni-tape lay-up subjected to creep test at 32 MPa in steam at 1100 °C (t_f = 3.45h).

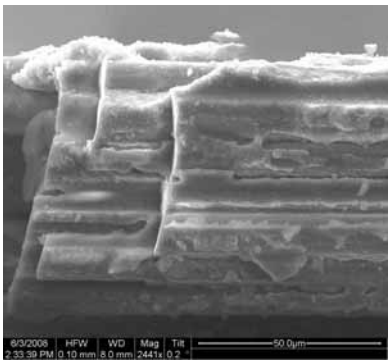

Figure A.18: Fracture surface of the N610/Al_2O_3-$LaPO_4$ specimen with 10ply 0°/90° uni-tape lay-up subjected to creep test at 32 MPa in steam at 1100 °C (t_f = 3.45h).

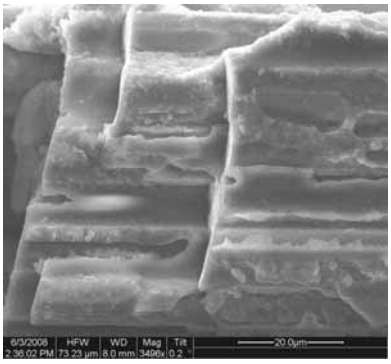

Figure A.19: Fracture surface of the N610/Al_2O_3-$LaPO_4$ specimen with 10ply 0°/90° uni-tape lay-up subjected to creep test at 32 MPa in steam at 1100 °C (t_f = 3.45h).

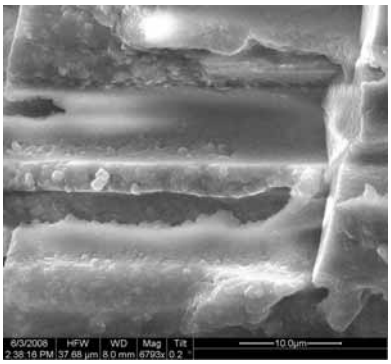

Figure A.20: Fracture surface of the N610/Al_2O_3-$LaPO_4$ specimen with 10ply 0°/90° uni-tape lay-up subjected to creep test at 32 MPa in steam at 1100 °C (t_f = 3.45h).

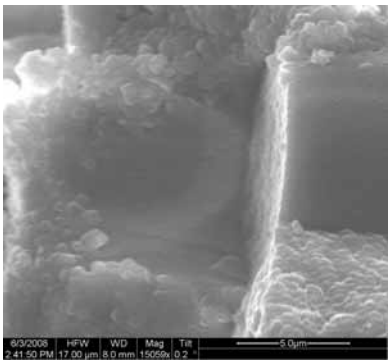

Figure A.21: Fracture surface of the N610/Al_2O_3-$LaPO_4$ specimen with 10ply 0°/90° uni-tape lay-up subjected to creep test at 32 MPa in steam at 1100 °C (t_f = 3.45h).

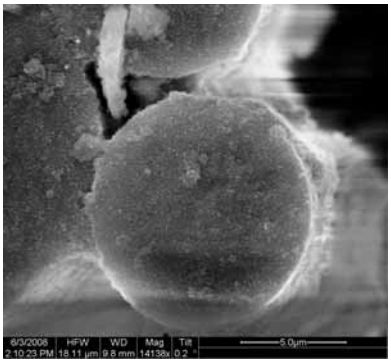

Figure A.22: Fracture surface of the N610/Al_2O_3-$LaPO_4$ specimen with 10ply 0°/90° uni-tape lay-up subjected to creep test at 32 MPa in steam at 1100 °C (t_f = 3.45h).

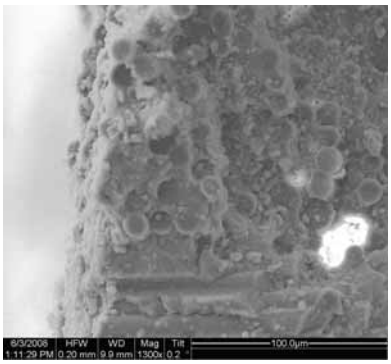

Figure A.23: Fracture surface of the N610/Al_2O_3-$LaPO_4$ specimen with 10ply 0°/90° uni-tape lay-up subjected to creep test at 32 MPa in steam at 1100 °C (t_f = 3.45h).

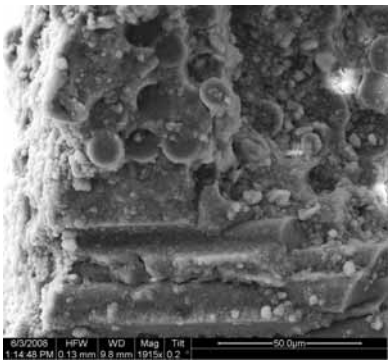

Figure A.24: Fracture surface of the N610/Al_2O_3-$LaPO_4$ specimen with 10ply 0°/90° uni-tape lay-up subjected to creep test at 32 MPa in steam at 1100 °C (t_f = 3.45h).

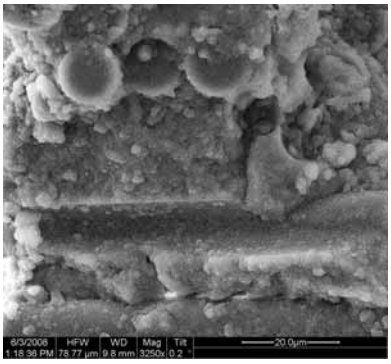

Figure A.25: Fracture surface of the N610/Al_2O_3-$LaPO_4$ specimen with 10ply 0°/90° uni-tape lay-up subjected to creep test at 32 MPa in steam at 1100 °C (t_f = 3.45h).

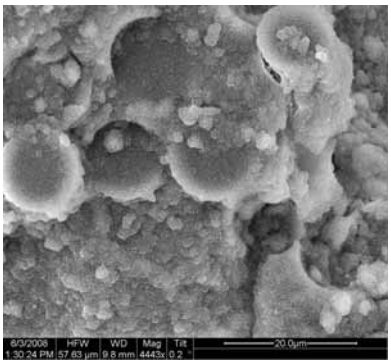

Figure A.26: Fracture surface of the N610/Al_2O_3-$LaPO_4$ specimen with 10ply 0°/90° uni-tape lay-up subjected to creep test at 32 MPa in steam at 1100 °C (t_f = 3.45h).

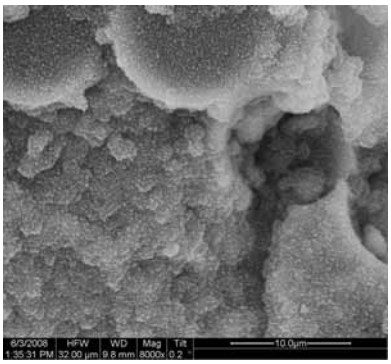

Figure A.27: Fracture surface of the N610/Al_2O_3-$LaPO_4$ specimen with 10ply 0°/90° uni-tape lay-up subjected to creep test at 32 MPa in steam at 1100 °C (t_f = 3.45h).

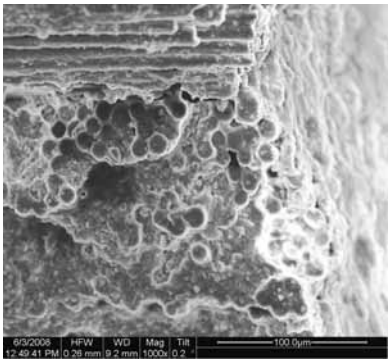

Figure A.28: Fracture surface of the N610/Al_2O_3-$LaPO_4$ specimen with 10ply 0°/90° uni-tape lay-up subjected to creep test at 32 MPa in steam at 1100 °C (t_f = 3.45h).

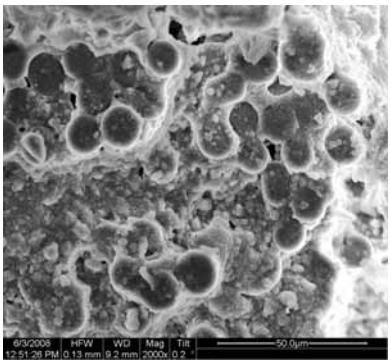

Figure A.29: Fracture surface of the N610/Al_2O_3-$LaPO_4$ specimen with 10ply 0°/90° uni-tape lay-up subjected to creep test at 32 MPa in steam at 1100 °C (t_f = 3.45h).

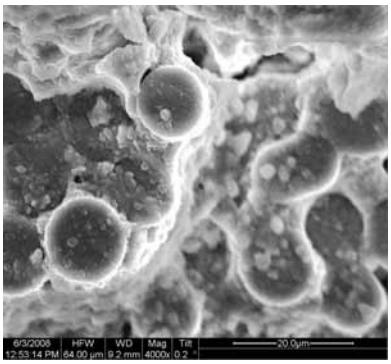

Figure A.30: Fracture surface of the N610/Al_2O_3-$LaPO_4$ specimen with 10ply 0°/90° uni-tape lay-up subjected to creep test at 32 MPa in steam at 1100 °C (t_f = 3.45h).

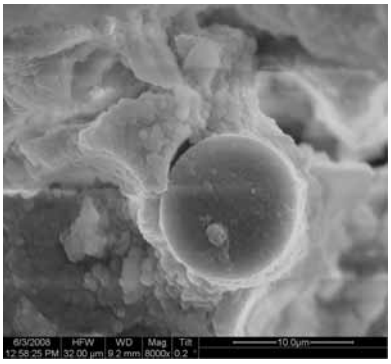

Figure A.31: Fracture surface of the N610/Al_2O_3-$LaPO_4$ specimen with 10ply 0°/90° uni-tape lay-up subjected to creep test at 32 MPa in steam at 1100 °C (t_f = 3.45h).

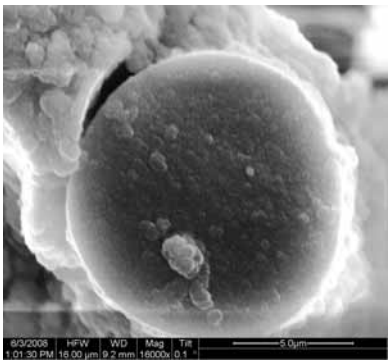

Figure A.32: Fracture surface of the N610/Al_2O_3-$LaPO_4$ specimen with 10ply 0°/90° uni-tape lay-up subjected to creep test at 32 MPa in steam at 1100 °C (t_f = 3.45h).

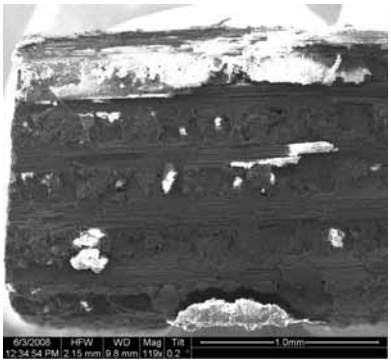

Figure A.33: Fracture surface of the N610/Al_2O_3-$LaPO_4$ specimen with 10ply 0°/90° uni-tape lay-up subjected to creep test at 32 MPa in steam at 1100 °C (t_f = 3.45h).

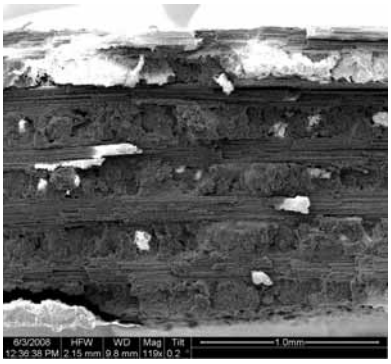

Figure A.34: Fracture surface of the N610/Al_2O_3-$LaPO_4$ specimen with 10ply 0°/90° uni-tape lay-up subjected to creep test at 32 MPa in steam at 1100 °C (t_f = 3.45h).

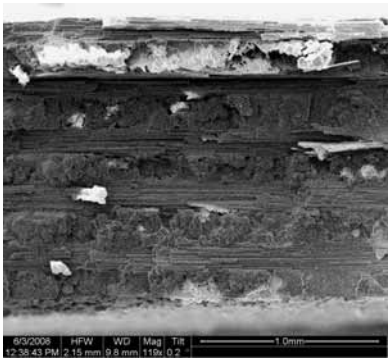

Figure A.35: Fracture surface of the N610/Al_2O_3-$LaPO_4$ specimen with 10ply 0°/90° uni-tape lay-up subjected to creep test at 32 MPa in steam at 1100 °C (t_f = 3.45h).

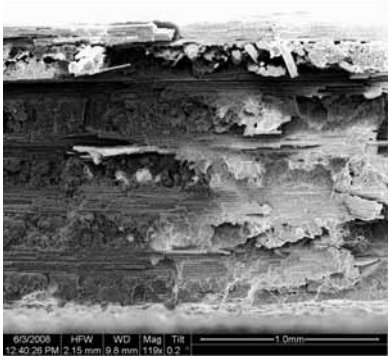

Figure A.36: Fracture surface of the N610/Al_2O_3-$LaPO_4$ specimen with 10ply 0°/90° uni-tape lay-up subjected to creep test at 32 MPa in steam at 1100 °C (t_f = 3.45h).

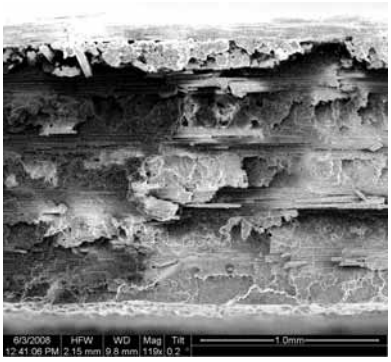

Figure A.37: Fracture surface of the N610/Al_2O_3-$LaPO_4$ specimen with 10ply 0°/90° uni-tape lay-up subjected to creep test at 32 MPa in steam at 1100 °C (t_f = 3.45h).

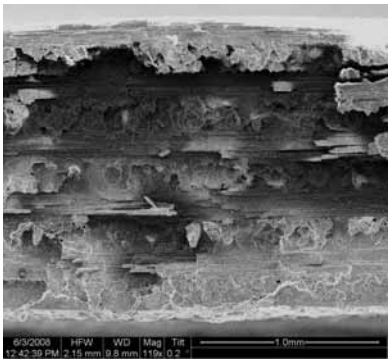

Figure A.38: Fracture surface of the N610/Al_2O_3-$LaPO_4$ specimen with 10ply 0°/90° uni-tape lay-up subjected to creep test at 32 MPa in steam at 1100 °C (t_f = 3.45h).

Figure A.39: Fracture surface of the N610/Al_2O_3-$LaPO_4$ specimen with 10ply 0°/90° uni-tape lay-up subjected to creep test at 32 MPa in steam at 1100 °C (t_f = 3.45h).

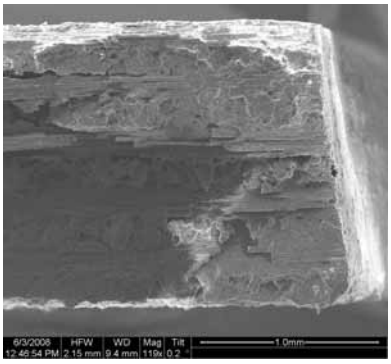

Figure A.40: Fracture surface of the N610/Al_2O_3-$LaPO_4$ specimen with 10ply 0°/90° uni-tape lay-up subjected to creep test at 32 MPa in steam at 1100 °C (t_f = 3.45h).

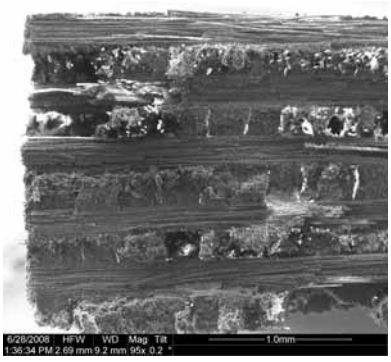

Figure A.41: Fracture surface of the N610/$LaPO_4$/Al_2O_3 specimen with 10ply 0°/90° uni-tape lay-up subjected to creep test at 85 MPa in air at 1100 °C (t_f = 16.23h).

Figure A.42: Fracture surface of the N610/$LaPO_4$/Al_2O_3 specimen with 10ply 0°/90° uni-tape lay-up subjected to creep test at 85 MPa in air at 1100 °C (t_f = 16.23h).

Figure A.43: Fracture surface of the N610/$LaPO_4$/Al_2O_3 specimen with 10ply 0°/90° uni-tape lay-up subjected to creep test at 85 MPa in air at 1100 °C (t_f = 16.23h).

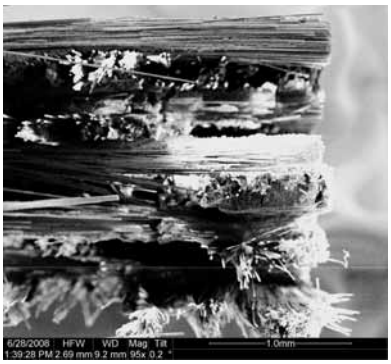

Figure A.44: Fracture surface of the N610/$LaPO_4$/Al_2O_3 specimen with 10ply 0°/90° uni-tape lay-up subjected to creep test at 85 MPa in air at 1100 °C (t_f = 16.23h).

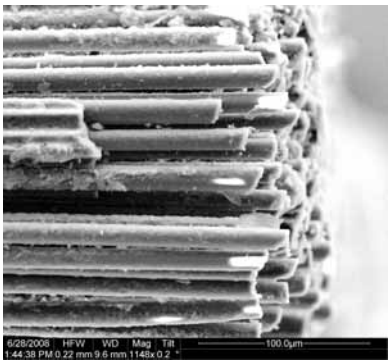

Figure A.45: Fracture surface of the N610/$LaPO_4$/Al_2O_3 specimen with 10ply 0°/90° uni-tape lay-up subjected to creep test at 85 MPa in air at 1100 °C (t_f = 16.23h).

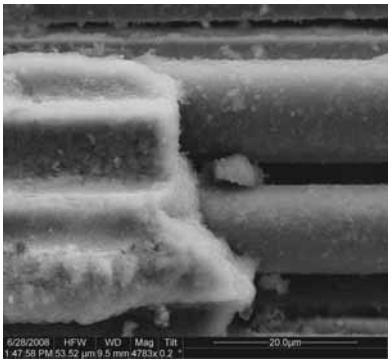

Figure A.46: Fracture surface of the N610/$LaPO_4$/Al_2O_3 specimen with 10ply 0°/90° uni-tape lay-up subjected to creep test at 85 MPa in air at 1100 °C (t_f = 16.23h).

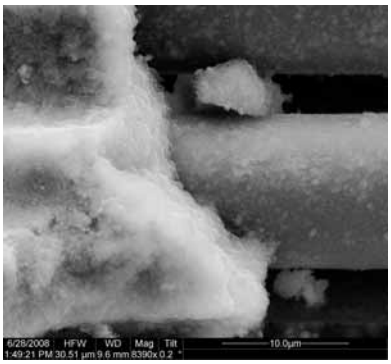

Figure A.47: Fracture surface of the N610/$LaPO_4$/Al_2O_3 specimen with 10ply 0°/90° uni-tape lay-up subjected to creep test at 85 MPa in air at 1100 °C (t_f = 16.23h).

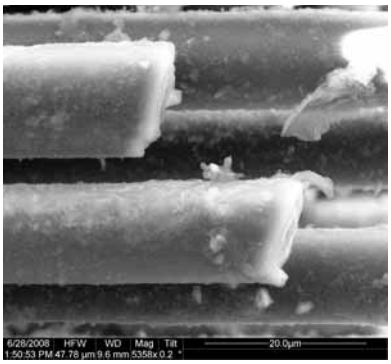

Figure A.48: Fracture surface of the N610/$LaPO_4$/Al_2O_3 specimen with 10ply 0°/90° uni-tape lay-up subjected to creep test at 85 MPa in air at 1100 °C (t_f = 16.23h).

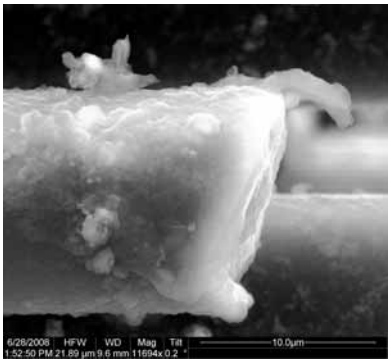

Figure A.49: Fracture surface of the N610/$LaPO_4$/Al_2O_3 specimen with 10ply 0°/90° uni-tape lay-up subjected to creep test at 85 MPa in air at 1100 °C (t_f = 16.23h).

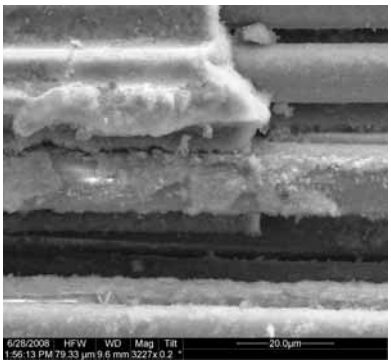

Figure A.50: Fracture surface of the N610/$LaPO_4$/Al_2O_3 specimen with 10ply 0°/90° uni-tape lay-up subjected to creep test at 85 MPa in air at 1100 °C (t_f = 16.23h).

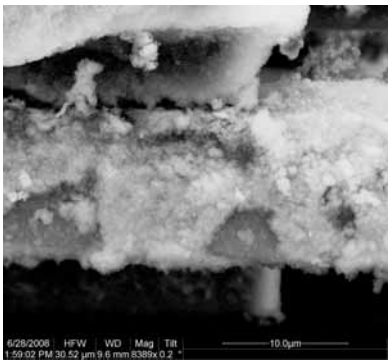

Figure A.51: Fracture surface of the N610/$LaPO_4$/Al_2O_3 specimen with 10ply 0°/90° uni-tape lay-up subjected to creep test at 85 MPa in air at 1100 °C (t_f = 16.23h).

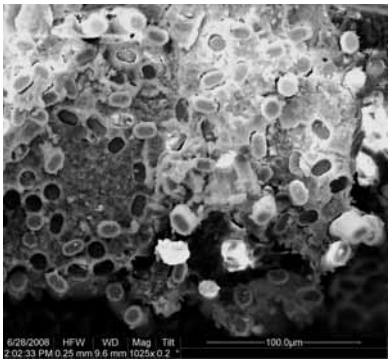

Figure A.52: Fracture surface of the N610/$LaPO_4$/Al_2O_3 specimen with 10ply 0°/90° uni-tape lay-up subjected to creep test at 85 MPa in air at 1100 °C (t_f = 16.23h).

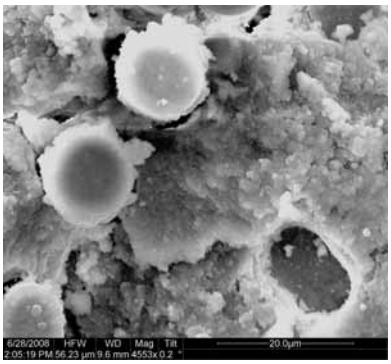

Figure A.53: Fracture surface of the N610/$LaPO_4$/Al_2O_3 specimen with 10ply 0°/90° uni-tape lay-up subjected to creep test at 85 MPa in air at 1100 °C (t_f = 16.23h).

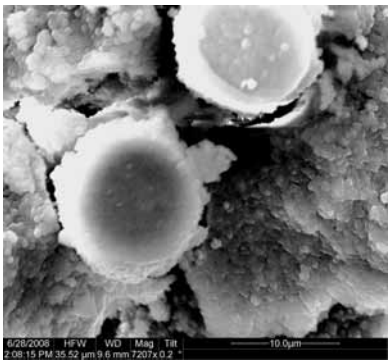

Figure A.54: Fracture surface of the N610/$LaPO_4$/Al_2O_3 specimen with 10ply 0°/90° uni-tape lay-up subjected to creep test at 85 MPa in air at 1100 °C (t_f = 16.23h).

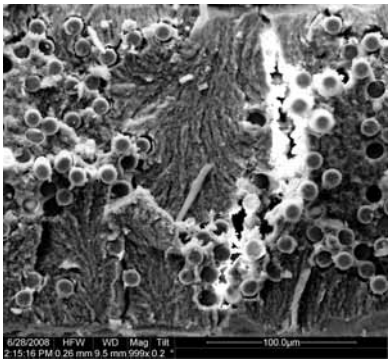

Figure A.55: Fracture surface of the N610/$LaPO_4$/Al_2O_3 specimen with 10ply 0°/90° uni-tape lay-up subjected to creep test at 85 MPa in air at 1100 °C (t_f = 16.23h).

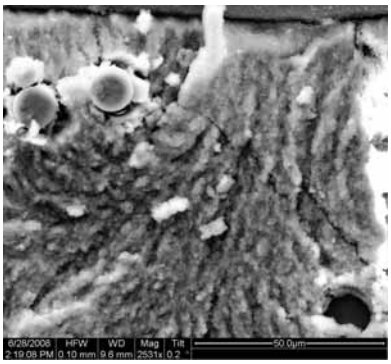

Figure A.56: Fracture surface of the N610/$LaPO_4$/Al_2O_3 specimen with 10ply 0°/90° uni-tape lay-up subjected to creep test at 85 MPa in air at 1100 °C (t_f = 16.23h).

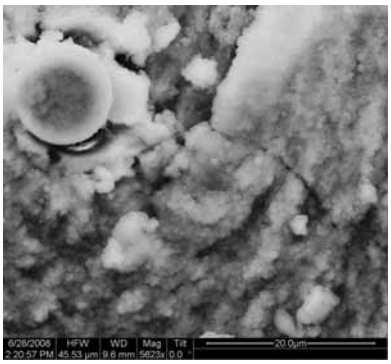

Figure A.57: Fracture surface of the N610/$LaPO_4$/Al_2O_3 specimen with 10ply 0°/90° uni-tape lay-up subjected to creep test at 85 MPa in air at 1100 °C (t_f = 16.23h).

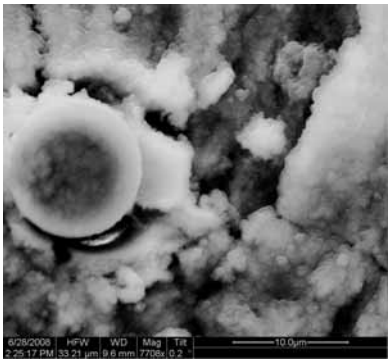

Figure A.58: Fracture surface of the N610/$LaPO_4$/Al_2O_3 specimen with 10ply 0°/90° uni-tape lay-up subjected to creep test at 85 MPa in air at 1100 °C (t_f = 16.23h).

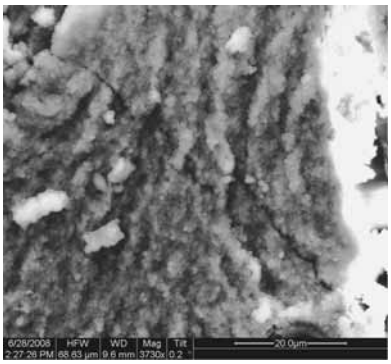

Figure A.59: Fracture surface of the N610/$LaPO_4$/Al_2O_3 specimen with 10ply 0°/90° uni-tape lay-up subjected to creep test at 85 MPa in air at 1100 °C (t_f = 16.23h).

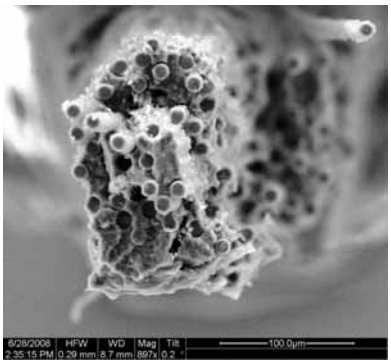

Figure A.60: Fracture surface of the N610/$LaPO_4$/Al_2O_3 specimen with 10ply 0°/90° uni-tape lay-up subjected to creep test at 85 MPa in air at 1100 °C (t_f = 16.23h).

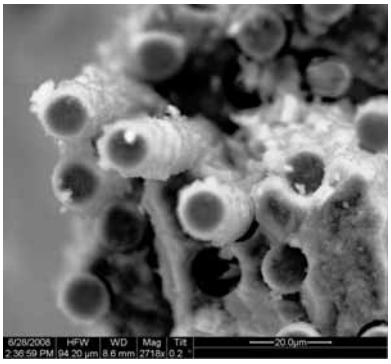

Figure A.61: Fracture surface of the N610/$LaPO_4$/Al_2O_3 specimen with 10ply 0°/90° uni-tape lay-up subjected to creep test at 85 MPa in air at 1100 °C (t_f = 16.23h).

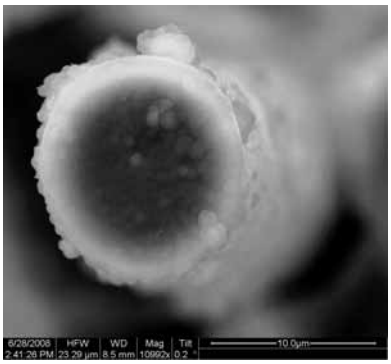

Figure A.62: Fracture surface of the N610/$LaPO_4$/Al_2O_3 specimen with 10ply 0°/90° uni-tape lay-up subjected to creep test at 85 MPa in air at 1100 °C (t_f = 16.23h).

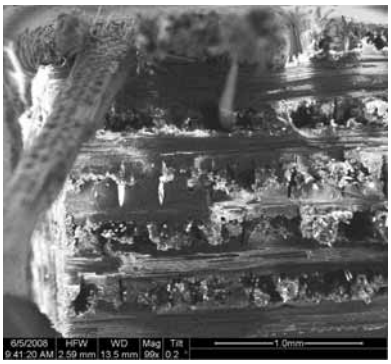

Figure A.63: Fracture surface of the N610/$LaPO_4$/Al_2O_3 specimen with 10ply 0°/90° uni-tape lay-up subjected to creep test at 120 MPa in steam at 1100 °C (t_f = 0.0313h).

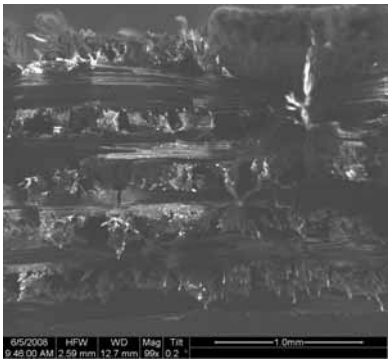

Figure A.64: Fracture surface of the N610/$LaPO_4$/Al_2O_3 specimen with 10ply 0°/90° uni-tape lay-up subjected to creep test at 120 MPa in steam at 1100 °C (t_f = 0.0313h).

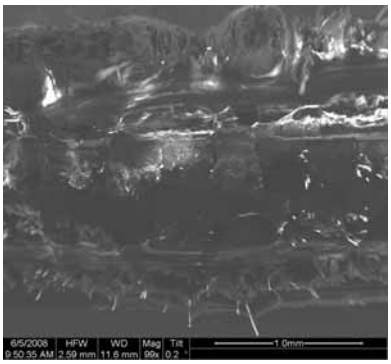

Figure A.65: Fracture surface of the N610/$LaPO_4$/Al_2O_3 specimen with 10ply 0°/90° uni-tape lay-up subjected to creep test at 120 MPa in steam at 1100 °C (t_f = 0.0313h).

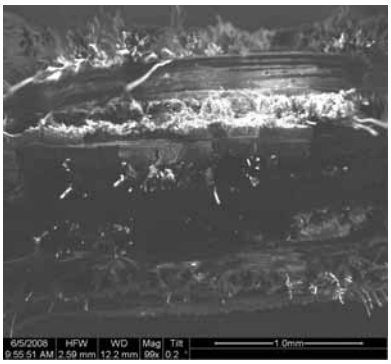

Figure A.66: Fracture surface of the N610/$LaPO_4$/Al_2O_3 specimen with 10ply 0°/90° uni-tape lay-up subjected to creep test at 120 MPa in steam at 1100 °C (t_f = 0.0313h).

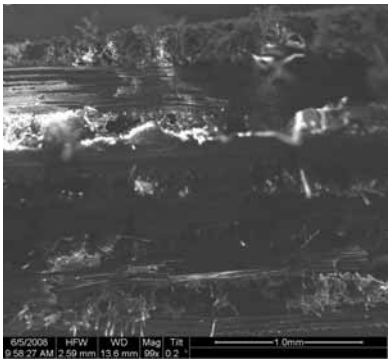

Figure A.67: Fracture surface of the N610/$LaPO_4$/Al_2O_3 specimen with 10ply 0°/90° uni-tape lay-up subjected to creep test at 120 MPa in steam at 1100 °C (t_f = 0.0313h).

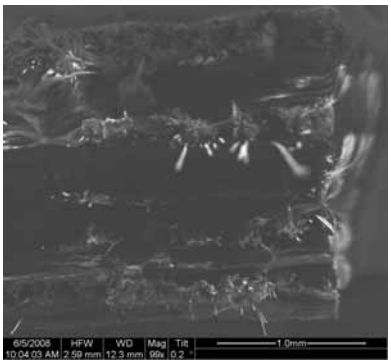

Figure A.68: Fracture surface of the N610/$LaPO_4$/Al_2O_3 specimen with 10ply 0°/90° uni-tape lay-up subjected to creep test at 120 MPa in steam at 1100 °C (t_f = 0.0313h).

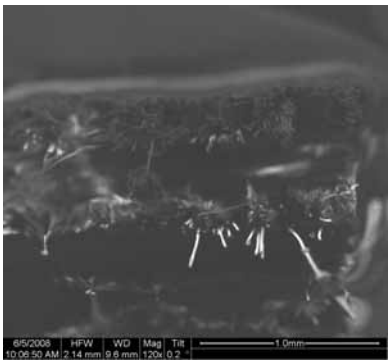

Figure A.69: Fracture surface of the N610/$LaPO_4$/Al_2O_3 specimen with 10ply 0°/90° uni-tape lay-up subjected to creep test at 120 MPa in steam at 1100 °C (t_f = 0.0313h).

Figure A.70: Fracture surface of the N610/$LaPO_4$/Al_2O_3 specimen with 10ply 0°/90° uni-tape lay-up subjected to creep test at 120 MPa in steam at 1100 °C (t_f = 0.0313h).

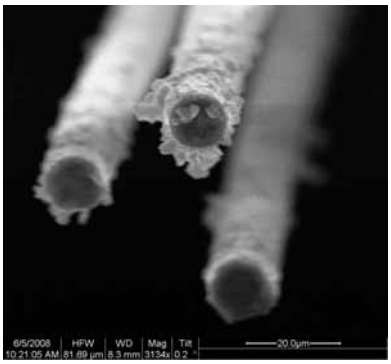

Figure A.71: Fracture surface of the N610/$LaPO_4$/Al_2O_3 specimen with 10ply 0°/90° uni-tape lay-up subjected to creep test at 120 MPa in steam at 1100 °C (t_f = 0.0313h).

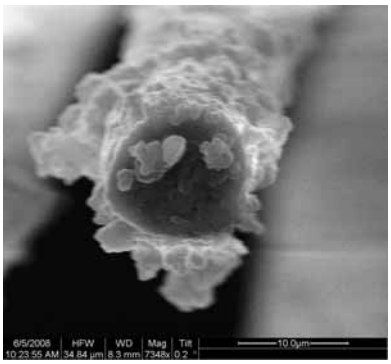

Figure A.72: Fracture surface of the N610/$LaPO_4$/Al_2O_3 specimen with 10ply 0°/90° uni-tape lay-up subjected to creep test at 120 MPa in steam at 1100 °C (t_f = 0.0313h).

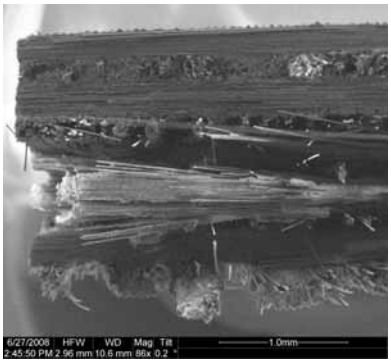

Figure A.73: Fracture surface of the N610/$LaPO_4$/Al_2O_3 specimen with 10ply 0°/90° uni-tape lay-up subjected to creep test at 120 MPa in air at 1100 °C (t_f = 0.748h).

Figure A.74: Fracture surface of the N610/$LaPO_4$/Al_2O_3 specimen with 10ply 0°/90° uni-tape lay-up subjected to creep test at 120 MPa in air at 1100 °C (t_f = 0.748h).

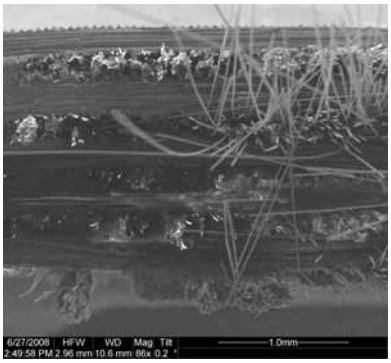

Figure A.75: Fracture surface of the N610/$LaPO_4$/Al_2O_3 specimen with 10ply 0°/90° uni-tape lay-up subjected to creep test at 120 MPa in air at 1100 °C (t_f = 0.748h).

Figure A.76: Fracture surface of the N610/$LaPO_4$/Al_2O_3 specimen with 10ply 0°/90° uni-tape lay-up subjected to creep test at 120 MPa in air at 1100 °C (t_f = 0.748h).

Figure A.77: Fracture surface of the N610/$LaPO_4$/Al_2O_3 specimen with 10ply 0°/90° uni-tape lay-up subjected to creep test at 120 MPa in air at 1100 °C (t_f = 0.748h).

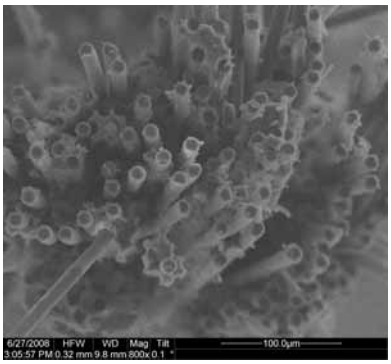

Figure A.78: Fracture surface of the N610/$LaPO_4$/Al_2O_3 specimen with 10ply 0°/90° uni-tape lay-up subjected to creep test at 120 MPa in air at 1100 °C (t_f = 0.748h).

Figure A.79: Fracture surface of the N610/$LaPO_4$/Al_2O_3 specimen with 10ply 0°/90° uni-tape lay-up subjected to creep test at 120 MPa in air at 1100 °C (t_f = 0.748h).

Figure A.80: Fracture surface of the N610/$LaPO_4$/Al_2O_3 specimen with 10ply 0°/90° uni-tape lay-up subjected to creep test at 120 MPa in air at 1100 °C (t_f = 0.748h).

Figure A.81: Fracture surface of the N610/$LaPO_4$/Al_2O_3 specimen with 10ply 0°/90° uni-tape lay-up subjected to creep test at 120 MPa in air at 1100 °C (t_f = 0.748h).

Figure A.82: Fracture surface of the N610/$LaPO_4$/Al_2O_3 specimen with 10ply 0°/90° uni-tape lay-up subjected to creep test at 120 MPa in air at 1100 °C (t_f = 0.748h).

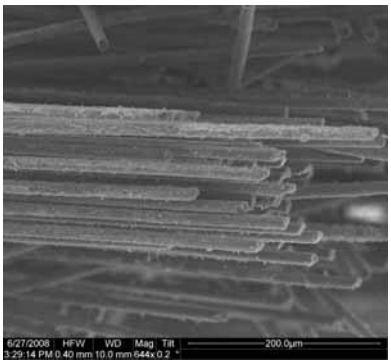

Figure A.83: Fracture surface of the N610/$LaPO_4$/Al_2O_3 specimen with 10ply 0°/90° uni-tape lay-up subjected to creep test at 120 MPa in air at 1100 °C (t_f = 0.748h).

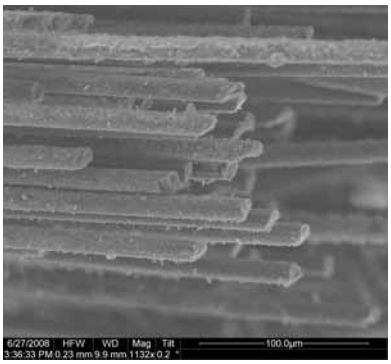

Figure A.84: Fracture surface of the N610/$LaPO_4$/Al_2O_3 specimen with 10ply 0°/90° uni-tape lay-up subjected to creep test at 120 MPa in air at 1100 °C (t_f = 0.748h).

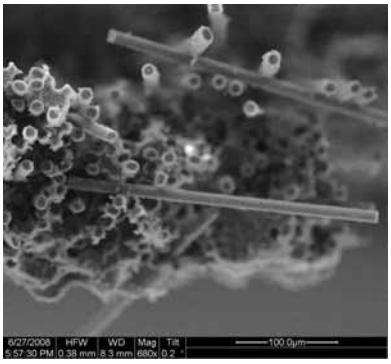

Figure A.85: Fracture surface of the N610/$LaPO_4$/Al_2O_3 specimen with 10ply 0°/90° uni-tape lay-up subjected to creep test at 120 MPa in air at 1100 °C (t_f = 0.748h).

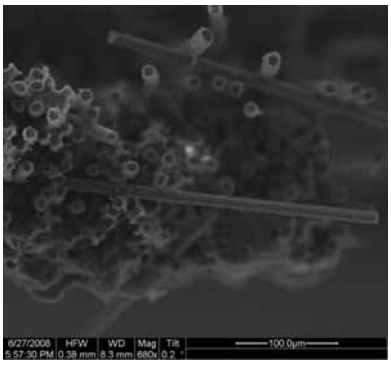

Figure A.86: Fracture surface of the N610/$LaPO_4$/Al_2O_3 specimen with 10ply 0°/90° uni-tape lay-up subjected to creep test at 120 MPa in air at 1100 °C (t_f = 0.748h).

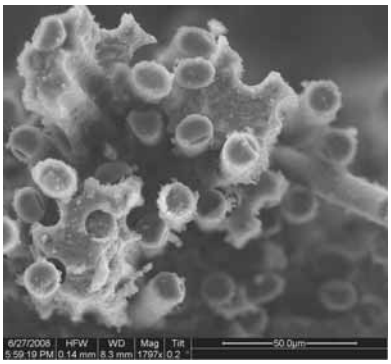

Figure A.87: Fracture surface of the N610/$LaPO_4$/Al_2O_3 specimen with 10ply 0°/90° uni-tape lay-up subjected to creep test at 120 MPa in air at 1100 °C (t_f = 0.748h).

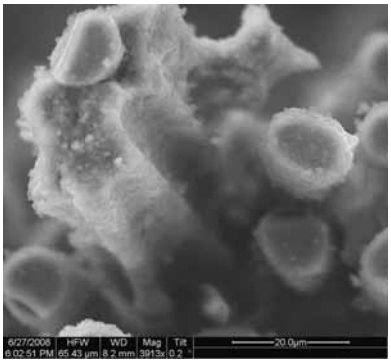

Figure A.88: Fracture surface of the N610/$LaPO_4$/Al_2O_3 specimen with 10ply 0°/90° uni-tape lay-up subjected to creep test at 120 MPa in air at 1100 °C (t_f = 0.748h).

Figure A.89: Fracture surface of the N610/$LaPO_4$/Al_2O_3 specimen with 10ply 0°/90° uni-tape lay-up subjected to creep test at 120 MPa in air at 1100 °C (t_f = 0.748h).

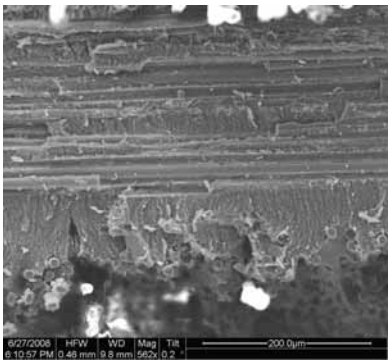

Figure A.90: Fracture surface of the N610/$LaPO_4$/Al_2O_3 specimen with 10ply 0°/90° uni-tape lay-up subjected to creep test at 120 MPa in air at 1100 °C (t_f = 0.748h).

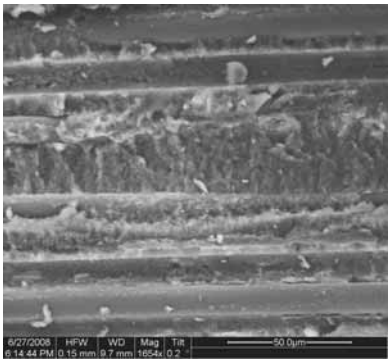

Figure A.91: Fracture surface of the N610/$LaPO_4$/Al_2O_3 specimen with 10ply 0°/90° uni-tape lay-up subjected to creep test at 120 MPa in air at 1100 °C (t_f = 0.748h).

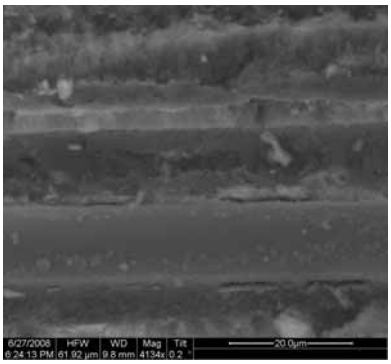

Figure A.92: Fracture surface of the N610/$LaPO_4$/Al_2O_3 specimen with 10ply 0°/90° uni-tape lay-up subjected to creep test at 120 MPa in air at 1100 °C (t_f = 0.748h).

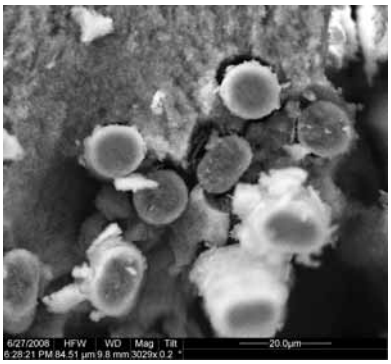

Figure A.93: Fracture surface of the N610/$LaPO_4$/Al_2O_3 specimen with 10ply 0°/90° uni-tape lay-up subjected to creep test at 120 MPa in air at 1100 °C (t_f = 0.748h).

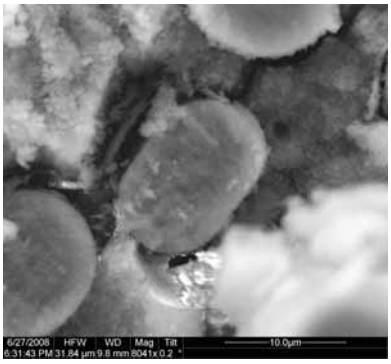

Figure A.94: Fracture surface of the N610/$LaPO_4$/Al_2O_3 specimen with 10ply 0°/90° uni-tape lay-up subjected to creep test at 120 MPa in air at 1100 °C (t_f = 0.748h).

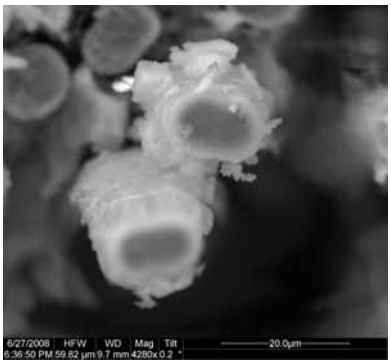

Figure A.95: Fracture surface of the N610/$LaPO_4$/Al_2O_3 specimen with 10ply 0°/90° uni-tape lay-up subjected to creep test at 120 MPa in air at 1100 °C (t_f = 0.748h).

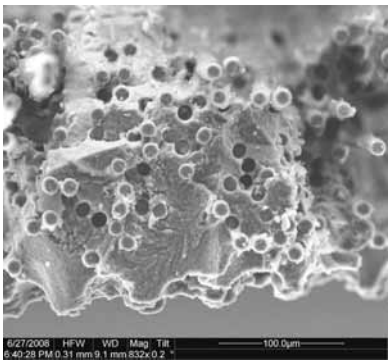

Figure A.96: Fracture surface of the N610/$LaPO_4$/Al_2O_3 specimen with 10ply 0°/90° uni-tape lay-up subjected to creep test at 120 MPa in air at 1100 °C (t_f = 0.748h).

Figure A.97: Fracture surface of the N610/$LaPO_4$/Al_2O_3 specimen with 10ply 0°/90° uni-tape lay-up subjected to creep test at 120 MPa in air at 1100 °C (t_f = 0.748h).

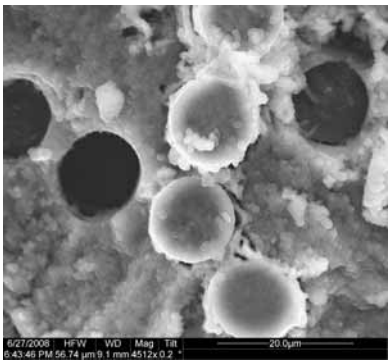

Figure A.98: Fracture surface of the N610/$LaPO_4$/Al_2O_3 specimen with 10ply 0°/90° uni-tape lay-up subjected to creep test at 120 MPa in air at 1100 °C (t_f = 0.748h).

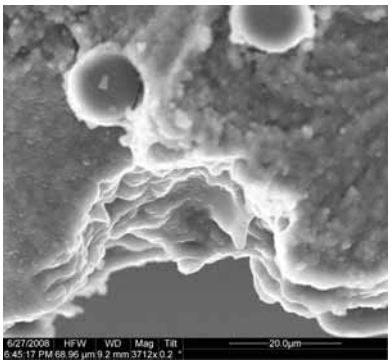

Figure A.99: Fracture surface of the N610/$LaPO_4$/Al_2O_3 specimen with 10ply 0°/90° uni-tape lay-up subjected to creep test at 120 MPa in air at 1100 °C (t_f = 0.748h).

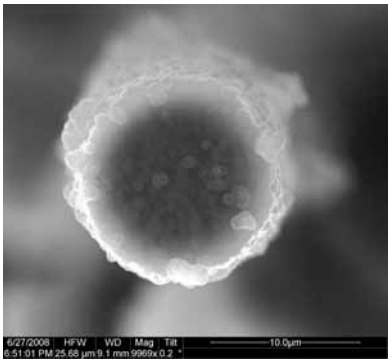

Figure A.100: Fracture surface of the N610/$LaPO_4$/Al_2O_3 specimen with 10ply 0°/90° uni-tape lay-up subjected to creep test at 120 MPa in air at 1100 °C (t_f = 0.748h).

Figure A.101: Fracture surface of the N610/$LaPO_4$/Al_2O_3 specimen with 10ply 0°/90° uni-tape lay-up subjected to creep test at 120 MPa in air at 1100 °C (t_f = 0.748h).

Figure A.102: Fracture surface of the N610/$LaPO_4$/Al_2O_3 specimen with 10ply 0°/90° uni-tape lay-up subjected to creep test at 120 MPa in air at 1100 °C (t_f = 0.748h).

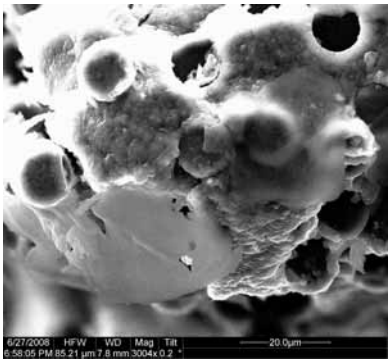

Figure A.103: Fracture surface of the N610/$LaPO_4$/Al_2O_3 specimen with 10ply 0°/90° uni-tape lay-up subjected to creep test at 120 MPa in air at 1100 °C (t_f = 0.748h).

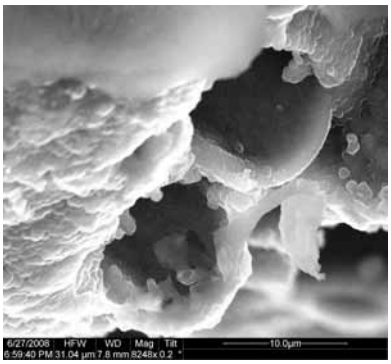

Figure A.104: Fracture surface of the N610/$LaPO_4$/Al_2O_3 specimen with 10ply 0°/90° uni-tape lay-up subjected to creep test at 120 MPa in air at 1100 °C (t_f = 0.748h).

Figure A.105: Fracture surface of the N610/$LaPO_4$/Al_2O_3 specimen with 10ply 0°/90° uni-tape lay-up subjected to creep test at 120 MPa in air at 1100 °C (t_f = 0.748h).

Figure A.106: Fracture surface of the N610/$LaPO_4$/Al_2O_3 specimen with 10ply 0°/90° uni-tape lay-up subjected to creep test at 120 MPa in air at 1100 °C (t_f = 0.748h).

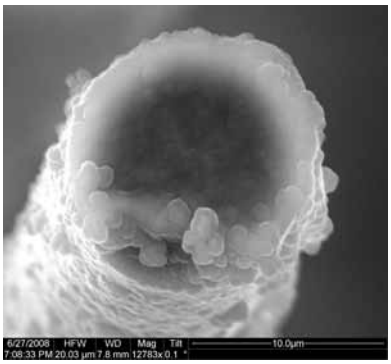

Figure A.107: Fracture surface of the N610/$LaPO_4$/Al_2O_3 specimen with 10ply 0°/90° uni-tape lay-up subjected to creep test at 120 MPa in air at 1100 °C (t_f = 0.748h).

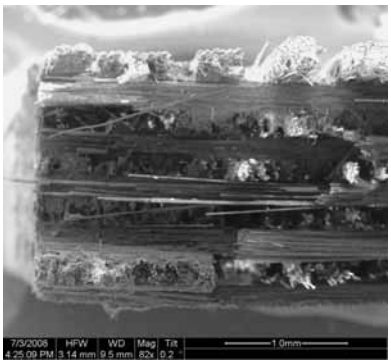

Figure A.108: Fracture surface of the N610/$LaPO_4$/Al_2O_3 specimen with 10ply 0°/90° uni-tape lay-up subjected to creep test at 85 MPa in steam at 1100 °C (t_f = 8.183h).

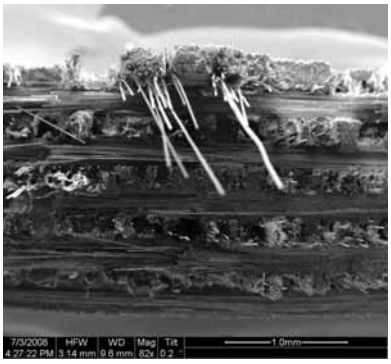

Figure A.109: Fracture surface of the N610/$LaPO_4$/Al_2O_3 specimen with 10ply 0°/90° uni-tape lay-up subjected to creep test at 85 MPa in steam at 1100 °C (t_f = 8.183h).

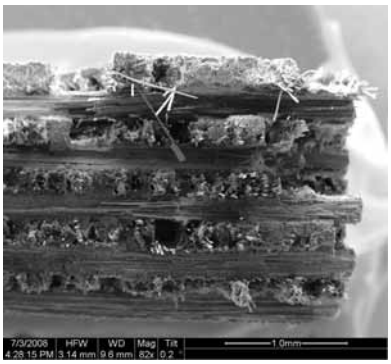

Figure A.110: Fracture surface of the N610/$LaPO_4$/Al_2O_3 specimen with 10ply 0°/90° uni-tape lay-up subjected to creep test at 85 MPa in steam at 1100 °C (t_f = 8.183h).

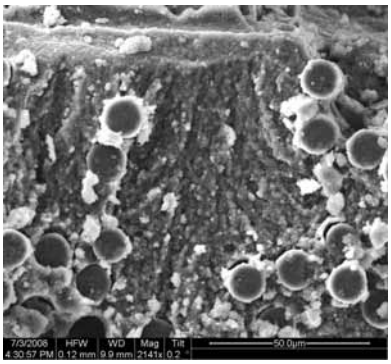

Figure A.111: Fracture surface of the N610/$LaPO_4$/Al_2O_3 specimen with 10ply 0°/90° uni-tape lay-up subjected to creep test at 85 MPa in steam at 1100 °C (t_f = 8.183h).

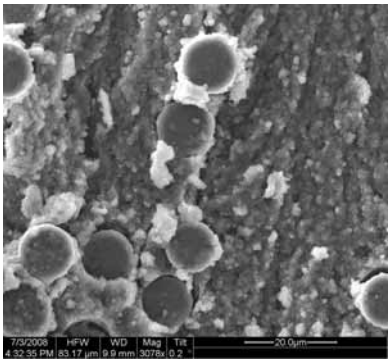

Figure A.112: Fracture surface of the N610/$LaPO_4$/Al_2O_3 specimen with 10ply 0°/90° uni-tape lay-up subjected to creep test at 85 MPa in steam at 1100 °C (t_f = 8.183h).

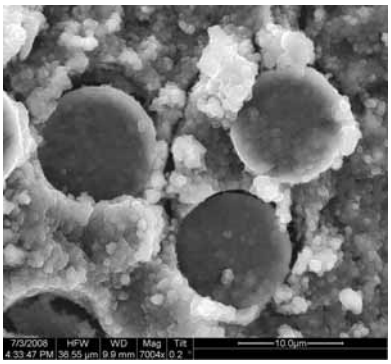

Figure A.113: Fracture surface of the N610/$LaPO_4$/Al_2O_3 specimen with 10ply 0°/90° uni-tape lay-up subjected to creep test at 85 MPa in steam at 1100 °C (t_f = 8.183h).

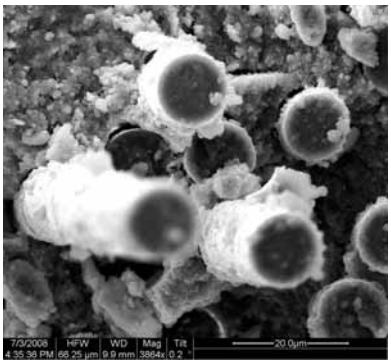

Figure A.114: Fracture surface of the N610/$LaPO_4$/Al_2O_3 specimen with 10ply 0°/90° uni-tape lay-up subjected to creep test at 85 MPa in steam at 1100 °C (t_f = 8.183h).

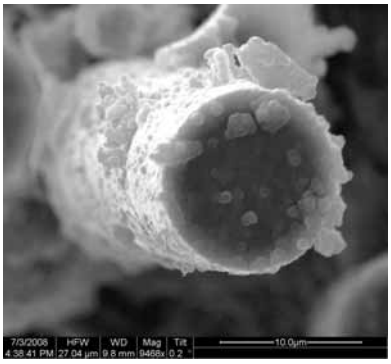

Figure A.115: Fracture surface of the N610/$LaPO_4$/Al_2O_3 specimen with 10ply 0°/90° uni-tape lay-up subjected to creep test at 85 MPa in steam at 1100 °C (t_f = 8.183h).

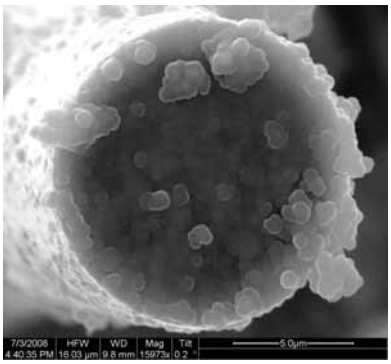

Figure A.116: Fracture surface of the N610/$LaPO_4$/Al_2O_3 specimen with 10ply 0°/90° uni-tape lay-up subjected to creep test at 85 MPa in steam at 1100 °C (t_f = 8.183h).

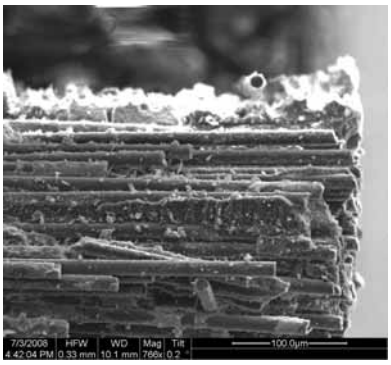

Figure A.117: Fracture surface of the N610/$LaPO_4$/Al_2O_3 specimen with 10ply 0°/90° uni-tape lay-up subjected to creep test at 85 MPa in steam at 1100 °C (t_f = 8.183h).

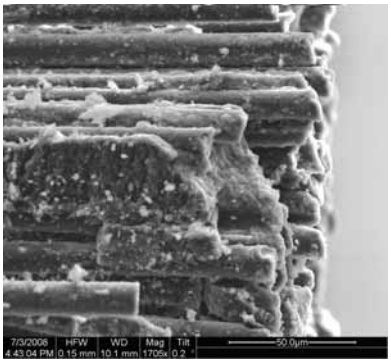

Figure A.118: Fracture surface of the N610/$LaPO_4$/Al_2O_3 specimen with 10ply 0°/90° uni-tape lay-up subjected to creep test at 85 MPa in steam at 1100 °C (t_f = 8.183h).

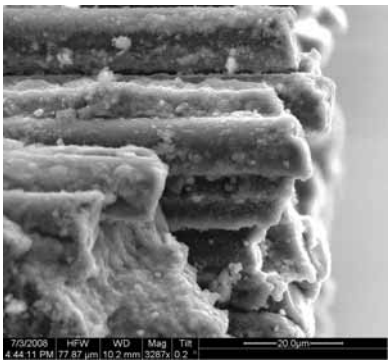

Figure A.119: Fracture surface of the N610/$LaPO_4$/Al_2O_3 specimen with 10ply 0°/90° uni-tape lay-up subjected to creep test at 85 MPa in steam at 1100 °C (t_f = 8.183h).

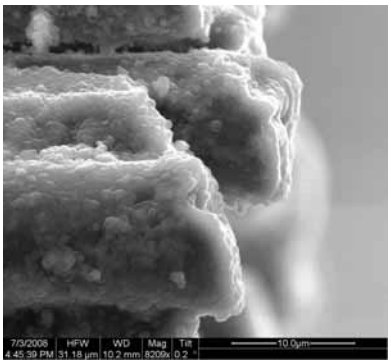

Figure A.120: Fracture surface of the N610/$LaPO_4$/Al_2O_3 specimen with 10ply 0°/90° uni-tape lay-up subjected to creep test at 85 MPa in steam at 1100 °C (t_f = 8.183h).

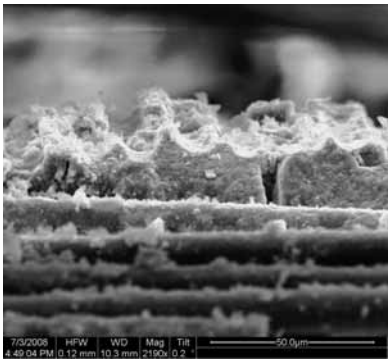

Figure A.121: Fracture surface of the N610/$LaPO_4$/Al_2O_3 specimen with 10ply 0°/90° uni-tape lay-up subjected to creep test at 85 MPa in steam at 1100 °C (t_f = 8.183h).

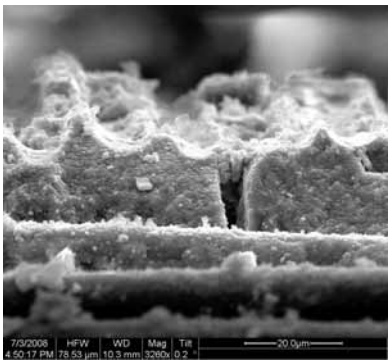

Figure A.122: Fracture surface of the N610/$LaPO_4$/Al_2O_3 specimen with 10ply 0°/90° uni-tape lay-up subjected to creep test at 85 MPa in steam at 1100 °C (t_f = 8.183h).

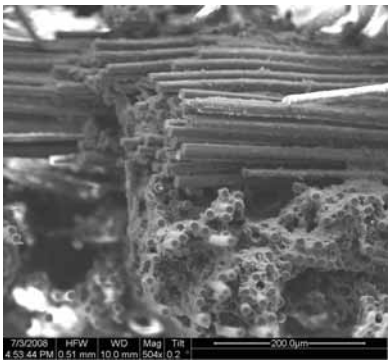

Figure A.123: Fracture surface of the N610/$LaPO_4$/Al_2O_3 specimen with 10ply 0°/90° uni-tape lay-up subjected to creep test at 85 MPa in steam at 1100 °C (t_f = 8.183h).

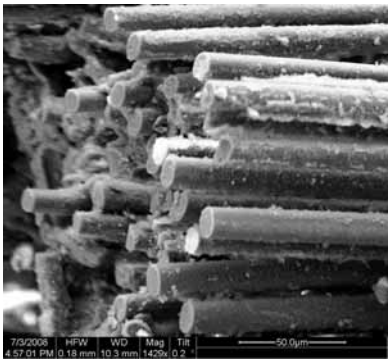

Figure A.124: Fracture surface of the N610/$LaPO_4$/Al_2O_3 specimen with 10ply 0°/90° uni-tape lay-up subjected to creep test at 85 MPa in steam at 1100 °C (t_f = 8.183h).

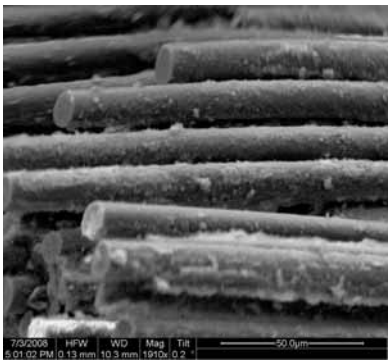

Figure A.125: Fracture surface of the N610/$LaPO_4$/Al_2O_3 specimen with 10ply 0°/90° uni-tape lay-up subjected to creep test at 85 MPa in steam at 1100 °C (t_f = 8.183h).

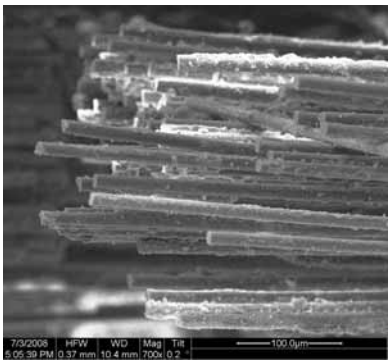

Figure A.126: Fracture surface of the N610/$LaPO_4$/Al_2O_3 specimen with 10ply 0°/90° uni-tape lay-up subjected to creep test at 85 MPa in steam at 1100 °C (t_f = 8.183h).

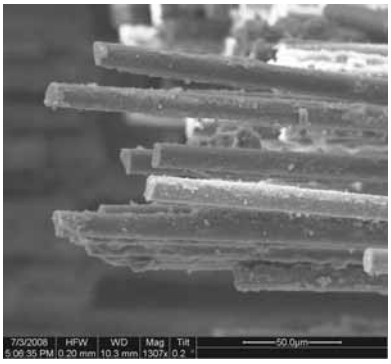

Figure A.127: Fracture surface of the N610/$LaPO_4$/Al_2O_3 specimen with 10ply 0°/90° uni-tape lay-up subjected to creep test at 85 MPa in steam at 1100 °C (t_f = 8.183h).

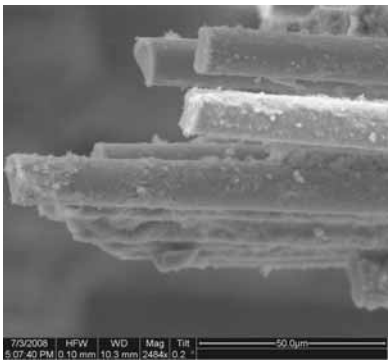

Figure A.128: Fracture surface of the N610/$LaPO_4$/Al_2O_3 specimen with 10ply 0°/90° uni-tape lay-up subjected to creep test at 85 MPa in steam at 1100 °C (t_f = 8.183h).

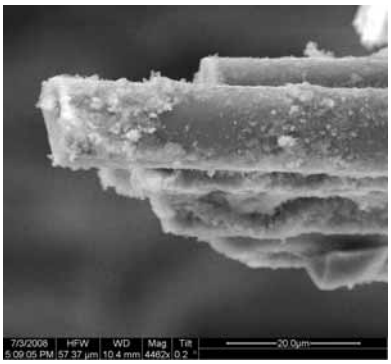

Figure A.129: Fracture surface of the N610/$LaPO_4$/Al_2O_3 specimen with 10ply 0°/90° uni-tape lay-up subjected to creep test at 85 MPa in steam at 1100 °C (t_f = 8.183h).

Figure A.130: Fracture surface of the N610/$LaPO_4$/Al_2O_3 specimen with 10ply 0°/90° uni-tape lay-up subjected to creep test at 85 MPa in steam at 1100 °C (t_f = 8.183h).

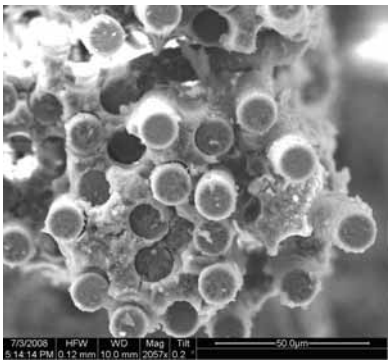

Figure A.131: Fracture surface of the N610/$LaPO_4$/Al_2O_3 specimen with 10ply 0°/90° uni-tape lay-up subjected to creep test at 85 MPa in steam at 1100 °C (t_f = 8.183h).

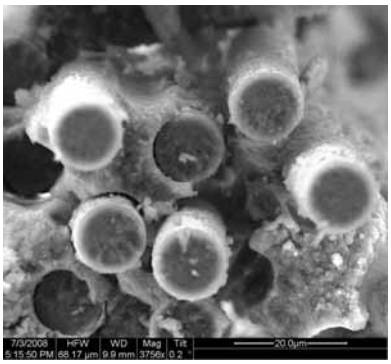

Figure A.132: Fracture surface of the N610/$LaPO_4$/Al_2O_3 specimen with 10ply 0°/90° uni-tape lay-up subjected to creep test at 85 MPa in steam at 1100 °C (t_f = 8.183h).

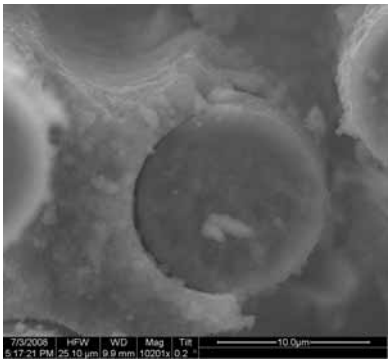

Figure A.133: Fracture surface of the N610/$LaPO_4$/Al_2O_3 specimen with 10ply 0°/90° uni-tape lay-up subjected to creep test at 85 MPa in steam at 1100 °C (t_f = 8.183h).

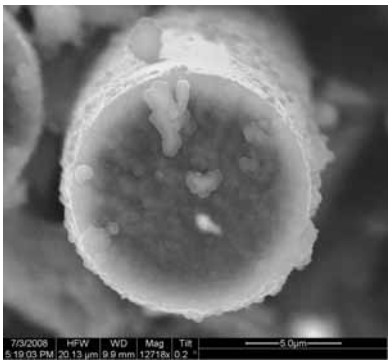

Figure A.134: Fracture surface of the N610/$LaPO_4$/Al_2O_3 specimen with 10ply 0°/90° uni-tape lay-up subjected to creep test at 85 MPa in steam at 1100 °C (t_f = 8.183h).

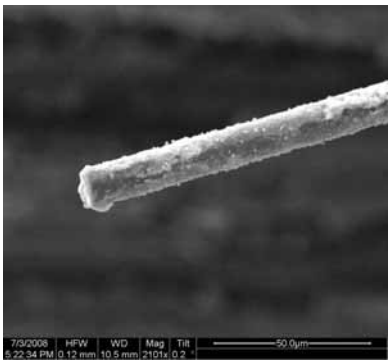

Figure A.135: Fracture surface of the N610/$LaPO_4$/Al_2O_3 specimen with 10ply 0°/90° uni-tape lay-up subjected to creep test at 85 MPa in steam at 1100 °C (t_f = 8.183h).

Figure A.136: Fracture surface of the N610/$LaPO_4$/Al_2O_3 specimen with 10ply 0°/90° uni-tape lay-up subjected to creep test at 85 MPa in steam at 1100 °C (t_f = 8.183h).

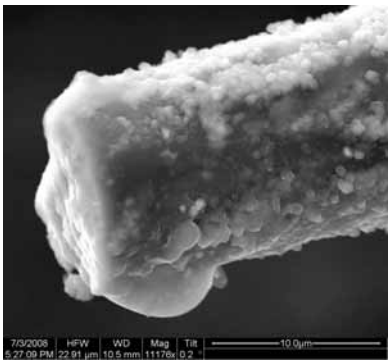

Figure A.137: Fracture surface of the N610/$LaPO_4$/Al_2O_3 specimen with 10ply 0°/90° uni-tape lay-up subjected to creep test at 85 MPa in steam at 1100 °C (t_f = 8.183h).

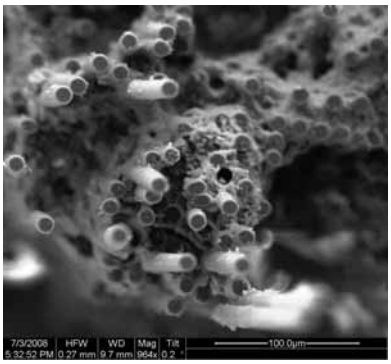

Figure A.138: Fracture surface of the N610/$LaPO_4$/Al_2O_3 specimen with 10ply 0°/90° uni-tape lay-up subjected to creep test at 85 MPa in steam at 1100 °C (t_f = 8.183h).

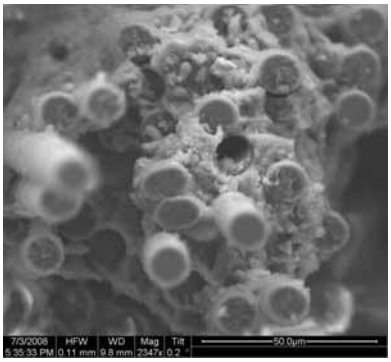

Figure A.139: Fracture surface of the N610/$LaPO_4$/Al_2O_3 specimen with 10ply 0°/90° uni-tape lay-up subjected to creep test at 85 MPa in steam at 1100 °C (t_f = 8.183h).

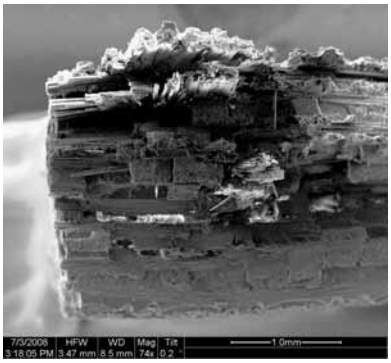

Figure A.140: Fracture surface of the N610/$LaPO_4$/Al_2O_3 specimen with 8ply HSW subjected to creep test at 32 MPa in air at 1100 °C (t_f = 100h).

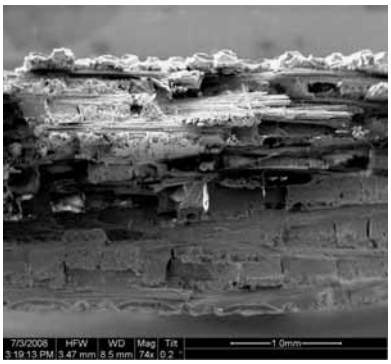

Figure A.141: Fracture surface of the N610/$LaPO_4$/Al_2O_3 specimen with 8ply HSW subjected to creep test at 32 MPa in air at 1100 °C (t_f = 100h).

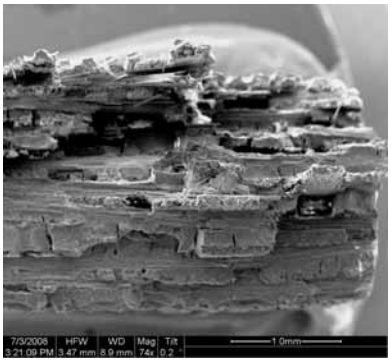

Figure A.142: Fracture surface of the N610/$LaPO_4$/Al_2O_3 specimen with 8ply HSW subjected to creep test at 32 MPa in air at 1100 °C (t_f = 100h).

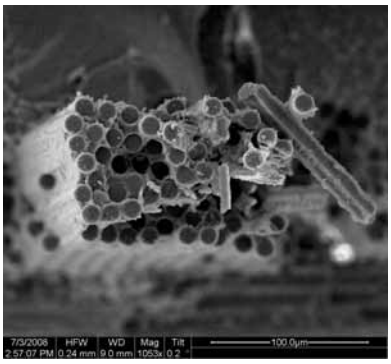

Figure A.143: Fracture surface of the N610/$LaPO_4$/Al_2O_3 specimen with 8ply HSW subjected to creep test at 32 MPa in air at 1100 °C (t_f = 100h).

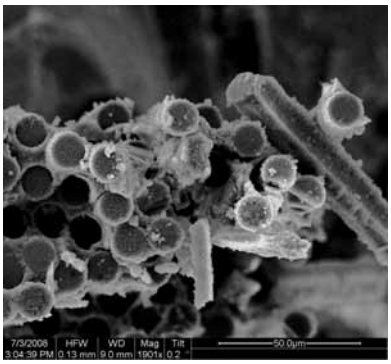

Figure A.144: Fracture surface of the N610/$LaPO_4$/Al_2O_3 specimen with 8ply HSW subjected to creep test at 32 MPa in air at 1100 °C (t_f = 100h).

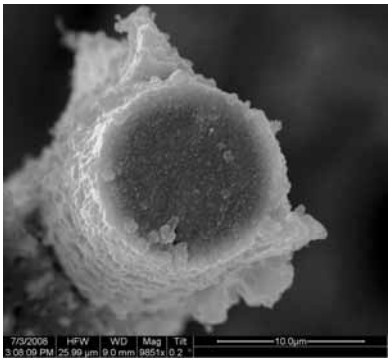

Figure A.145: Fracture surface of the N610/$LaPO_4$/Al_2O_3 specimen with 8ply HSW subjected to creep test at 32 MPa in air at 1100 °C (t_f = 100h).

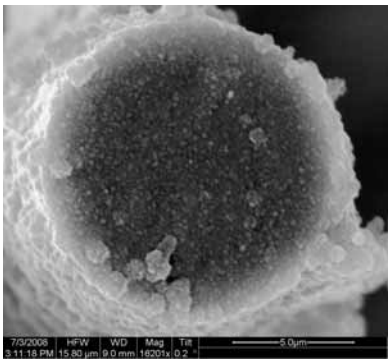

Figure A.146: Fracture surface of the N610/$LaPO_4$/Al_2O_3 specimen with 8ply HSW subjected to creep test at 32 MPa in air at 1100 °C (t_f = 100h).

Figure A.147: Fracture surface of the N610/$LaPO_4$/Al_2O_3 specimen with 8ply HSW subjected to creep test at 32 MPa in air at 1100 °C (t_f = 100h).

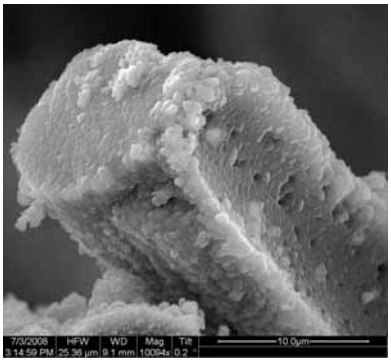

Figure A.148: Fracture surface of the N610/$LaPO_4$/Al_2O_3 specimen with 8ply HSW subjected to creep test at 32 MPa in air at 1100 °C (t_f = 100h).

Figure A.149: Fracture surface of the N610/$LaPO_4$/Al_2O_3 specimen with 8ply HSW subjected to creep test at 32 MPa in air at 1100 °C (t_f = 100h).

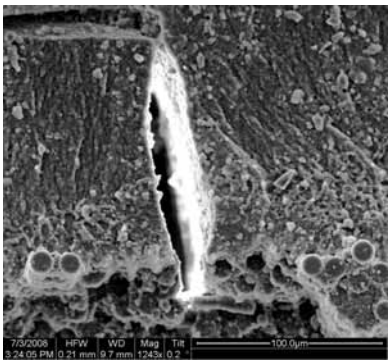

Figure A.150: Fracture surface of the N610/$LaPO_4$/Al_2O_3 specimen with 8ply HSW subjected to creep test at 32 MPa in air at 1100 °C (t_f = 100h).

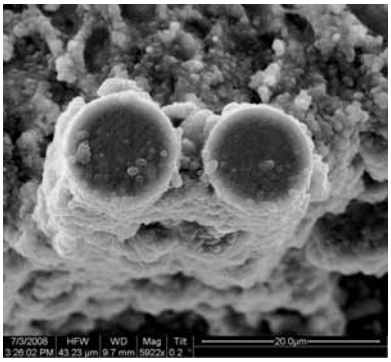

Figure A.151: Fracture surface of the N610/$LaPO_4$/Al_2O_3 specimen with 8ply HSW subjected to creep test at 32 MPa in air at 1100 °C (t_f = 100h).

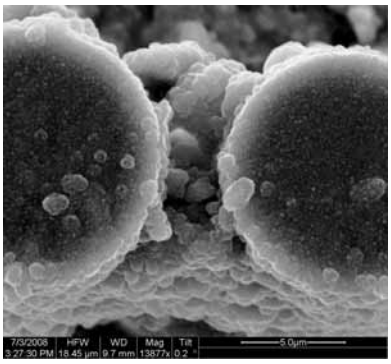

Figure A.152: Fracture surface of the N610/$LaPO_4$/Al_2O_3 specimen with 8ply HSW subjected to creep test at 32 MPa in air at 1100 °C (t_f = 100h).

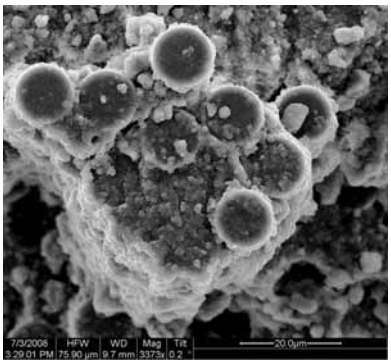

Figure A.153: Fracture surface of the N610/$LaPO_4$/Al_2O_3 specimen with 8ply HSW subjected to creep test at 32 MPa in air at 1100 °C (t_f = 100h).

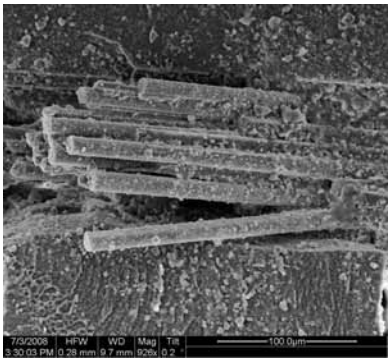

Figure A.154: Fracture surface of the N610/$LaPO_4$/Al_2O_3 specimen with 8ply HSW subjected to creep test at 32 MPa in air at 1100 °C (t_f = 100h).

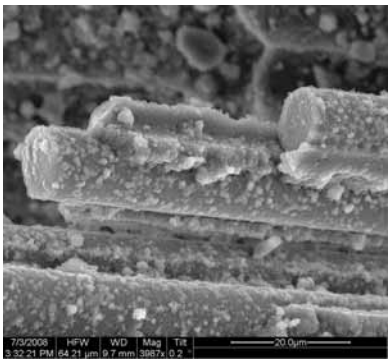

Figure A.155: Fracture surface of the N610/$LaPO_4$/Al_2O_3 specimen with 8ply HSW subjected to creep test at 32 MPa in air at 1100 °C (t_f = 100h).

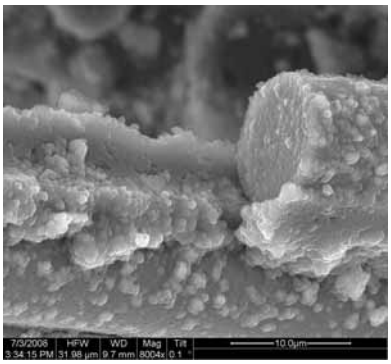

Figure A.156: Fracture surface of the N610/$LaPO_4$/Al_2O_3 specimen with 8ply HSW subjected to creep test at 32 MPa in air at 1100 °C (t_f = 100h).

Figure A.157: Fracture surface of the N610/$LaPO_4$/Al_2O_3 specimen with 8ply HSW subjected to creep test at 32 MPa in air at 1100 °C (t_f = 100h).

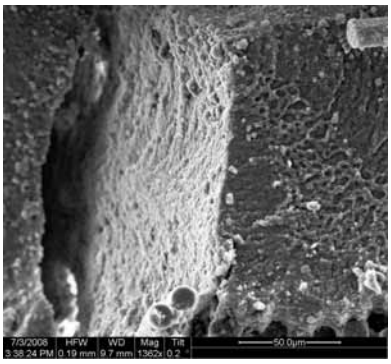

Figure A.158: Fracture surface of the N610/$LaPO_4$/Al_2O_3 specimen with 8ply HSW subjected to creep test at 32 MPa in air at 1100 °C (t_f = 100h).

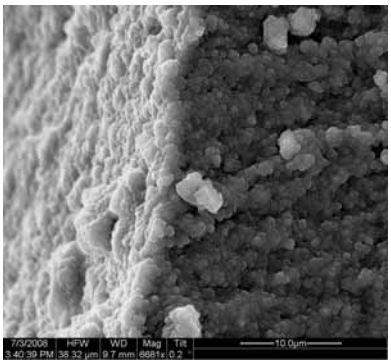

Figure A.159: Fracture surface of the N610/$LaPO_4$/Al_2O_3 specimen with 8ply HSW subjected to creep test at 32 MPa in air at 1100 °C (t_f = 100h).

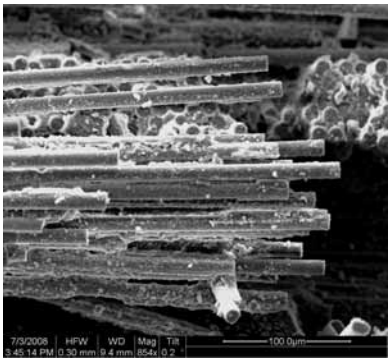

Figure A.160: Fracture surface of the N610/$LaPO_4$/Al_2O_3 specimen with 8ply HSW subjected to creep test at 32 MPa in air at 1100 °C (t_f = 100h).

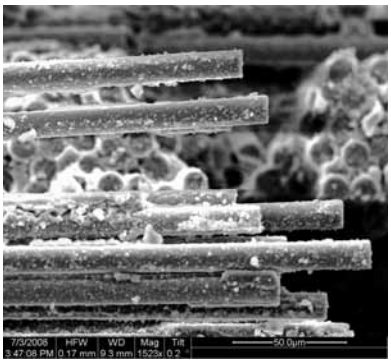

Figure A.161: Fracture surface of the N610/$LaPO_4$/Al_2O_3 specimen with 8ply HSW subjected to creep test at 32 MPa in air at 1100 °C (t_f = 100h).

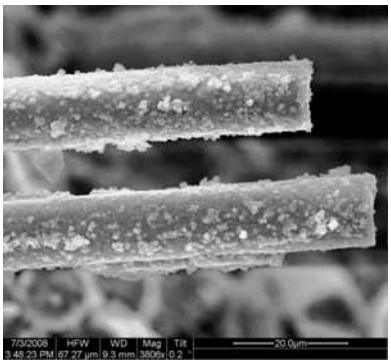

Figure A.162: Fracture surface of the N610/$LaPO_4$/Al_2O_3 specimen with 8ply HSW subjected to creep test at 32 MPa in air at 1100 °C (t_f = 100h).

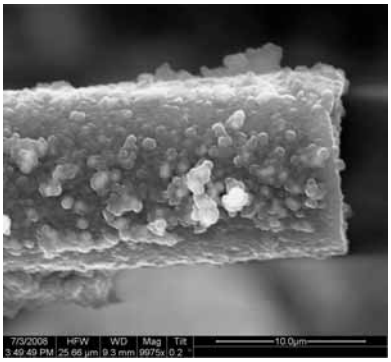

Figure A.163: Fracture surface of the N610/$LaPO_4$/Al_2O_3 specimen with 8ply HSW subjected to creep test at 32 MPa in air at 1100 °C (t_f = 100h).

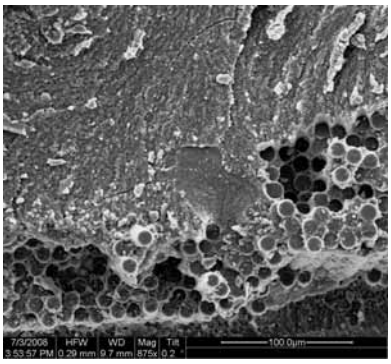

Figure A.164: Fracture surface of the N610/$LaPO_4$/Al_2O_3 specimen with 8ply HSW subjected to creep test at 32 MPa in air at 1100 °C (t_f = 100h).

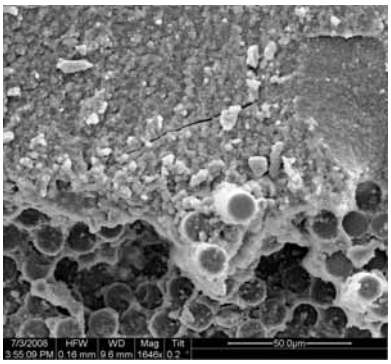

Figure A.165: Fracture surface of the N610/$LaPO_4$/Al_2O_3 specimen with 8ply HSW subjected to creep test at 32 MPa in air at 1100 °C (t_f = 100h).

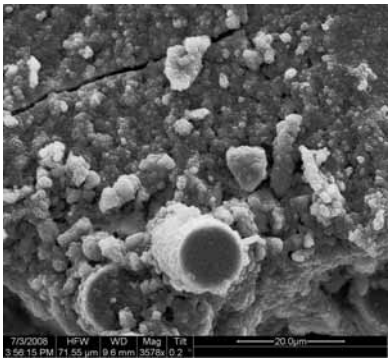

Figure A.166: Fracture surface of the N610/$LaPO_4$/Al_2O_3 specimen with 8ply HSW subjected to creep test at 32 MPa in air at 1100 °C (t_f = 100h).

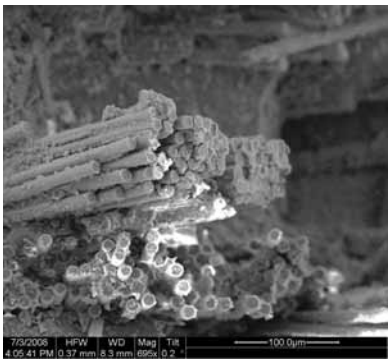

Figure A.167: Fracture surface of the N610/$LaPO_4$/Al_2O_3 specimen with 8ply HSW subjected to creep test at 32 MPa in air at 1100 °C (t_f = 100h).

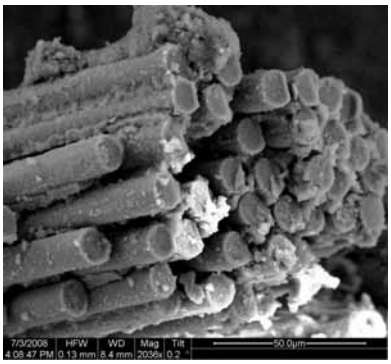

Figure A.168: Fracture surface of the N610/$LaPO_4$/Al_2O_3 specimen with 8ply HSW subjected to creep test at 32 MPa in air at 1100 °C (t_f = 100h).

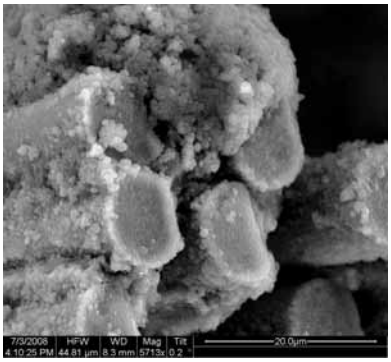

Figure A.169: Fracture surface of the N610/$LaPO_4$/Al_2O_3 specimen with 8ply HSW subjected to creep test at 32 MPa in air at 1100 °C (t_f = 100h).

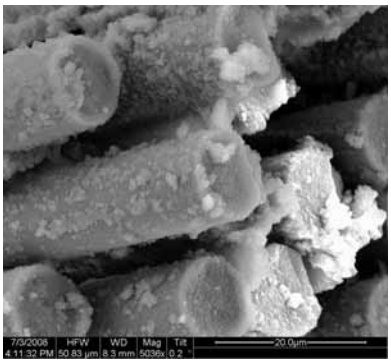

Figure A.170: Fracture surface of the N610/$LaPO_4$/Al_2O_3 specimen with 8ply HSW subjected to creep test at 32 MPa in air at 1100 °C (t_f = 100h).

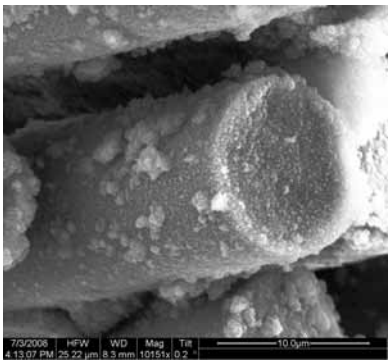

Figure A.171: Fracture surface of the N610/$LaPO_4$/Al_2O_3 specimen with 8ply HSW subjected to creep test at 32 MPa in air at 1100 °C (t_f = 100h).

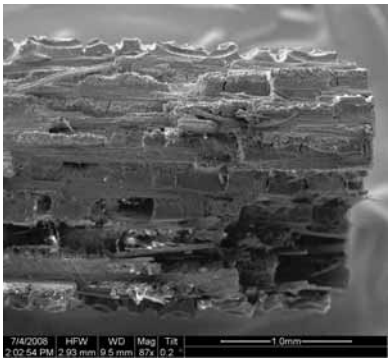

Figure A.172: Fracture surface of the N610/$LaPO_4$/Al_2O_3 specimen with 8ply HSW subjected to creep test at 32 MPa in steam at 1100 °C (t_f = 51.9h).

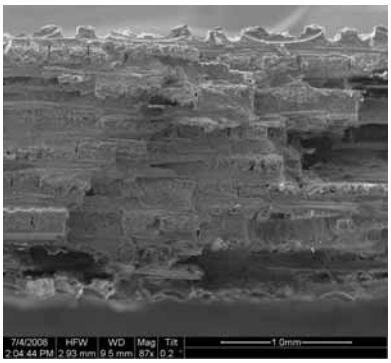

Figure A.173: Fracture surface of the N610/$LaPO_4$/Al_2O_3 specimen with 8ply HSW subjected to creep test at 32 MPa in steam at 1100 °C (t_f = 51.9h).

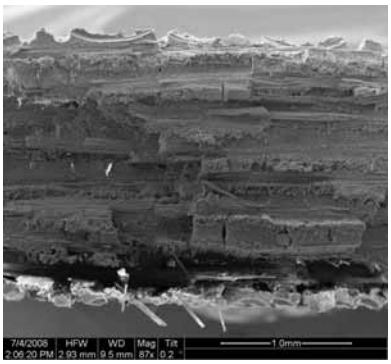

Figure A.174: Fracture surface of the N610/$LaPO_4$/Al_2O_3 specimen with 8ply HSW subjected to creep test at 32 MPa in steam at 1100 °C (t_f = 51.9h).

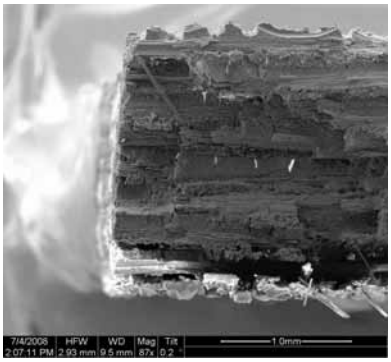

Figure A.175: Fracture surface of the N610/$LaPO_4$/Al_2O_3 specimen with 8ply HSW subjected to creep test at 32 MPa in steam at 1100 °C (t_f = 51.9h).

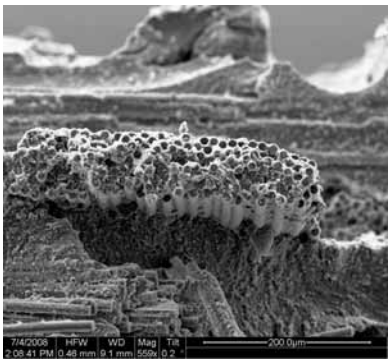

Figure A.176: Fracture surface of the N610/$LaPO_4$/Al_2O_3 specimen with 8ply HSW subjected to creep test at 32 MPa in steam at 1100 °C (t_f = 51.9h).

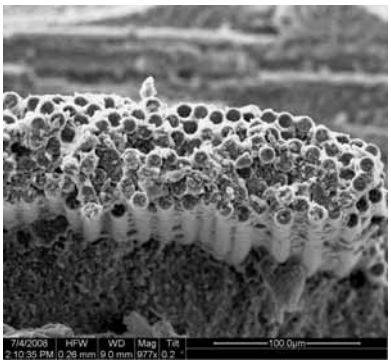

Figure A.177: Fracture surface of the N610/$LaPO_4$/Al_2O_3 specimen with 8ply HSW subjected to creep test at 32 MPa in steam at 1100 °C (t_f = 51.9h).

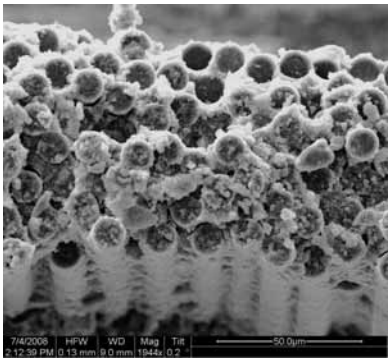

Figure A.178: Fracture surface of the N610/$LaPO_4$/Al_2O_3 specimen with 8ply HSW subjected to creep test at 32 MPa in steam at 1100 °C (t_f = 51.9h).

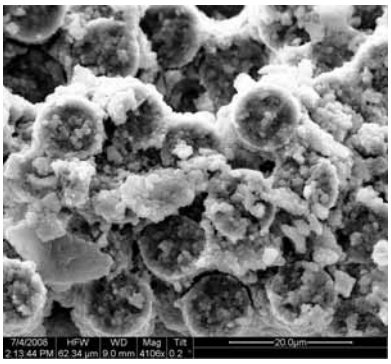

Figure A.179: Fracture surface of the N610/$LaPO_4$/Al_2O_3 specimen with 8ply HSW subjected to creep test at 32 MPa in steam at 1100 °C (t_f = 51.9h).

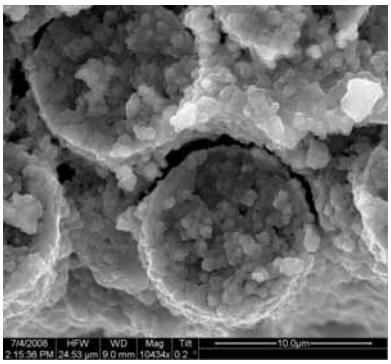

Figure A.180: Fracture surface of the N610/$LaPO_4$/Al_2O_3 specimen with 8ply HSW subjected to creep test at 32 MPa in steam at 1100 °C (t_f = 51.9h).

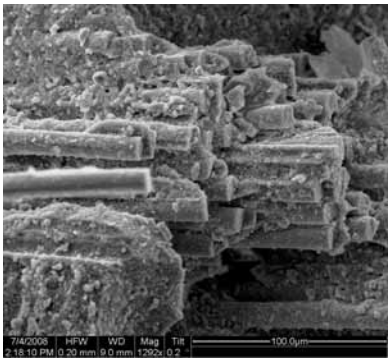

Figure A.181: Fracture surface of the N610/$LaPO_4$/Al_2O_3 specimen with 8ply HSW subjected to creep test at 32 MPa in steam at 1100 °C (t_f = 51.9h).

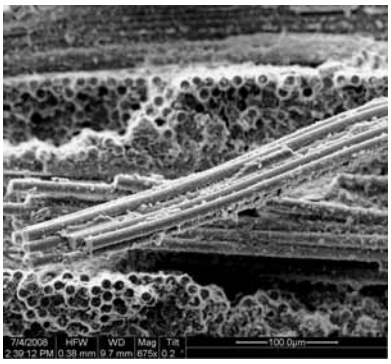

Figure A.182: Fracture surface of the N610/$LaPO_4$/Al_2O_3 specimen with 8ply HSW subjected to creep test at 32 MPa in steam at 1100 °C (t_f = 51.9h).

Figure A.183: Fracture surface of the N610/$LaPO_4$/Al_2O_3 specimen with 8ply HSW subjected to creep test at 32 MPa in steam at 1100 °C (t_f = 51.9h).

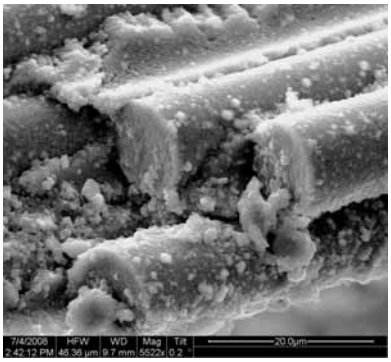

Figure A.184: Fracture surface of the N610/$LaPO_4$/Al_2O_3 specimen with 8ply HSW subjected to creep test at 32 MPa in steam at 1100 °C (t_f = 51.9h).

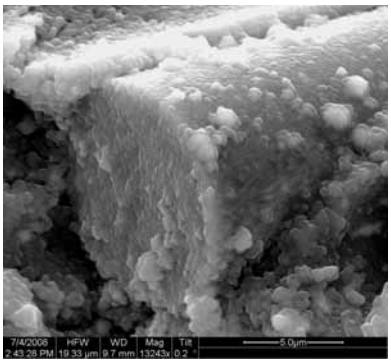

Figure A.185: Fracture surface of the N610/$LaPO_4$/Al_2O_3 specimen with 8ply HSW subjected to creep test at 32 MPa in steam at 1100 °C (t_f = 51.9h).

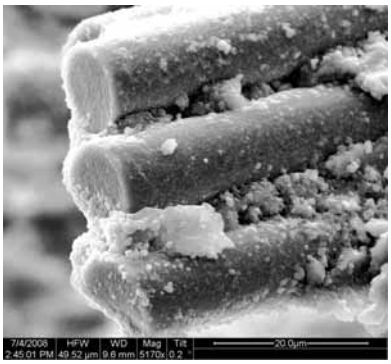

Figure A.186: Fracture surface of the N610/$LaPO_4$/Al_2O_3 specimen with 8ply HSW subjected to creep test at 32 MPa in steam at 1100 °C (t_f = 51.9h).

Figure A.187: Fracture surface of the N610/$LaPO_4$/Al_2O_3 specimen with 8ply HSW subjected to creep test at 32 MPa in steam at 1100 °C (t_f = 51.9h).

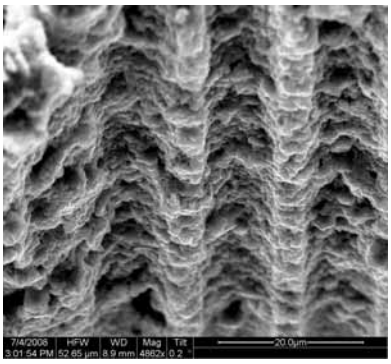

Figure A.188: Fracture surface of the N610/$LaPO_4$/Al_2O_3 specimen with 8ply HSW subjected to creep test at 32 MPa in steam at 1100 °C (t_f = 51.9h).

Figure A.189: Fracture surface of the N610/$LaPO_4$/Al_2O_3 specimen with 8ply HSW subjected to creep test at 32 MPa in steam at 1100 °C (t_f = 51.9h).

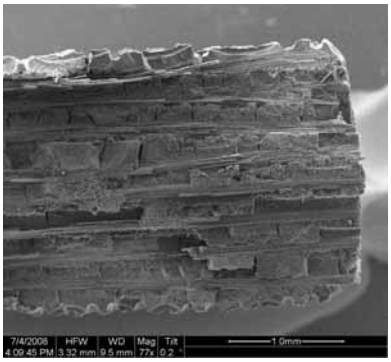

Figure A.190: Fracture surface of the N610/$LaPO_4$/Al_2O_3 specimen with 8ply HSW subjected to creep test at 72 MPa in air at 1100 °C (t_f = 100h).

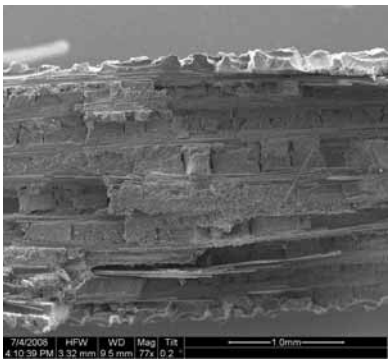

Figure A.191: Fracture surface of the N610/$LaPO_4$/Al_2O_3 specimen with 8ply HSW subjected to creep test at 72 MPa in air at 1100 °C (t_f = 100h).

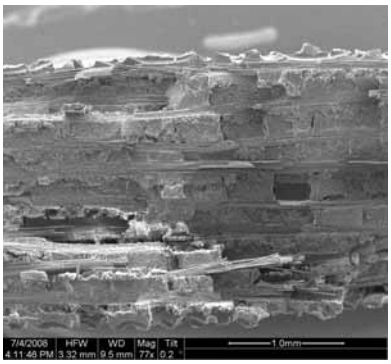

Figure A.192: Fracture surface of the N610/$LaPO_4$/Al_2O_3 specimen with 8ply HSW subjected to creep test at 72 MPa in air at 1100 °C (t_f = 100h).

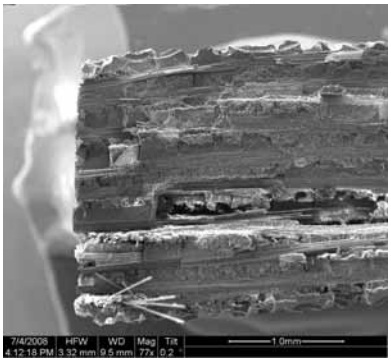

Figure A.193: Fracture surface of the N610/$LaPO_4$/Al_2O_3 specimen with 8ply HSW subjected to creep test at 72 MPa in air at 1100 °C (t_f = 100h).

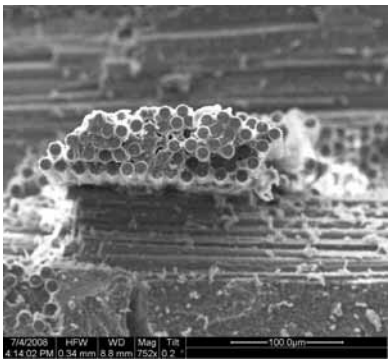

Figure A.194: Fracture surface of the N610/$LaPO_4$/Al_2O_3 specimen with 8ply HSW subjected to creep test at 72 MPa in air at 1100 °C (t_f = 100h).

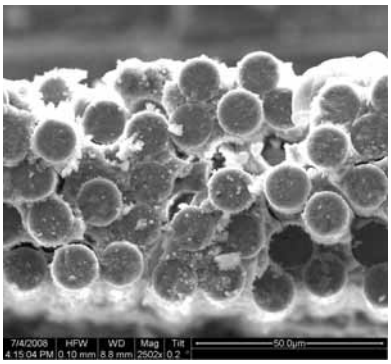

Figure A.195: Fracture surface of the N610/$LaPO_4$/Al_2O_3 specimen with 8ply HSW subjected to creep test at 72 MPa in air at 1100 °C (t_f = 100h).

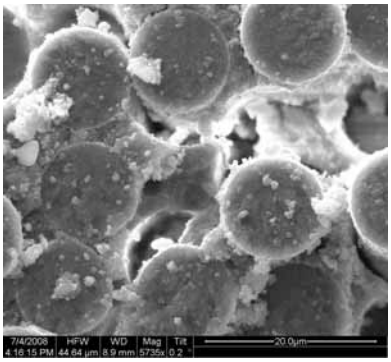

Figure A.196: Fracture surface of the N610/$LaPO_4$/Al_2O_3 specimen with 8ply HSW subjected to creep test at 72 MPa in air at 1100 °C (t_f = 100h).

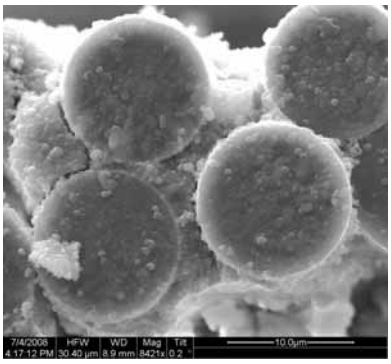

Figure A.197: Fracture surface of the N610/$LaPO_4$/Al_2O_3 specimen with 8ply HSW subjected to creep test at 72 MPa in air at 1100 °C (t_f = 100h).

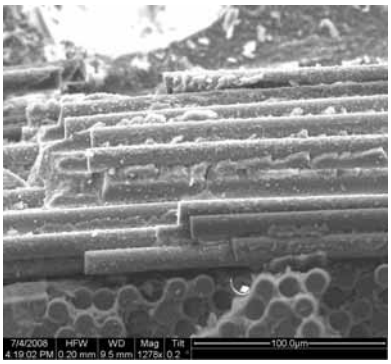

Figure A.198: Fracture surface of the N610/$LaPO_4$/Al_2O_3 specimen with 8ply HSW subjected to creep test at 72 MPa in air at 1100 °C (t_f = 100h).

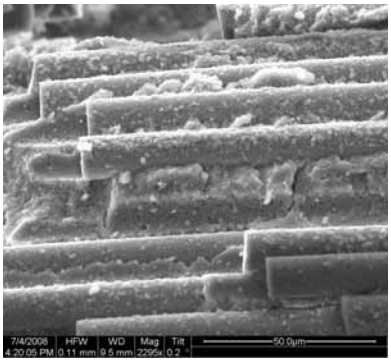

Figure A.199: Fracture surface of the N610/$LaPO_4$/Al_2O_3 specimen with 8ply HSW subjected to creep test at 72 MPa in air at 1100 °C (t_f = 100h).

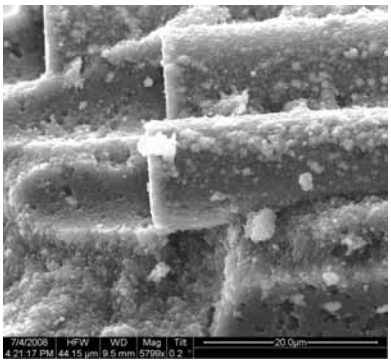

Figure A.200: Fracture surface of the N610/$LaPO_4$/Al_2O_3 specimen with 8ply HSW subjected to creep test at 72 MPa in air at 1100 °C (t_f = 100h).

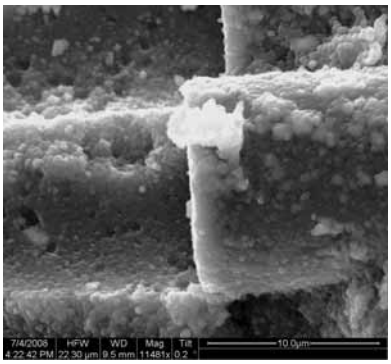

Figure A.201: Fracture surface of the N610/$LaPO_4$/Al_2O_3 specimen with 8ply HSW subjected to creep test at 72 MPa in air at 1100 °C (t_f = 100h).

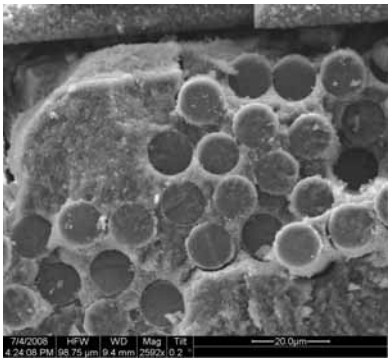

Figure A.202: Fracture surface of the N610/$LaPO_4$/Al_2O_3 specimen with 8ply HSW subjected to creep test at 72 MPa in air at 1100 °C (t_f = 100h).

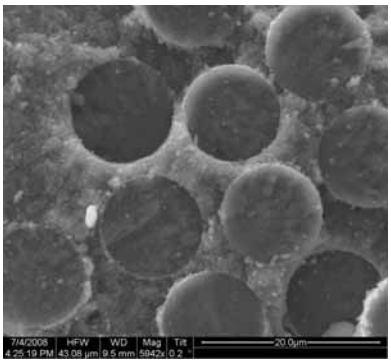

Figure A.203: Fracture surface of the N610/$LaPO_4$/Al_2O_3 specimen with 8ply HSW subjected to creep test at 72 MPa in air at 1100 °C (t_f = 100h).

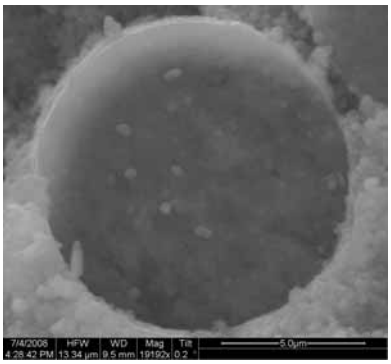

Figure A.204: Fracture surface of the N610/$LaPO_4$/Al_2O_3 specimen with 8ply HSW subjected to creep test at 72 MPa in air at 1100 °C (t_f = 100h).

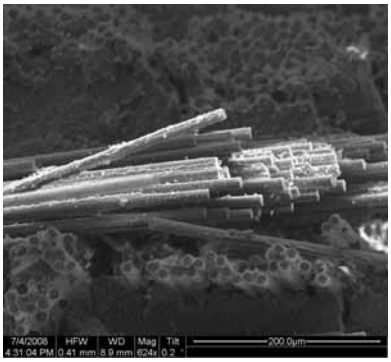

Figure A.205: Fracture surface of the N610/$LaPO_4$/Al_2O_3 specimen with 8ply HSW subjected to creep test at 72 MPa in air at 1100 °C (t_f = 100h).

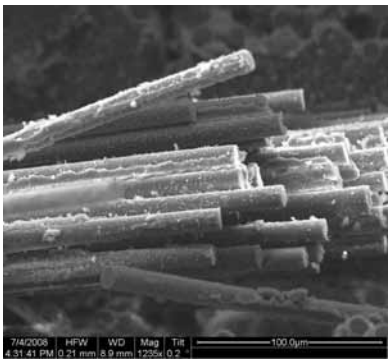

Figure A.206: Fracture surface of the N610/$LaPO_4$/Al_2O_3 specimen with 8ply HSW subjected to creep test at 72 MPa in air at 1100 °C (t_f = 100h).

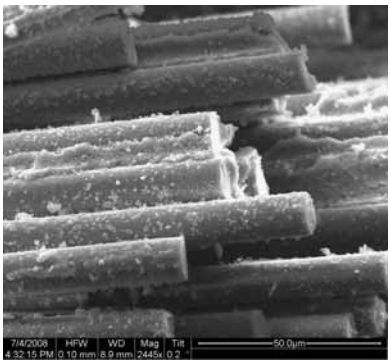

Figure A.207: Fracture surface of the N610/$LaPO_4$/Al_2O_3 specimen with 8ply HSW subjected to creep test at 72 MPa in air at 1100 °C (t_f = 100h).

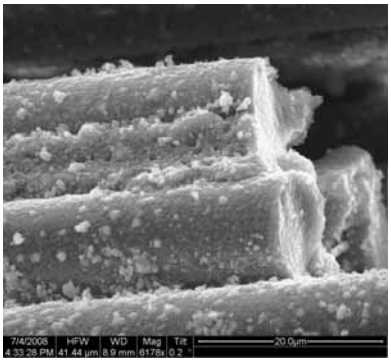

Figure A.208: Fracture surface of the N610/$LaPO_4$/Al_2O_3 specimen with 8ply HSW subjected to creep test at 72 MPa in air at 1100 °C (t_f = 100h).

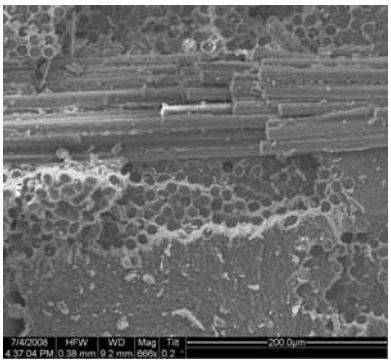

Figure A.209: Fracture surface of the N610/$LaPO_4$/Al_2O_3 specimen with 8ply HSW subjected to creep test at 72 MPa in air at 1100 °C (t_f = 100h).

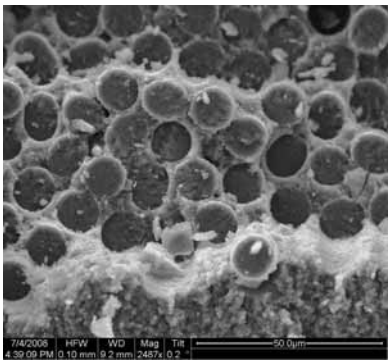

Figure A.210: Fracture surface of the N610/$LaPO_4$/Al_2O_3 specimen with 8ply HSW subjected to creep test at 72 MPa in air at 1100 °C (t_f = 100h).

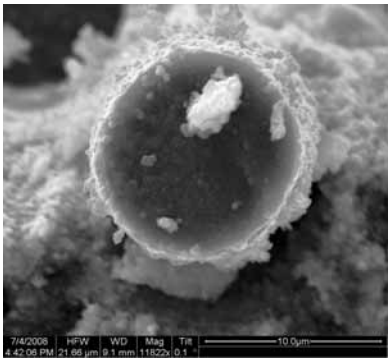

Figure A.211: Fracture surface of the N610/$LaPO_4$/Al_2O_3 specimen with 8ply HSW subjected to creep test at 72 MPa in air at 1100 °C (t_f = 100h).

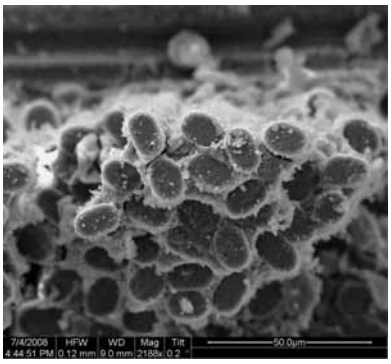

Figure A.212: Fracture surface of the N610/$LaPO_4$/Al_2O_3 specimen with 8ply HSW subjected to creep test at 72 MPa in air at 1100 °C (t_f = 100h).

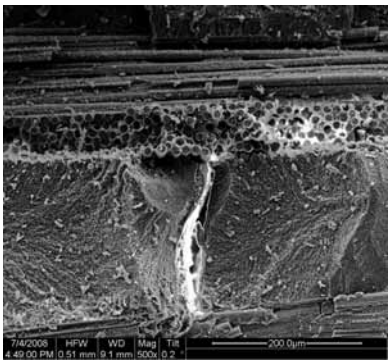

Figure A.213: Fracture surface of the N610/$LaPO_4$/Al_2O_3 specimen with 8ply HSW subjected to creep test at 72 MPa in air at 1100 °C (t_f = 100h).

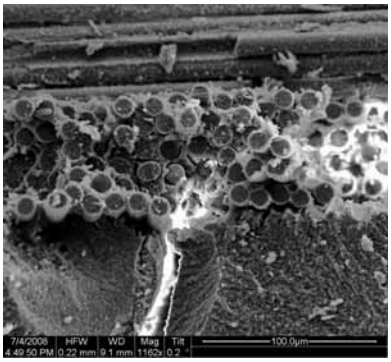

Figure A.214: Fracture surface of the N610/$LaPO_4$/Al_2O_3 specimen with 8ply HSW subjected to creep test at 72 MPa in air at 1100 °C (t_f = 100h).

Figure A.215: Fracture surface of the N610/$LaPO_4$/Al_2O_3 specimen with 8ply HSW subjected to creep test at 72 MPa in air at 1100 °C (t_f = 100h).

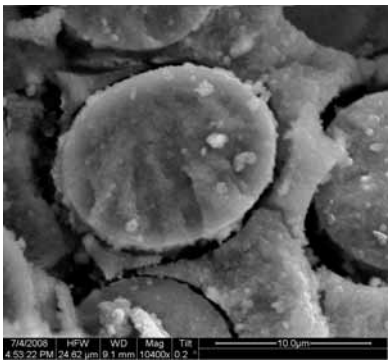

Figure A.216: Fracture surface of the N610/$LaPO_4$/Al_2O_3 specimen with 8ply HSW subjected to creep test at 72 MPa in air at 1100 °C (t_f = 100h).

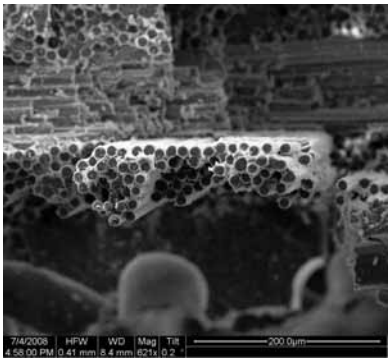

Figure A.217: Fracture surface of the N610/$LaPO_4$/Al_2O_3 specimen with 8ply HSW subjected to creep test at 72 MPa in air at 1100 °C (t_f = 100h).

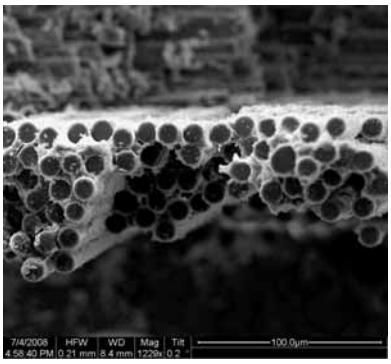

Figure A.218: Fracture surface of the N610/$LaPO_4$/Al_2O_3 specimen with 8ply HSW subjected to creep test at 72 MPa in air at 1100 °C (t_f = 100h).

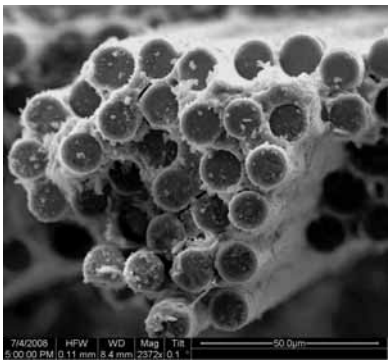

Figure A.219: Fracture surface of the N610/$LaPO_4$/Al_2O_3 specimen with 8ply HSW subjected to creep test at 72 MPa in air at 1100 °C (t_f = 100h).

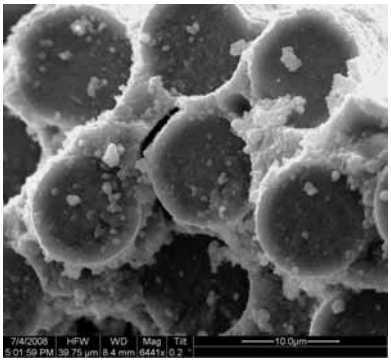

Figure A.220: Fracture surface of the N610/$LaPO_4$/Al_2O_3 specimen with 8ply HSW subjected to creep test at 72 MPa in air at 1100 °C (t_f = 100h).

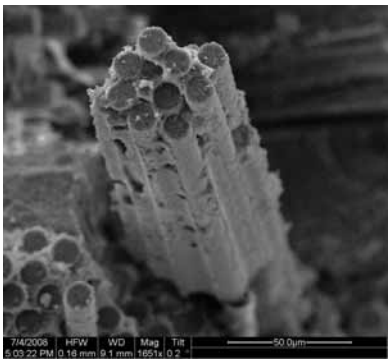

Figure A.221: Fracture surface of the N610/$LaPO_4$/Al_2O_3 specimen with 8ply HSW subjected to creep test at 72 MPa in air at 1100 °C (t_f = 100h).

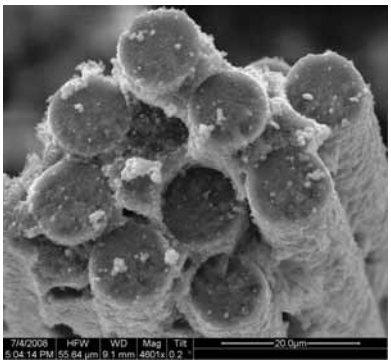

Figure A.222: Fracture surface of the N610/$LaPO_4$/Al_2O_3 specimen with 8ply HSW subjected to creep test at 72 MPa in air at 1100 °C (t_f = 100h).

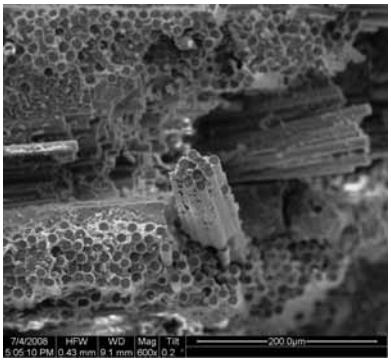

Figure A.223: Fracture surface of the N610/$LaPO_4$/Al_2O_3 specimen with 8ply HSW subjected to creep test at 72 MPa in air at 1100 °C (t_f = 100h).

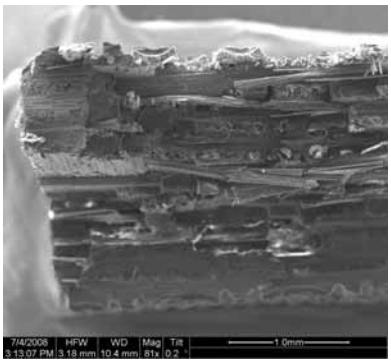

Figure A.224: Fracture surface of the N610/$LaPO_4$/Al_2O_3 specimen with 8ply HSW subjected to creep test at 72 MPa in steam at 1100 °C (t_f = 2.24h).

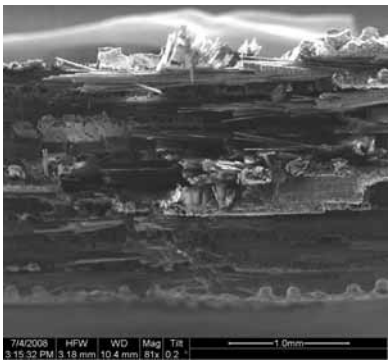

Figure A.225: Fracture surface of the N610/$LaPO_4$/Al_2O_3 specimen with 8ply HSW subjected to creep test at 72 MPa in steam at 1100 °C (t_f = 2.24h).

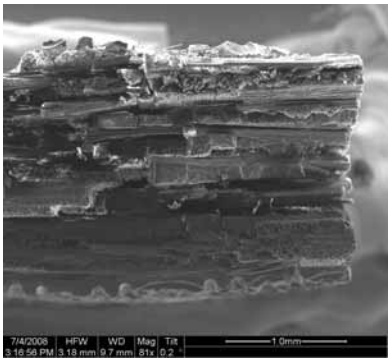

Figure A.226: Fracture surface of the N610/$LaPO_4$/Al_2O_3 specimen with 8ply HSW subjected to creep test at 72 MPa in steam at 1100 °C (t_f = 2.24h).

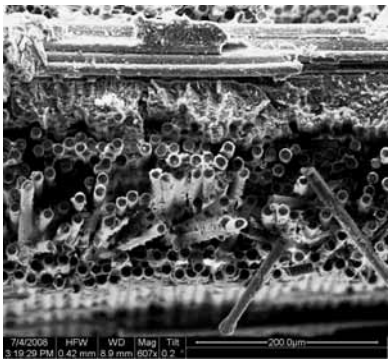

Figure A.227: Fracture surface of the N610/$LaPO_4$/Al_2O_3 specimen with 8ply HSW subjected to creep test at 72 MPa in steam at 1100 °C (t_f = 2.24h).

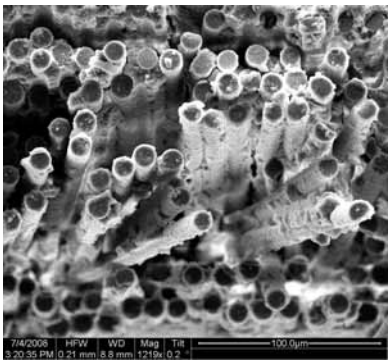

Figure A.228: Fracture surface of the N610/$LaPO_4$/Al_2O_3 specimen with 8ply HSW subjected to creep test at 72 MPa in steam at 1100 °C (t_f = 2.24h).

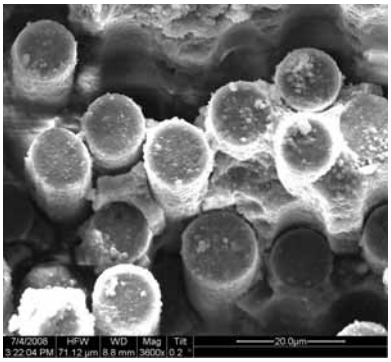

Figure A.229: Fracture surface of the N610/$LaPO_4$/Al_2O_3 specimen with 8ply HSW subjected to creep test at 72 MPa in steam at 1100 °C (t_f = 2.24h).

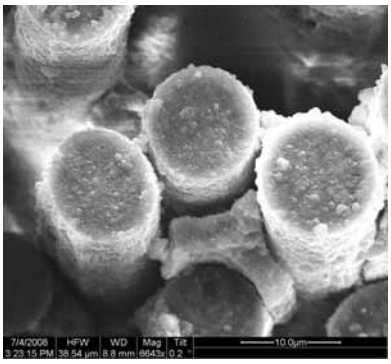

Figure A.230: Fracture surface of the N610/$LaPO_4$/Al_2O_3 specimen with 8ply HSW subjected to creep test at 72 MPa in steam at 1100 °C (t_f = 2.24h).

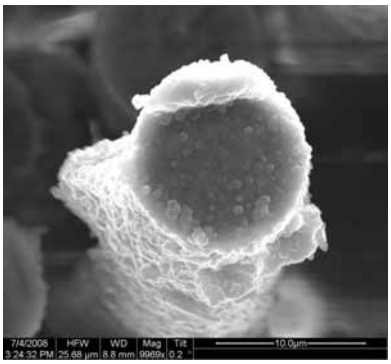

Figure A.231: Fracture surface of the N610/$LaPO_4$/Al_2O_3 specimen with 8ply HSW subjected to creep test at 72 MPa in steam at 1100 °C (t_f = 2.24h).

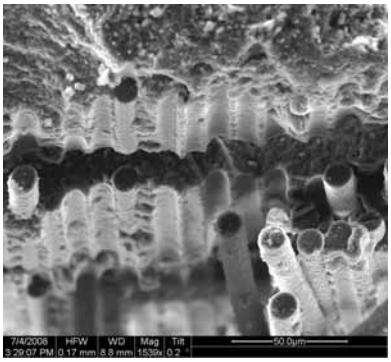

Figure A.232: Fracture surface of the N610/$LaPO_4$/Al_2O_3 specimen with 8ply HSW subjected to creep test at 72 MPa in steam at 1100 °C (t_f = 2.24h).

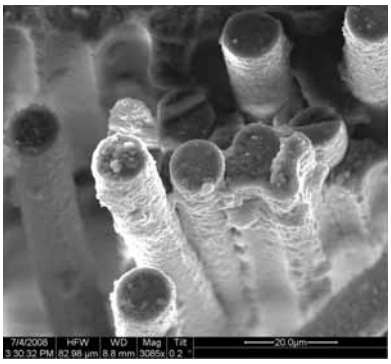

Figure A.233: Fracture surface of the N610/$LaPO_4$/Al_2O_3 specimen with 8ply HSW subjected to creep test at 72 MPa in steam at 1100 °C (t_f = 2.24h).

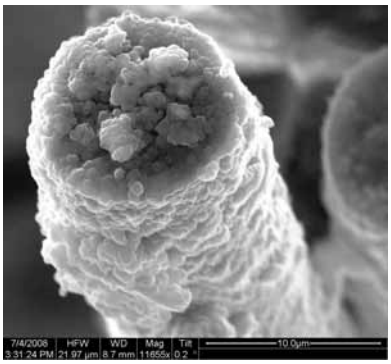

Figure A.234: Fracture surface of the N610/$LaPO_4$/Al_2O_3 specimen with 8ply HSW subjected to creep test at 72 MPa in steam at 1100 °C (t_f = 2.24h).

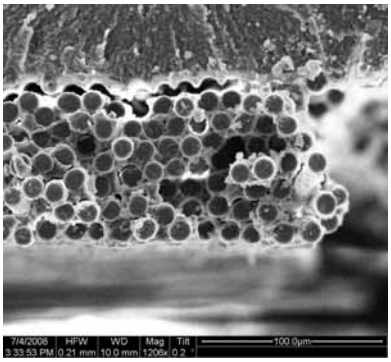

Figure A.235: Fracture surface of the N610/$LaPO_4$/Al_2O_3 specimen with 8ply HSW subjected to creep test at 72 MPa in steam at 1100 °C (t_f = 2.24h).

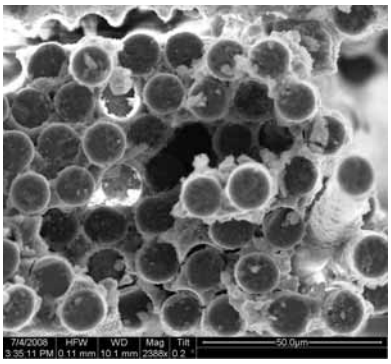

Figure A.236: Fracture surface of the N610/$LaPO_4$/Al_2O_3 specimen with 8ply HSW subjected to creep test at 72 MPa in steam at 1100 °C (t_f = 2.24h).

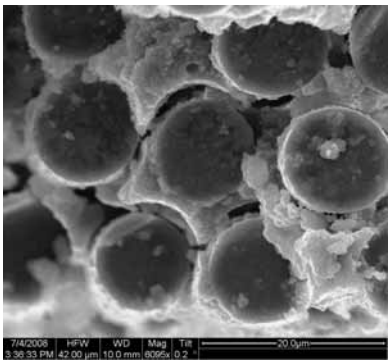

Figure A.237: Fracture surface of the N610/$LaPO_4$/Al_2O_3 specimen with 8ply HSW subjected to creep test at 72 MPa in steam at 1100 °C (t_f = 2.24h).

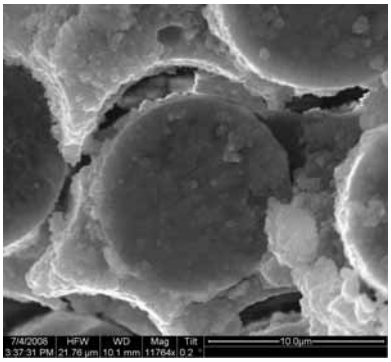

Figure A.238: Fracture surface of the N610/$LaPO_4$/Al_2O_3 specimen with 8ply HSW subjected to creep test at 72 MPa in steam at 1100 °C (t_f = 2.24h).

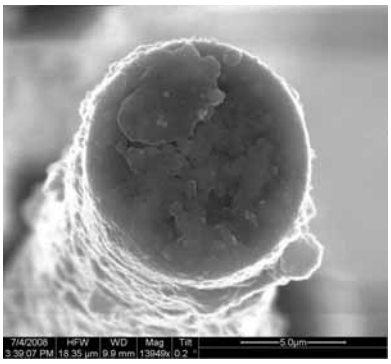

Figure A.239: Fracture surface of the N610/$LaPO_4$/Al_2O_3 specimen with 8ply HSW subjected to creep test at 72 MPa in steam at 1100 °C (t_f = 2.24h).

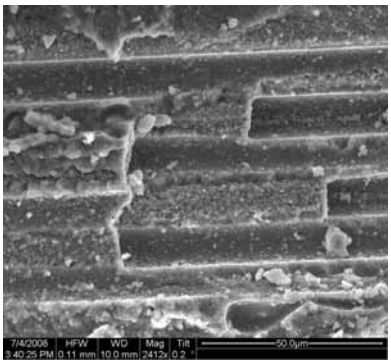

Figure A.240: Fracture surface of the N610/$LaPO_4$/Al_2O_3 specimen with 8ply HSW subjected to creep test at 72 MPa in steam at 1100 °C (t_f = 2.24h).

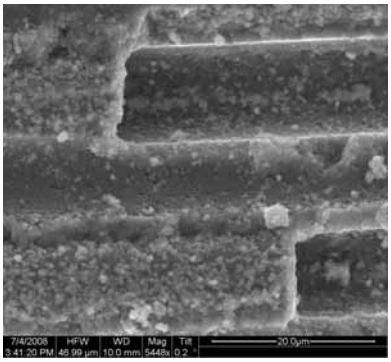

Figure A.241: Fracture surface of the N610/$LaPO_4$/Al_2O_3 specimen with 8ply HSW subjected to creep test at 72 MPa in steam at 1100 °C (t_f = 2.24h).

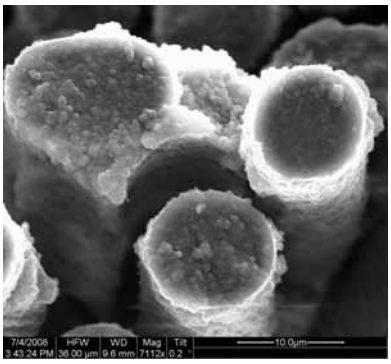

Figure A.242: Fracture surface of the N610/$LaPO_4$/Al_2O_3 specimen with 8ply HSW subjected to creep test at 72 MPa in steam at 1100 °C (t_f = 2.24h).

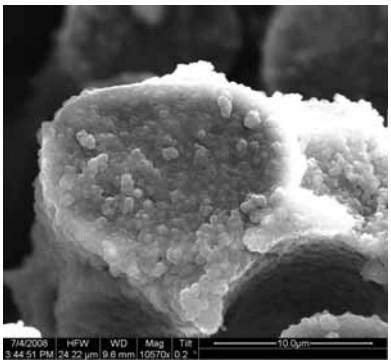

Figure A.243: Fracture surface of the N610/$LaPO_4$/Al_2O_3 specimen with 8ply HSW subjected to creep test at 72 MPa in steam at 1100 °C (t_f = 2.24h).

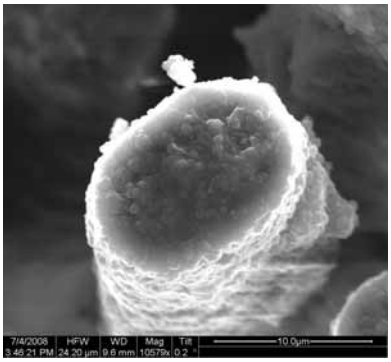

Figure A.244: Fracture surface of the N610/$LaPO_4$/Al_2O_3 specimen with 8ply HSW subjected to creep test at 72 MPa in steam at 1100 °C (t_f = 2.24h).

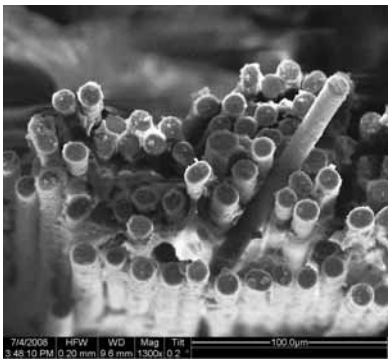

Figure A.245: Fracture surface of the N610/$LaPO_4$/Al_2O_3 specimen with 8ply HSW subjected to creep test at 72 MPa in steam at 1100 °C (t_f = 2.24h).

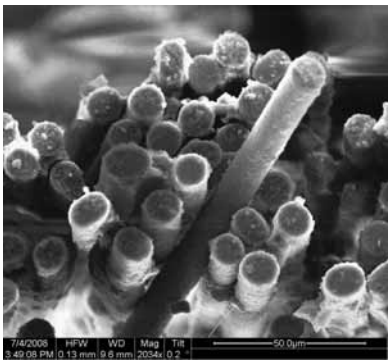

Figure A.246: Fracture surface of the N610/$LaPO_4$/Al_2O_3 specimen with 8ply HSW subjected to creep test at 72 MPa in steam at 1100 °C (t_f = 2.24h).

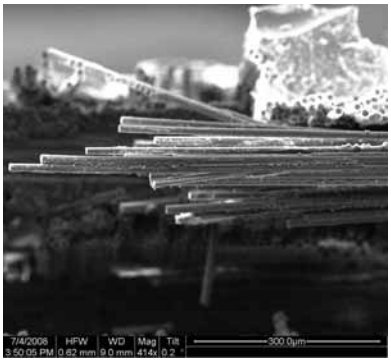

Figure A.247: Fracture surface of the N610/$LaPO_4$/Al_2O_3 specimen with 8ply HSW subjected to creep test at 72 MPa in steam at 1100 °C (t_f = 2.24h).

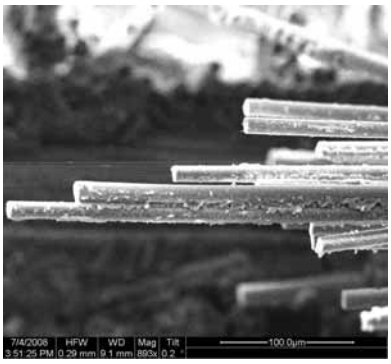

Figure A.248: Fracture surface of the N610/$LaPO_4$/Al_2O_3 specimen with 8ply HSW subjected to creep test at 72 MPa in steam at 1100 °C (t_f = 2.24h).

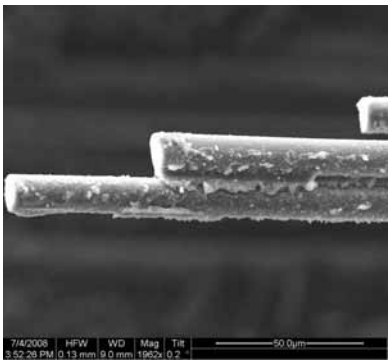

Figure A.249: Fracture surface of the N610/$LaPO_4$/Al_2O_3 specimen with 8ply HSW subjected to creep test at 72 MPa in steam at 1100 °C (t_f = 2.24h).

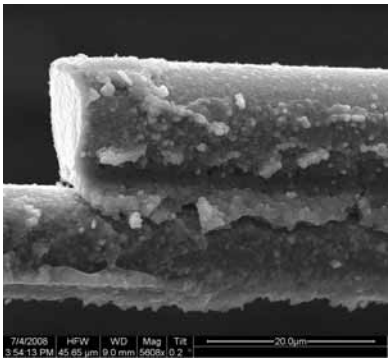

Figure A.250: Fracture surface of the N610/$LaPO_4$/Al_2O_3 specimen with 8ply HSW subjected to creep test at 72 MPa in steam at 1100 °C (t_f = 2.24h).

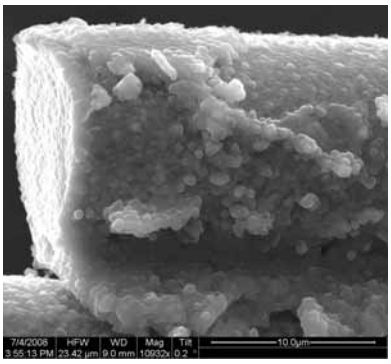

Figure A.251: Fracture surface of the N610/$LaPO_4$/Al_2O_3 specimen with 8ply HSW subjected to creep test at 72 MPa in steam at 1100 °C (t_f = 2.24h).

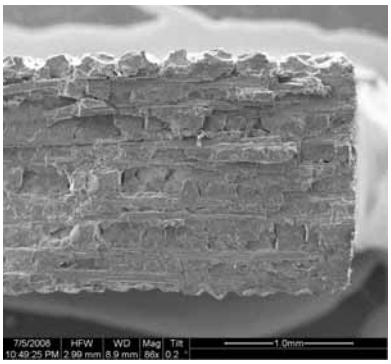

Figure A.252: Fracture surface of the N610/Al_2O_3 specimen with 8ply HSW subjected to creep test at 30 MPa in steam at 1100 °C (t_f = 16.1h).

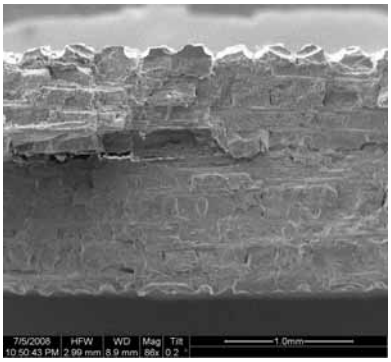

Figure A.253: Fracture surface of the N610/Al_2O_3 specimen with 8ply HSW subjected to creep test at 30 MPa in steam at 1100 °C (t_f = 16.1h).

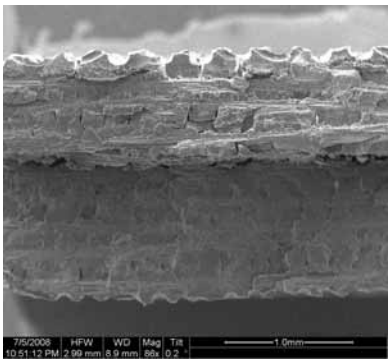

Figure A.254: Fracture surface of the N610/Al_2O_3 specimen with 8ply HSW subjected to creep test at 30 MPa in steam at 1100 °C (t_f = 16.1h).

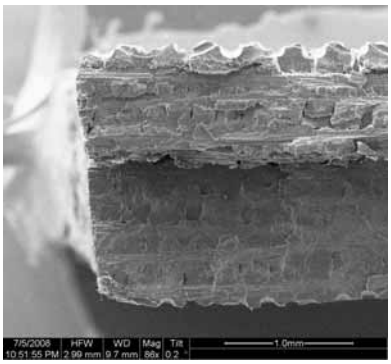

Figure A.255: Fracture surface of the N610/Al_2O_3 specimen with 8ply HSW subjected to creep test at 30 MPa in steam at 1100 °C (t_f = 16.1h).

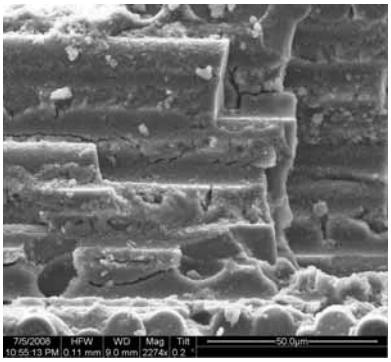

Figure A.256: Fracture surface of the N610/Al_2O_3 specimen with 8ply HSW subjected to creep test at 30 MPa in steam at 1100 °C (t_f = 16.1h).

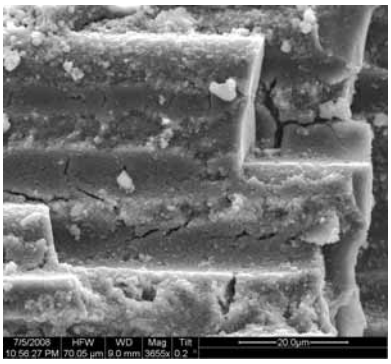

Figure A.257: Fracture surface of the N610/Al_2O_3 specimen with 8ply HSW subjected to creep test at 30 MPa in steam at 1100 °C (t_f = 16.1h).

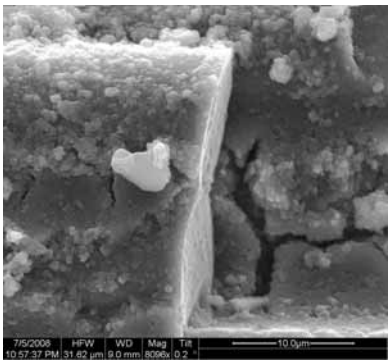

Figure A.258: Fracture surface of the N610/Al_2O_3 specimen with 8ply HSW subjected to creep test at 30 MPa in steam at 1100 °C (t_f = 16.1h).

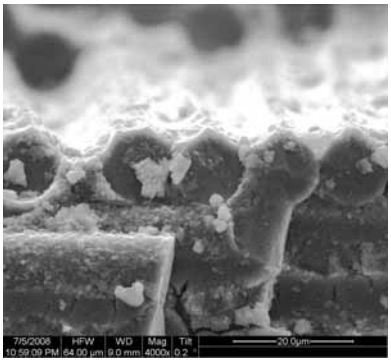

Figure A.259: Fracture surface of the N610/Al_2O_3 specimen with 8ply HSW subjected to creep test at 30 MPa in steam at 1100 °C (t_f = 16.1h).

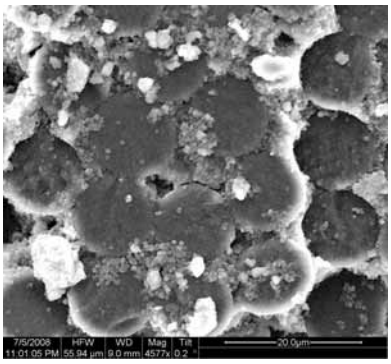

Figure A.260: Fracture surface of the N610/Al_2O_3 specimen with 8ply HSW subjected to creep test at 30 MPa in steam at 1100 °C (t_f = 16.1h).

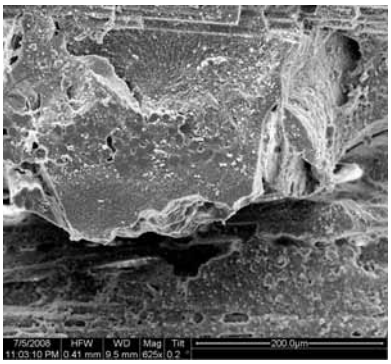

Figure A.261: Fracture surface of the N610/Al_2O_3 specimen with 8ply HSW subjected to creep test at 30 MPa in steam at 1100 °C (t_f = 16.1h).

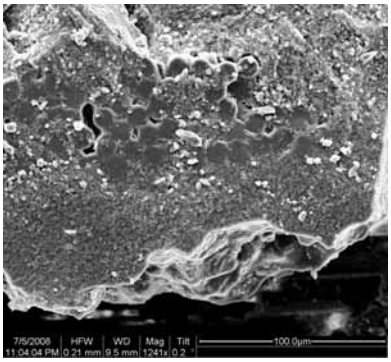

Figure A.262: Fracture surface of the N610/Al_2O_3 specimen with 8ply HSW subjected to creep test at 30 MPa in steam at 1100 °C (t_f = 16.1h).

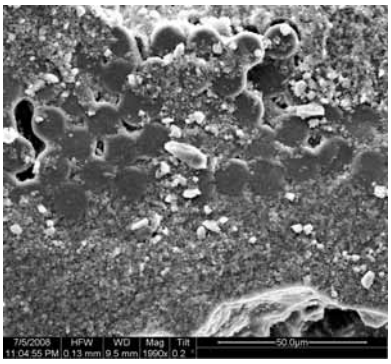

Figure A.263: Fracture surface of the N610/Al_2O_3 specimen with 8ply HSW subjected to creep test at 30 MPa in steam at 1100 °C (t_f = 16.1h).

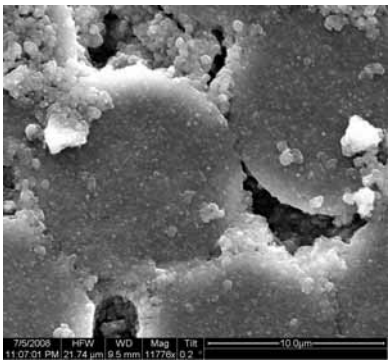

Figure A.264: Fracture surface of the N610/Al_2O_3 specimen with 8ply HSW subjected to creep test at 30 MPa in steam at 1100 °C (t_f = 16.1h).

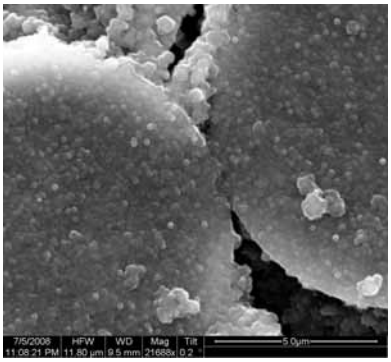

Figure A.265: Fracture surface of the N610/Al_2O_3 specimen with 8ply HSW subjected to creep test at 30 MPa in steam at 1100 °C (t_f = 16.1h).

Figure A.266: Fracture surface of the N610/Al_2O_3 specimen with 8ply HSW subjected to creep test at 30 MPa in steam at 1100 °C (t_f = 16.1h).

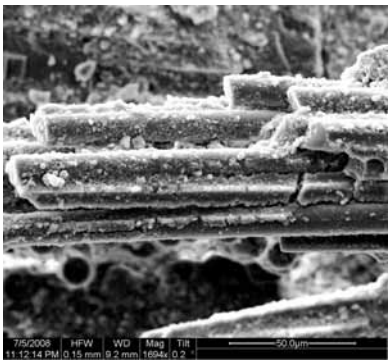

Figure A.267: Fracture surface of the N610/Al_2O_3 specimen with 8ply HSW subjected to creep test at 30 MPa in steam at 1100 °C (t_f = 16.1h).

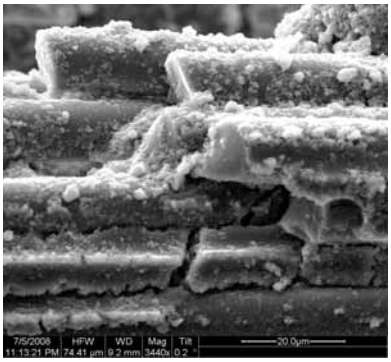

Figure A.268: Fracture surface of the N610/Al_2O_3 specimen with 8ply HSW subjected to creep test at 30 MPa in steam at 1100 °C (t_f = 16.1h).

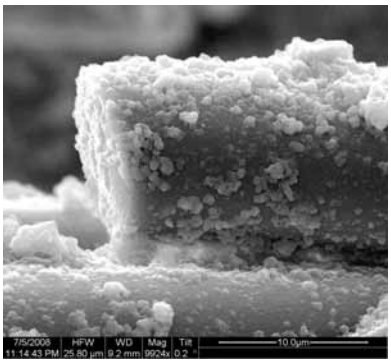

Figure A.269: Fracture surface of the N610/Al_2O_3 specimen with 8ply HSW subjected to creep test at 30 MPa in steam at 1100 °C (t_f = 16.1h).

Figure A.270: Fracture surface of the N610/Al_2O_3 specimen with 8ply HSW subjected to creep test at 30 MPa in steam at 1100 °C (t_f = 16.1h).

Figure A.271: Fracture surface of the N610/Al_2O_3 specimen with 8ply HSW subjected to creep test at 30 MPa in steam at 1100 °C (t_f = 16.1h).

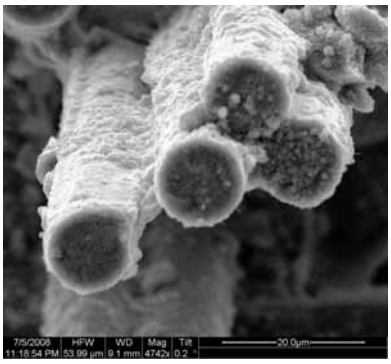

Figure A.272: Fracture surface of the N610/Al_2O_3 specimen with 8ply HSW subjected to creep test at 30 MPa in steam at 1100 °C (t_f = 16.1h).

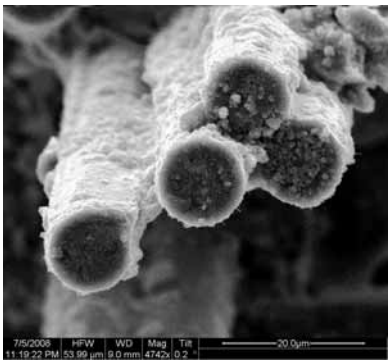

Figure A.273: Fracture surface of the N610/Al_2O_3 specimen with 8ply HSW subjected to creep test at 30 MPa in steam at 1100 °C (t_f = 16.1h).

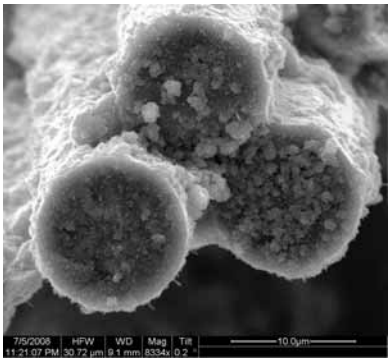

Figure A.274: Fracture surface of the N610/Al_2O_3 specimen with 8ply HSW subjected to creep test at 30 MPa in steam at 1100 °C (t_f = 16.1h).

Figure A.275: Fracture surface of the N610/Al_2O_3 specimen with 8ply HSW subjected to creep test at 30 MPa in steam at 1100 °C (t_f = 16.1h).

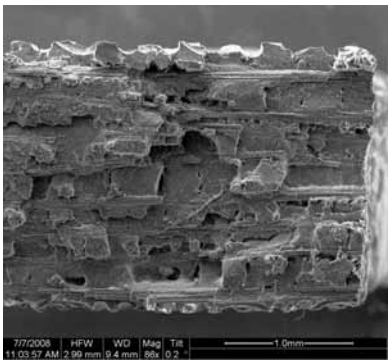

Figure A.276: Fracture surface of the N610/Al_2O_3 specimen with 8ply HSW subjected to creep test at 40.5 MPa in air at 1100 °C (t_f = 3.34h).

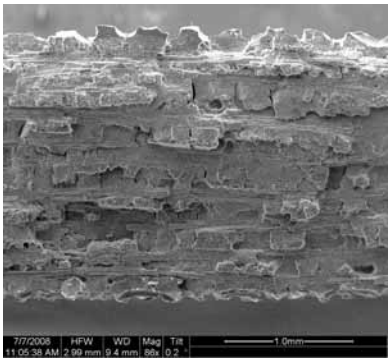

Figure A.277: Fracture surface of the N610/Al_2O_3 specimen with 8ply HSW subjected to creep test at 40.5 MPa in air at 1100 °C (t_f = 3.34h).

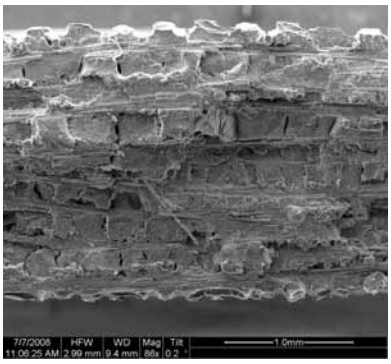

Figure A.278: Fracture surface of the N610/Al_2O_3 specimen with 8ply HSW subjected to creep test at 40.5 MPa in air at 1100 °C (t_f = 3.34h).

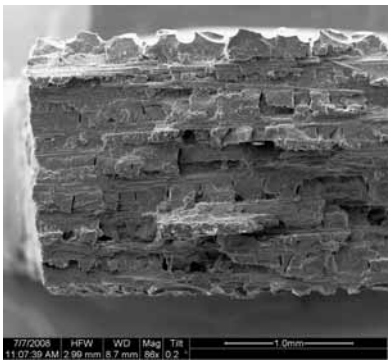

Figure A.279: Fracture surface of the N610/Al_2O_3 specimen with 8ply HSW subjected to creep test at 40.5 MPa in air at 1100 °C (t_f = 3.34h).

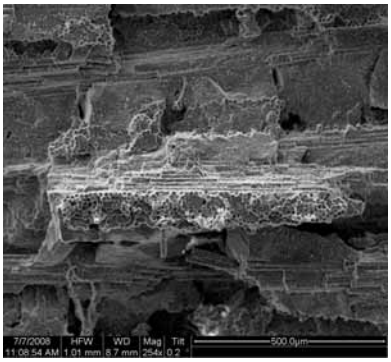

Figure A.280: Fracture surface of the N610/Al_2O_3 specimen with 8ply HSW subjected to creep test at 40.5 MPa in air at 1100 °C (t_f = 3.34h).

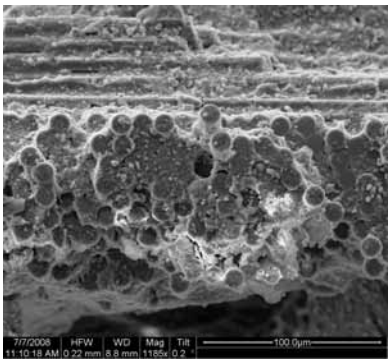

Figure A.281: Fracture surface of the N610/Al_2O_3 specimen with 8ply HSW subjected to creep test at 40.5 MPa in air at 1100 °C (t_f = 3.34h).

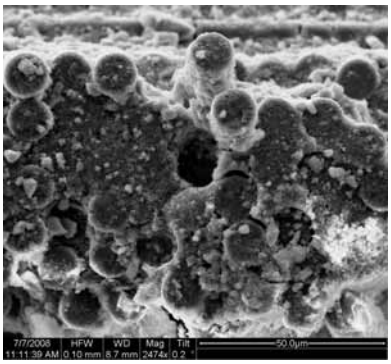

Figure A.282: Fracture surface of the N610/Al_2O_3 specimen with 8ply HSW subjected to creep test at 40.5 MPa in air at 1100 °C (t_f = 3.34h).

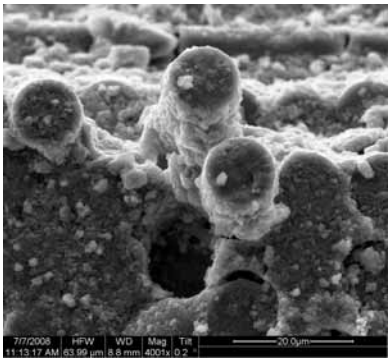

Figure A.283: Fracture surface of the N610/Al_2O_3 specimen with 8ply HSW subjected to creep test at 40.5 MPa in air at 1100 °C (t_f = 3.34h).

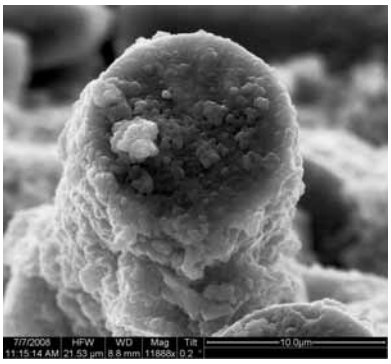

Figure A.284: Fracture surface of the N610/Al_2O_3 specimen with 8ply HSW subjected to creep test at 40.5 MPa in air at 1100 °C (t_f = 3.34h).

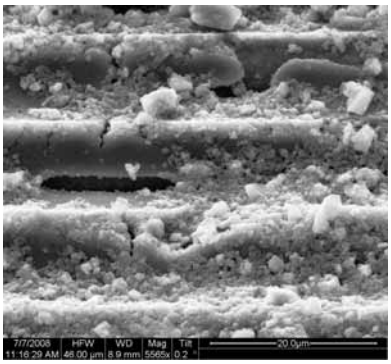

Figure A.285: Fracture surface of the N610/Al_2O_3 specimen with 8ply HSW subjected to creep test at 40.5 MPa in air at 1100 °C (t_f = 3.34h).

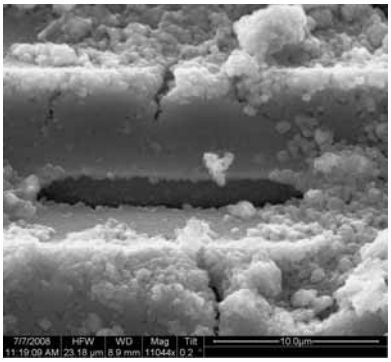

Figure A.286: Fracture surface of the N610/Al_2O_3 specimen with 8ply HSW subjected to creep test at 40.5 MPa in air at 1100 °C (t_f = 3.34h).

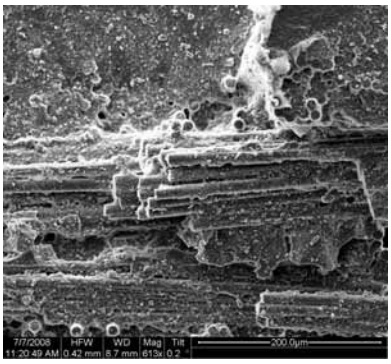

Figure A.287: Fracture surface of the N610/Al_2O_3 specimen with 8ply HSW subjected to creep test at 40.5 MPa in air at 1100 °C (t_f = 3.34h).

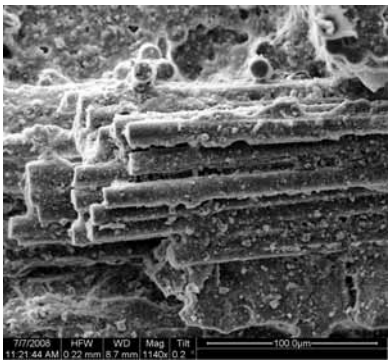

Figure A.288: Fracture surface of the N610/Al_2O_3 specimen with 8ply HSW subjected to creep test at 40.5 MPa in air at 1100 °C (t_f = 3.34h).

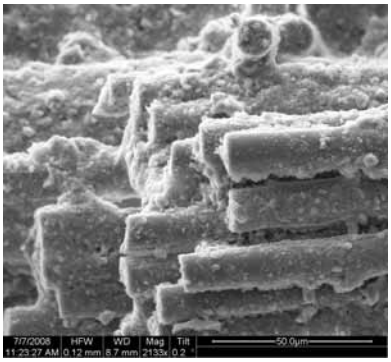

Figure A.289: Fracture surface of the N610/Al_2O_3 specimen with 8ply HSW subjected to creep test at 40.5 MPa in air at 1100 °C (t_f = 3.34h).

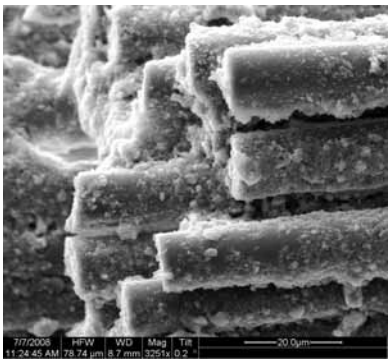

Figure A.290: Fracture surface of the N610/Al_2O_3 specimen with 8ply HSW subjected to creep test at 40.5 MPa in air at 1100 °C (t_f = 3.34h).

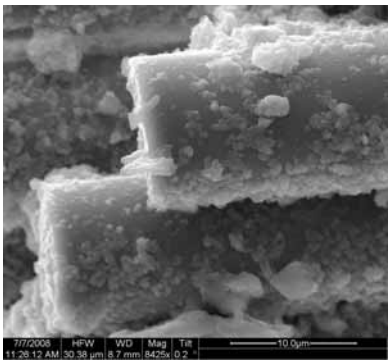

Figure A.291: Fracture surface of the N610/Al_2O_3 specimen with 8ply HSW subjected to creep test at 40.5 MPa in air at 1100 °C (t_f = 3.34h).

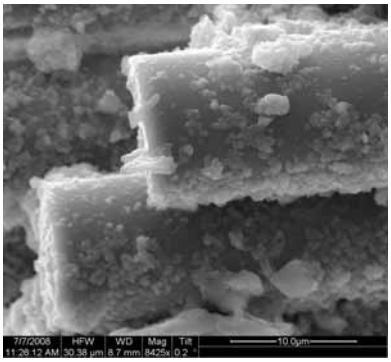

Figure A.292: Fracture surface of the N610/Al_2O_3 specimen with 8ply HSW subjected to creep test at 40.5 MPa in air at 1100 °C (t_f = 3.34h).

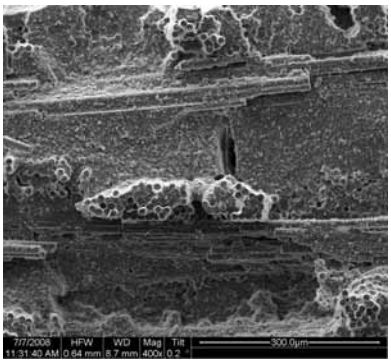

Figure A.293: Fracture surface of the N610/Al_2O_3 specimen with 8ply HSW subjected to creep test at 40.5 MPa in air at 1100 °C (t_f = 3.34h).

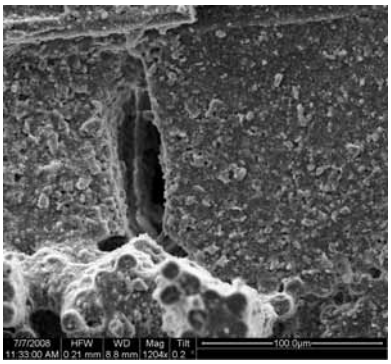

Figure A.294: Fracture surface of the N610/Al_2O_3 specimen with 8ply HSW subjected to creep test at 40.5 MPa in air at 1100 °C (t_f = 3.34h).

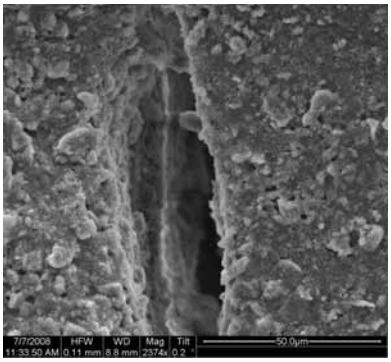

Figure A.295: Fracture surface of the N610/Al_2O_3 specimen with 8ply HSW subjected to creep test at 40.5 MPa in air at 1100 °C (t_f = 3.34h).

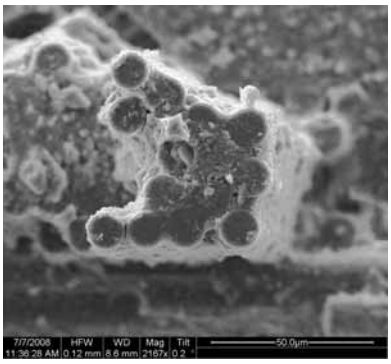

Figure A.296: Fracture surface of the N610/Al_2O_3 specimen with 8ply HSW subjected to creep test at 40.5 MPa in air at 1100 °C (t_f = 3.34h).

Figure A.297: Fracture surface of the N610/Al_2O_3 specimen with 8ply HSW subjected to creep test at 40.5 MPa in air at 1100 °C (t_f = 3.34h).

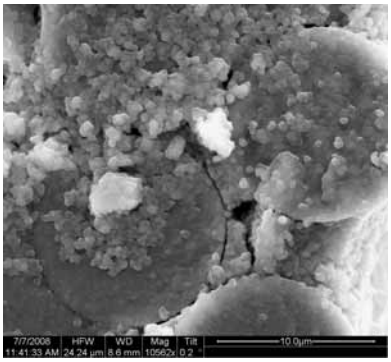

Figure A.298: Fracture surface of the N610/Al_2O_3 specimen with 8ply HSW subjected to creep test at 40.5 MPa in air at 1100 °C (t_f = 3.34h).

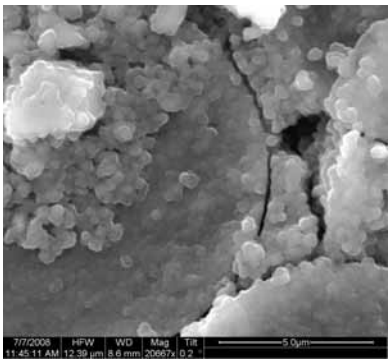

Figure A.299: Fracture surface of the N610/Al_2O_3 specimen with 8ply HSW subjected to creep test at 40.5 MPa in air at 1100 °C (t_f = 3.34h).

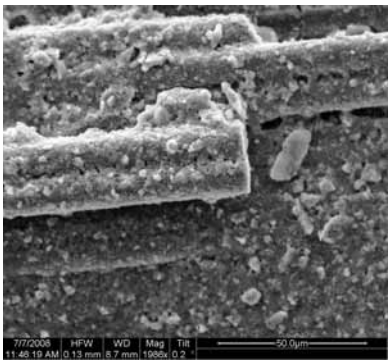

Figure A.300: Fracture surface of the N610/Al_2O_3 specimen with 8ply HSW subjected to creep test at 40.5 MPa in air at 1100 °C (t_f = 3.34h).

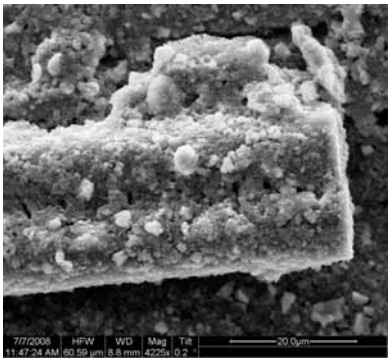

Figure A.301: Fracture surface of the N610/Al_2O_3 specimen with 8ply HSW subjected to creep test at 40.5 MPa in air at 1100 °C (t_f = 3.34h).

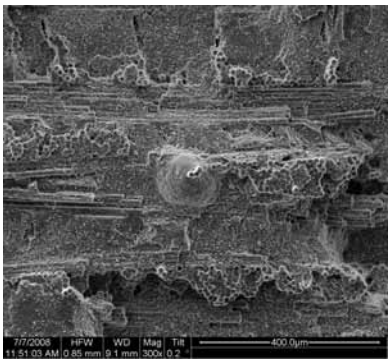

Figure A.302: Fracture surface of the N610/Al_2O_3 specimen with 8ply HSW subjected to creep test at 40.5 MPa in air at 1100 °C (t_f = 3.34h).

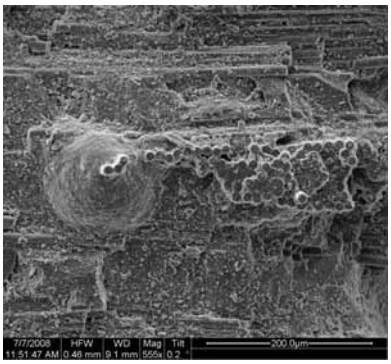

Figure A.303: Fracture surface of the N610/Al_2O_3 specimen with 8ply HSW subjected to creep test at 40.5 MPa in air at 1100 °C (t_f = 3.34h).

Figure A.304: Fracture surface of the N610/Al_2O_3 specimen with 8ply HSW subjected to creep test at 40.5 MPa in air at 1100 °C (t_f = 3.34h).

Figure A.305: Fracture surface of the N610/Al_2O_3 specimen with 8ply HSW subjected to creep test at 40.5 MPa in air at 1100 °C (t_f = 3.34h).

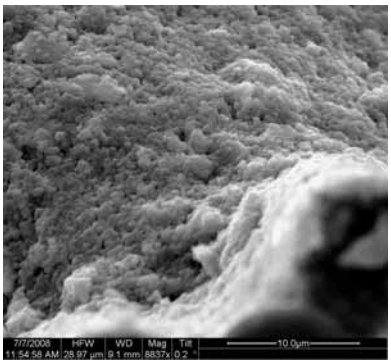

Figure A.306: Fracture surface of the N610/Al_2O_3 specimen with 8ply HSW subjected to creep test at 40.5 MPa in air at 1100 °C (t_f = 3.34h).

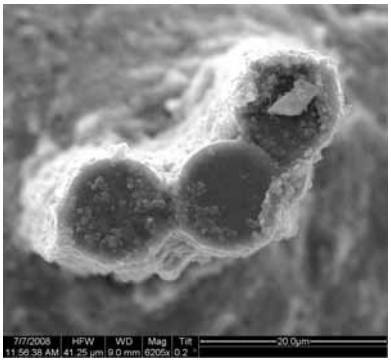

Figure A.307: Fracture surface of the N610/Al_2O_3 specimen with 8ply HSW subjected to creep test at 40.5 MPa in air at 1100 °C (t_f = 3.34h).

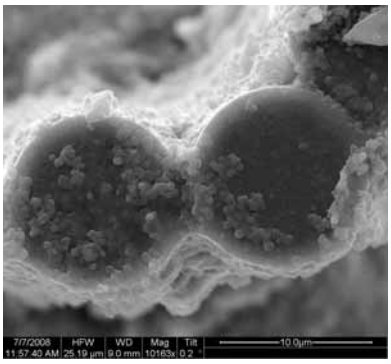

Figure A.308: Fracture surface of the N610/Al_2O_3 specimen with 8ply HSW subjected to creep test at 40.5 MPa in air at 1100 °C (t_f = 3.34h).

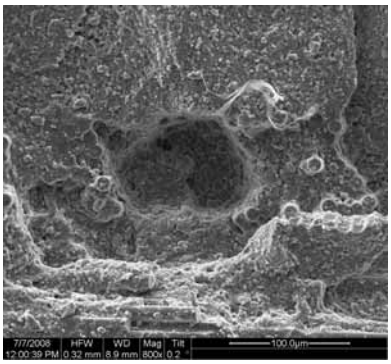

Figure A.309: Fracture surface of the N610/Al_2O_3 specimen with 8ply HSW subjected to creep test at 40.5 MPa in air at 1100 °C (t_f = 3.34h).

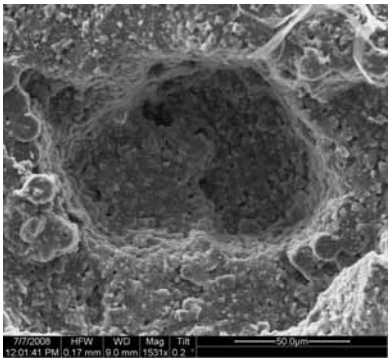

Figure A.310: Fracture surface of the N610/Al_2O_3 specimen with 8ply HSW subjected to creep test at 40.5 MPa in air at 1100 °C (t_f = 3.34h).

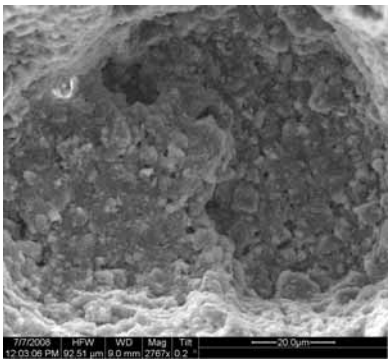

Figure A.311: Fracture surface of the N610/Al_2O_3 specimen with 8ply HSW subjected to creep test at 40.5 MPa in air at 1100 °C (t_f = 3.34h).

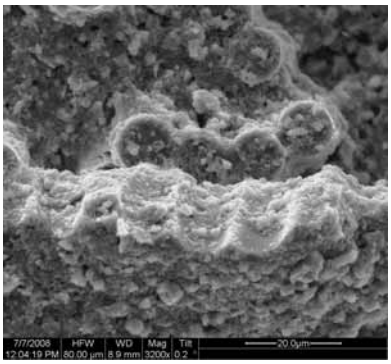

Figure A.312: Fracture surface of the N610/Al_2O_3 specimen with 8ply HSW subjected to creep test at 40.5 MPa in air at 1100 °C (t_f = 3.34h).

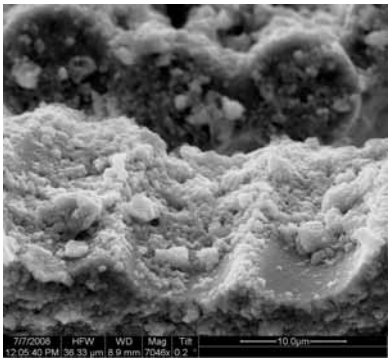

Figure A.313: Fracture surface of the N610/Al_2O_3 specimen with 8ply HSW subjected to creep test at 40.5 MPa in air at 1100 °C (t_f = 3.34h).

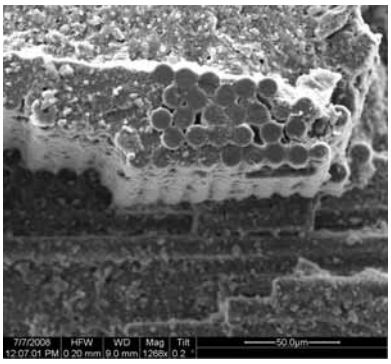

Figure A.314: Fracture surface of the N610/Al_2O_3 specimen with 8ply HSW subjected to creep test at 40.5 MPa in air at 1100 °C (t_f = 3.34h).

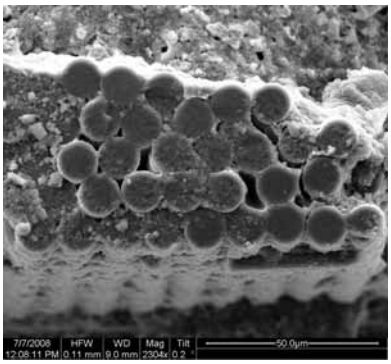

Figure A.315: Fracture surface of the N610/Al_2O_3 specimen with 8ply HSW subjected to creep test at 40.5 MPa in air at 1100 °C (t_f = 3.34h).

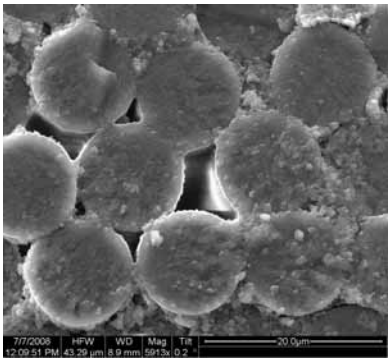

Figure A.316: Fracture surface of the N610/Al_2O_3 specimen with 8ply HSW subjected to creep test at 40.5 MPa in air at 1100 °C (t_f = 3.34h).

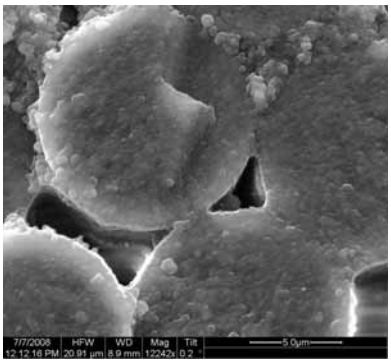

Figure A.317: Fracture surface of the N610/Al_2O_3 specimen with 8ply HSW subjected to creep test at 40.5 MPa in air at 1100 °C (t_f = 3.34h).

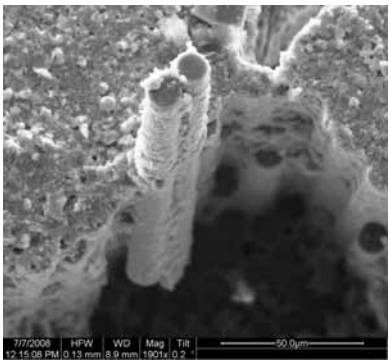

Figure A.318: Fracture surface of the N610/Al_2O_3 specimen with 8ply HSW subjected to creep test at 40.5 MPa in air at 1100 °C (t_f = 3.34h).

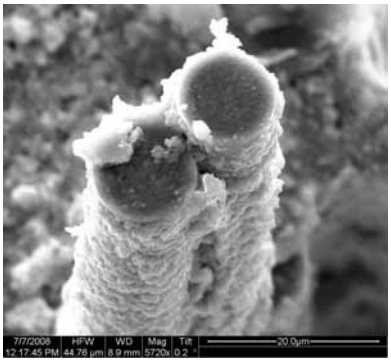

Figure A.319: Fracture surface of the N610/Al_2O_3 specimen with 8ply HSW subjected to creep test at 40.5 MPa in air at 1100 °C (t_f = 3.34h).

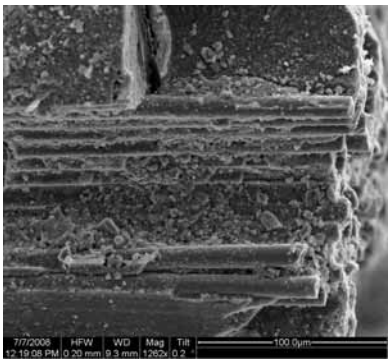

Figure A.320: Fracture surface of the N610/Al_2O_3 specimen with 8ply HSW subjected to creep test at 40.5 MPa in air at 1100 °C (t_f = 3.34h).

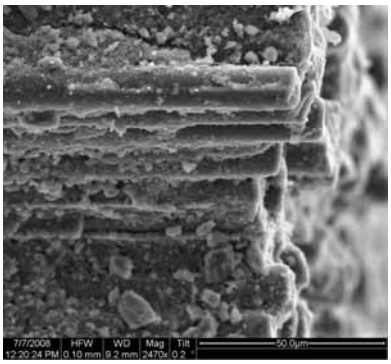

Figure A.321: Fracture surface of the N610/Al_2O_3 specimen with 8ply HSW subjected to creep test at 40.5 MPa in air at 1100 °C (t_f = 3.34h).

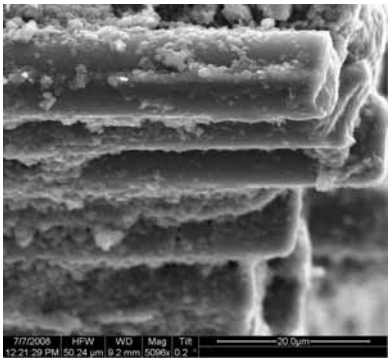

Figure A.322: Fracture surface of the N610/Al_2O_3 specimen with 8ply HSW subjected to creep test at 40.5 MPa in air at 1100 °C (t_f = 3.34h).

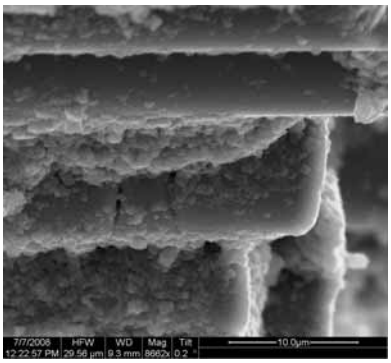

Figure A.323: Fracture surface of the N610/Al_2O_3 specimen with 8ply HSW subjected to creep test at 40.5 MPa in air at 1100 °C (t_f = 3.34h).

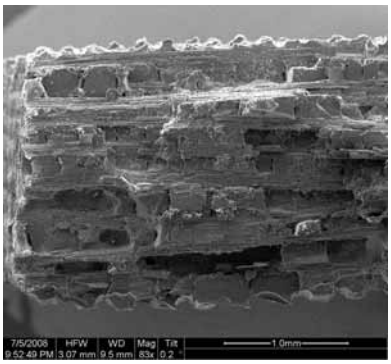

Figure A.324: Fracture surface of the N610/Al_2O_3 specimen with 8ply HSW subjected to creep test at 40.5 MPa in steam at 1100 °C (t_f = 0.01h).

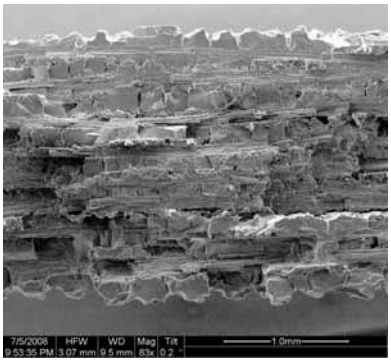

Figure A.325: Fracture surface of the N610/Al_2O_3 specimen with 8ply HSW subjected to creep test at 40.5 MPa in steam at 1100 °C (t_f = 0.01h).

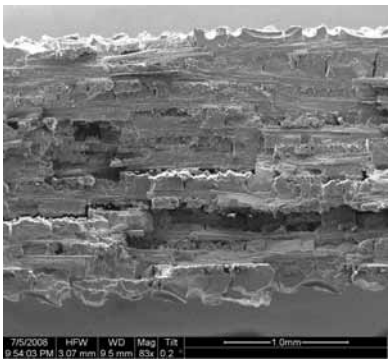

Figure A.326: Fracture surface of the N610/Al_2O_3 specimen with 8ply HSW subjected to creep test at 40.5 MPa in steam at 1100 °C (t_f = 0.01h).

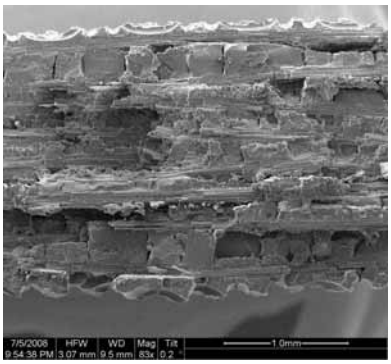

Figure A.327: Fracture surface of the N610/Al_2O_3 specimen with 8ply HSW subjected to creep test at 40.5 MPa in steam at 1100 °C (t_f = 0.01h).

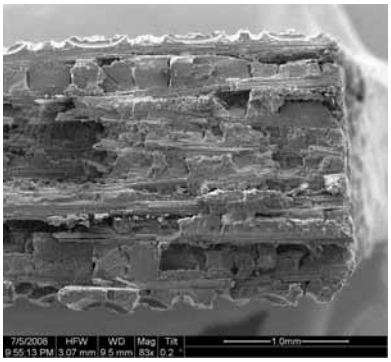

Figure A.328: Fracture surface of the N610/Al_2O_3 specimen with 8ply HSW subjected to creep test at 40.5 MPa in steam at 1100 °C (t_f = 0.01h).

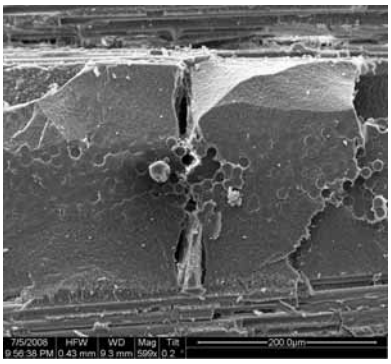

Figure A.329: Fracture surface of the N610/Al_2O_3 specimen with 8ply HSW subjected to creep test at 40.5 MPa in steam at 1100 °C (t_f = 0.01h).

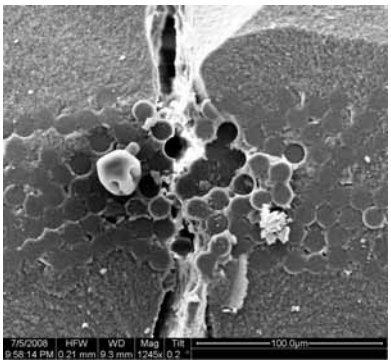

Figure A.330: Fracture surface of the N610/Al_2O_3 specimen with 8ply HSW subjected to creep test at 40.5 MPa in steam at 1100 °C (t_f = 0.01h).

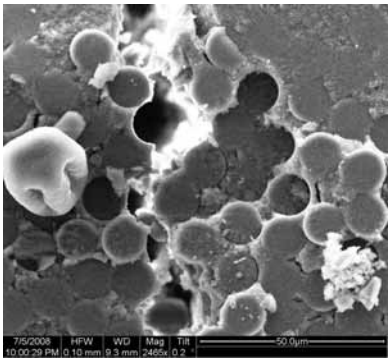

Figure A.331: Fracture surface of the N610/Al_2O_3 specimen with 8ply HSW subjected to creep test at 40.5 MPa in steam at 1100 °C (t_f = 0.01h).

Figure A.332: Fracture surface of the N610/Al_2O_3 specimen with 8ply HSW subjected to creep test at 40.5 MPa in steam at 1100 °C (t_f = 0.01h).

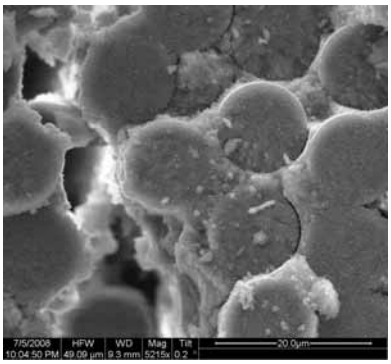

Figure A.333: Fracture surface of the N610/Al_2O_3 specimen with 8ply HSW subjected to creep test at 40.5 MPa in steam at 1100 °C (t_f = 0.01h).

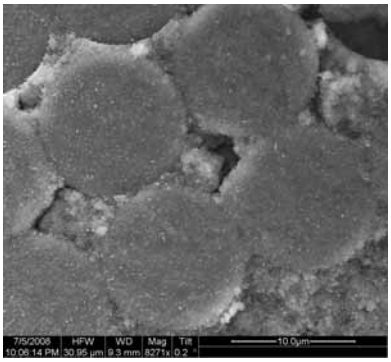

Figure A.334: Fracture surface of the N610/Al_2O_3 specimen with 8ply HSW subjected to creep test at 40.5 MPa in steam at 1100 °C (t_f = 0.01h).

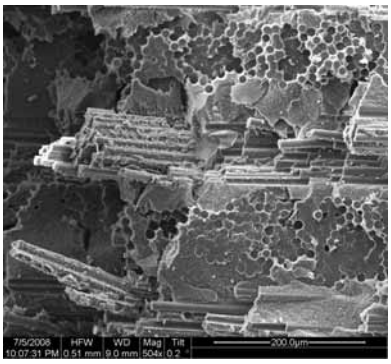

Figure A.335: Fracture surface of the N610/Al_2O_3 specimen with 8ply HSW subjected to creep test at 40.5 MPa in steam at 1100 °C (t_f = 0.01h).

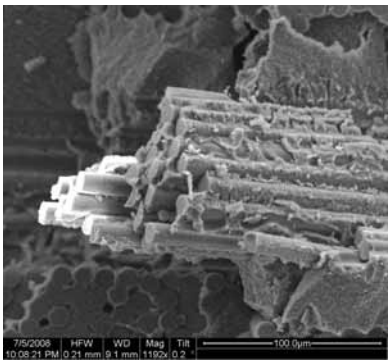

Figure A.336: Fracture surface of the N610/Al_2O_3 specimen with 8ply HSW subjected to creep test at 40.5 MPa in steam at 1100 °C (t_f = 0.01h).

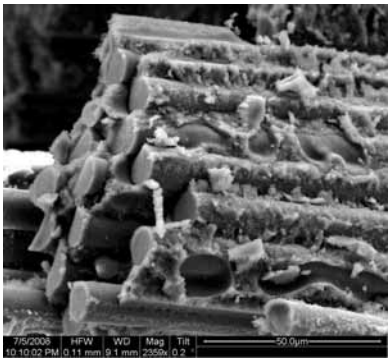

Figure A.337: Fracture surface of the N610/Al_2O_3 specimen with 8ply HSW subjected to creep test at 40.5 MPa in steam at 1100 °C (t_f = 0.01h).

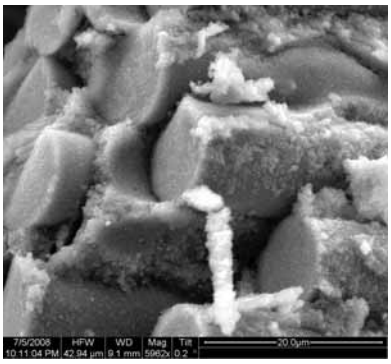

Figure A.338: Fracture surface of the N610/Al_2O_3 specimen with 8ply HSW subjected to creep test at 40.5 MPa in steam at 1100 °C (t_f = 0.01h).

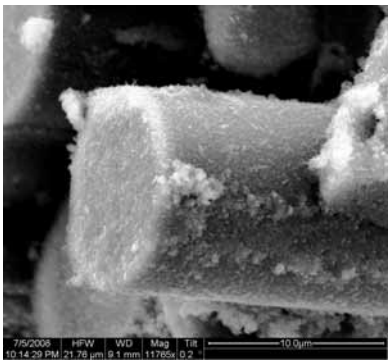

Figure A.339: Fracture surface of the N610/Al_2O_3 specimen with 8ply HSW subjected to creep test at 40.5 MPa in steam at 1100 °C (t_f = 0.01h).

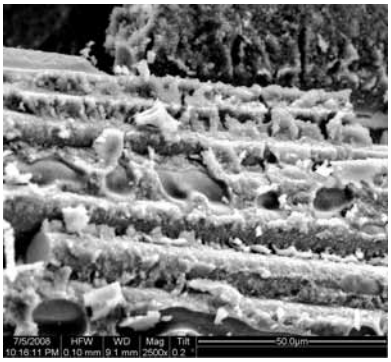

Figure A.340: Fracture surface of the N610/Al_2O_3 specimen with 8ply HSW subjected to creep test at 40.5 MPa in steam at 1100 °C (t_f = 0.01h).

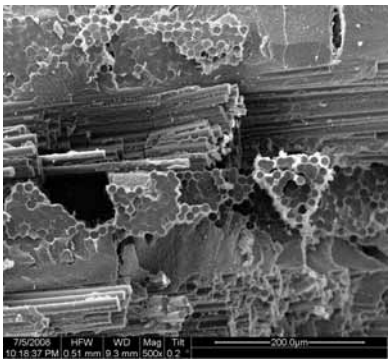

Figure A.341: Fracture surface of the N610/Al_2O_3 specimen with 8ply HSW subjected to creep test at 40.5 MPa in steam at 1100 °C (t_f = 0.01h).

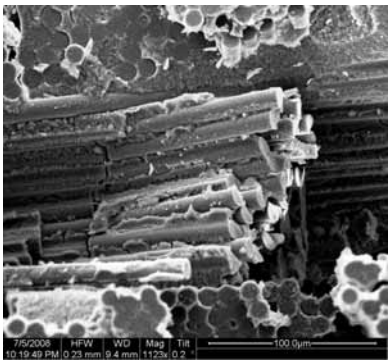

Figure A.342: Fracture surface of the N610/Al_2O_3 specimen with 8ply HSW subjected to creep test at 40.5 MPa in steam at 1100 °C (t_f = 0.01h).

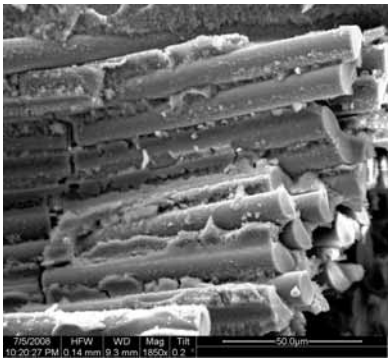

Figure A.343: Fracture surface of the N610/Al_2O_3 specimen with 8ply HSW subjected to creep test at 40.5 MPa in steam at 1100 °C (t_f = 0.01h).

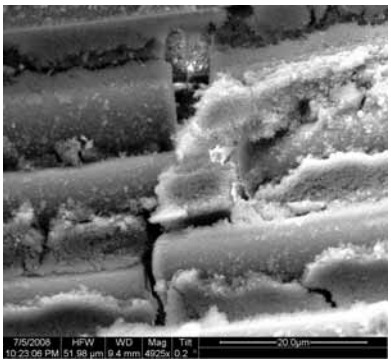

Figure A.344: Fracture surface of the N610/Al_2O_3 specimen with 8ply HSW subjected to creep test at 40.5 MPa in steam at 1100 °C (t_f = 0.01h).

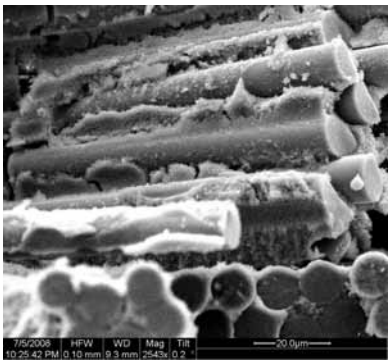

Figure A.345: Fracture surface of the N610/Al_2O_3 specimen with 8ply HSW subjected to creep test at 40.5 MPa in steam at 1100 °C (t_f = 0.01h).

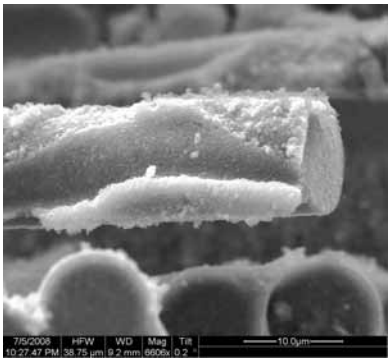

Figure A.346: Fracture surface of the N610/Al_2O_3 specimen with 8ply HSW subjected to creep test at 40.5 MPa in steam at 1100 °C (t_f = 0.01h).

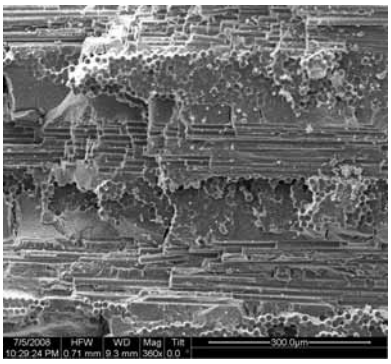

Figure A.347: Fracture surface of the N610/Al_2O_3 specimen with 8ply HSW subjected to creep test at 40.5 MPa in steam at 1100 °C (t_f = 0.01h).

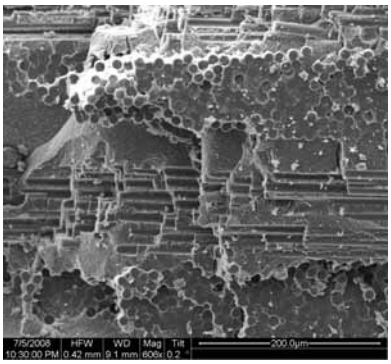

Figure A.348: Fracture surface of the N610/Al_2O_3 specimen with 8ply HSW subjected to creep test at 40.5 MPa in steam at 1100 °C (t_f = 0.01h).

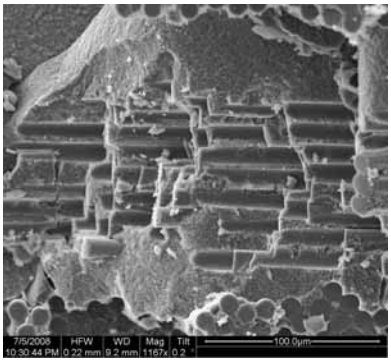

Figure A.349: Fracture surface of the N610/Al_2O_3 specimen with 8ply HSW subjected to creep test at 40.5 MPa in steam at 1100 °C (t_f = 0.01h).

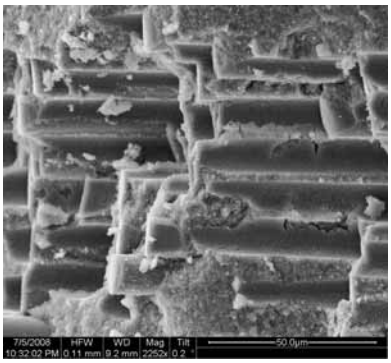

Figure A.350: Fracture surface of the N610/Al_2O_3 specimen with 8ply HSW subjected to creep test at 40.5 MPa in steam at 1100 °C (t_f = 0.01h).

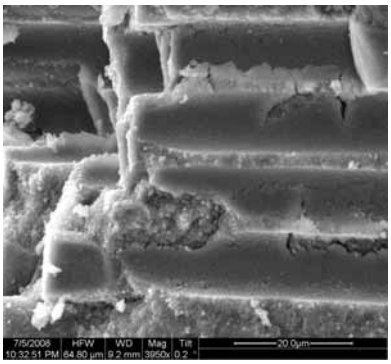

Figure A.351: Fracture surface of the N610/Al_2O_3 specimen with 8ply HSW subjected to creep test at 40.5 MPa in steam at 1100 °C (t_f = 0.01h).

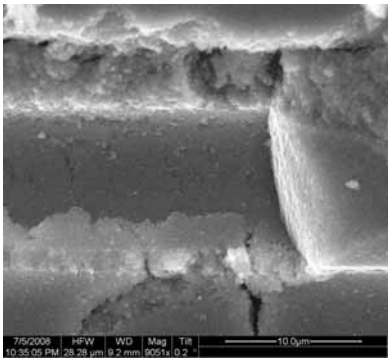

Figure A.352: Fracture surface of the N610/Al_2O_3 specimen with 8ply HSW subjected to creep test at 40.5 MPa in steam at 1100 °C (t_f = 0.01h).

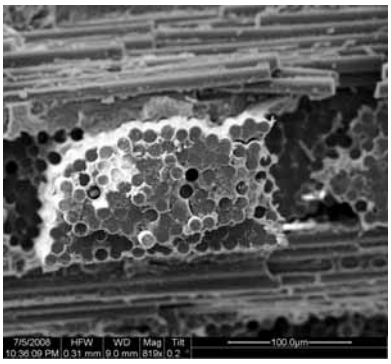

Figure A.353: Fracture surface of the N610/Al_2O_3 specimen with 8ply HSW subjected to creep test at 40.5 MPa in steam at 1100 °C (t_f = 0.01h).

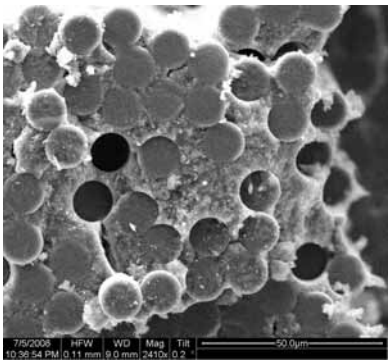

Figure A.354: Fracture surface of the N610/Al_2O_3 specimen with 8ply HSW subjected to creep test at 40.5 MPa in steam at 1100 °C (t_f = 0.01h).

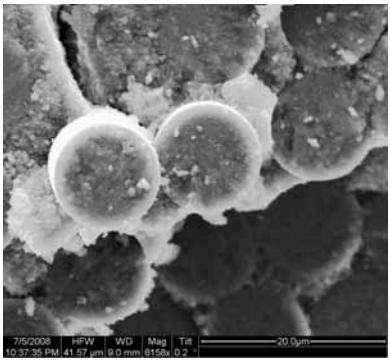

Figure A.355: Fracture surface of the N610/Al_2O_3 specimen with 8ply HSW subjected to creep test at 40.5 MPa in steam at 1100 °C (t_f = 0.01h).

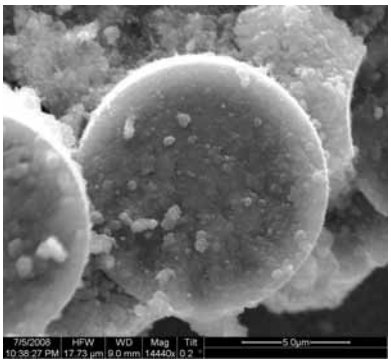

Figure A.356: Fracture surface of the N610/Al_2O_3 specimen with 8ply HSW subjected to creep test at 40.5 MPa in steam at 1100 °C (t_f = 0.01h).

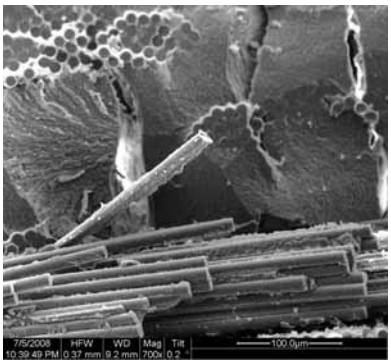

Figure A.357: Fracture surface of the N610/Al_2O_3 specimen with 8ply HSW subjected to creep test at 40.5 MPa in steam at 1100 °C (t_f = 0.01h).

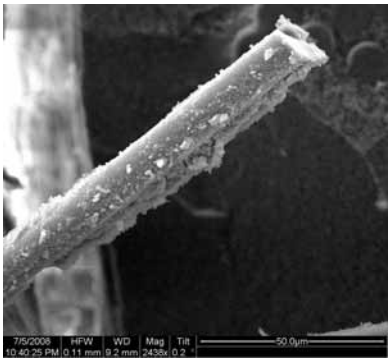

Figure A.358: Fracture surface of the N610/Al_2O_3 specimen with 8ply HSW subjected to creep test at 40.5 MPa in steam at 1100 °C (t_f = 0.01h).

Figure A.359: Fracture surface of the N610/Al_2O_3 specimen with 8ply HSW subjected to creep test at 40.5 MPa in steam at 1100 °C (t_f = 0.01h).

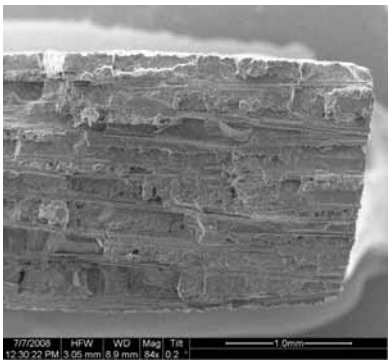

Figure A.360: Fracture surface of the N610/$LaPO_4$/Al_2O_3-$LaPO_4$-AlOCl specimen with 8ply HSW subjected to creep test at 32 MPa in air at 1100 °C (t_f = 100h).

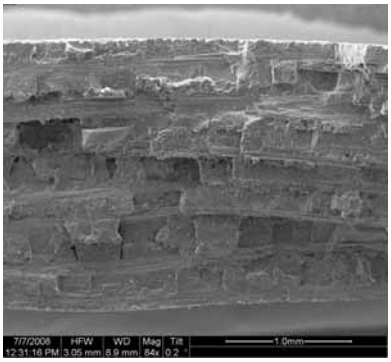

Figure A.361: Fracture surface of the N610/$LaPO_4$/Al_2O_3-$LaPO_4$-AlOCl specimen with 8ply HSW subjected to creep test at 32 MPa in air at 1100 °C (t_f = 100h).

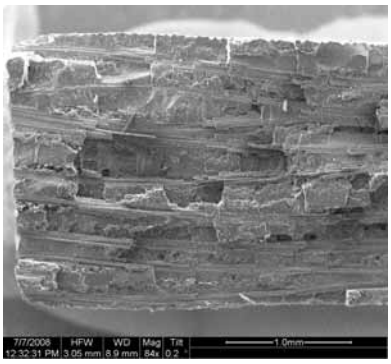

Figure A.362: Fracture surface of the N610/$LaPO_4$/Al_2O_3-$LaPO_4$-AlOCl specimen with 8ply HSW subjected to creep test at 32 MPa in air at 1100 °C (t_f = 100h).

Figure A.363: Fracture surface of the N610/$LaPO_4$/Al_2O_3-$LaPO_4$-AlOCl specimen with 8ply HSW subjected to creep test at 32 MPa in air at 1100 °C (t_f = 100h).

Figure A.364: Fracture surface of the N610/$LaPO_4$/Al_2O_3-$LaPO_4$-AlOCl specimen with 8ply HSW subjected to creep test at 32 MPa in air at 1100 °C (t_f = 100h).

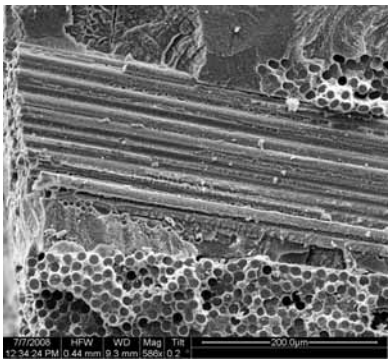

Figure A.365: Fracture surface of the N610/$LaPO_4$/Al_2O_3-$LaPO_4$-AlOCl specimen with 8ply HSW subjected to creep test at 32 MPa in air at 1100 °C (t_f = 100h).

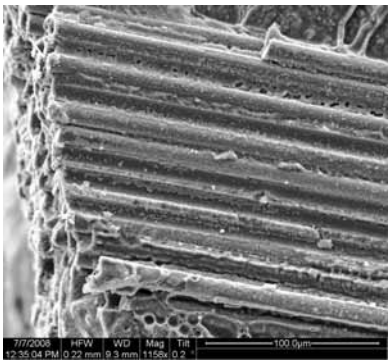

Figure A.366: Fracture surface of the N610/$LaPO_4$/Al_2O_3-$LaPO_4$-AlOCl specimen with 8ply HSW subjected to creep test at 32 MPa in air at 1100 °C (t_f = 100h).

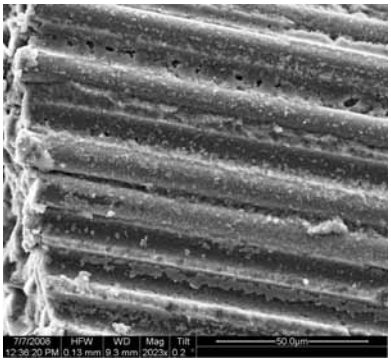

Figure A.367: Fracture surface of the N610/$LaPO_4$/Al_2O_3-$LaPO_4$-AlOCl specimen with 8ply HSW subjected to creep test at 32 MPa in air at 1100 °C (t_f = 100h).

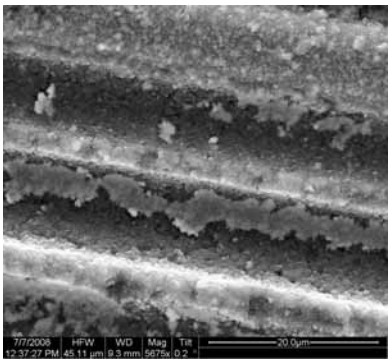

Figure A.368: Fracture surface of the N610/$LaPO_4$/Al_2O_3-$LaPO_4$-AlOCl specimen with 8ply HSW subjected to creep test at 32 MPa in air at 1100 °C (t_f = 100h).

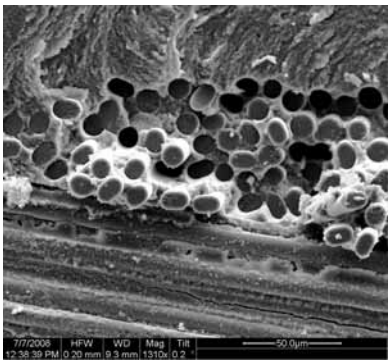

Figure A.369: Fracture surface of the N610/$LaPO_4$/Al_2O_3-$LaPO_4$-AlOCl specimen with 8ply HSW subjected to creep test at 32 MPa in air at 1100 °C (t_f = 100h).

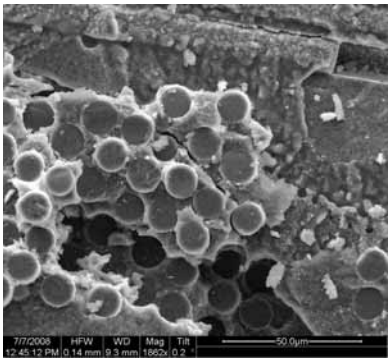

Figure A.370: Fracture surface of the N610/$LaPO_4$/Al_2O_3-$LaPO_4$-AlOCl specimen with 8ply HSW subjected to creep test at 32 MPa in air at 1100 °C (t_f = 100h).

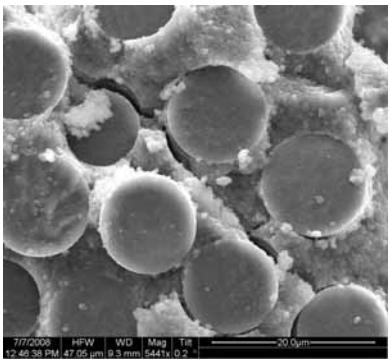

Figure A.371: Fracture surface of the N610/$LaPO_4$/Al_2O_3-$LaPO_4$-AlOCl specimen with 8ply HSW subjected to creep test at 32 MPa in air at 1100 °C (t_f = 100h).

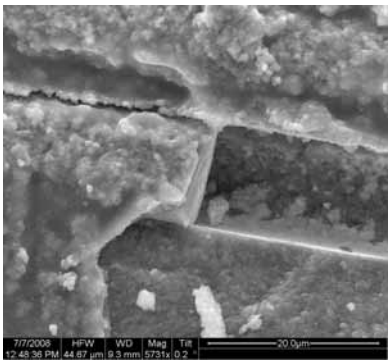

Figure A.372: Fracture surface of the N610/$LaPO_4$/Al_2O_3-$LaPO_4$-AlOCl specimen with 8ply HSW subjected to creep test at 32 MPa in air at 1100 °C (t_f = 100h).

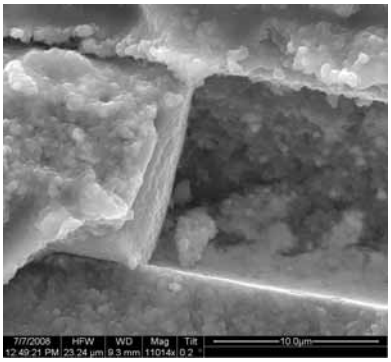

Figure A.373: Fracture surface of the N610/$LaPO_4$/Al_2O_3-$LaPO_4$-AlOCl specimen with 8ply HSW subjected to creep test at 32 MPa in air at 1100 °C (t_f = 100h).

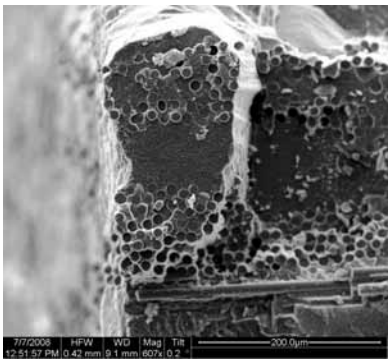

Figure A.374: Fracture surface of the N610/$LaPO_4$/Al_2O_3-$LaPO_4$-AlOCl specimen with 8ply HSW subjected to creep test at 32 MPa in air at 1100 °C (t_f = 100h).

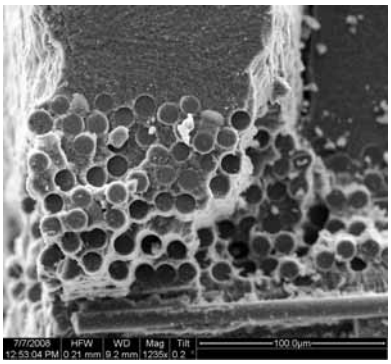

Figure A.375: Fracture surface of the N610/$LaPO_4$/Al_2O_3-$LaPO_4$-AlOCl specimen with 8ply HSW subjected to creep test at 32 MPa in air at 1100 °C (t_f = 100h).

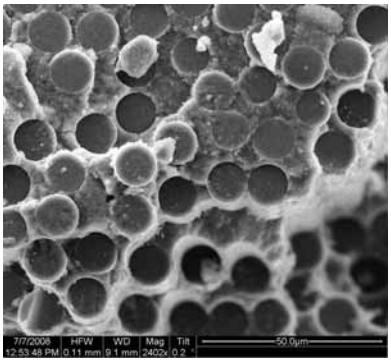

Figure A.376: Fracture surface of the N610/$LaPO_4$/Al_2O_3-$LaPO_4$-AlOCl specimen with 8ply HSW subjected to creep test at 32 MPa in air at 1100 °C (t_f = 100h).

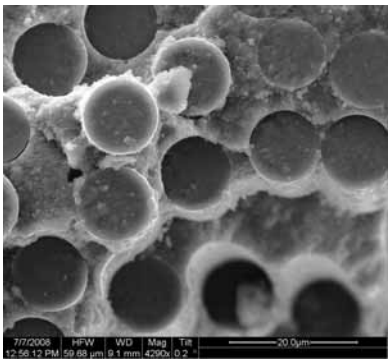

Figure A.377: Fracture surface of the N610/$LaPO_4$/Al_2O_3-$LaPO_4$-AlOCl specimen with 8ply HSW subjected to creep test at 32 MPa in air at 1100 °C (t_f = 100h).

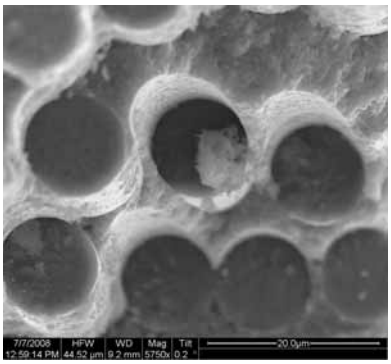

Figure A.378: Fracture surface of the N610/$LaPO_4$/Al_2O_3-$LaPO_4$-AlOCl specimen with 8ply HSW subjected to creep test at 32 MPa in air at 1100 °C (t_f = 100h).

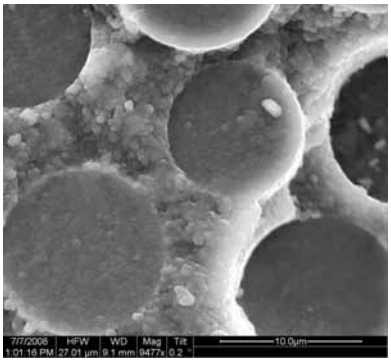

Figure A.379: Fracture surface of the N610/$LaPO_4$/Al_2O_3-$LaPO_4$-AlOCl specimen with 8ply HSW subjected to creep test at 32 MPa in air at 1100 °C (t_f = 100h).

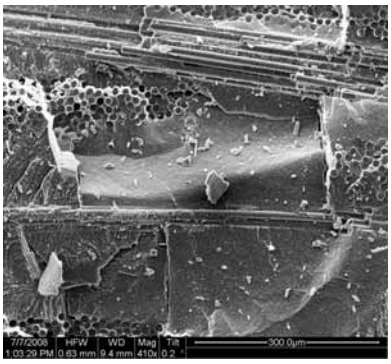

Figure A.380: Fracture surface of the N610/$LaPO_4$/Al_2O_3-$LaPO_4$-AlOCl specimen with 8ply HSW subjected to creep test at 32 MPa in air at 1100 °C (t_f = 100h).

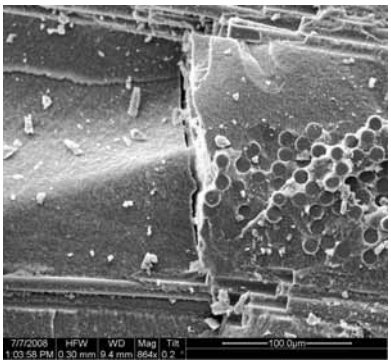

Figure A.381: Fracture surface of the N610/$LaPO_4$/Al_2O_3-$LaPO_4$-AlOCl specimen with 8ply HSW subjected to creep test at 32 MPa in air at 1100 °C (t_f = 100h).

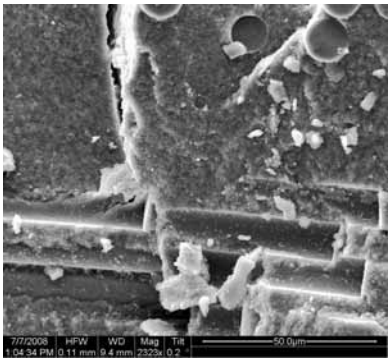

Figure A.382: Fracture surface of the N610/$LaPO_4$/Al_2O_3-$LaPO_4$-AlOCl specimen with 8ply HSW subjected to creep test at 32 MPa in air at 1100 °C (t_f = 100h).

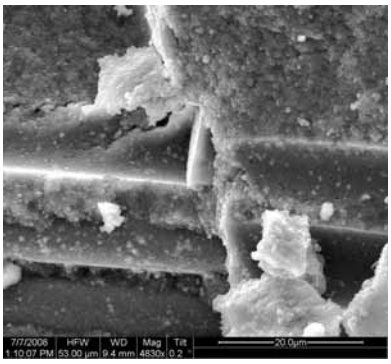

Figure A.383: Fracture surface of the N610/$LaPO_4$/Al_2O_3-$LaPO_4$-AlOCl specimen with 8ply HSW subjected to creep test at 32 MPa in air at 1100 °C (t_f = 100h).

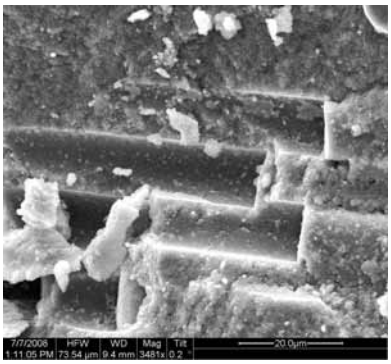

Figure A.384: Fracture surface of the N610/$LaPO_4$/Al_2O_3-$LaPO_4$-AlOCl specimen with 8ply HSW subjected to creep test at 32 MPa in air at 1100 °C (t_f = 100h).

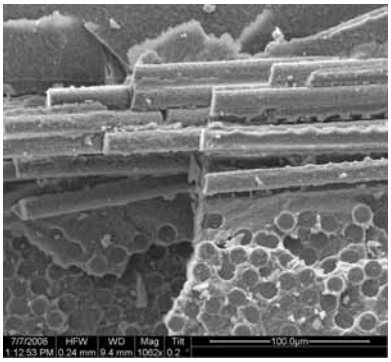

Figure A.385: Fracture surface of the N610/$LaPO_4$/Al_2O_3-$LaPO_4$-AlOCl specimen with 8ply HSW subjected to creep test at 32 MPa in air at 1100 °C (t_f = 100h).

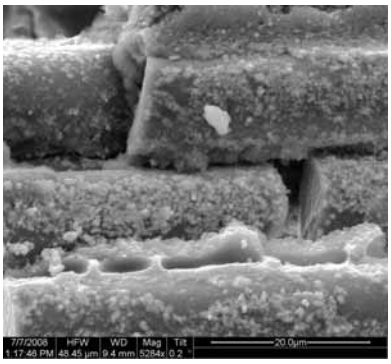

Figure A.386: Fracture surface of the N610/$LaPO_4$/Al_2O_3-$LaPO_4$-AlOCl specimen with 8ply HSW subjected to creep test at 32 MPa in air at 1100 °C (t_f = 100h).

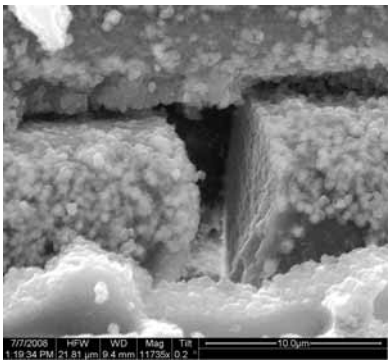

Figure A.387: Fracture surface of the N610/$LaPO_4$/Al_2O_3-$LaPO_4$-AlOCl specimen with 8ply HSW subjected to creep test at 32 MPa in air at 1100 °C (t_f = 100h).

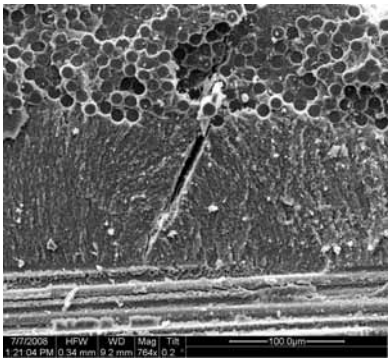

Figure A.388: Fracture surface of the N610/$LaPO_4$/Al_2O_3-$LaPO_4$-AlOCl specimen with 8ply HSW subjected to creep test at 32 MPa in air at 1100 °C (t_f = 100h).

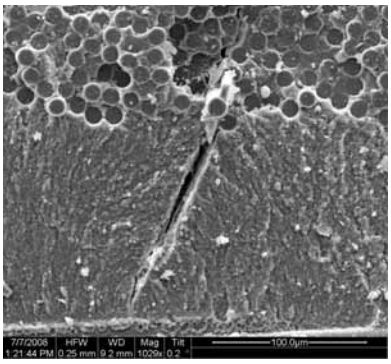

Figure A.389: Fracture surface of the N610/$LaPO_4$/Al_2O_3-$LaPO_4$-AlOCl specimen with 8ply HSW subjected to creep test at 32 MPa in air at 1100 °C (t_f = 100h).

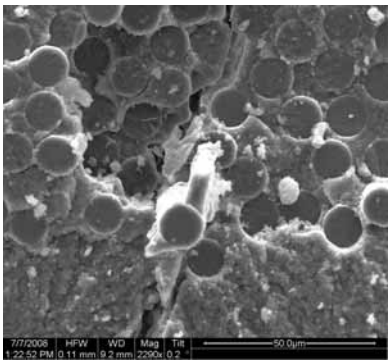

Figure A.390: Fracture surface of the N610/$LaPO_4$/Al_2O_3-$LaPO_4$-AlOCl specimen with 8ply HSW subjected to creep test at 32 MPa in air at 1100 °C (t_f = 100h).

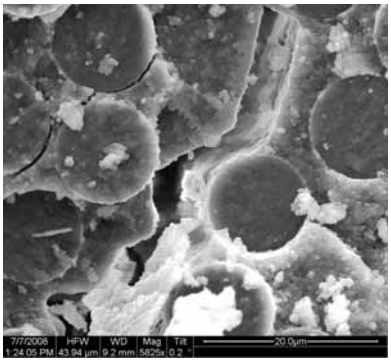

Figure A.391: Fracture surface of the N610/$LaPO_4$/Al_2O_3-$LaPO_4$-AlOCl specimen with 8ply HSW subjected to creep test at 32 MPa in air at 1100 °C (t_f = 100h).

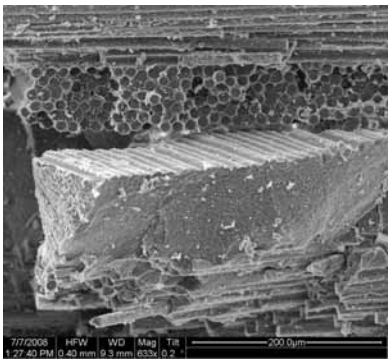

Figure A.392: Fracture surface of the N610/$LaPO_4$/Al_2O_3-$LaPO_4$-AlOCl specimen with 8ply HSW subjected to creep test at 32 MPa in air at 1100 °C (t_f = 100h).

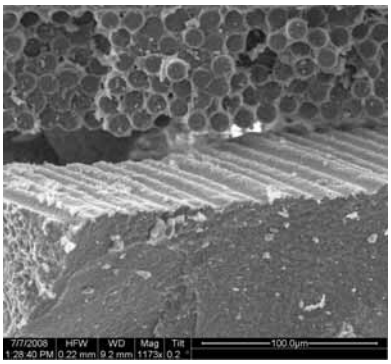

Figure A.393: Fracture surface of the N610/$LaPO_4$/Al_2O_3-$LaPO_4$-AlOCl specimen with 8ply HSW subjected to creep test at 32 MPa in air at 1100 °C (t_f = 100h).

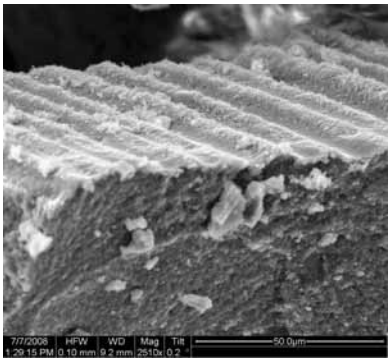

Figure A.394: Fracture surface of the N610/$LaPO_4$/Al_2O_3-$LaPO_4$-AlOCl specimen with 8ply HSW subjected to creep test at 32 MPa in air at 1100 °C (t_f = 100h).

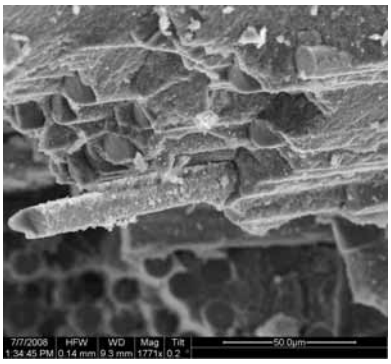

Figure A.395: Fracture surface of the N610/$LaPO_4$/Al_2O_3-$LaPO_4$-AlOCl specimen with 8ply HSW subjected to creep test at 32 MPa in air at 1100 °C (t_f = 100h).

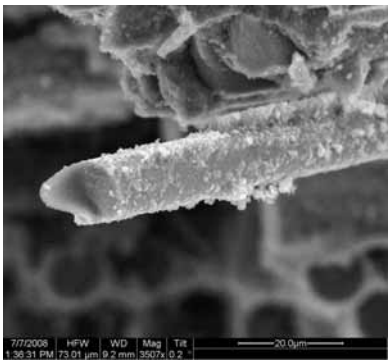

Figure A.396: Fracture surface of the N610/$LaPO_4$/Al_2O_3-$LaPO_4$-AlOCl specimen with 8ply HSW subjected to creep test at 32 MPa in air at 1100 °C (t_f = 100h).

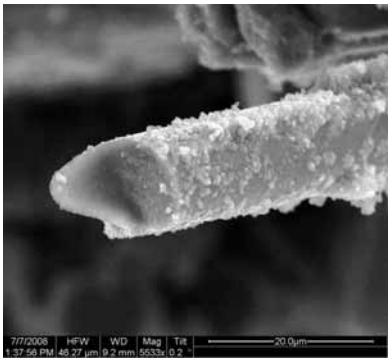

Figure A.397: Fracture surface of the N610/$LaPO_4$/Al_2O_3-$LaPO_4$-AlOCl specimen with 8ply HSW subjected to creep test at 32 MPa in air at 1100 °C (t_f = 100h).

Figure A.398: Fracture surface of the N610/$LaPO_4$/Al_2O_3-$LaPO_4$-AlOCl specimen with 8ply HSW subjected to creep test at 32 MPa in air at 1100 °C (t_f = 100h).

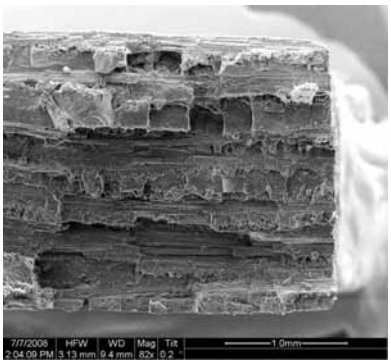

Figure A.399: Fracture surface of the N610/$LaPO_4$/Al_2O_3-$LaPO_4$-AlOCl specimen with 8ply HSW subjected to creep test at 32 MPa in steam at 1100 °C (t_f = 3.47h).

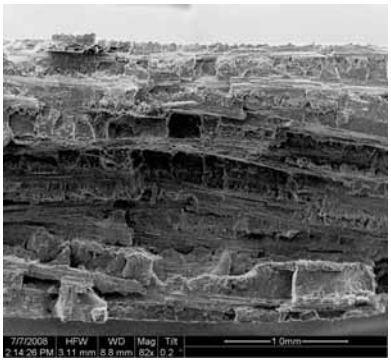

Figure A.400: Fracture surface of the N610/$LaPO_4$/Al_2O_3-$LaPO_4$-AlOCl specimen with 8ply HSW subjected to creep test at 32 MPa in steam at 1100 °C (t_f = 3.47h).

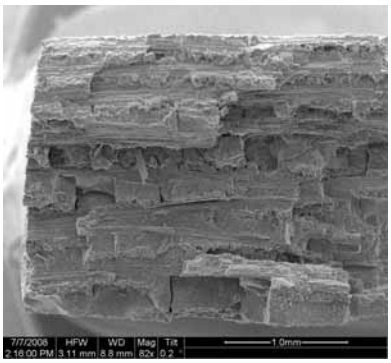

Figure A.401: Fracture surface of the N610/$LaPO_4$/Al_2O_3-$LaPO_4$-AlOCl specimen with 8ply HSW subjected to creep test at 32 MPa in steam at 1100 °C (t_f = 3.47h).

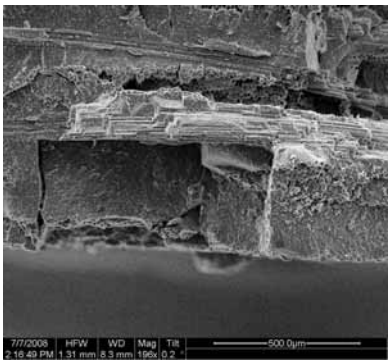

Figure A.402: Fracture surface of the N610/$LaPO_4$/Al_2O_3-$LaPO_4$-AlOCl specimen with 8ply HSW subjected to creep test at 32 MPa in steam at 1100 °C (t_f = 3.47h).

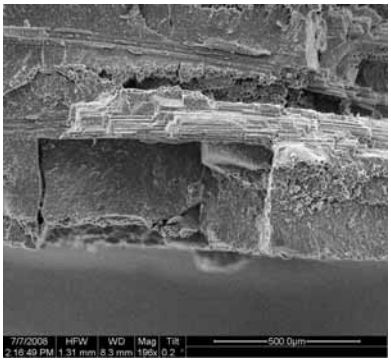

Figure A.403: Fracture surface of the N610/$LaPO_4$/Al_2O_3-$LaPO_4$-AlOCl specimen with 8ply HSW subjected to creep test at 32 MPa in steam at 1100 °C (t_f = 3.47h).

Figure A.404: Fracture surface of the N610/$LaPO_4$/Al_2O_3-$LaPO_4$-AlOCl specimen with 8ply HSW subjected to creep test at 32 MPa in steam at 1100 °C (t_f = 3.47h).

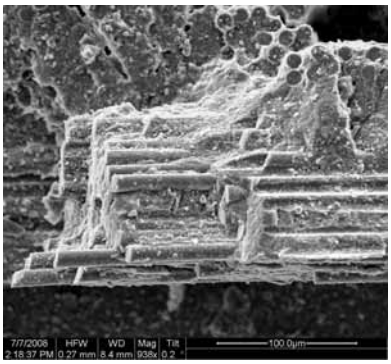

Figure A.405: Fracture surface of the N610/$LaPO_4$/Al_2O_3-$LaPO_4$-AlOCl specimen with 8ply HSW subjected to creep test at 32 MPa in steam at 1100 °C (t_f = 3.47h).

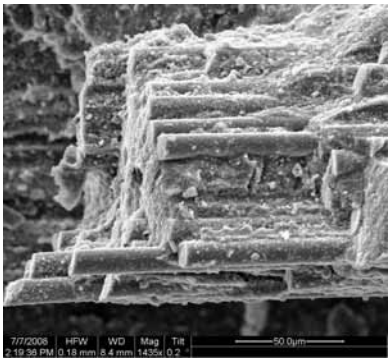

Figure A.406: Fracture surface of the N610/$LaPO_4$/Al_2O_3-$LaPO_4$-AlOCl specimen with 8ply HSW subjected to creep test at 32 MPa in steam at 1100 °C (t_f = 3.47h).

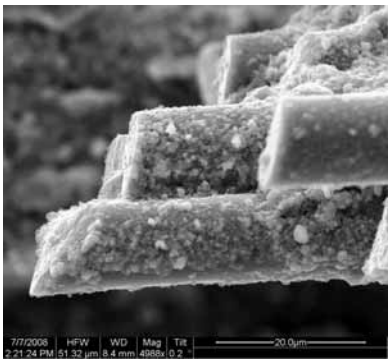

Figure A.407: Fracture surface of the N610/$LaPO_4$/Al_2O_3-$LaPO_4$-AlOCl specimen with 8ply HSW subjected to creep test at 32 MPa in steam at 1100 °C (t_f = 3.47h).

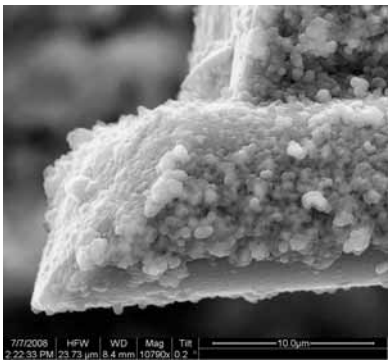

Figure A.408: Fracture surface of the N610/$LaPO_4$/Al_2O_3-$LaPO_4$-AlOCl specimen with 8ply HSW subjected to creep test at 32 MPa in steam at 1100 °C (t_f = 3.47h).

Figure A.409: Fracture surface of the N610/$LaPO_4$/Al_2O_3-$LaPO_4$-AlOCl specimen with 8ply HSW subjected to creep test at 32 MPa in steam at 1100 °C (t_f = 3.47h).

Figure A.410: Fracture surface of the N610/$LaPO_4$/Al_2O_3-$LaPO_4$-AlOCl specimen with 8ply HSW subjected to creep test at 32 MPa in steam at 1100 °C (t_f = 3.47h).

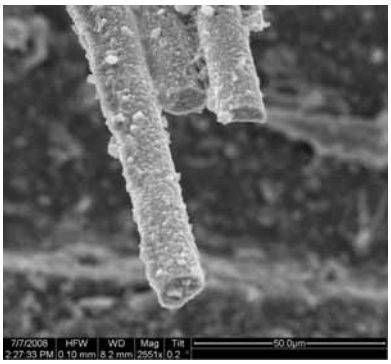

Figure A.411: Fracture surface of the N610/$LaPO_4$/Al_2O_3-$LaPO_4$-AlOCl specimen with 8ply HSW subjected to creep test at 32 MPa in steam at 1100 °C (t_f = 3.47h).

Figure A.412: Fracture surface of the N610/$LaPO_4$/Al_2O_3-$LaPO_4$-AlOCl specimen with 8ply HSW subjected to creep test at 32 MPa in steam at 1100 °C (t_f = 3.47h).

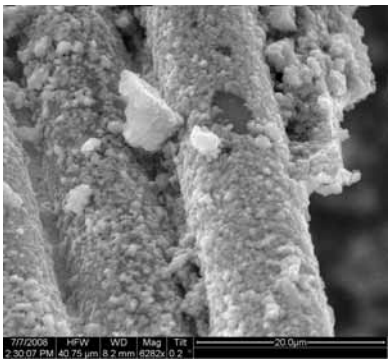

Figure A.413: Fracture surface of the N610/$LaPO_4$/Al_2O_3-$LaPO_4$-AlOCl specimen with 8ply HSW subjected to creep test at 32 MPa in steam at 1100 °C (t_f = 3.47h).

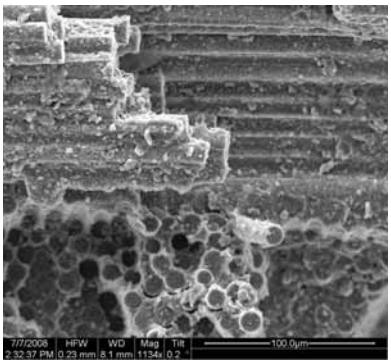

Figure A.414: Fracture surface of the N610/$LaPO_4$/Al_2O_3-$LaPO_4$-AlOCl specimen with 8ply HSW subjected to creep test at 32 MPa in steam at 1100 °C (t_f = 3.47h).

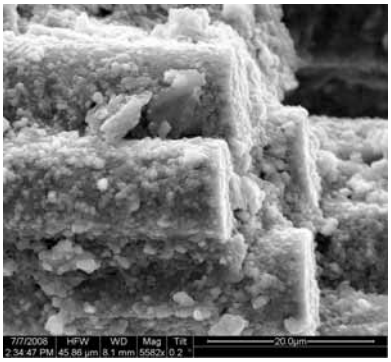

Figure A.415: Fracture surface of the N610/$LaPO_4$/Al_2O_3-$LaPO_4$-AlOCl specimen with 8ply HSW subjected to creep test at 32 MPa in steam at 1100 °C (t_f = 3.47h).

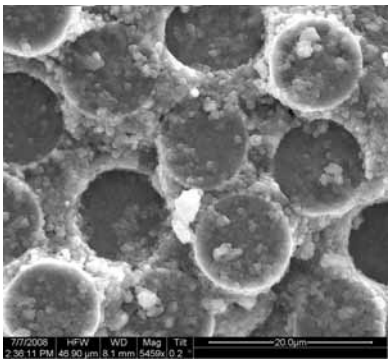

Figure A.416: Fracture surface of the N610/$LaPO_4$/Al_2O_3-$LaPO_4$-AlOCl specimen with 8ply HSW subjected to creep test at 32 MPa in steam at 1100 °C (t_f = 3.47h).

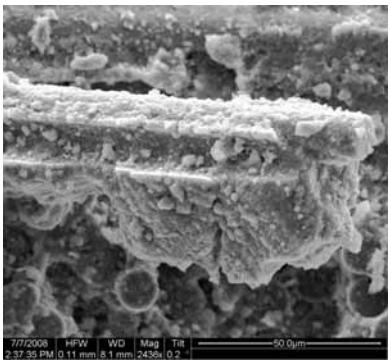

Figure A.417: Fracture surface of the N610/$LaPO_4$/Al_2O_3-$LaPO_4$-AlOCl specimen with 8ply HSW subjected to creep test at 32 MPa in steam at 1100 °C (t_f = 3.47h).

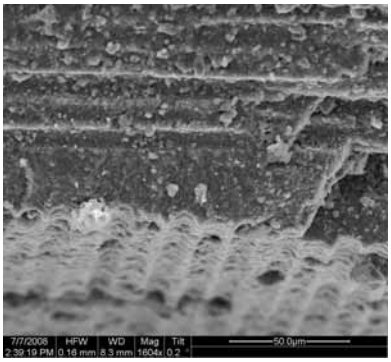

Figure A.418: Fracture surface of the N610/$LaPO_4$/Al_2O_3-$LaPO_4$-AlOCl specimen with 8ply HSW subjected to creep test at 32 MPa in steam at 1100 °C (t_f = 3.47h).

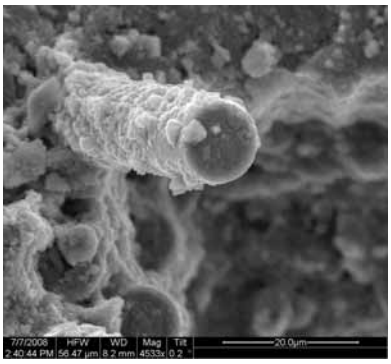

Figure A.419: Fracture surface of the N610/$LaPO_4$/Al_2O_3-$LaPO_4$-AlOCl specimen with 8ply HSW subjected to creep test at 32 MPa in steam at 1100 °C (t_f = 3.47h).

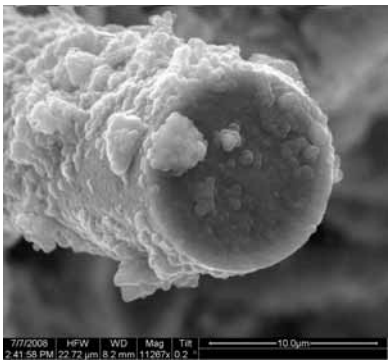

Figure A.420: Fracture surface of the N610/$LaPO_4$/Al_2O_3-$LaPO_4$-AlOCl specimen with 8ply HSW subjected to creep test at 32 MPa in steam at 1100 °C (t_f = 3.47h).

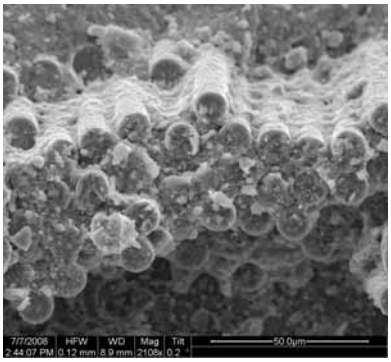

Figure A.421: Fracture surface of the N610/$LaPO_4$/Al_2O_3-$LaPO_4$-AlOCl specimen with 8ply HSW subjected to creep test at 32 MPa in steam at 1100 °C (t_f = 3.47h).

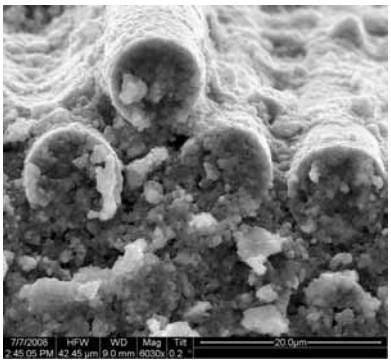

Figure A.422: Fracture surface of the N610/$LaPO_4$/Al_2O_3-$LaPO_4$-AlOCl specimen with 8ply HSW subjected to creep test at 32 MPa in steam at 1100 °C (t_f = 3.47h).

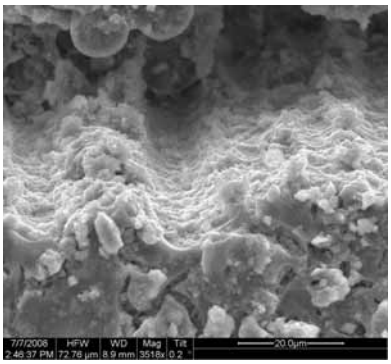

Figure A.423: Fracture surface of the N610/$LaPO_4$/Al_2O_3-$LaPO_4$-AlOCl specimen with 8ply HSW subjected to creep test at 32 MPa in steam at 1100 °C (t_f = 3.47h).

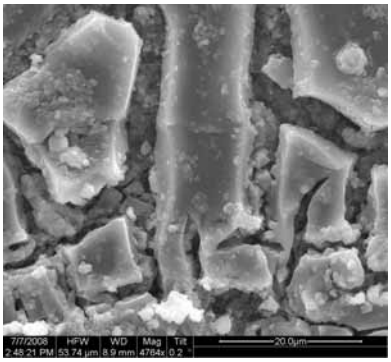

Figure A.424: Fracture surface of the N610/$LaPO_4$/Al_2O_3-$LaPO_4$-AlOCl specimen with 8ply HSW subjected to creep test at 32 MPa in steam at 1100 °C (t_f = 3.47h).

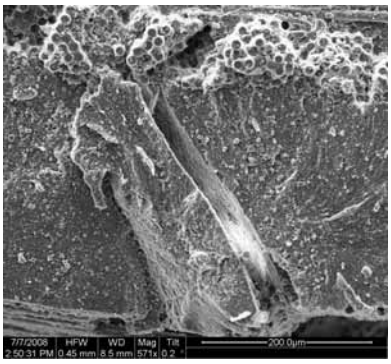

Figure A.425: Fracture surface of the N610/$LaPO_4$/Al_2O_3-$LaPO_4$-AlOCl specimen with 8ply HSW subjected to creep test at 32 MPa in steam at 1100 °C (t_f = 3.47h).

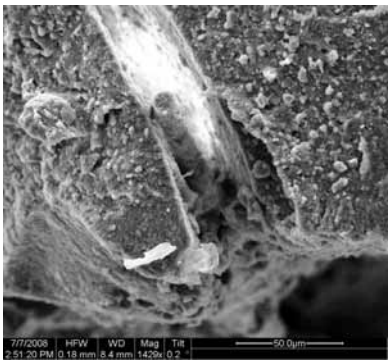

Figure A.426: Fracture surface of the N610/$LaPO_4$/Al_2O_3-$LaPO_4$-AlOCl specimen with 8ply HSW subjected to creep test at 32 MPa in steam at 1100 °C (t_f = 3.47h).

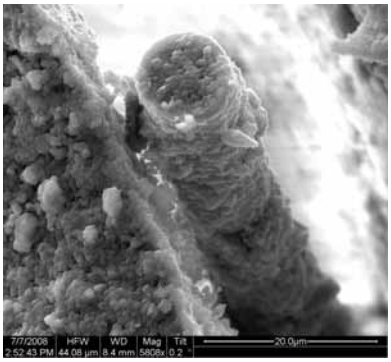

Figure A.427: Fracture surface of the N610/$LaPO_4$/Al_2O_3-$LaPO_4$-AlOCl specimen with 8ply HSW subjected to creep test at 32 MPa in steam at 1100 °C (t_f = 3.47h).

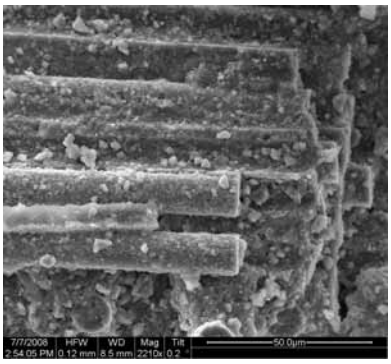

Figure A.428: Fracture surface of the N610/$LaPO_4$/Al_2O_3-$LaPO_4$-AlOCl specimen with 8ply HSW subjected to creep test at 32 MPa in steam at 1100 °C (t_f = 3.47h).

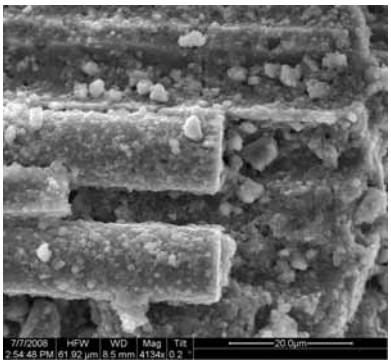

Figure A.429: Fracture surface of the N610/$LaPO_4$/Al_2O_3-$LaPO_4$-AlOCl specimen with 8ply HSW subjected to creep test at 32 MPa in steam at 1100 °C (t_f = 3.47h).

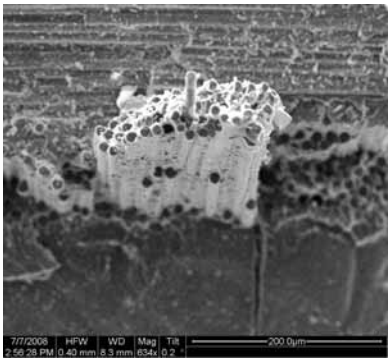

Figure A.430: Fracture surface of the N610/$LaPO_4$/Al_2O_3-$LaPO_4$-AlOCl specimen with 8ply HSW subjected to creep test at 32 MPa in steam at 1100 °C (t_f = 3.47h).

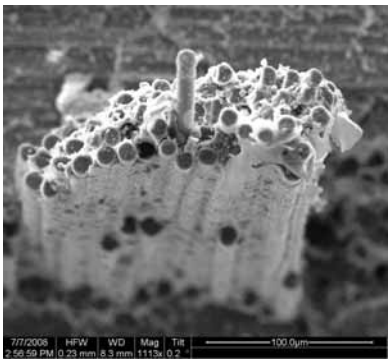

Figure A.431: Fracture surface of the N610/$LaPO_4$/Al_2O_3-$LaPO_4$-AlOCl specimen with 8ply HSW subjected to creep test at 32 MPa in steam at 1100 °C (t_f = 3.47h).

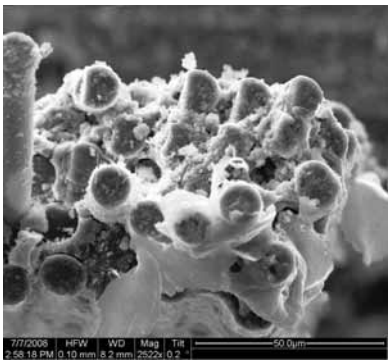

Figure A.432: Fracture surface of the N610/$LaPO_4$/Al_2O_3-$LaPO_4$-AlOCl specimen with 8ply HSW subjected to creep test at 32 MPa in steam at 1100 °C (t_f = 3.47h).

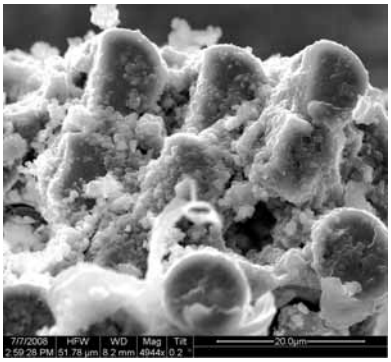

Figure A.433: Fracture surface of the N610/$LaPO_4$/Al_2O_3-$LaPO_4$-AlOCl specimen with 8ply HSW subjected to creep test at 32 MPa in steam at 1100 °C (t_f = 3.47h).

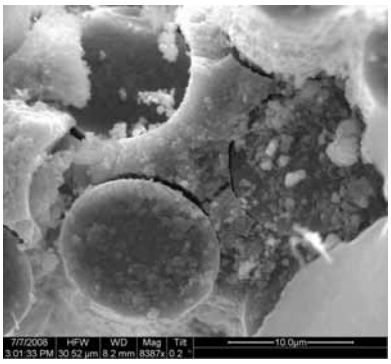

Figure A.434: Fracture surface of the N610/$LaPO_4$/Al_2O_3-$LaPO_4$-AlOCl specimen with 8ply HSW subjected to creep test at 32 MPa in steam at 1100 °C (t_f = 3.47h).

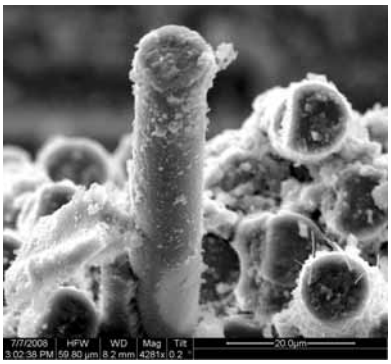

Figure A.435: Fracture surface of the N610/$LaPO_4$/Al_2O_3-$LaPO_4$-AlOCl specimen with 8ply HSW subjected to creep test at 32 MPa in steam at 1100 °C (t_f = 3.47h).

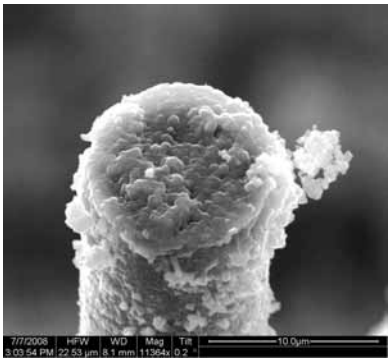

Figure A.436: Fracture surface of the N610/$LaPO_4$/Al_2O_3-$LaPO_4$-AlOCl specimen with 8ply HSW subjected to creep test at 32 MPa in steam at 1100 °C (t_f = 3.47h).

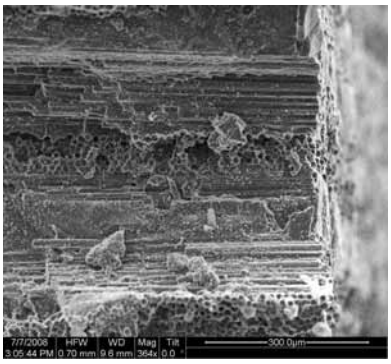

Figure A.437: Fracture surface of the N610/$LaPO_4$/Al_2O_3-$LaPO_4$-AlOCl specimen with 8ply HSW subjected to creep test at 32 MPa in steam at 1100 °C (t_f = 3.47h).

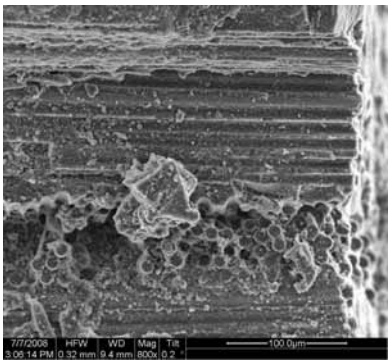

Figure A.438: Fracture surface of the N610/$LaPO_4$/Al_2O_3-$LaPO_4$-AlOCl specimen with 8ply HSW subjected to creep test at 32 MPa in steam at 1100 °C (t_f = 3.47h).

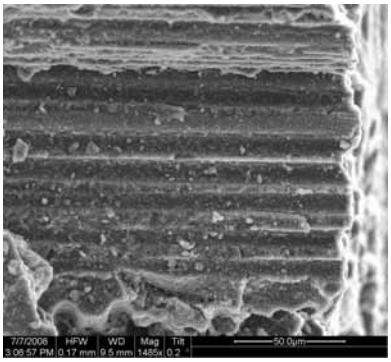

Figure A.439: Fracture surface of the N610/$LaPO_4$/Al_2O_3-$LaPO_4$-AlOCl specimen with 8ply HSW subjected to creep test at 32 MPa in steam at 1100 °C (t_f = 3.47h).

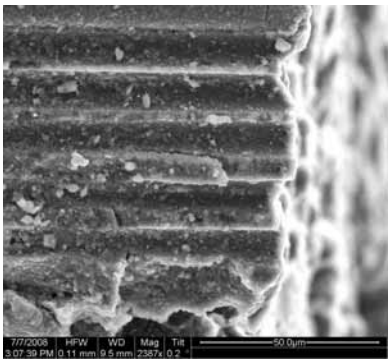

Figure A.440: Fracture surface of the N610/$LaPO_4$/Al_2O_3-$LaPO_4$-AlOCl specimen with 8ply HSW subjected to creep test at 32 MPa in steam at 1100 °C (t_f = 3.47h).

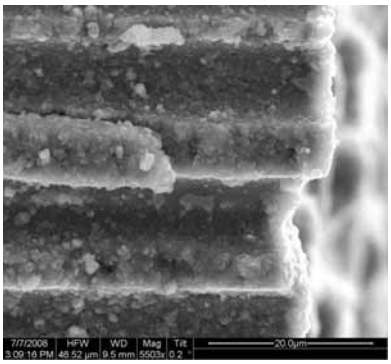

Figure A.441: Fracture surface of the N610/$LaPO_4$/Al_2O_3-$LaPO_4$-AlOCl specimen with 8ply HSW subjected to creep test at 32 MPa in steam at 1100 °C (t_f = 3.47h).

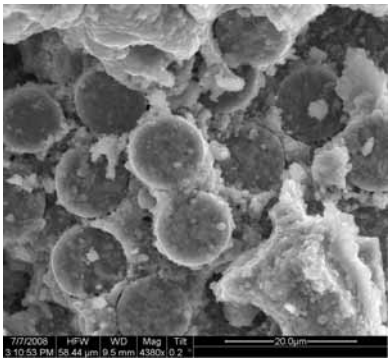

Figure A.442: Fracture surface of the N610/$LaPO_4$/Al_2O_3-$LaPO_4$-AlOCl specimen with 8ply HSW subjected to creep test at 32 MPa in steam at 1100 °C (t_f = 3.47h).

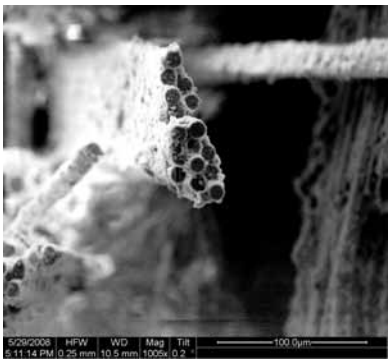

Figure A.443: Fracture surface of the N610/$LaPO_4$/Al_2O_3-$LaPO_4$-AlOCl specimen with 8ply HSW subjected to creep test at 48 MPa in steam at 1100 °C (t_f = 2.06h).

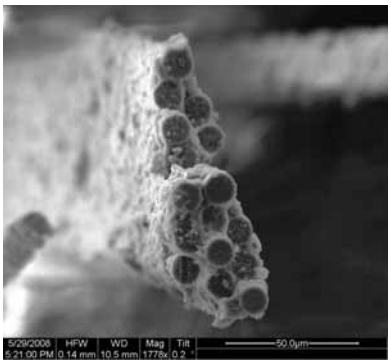

Figure A.444: Fracture surface of the N610/$LaPO_4$/Al_2O_3-$LaPO_4$-AlOCl specimen with 8ply HSW subjected to creep test at 48 MPa in steam at 1100 °C (t_f = 2.06h).

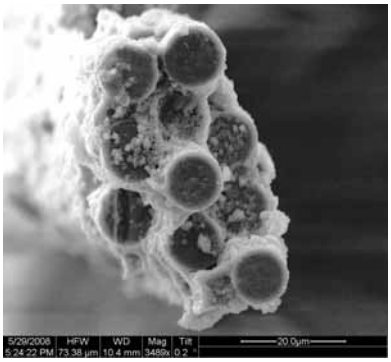

Figure A.445: Fracture surface of the N610/$LaPO_4$/Al_2O_3-$LaPO_4$-AlOCl specimen with 8ply HSW subjected to creep test at 48 MPa in steam at 1100 °C (t_f = 2.06h).

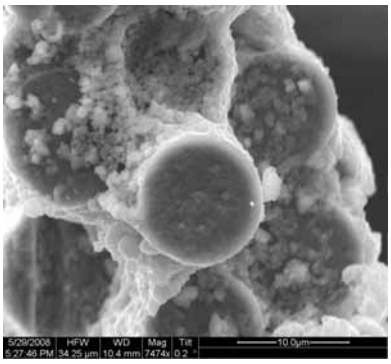

Figure A.446: Fracture surface of the N610/$LaPO_4$/Al_2O_3-$LaPO_4$-AlOCl specimen with 8ply HSW subjected to creep test at 48 MPa in steam at 1100 °C (t_f = 2.06h).

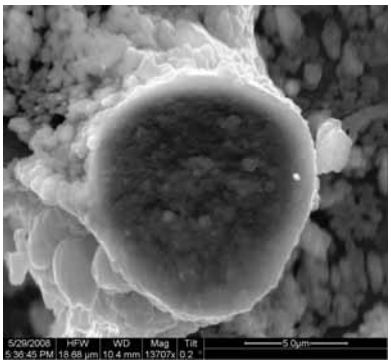

Figure A.447: Fracture surface of the N610/$LaPO_4$/Al_2O_3-$LaPO_4$-AlOCl specimen with 8ply HSW subjected to creep test at 48 MPa in steam at 1100 °C (t_f = 2.06h).

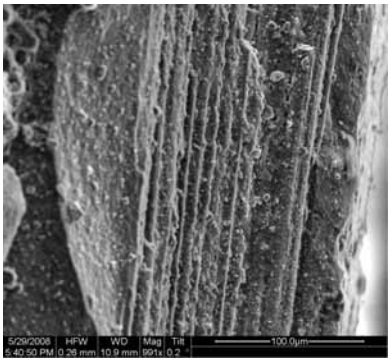

Figure A.448: Fracture surface of the N610/$LaPO_4$/Al_2O_3-$LaPO_4$-AlOCl specimen with 8ply HSW subjected to creep test at 48 MPa in steam at 1100 °C (t_f = 2.06h).

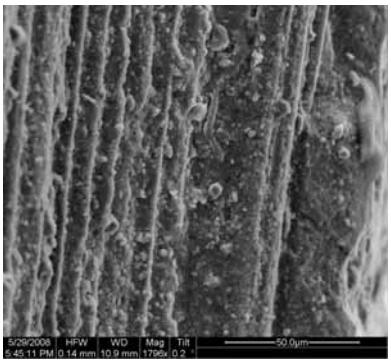

Figure A.449: Fracture surface of the N610/$LaPO_4$/Al_2O_3-$LaPO_4$-AlOCl specimen with 8ply HSW subjected to creep test at 48 MPa in steam at 1100 °C (t_f = 2.06h).

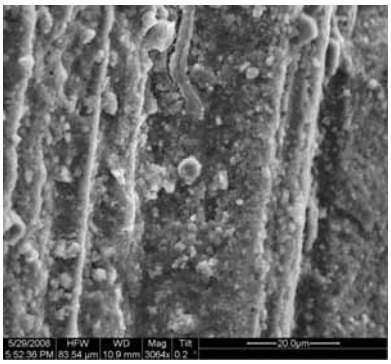

Figure A.450: Fracture surface of the N610/$LaPO_4$/Al_2O_3-$LaPO_4$-AlOCl specimen with 8ply HSW subjected to creep test at 48 MPa in steam at 1100 °C (t_f = 2.06h).

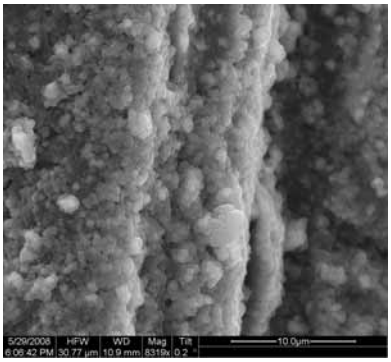

Figure A.451: Fracture surface of the N610/$LaPO_4$/Al_2O_3-$LaPO_4$-AlOCl specimen with 8ply HSW subjected to creep test at 48 MPa in steam at 1100 °C (t_f = 2.06h).

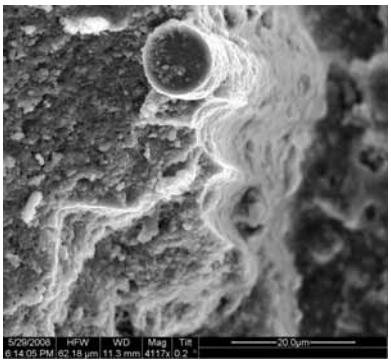

Figure A.452: Fracture surface of the N610/$LaPO_4$/Al_2O_3-$LaPO_4$-AlOCl specimen with 8ply HSW subjected to creep test at 48 MPa in steam at 1100 °C (t_f = 2.06h).

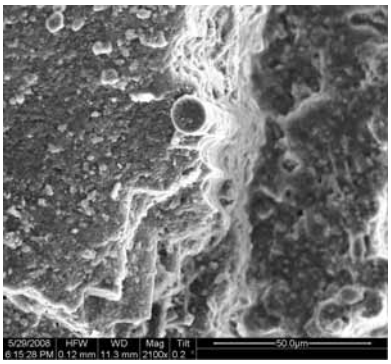

Figure A.453: Fracture surface of the N610/$LaPO_4$/Al_2O_3-$LaPO_4$-AlOCl specimen with 8ply HSW subjected to creep test at 48 MPa in steam at 1100 °C (t_f = 2.06h).

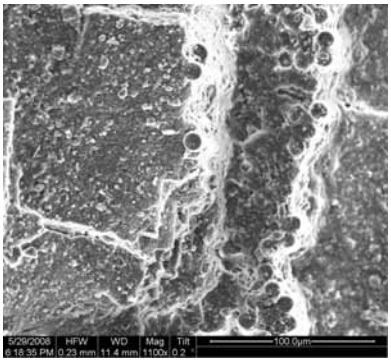

Figure A.454: Fracture surface of the N610/$LaPO_4$/Al_2O_3-$LaPO_4$-AlOCl specimen with 8ply HSW subjected to creep test at 48 MPa in steam at 1100 °C (t_f = 2.06h).

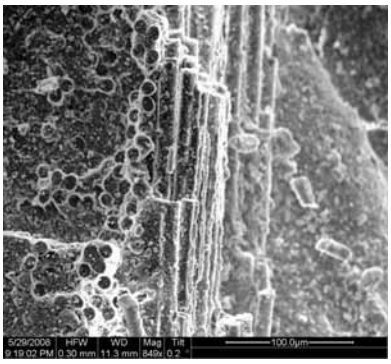

Figure A.455: Fracture surface of the N610/$LaPO_4$/Al_2O_3-$LaPO_4$-AlOCl specimen with 8ply HSW subjected to creep test at 48 MPa in steam at 1100 °C (t_f = 2.06h).

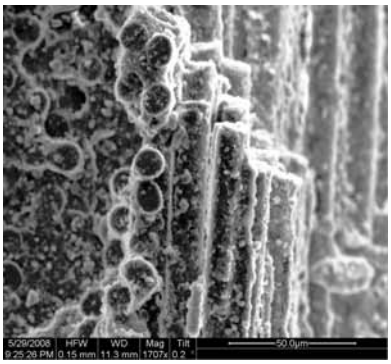

Figure A.456: Fracture surface of the N610/$LaPO_4$/Al_2O_3-$LaPO_4$-AlOCl specimen with 8ply HSW subjected to creep test at 48 MPa in steam at 1100 °C (t_f = 2.06h).

Figure A.457: Fracture surface of the N610/$LaPO_4$/Al_2O_3-$LaPO_4$-AlOCl specimen with 8ply HSW subjected to creep test at 48 MPa in steam at 1100 °C (t_f = 2.06h).

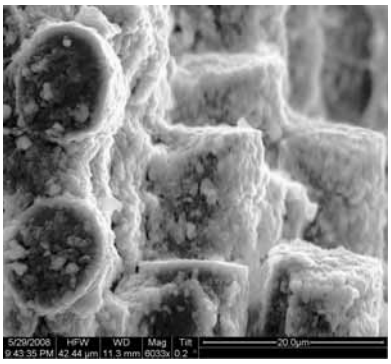

Figure A.458: Fracture surface of the N610/$LaPO_4$/Al_2O_3-$LaPO_4$-AlOCl specimen with 8ply HSW subjected to creep test at 48 MPa in steam at 1100 °C (t_f = 2.06h).

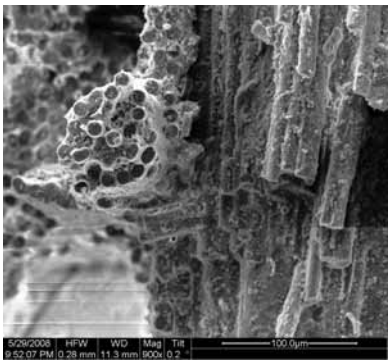

Figure A.459: Fracture surface of the N610/$LaPO_4$/Al_2O_3-$LaPO_4$-AlOCl specimen with 8ply HSW subjected to creep test at 48 MPa in steam at 1100 °C (t_f = 2.06h).

Figure A.460: Fracture surface of the N610/$LaPO_4$/Al_2O_3-$LaPO_4$-AlOCl specimen with 8ply HSW subjected to creep test at 48 MPa in steam at 1100 °C (t_f = 2.06h).

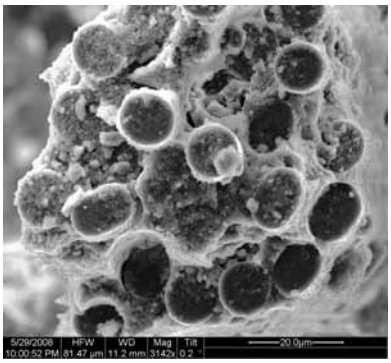

Figure A.461: Fracture surface of the N610/$LaPO_4$/Al_2O_3-$LaPO_4$-AlOCl specimen with 8ply HSW subjected to creep test at 48 MPa in steam at 1100 °C (t_f = 2.06h).

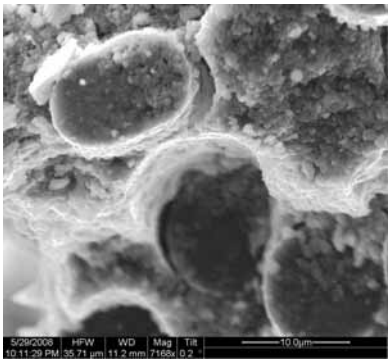

Figure A.462: Fracture surface of the N610/$LaPO_4$/Al_2O_3-$LaPO_4$-AlOCl specimen with 8ply HSW subjected to creep test at 48 MPa in steam at 1100 °C (t_f = 2.06h).

Figure A.463: Fracture surface of the N610/$LaPO_4$/Al_2O_3-$LaPO_4$-AlOCl specimen with 8ply HSW subjected to creep test at 48 MPa in steam at 1100 °C (t_f = 2.06h).

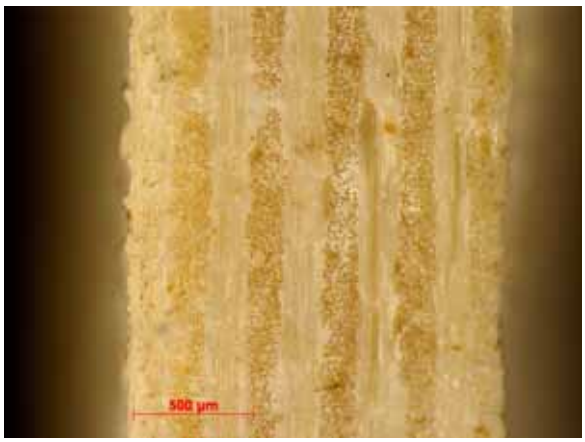

Figure B.1: Side view of the virgin N610/Al_2O_3-$LaPO_4$ specimen with 10ply 0°/90° uni-tape lay-up.

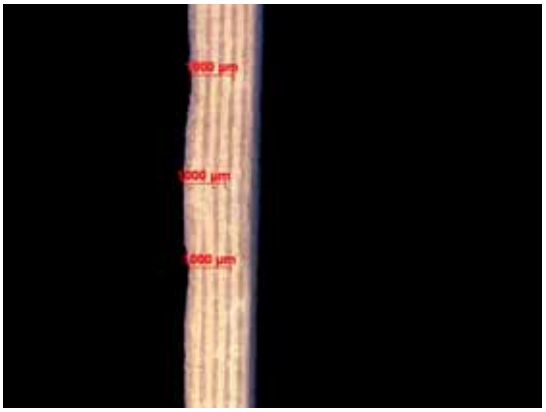

Figure B.2: Side view of the virgin N610/Al_2O_3-$LaPO_4$ specimen with 10ply 0°/90° uni-tape lay-up.

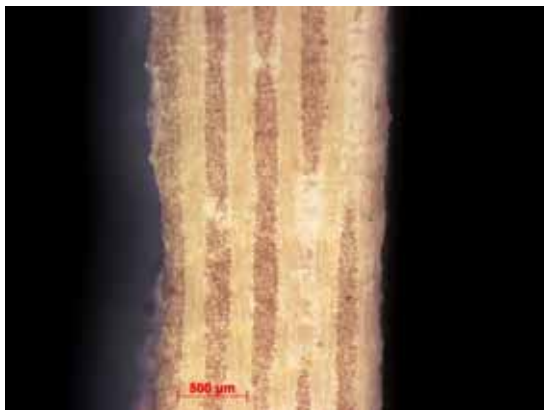

Figure B.3: Side view of the virgin N610/Al_2O_3-$LaPO_4$ specimen with 10ply 0°/90° uni-tape lay-up.

Figure B.4: Side view of the virgin N610/Al_2O_3-$LaPO_4$ specimen with 10ply 0°/90° uni-tape lay-up.

Figure B.5: Fracture surface of the N610/Al_2O_3-$LaPO_4$ specimen with 10ply 0°/90° uni-tape lay-up subjected tension to failure in laboratory air at 1100 °C.

Figure B.6: Fracture surface of the N610/Al_2O_3-$LaPO_4$ specimen with 10ply 0°/90° uni-tape lay-up subjected tension to failure in laboratory air at 1100 °C.

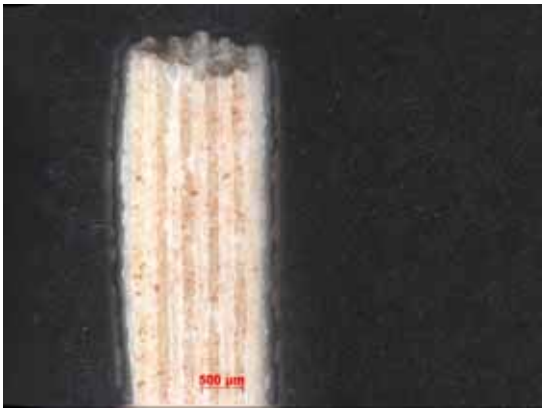

Figure B.7: Fracture surface of the N610/Al_2O_3-$LaPO_4$ specimen with 10ply 0°/90° uni-tape lay-up subjected tension to failure in laboratory air at 1100 °C.

Figure B.8: Fracture surface of the N610/Al_2O_3-$LaPO_4$ specimen with 10ply 0°/90° uni-tape lay-up subjected tension to failure in laboratory air at 1100 °C.

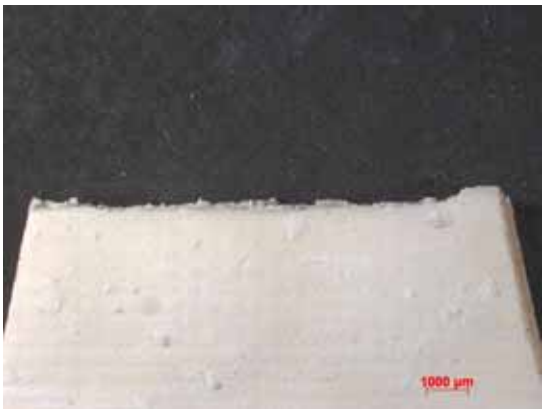

Figure B.9: Fracture surface of the N610/Al_2O_3-$LaPO_4$ specimen with 10ply 0°/90° uni-tape lay-up subjected tension to failure in laboratory air at 1100 °C.

Figure B.10: Fracture surface of the N610/Al_2O_3-$LaPO_4$ specimen with 10ply 0°/90° uni-tape lay-up subjected tension to failure in laboratory air at 1100 °C.

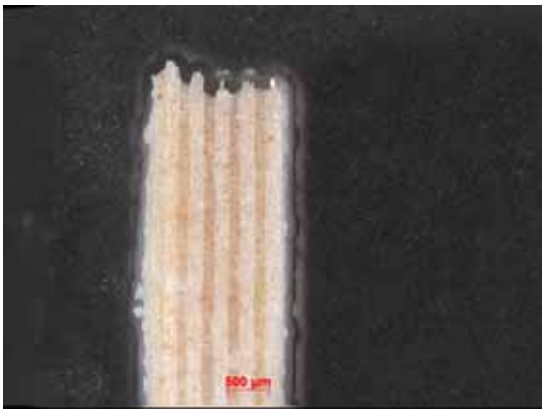

Figure B.11: Fracture surface of the N610/Al_2O_3-$LaPO_4$ specimen with 10ply 0°/90° uni-tape lay-up subjected tension to failure in laboratory air at 1100 °C.

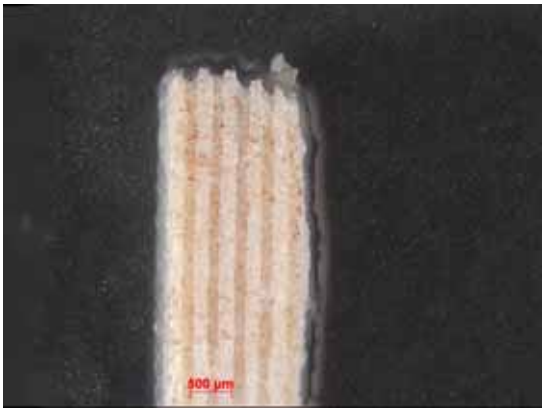

Figure B.12: Fracture surface of the N610/Al_2O_3-$LaPO_4$ specimen with 10ply 0°/90° uni-tape lay-up subjected tension to failure in laboratory air at 1100 °C.

Figure B.13: Fracture surface of the N610/Al_2O_3-$LaPO_4$ specimen with 10ply 0°/90° uni-tape lay-up subjected to creep test at 32 MPa in steam at 1100 °C (t_f = 3.45 h).

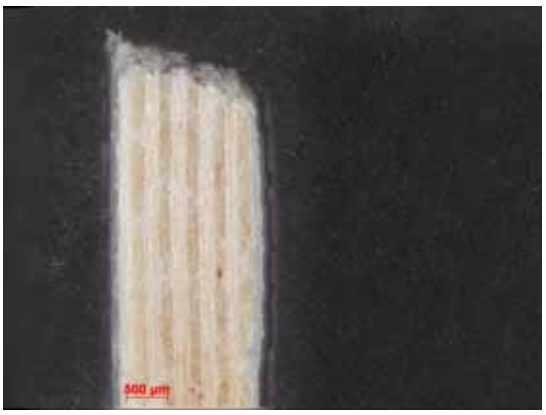

Figure B.14: Fracture surface of the N610/Al_2O_3-$LaPO_4$ specimen with 10ply 0°/90° uni-tape lay-up subjected to creep test at 32 MPa in steam at 1100 °C (t_f = 3.45 h).

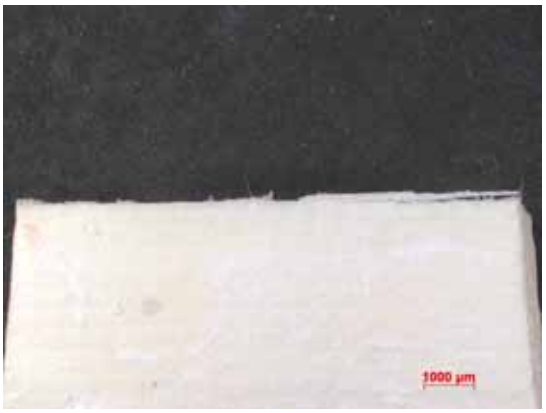

Figure B.15: Fracture surface of the N610/Al_2O_3-$LaPO_4$ specimen with 10ply 0°/90° uni-tape lay-up subjected to creep test at 32 MPa in steam at 1100 °C (t_f = 3.45 h).

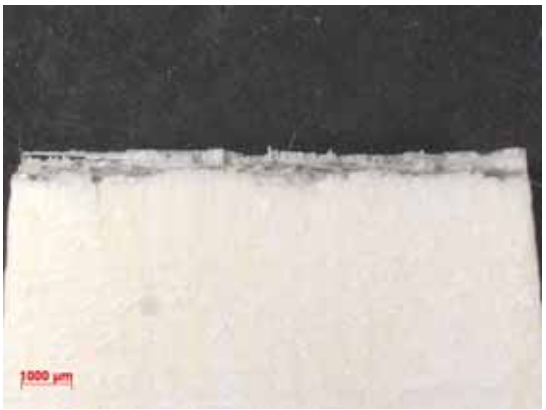

Figure B.16: Fracture surface of the N610/Al_2O_3-$LaPO_4$ specimen with 10ply 0°/90° uni-tape lay-up subjected to creep test at 32 MPa in steam at 1100 °C (t_f = 3.45 h).

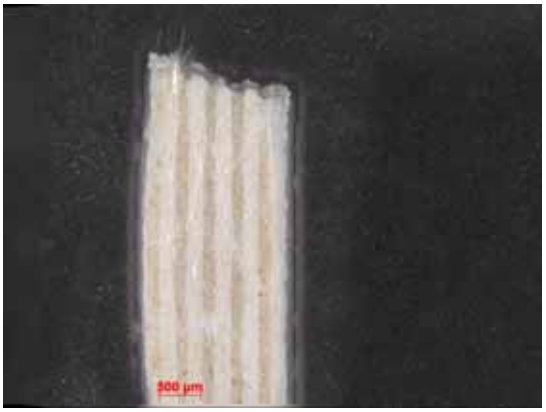

Figure B.17: Fracture surface of the N610/Al_2O_3-$LaPO_4$ specimen with 10ply 0°/90° uni-tape lay-up subjected to creep test at 32 MPa in steam at 1100 °C (t_f = 3.45 h).

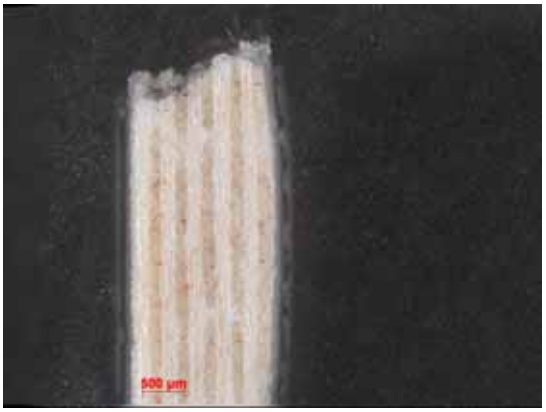

Figure B.18: Fracture surface of the N610/Al_2O_3-$LaPO_4$ specimen with 10ply 0°/90° uni-tape lay-up subjected to creep test at 32 MPa in steam at 1100 °C (t_f = 3.45 h).

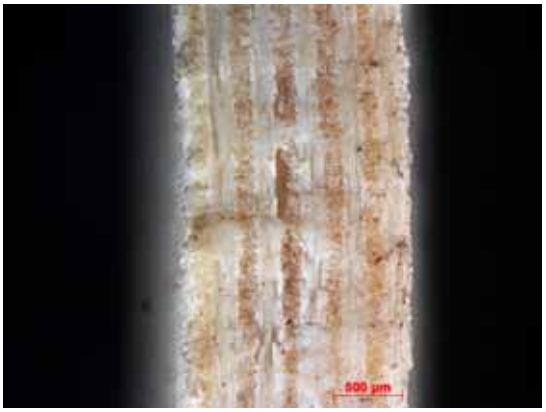

Figure B.19: Side view of the virgin N610/$LaPO_4$/Al_2O_3-$LaPO_4$ specimen with 10ply 0°/90° uni-tape lay-up.

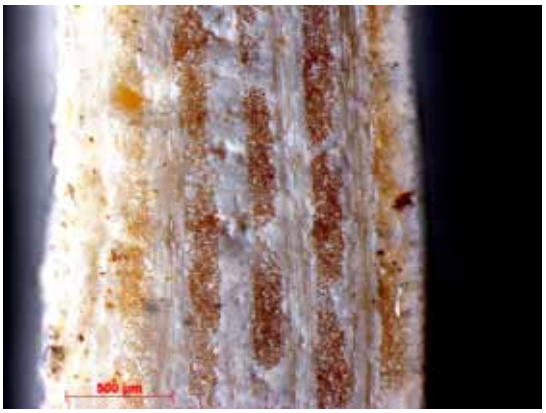

Figure B.20: Side view of the virgin N610/$LaPO_4$/Al_2O_3-$LaPO_4$ specimen with 10ply 0°/90° uni-tape lay-up.

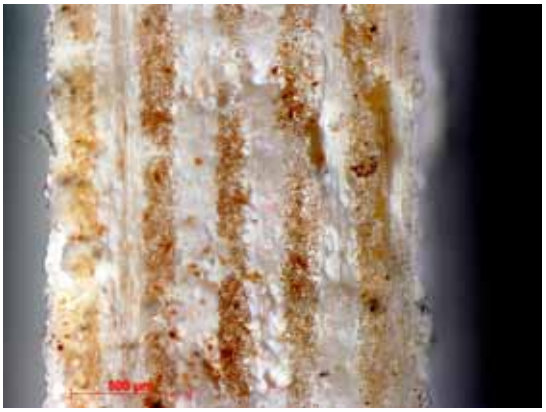

Figure B.21: Side view of the virgin N610/$LaPO_4$/Al_2O_3-$LaPO_4$ specimen with 10ply 0°/90° uni-tape lay-up.

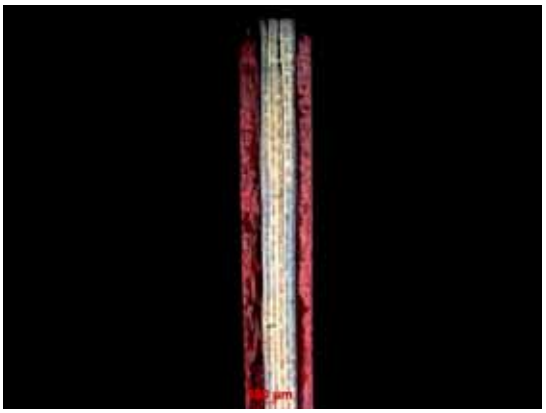

Figure B.22: Side view of the virgin N610/$LaPO_4$/Al_2O_3-$LaPO_4$ specimen with 10ply 0°/90° uni-tape lay-up.

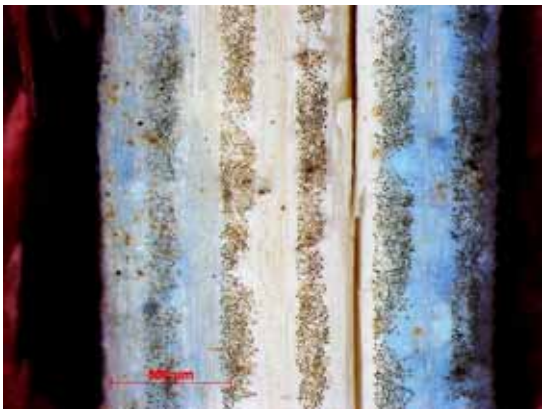

Figure B.23: Side view of the virgin N610/$LaPO_4$/Al_2O_3-$LaPO_4$ specimen with 10ply 0°/90° uni-tape lay-up.

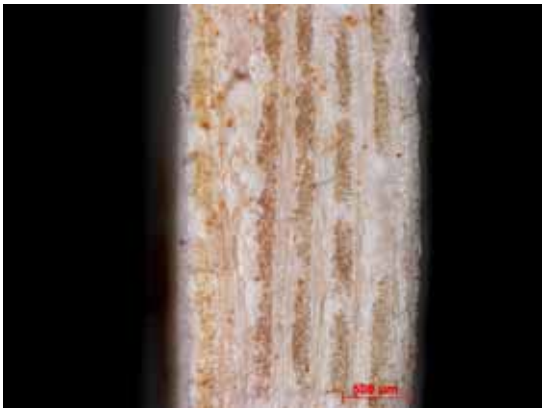

Figure B.24: Side view of the virgin N610/$LaPO_4$/Al_2O_3-$LaPO_4$ specimen with 10ply 0°/90° uni-tape lay-up.

Figure B.25: Fracture surface of the N610/$LaPO_4$/Al_2O_3-$LaPO_4$ specimen with 10ply 0°/90° uni-tape lay-up subjected tension to failure in laboratory air at 1100 °C.

Figure B.26: Fracture surface of the N610/$LaPO_4$/Al_2O_3-$LaPO_4$ specimen with 10ply 0°/90° uni-tape lay-up subjected tension to failure in laboratory air at 1100 °C.

Figure B.27: Fracture surface of the N610/$LaPO_4$/Al_2O_3-$LaPO_4$ specimen with 10ply 0°/90° uni-tape lay-up subjected tension to failure in laboratory air at 1100 °C.

Figure B.28: Fracture surface of the N610/$LaPO_4$/Al_2O_3-$LaPO_4$ specimen with 10ply 0°/90° uni-tape lay-up subjected tension to failure in laboratory air at 1100 °C.

Figure B.29: Fracture surface of the N610/$LaPO_4$/Al_2O_3-$LaPO_4$ specimen with 10ply 0°/90° uni-tape lay-up subjected tension to failure in laboratory air at 1100 °C.

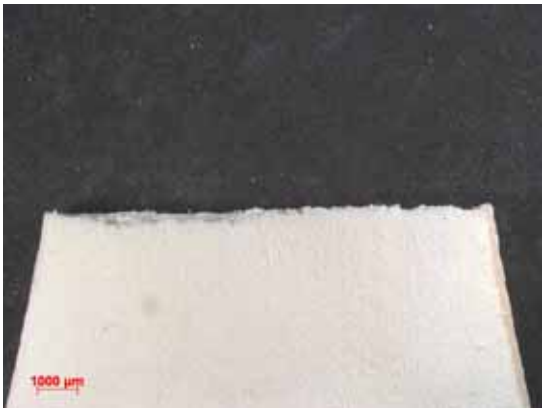

Figure B.30: Fracture surface of the N610/$LaPO_4$/Al_2O_3-$LaPO_4$ specimen with 10ply 0°/90° uni-tape lay-up subjected tension to failure in laboratory air at 1100 °C.

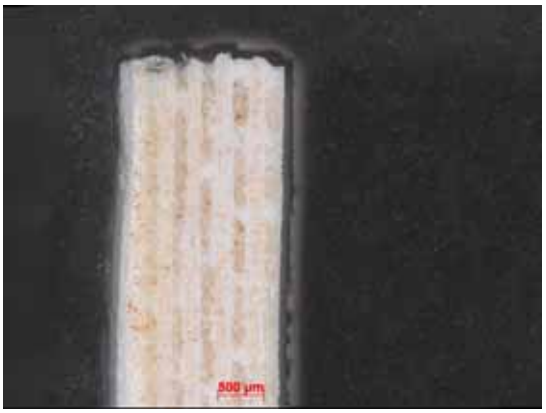

Figure B.31: Fracture surface of the N610/$LaPO_4$/Al_2O_3-$LaPO_4$ specimen with 10ply 0°/90° uni-tape lay-up subjected tension to failure in laboratory air at 1100 °C.

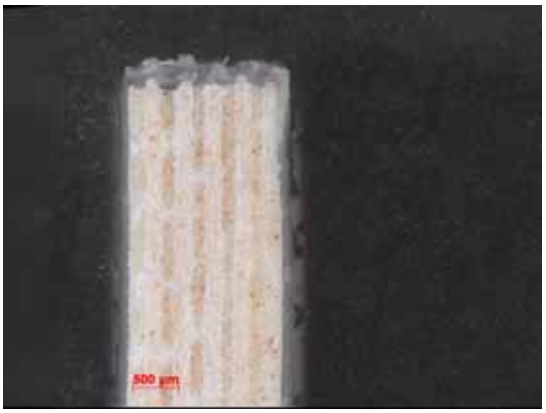

Figure B.32: Fracture surface of the N610/$LaPO_4$/Al_2O_3-$LaPO_4$ specimen with 10ply 0°/90° uni-tape lay-up subjected tension to failure in laboratory air at 1100 °C.

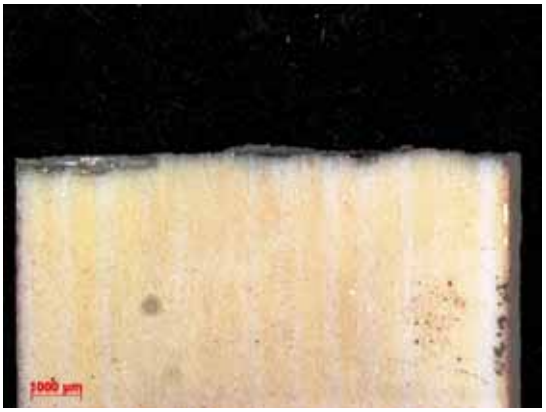

Figure B.33: Fracture surface of the N610/$LaPO_4$/Al_2O_3-$LaPO_4$ specimen with 10ply 0°/90° uni-tape lay-up subjected tension to failure in laboratory air at 1100 °C.

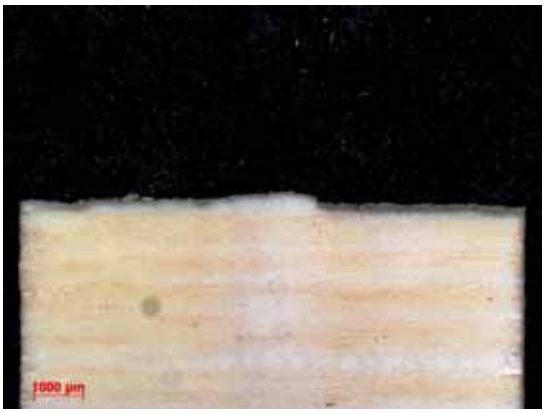

Figure B.34: Fracture surface of the N610/$LaPO_4$/Al_2O_3-$LaPO_4$ specimen with 10ply 0°/90° uni-tape lay-up subjected tension to failure in laboratory air at 1100 °C.

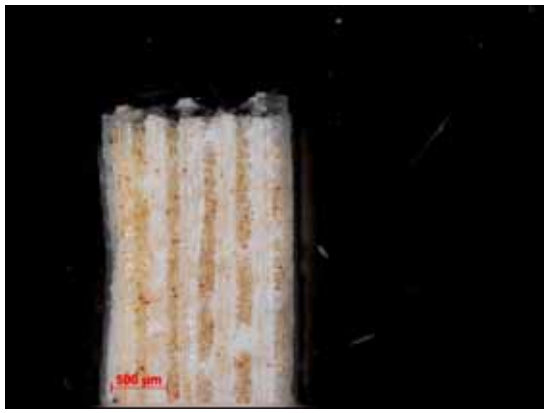

Figure B.35: Fracture surface of the N610/$LaPO_4$/Al_2O_3-$LaPO_4$ specimen with 10ply 0°/90° uni-tape lay-up subjected tension to failure in laboratory air at 1100 °C.

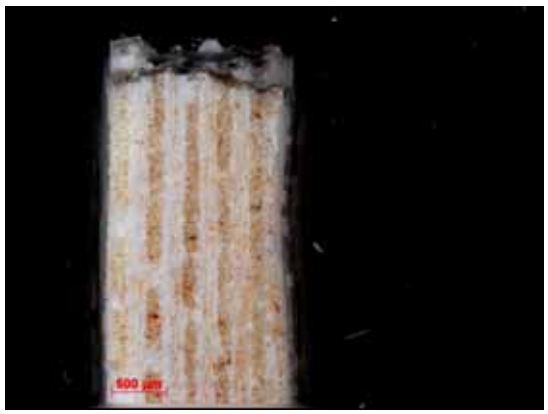

Figure B.36: Fracture surface of the N610/$LaPO_4$/Al_2O_3-$LaPO_4$ specimen with 10ply 0°/90° uni-tape lay-up subjected tension to failure in laboratory air at 1100 °C.

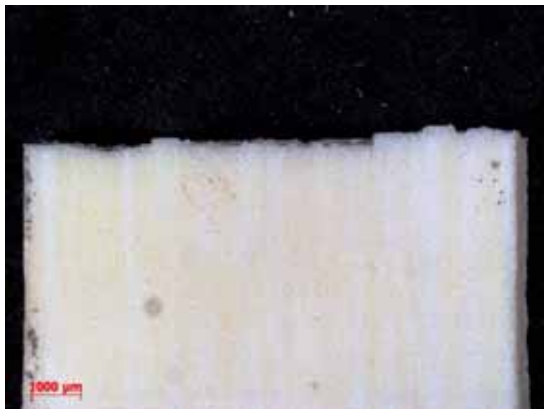

Figure B.37: Fracture surface of the N610/$LaPO_4$/Al_2O_3-$LaPO_4$ specimen with 10ply 0°/90° uni-tape lay-up subjected tension to failure in laboratory air at 1100 °C.

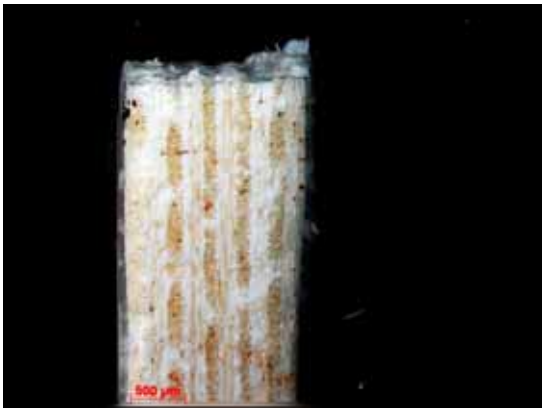

Figure B.38: Fracture surface of the N610/$LaPO_4$/Al_2O_3-$LaPO_4$ specimen with 10ply 0°/90° uni-tape lay-up subjected tension to failure in laboratory air at 1100 °C.

Figure B.39: Fracture surface of the N610/Al_2O_3-$LaPO_4$ specimen with 10ply 0°/90° uni-tape lay-up subjected to creep test at 25 MPa in steam at 1100 °C (t_f = 40.1 h).

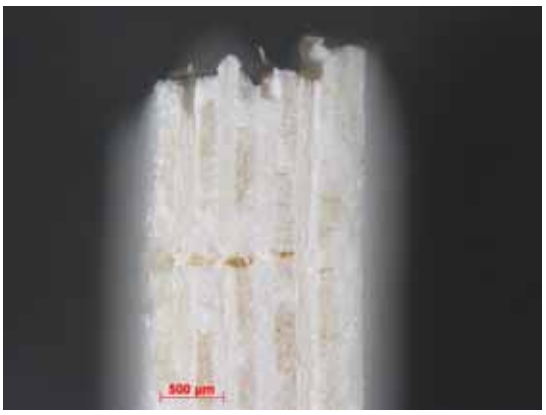

Figure B.40: Fracture surface of the N610/Al_2O_3-$LaPO_4$ specimen with 10ply 0°/90° uni-tape lay-up subjected to creep test at 25 MPa in steam at 1100 °C (t_f = 40.1 h).

Figure B.41: Fracture surface of the N610/Al_2O_3-$LaPO_4$ specimen with 10ply 0°/90° uni-tape lay-up subjected to creep test at 25 MPa in steam at 1100 °C (t_f = 40.1 h).

Figure B.42: Fracture surface of the N610/Al_2O_3-$LaPO_4$ specimen with 10ply 0°/90° uni-tape lay-up subjected to creep test at 25 MPa in steam at 1100 °C (t_f = 40.1 h).

Figure B.43: Fracture surface of the N610/Al_2O_3-$LaPO_4$ specimen with 10ply 0°/90° uni-tape lay-up subjected to creep test at 25 MPa in steam at 1100 °C (t_f = 40.1 h).

Figure B.44: Fracture surface of the N610/Al_2O_3-$LaPO_4$ specimen with 10ply 0°/90° uni-tape lay-up subjected to creep test at 25 MPa in steam at 1100 °C (t_f = 40.1 h).

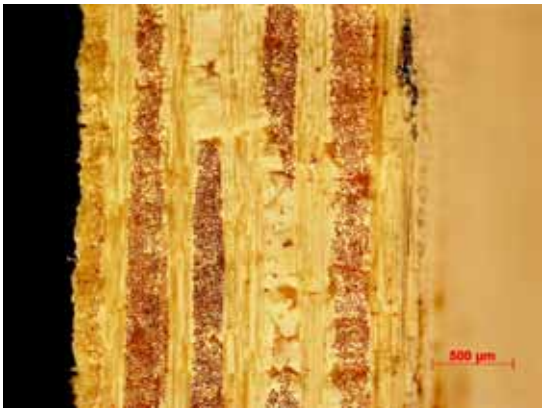

Figure B.45: Side view of the virgin N610/$LaPO_4$/Al_2O_3 specimen with 10ply 0°/90° uni-tape lay-up.

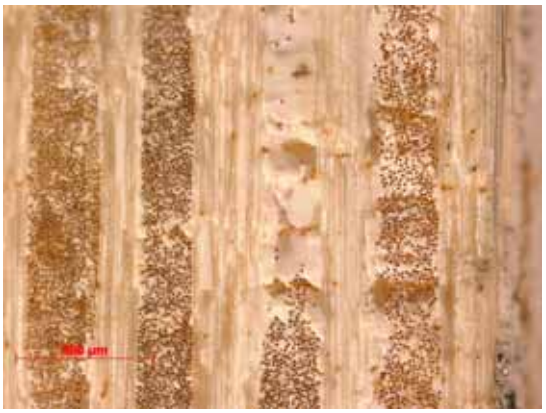

Figure B.46: Side view of the virgin N610/$LaPO_4$/Al_2O_3 specimen with 10ply 0°/90° uni-tape lay-up.

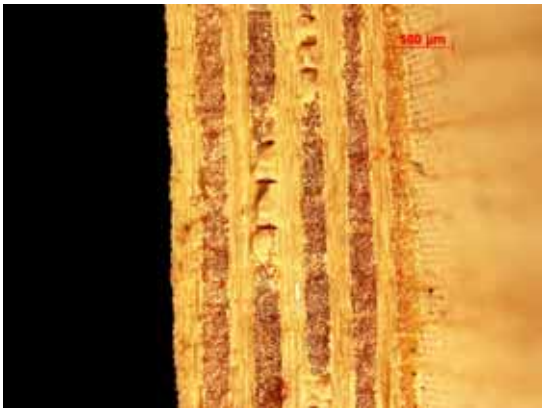

Figure B.47: Side view of the virgin N610/$LaPO_4$/Al_2O_3 specimen with 10ply 0°/90° uni-tape lay-up.

Figure B.48: Side view of the virgin N610/$LaPO_4$/Al_2O_3 specimen with 10ply 0°/90° uni-tape lay-up.

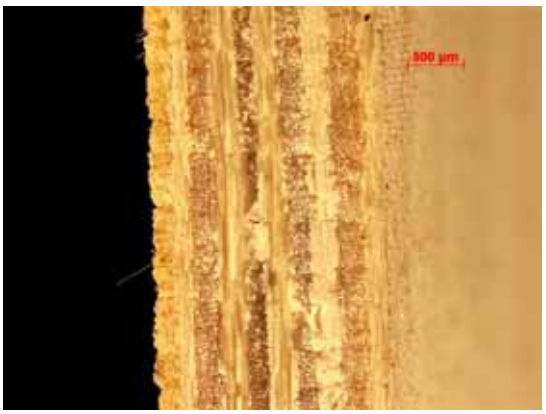

Figure B.49: Side view of the virgin N610/$LaPO_4$/Al_2O_3 specimen with 10ply 0°/90° uni-tape lay-up.

Figure B.50: Side view of the virgin N610/$LaPO_4$/Al_2O_3 specimen with 10ply 0°/90° uni-tape lay-up.

Figure B.51: Fracture surface of the N610/$LaPO_4$/Al_2O_3 specimen with 10ply 0°/90° uni-tape lay-up subjected tension to failure in laboratory air at 1100 °C.

Figure B.52: Fracture surface of the N610/$LaPO_4$/Al_2O_3 specimen with 10ply 0°/90° uni-tape lay-up subjected tension to failure in laboratory air at 1100 °C.

Figure B.53: Fracture surface of the N610/$LaPO_4$/Al_2O_3 specimen with 10ply 0°/90° uni-tape lay-up subjected tension to failure in laboratory air at 1100 °C.

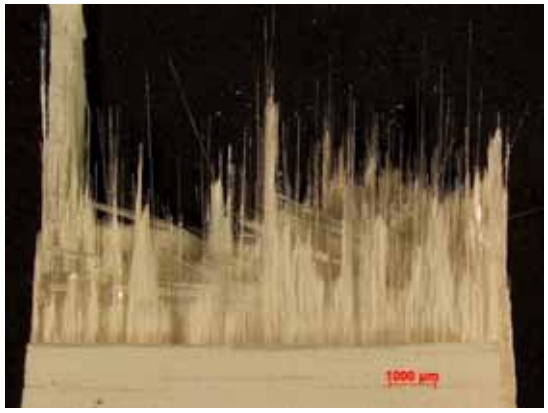

Figure B.54: Fracture surface of the N610/$LaPO_4$/Al_2O_3 specimen with 10ply 0°/90° uni-tape lay-up subjected tension to failure in laboratory air at 1100 °C.

Figure B.55: Fracture surface of the N610/$LaPO_4$/Al_2O_3 specimen with 10ply 0°/90° uni-tape lay-up subjected tension to failure in laboratory air at 1100 °C.

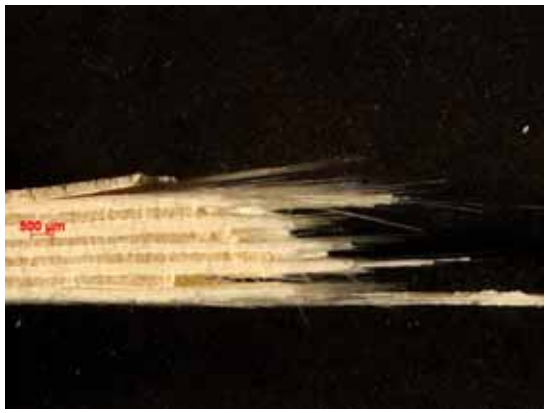

Figure B.56: Fracture surface of the N610/$LaPO_4$/Al_2O_3 specimen with 10ply 0°/90° uni-tape lay-up subjected tension to failure in laboratory air at 1100 °C.

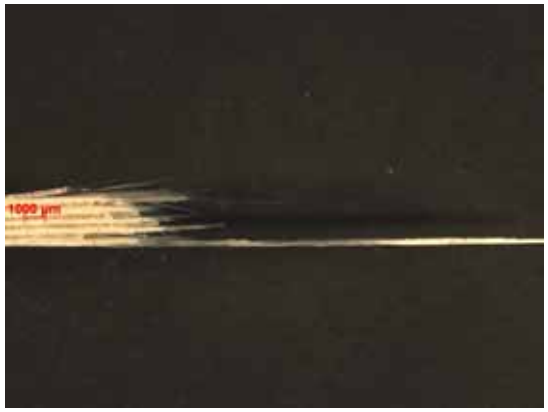

Figure B.57: Fracture surface of the N610/$LaPO_4$/Al_2O_3 specimen with 10ply 0°/90° uni-tape lay-up subjected tension to failure in laboratory air at 1100 °C.

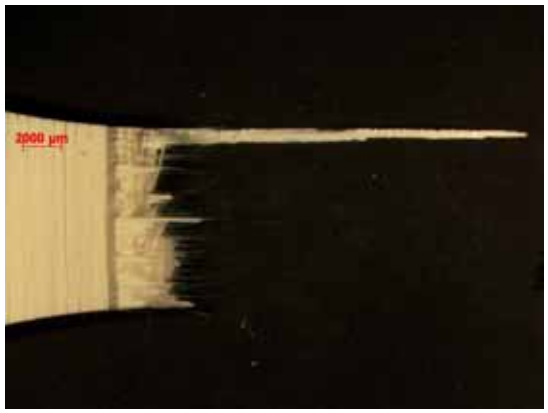

Figure B.58: Fracture surface of the N610/$LaPO_4$/Al_2O_3 specimen with 10ply 0°/90° uni-tape lay-up subjected tension to failure in laboratory air at 1100 °C.

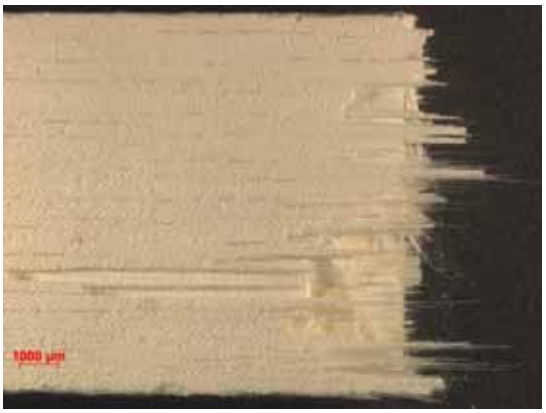

Figure B.59: Fracture surface of the N610/$LaPO_4$/Al_2O_3 specimen with 10ply 0°/90° uni-tape lay-up subjected to creep test at 85 MPa in air at 1100 °C (t_f = 16.2 h).

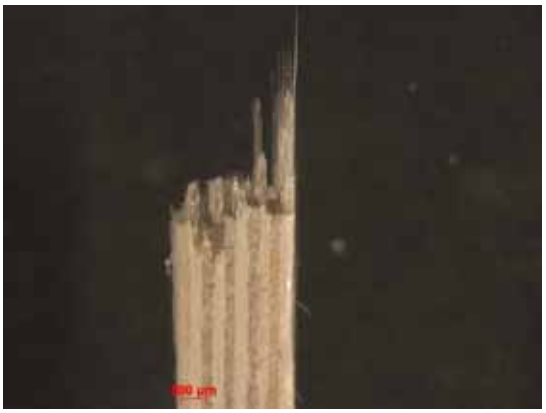

Figure B.60: Fracture surface of the N610/$LaPO_4$/Al_2O_3 specimen with 10ply 0°/90° uni-tape lay-up subjected to creep test at 85 MPa in air at 1100 °C (t_f = 16.2 h).

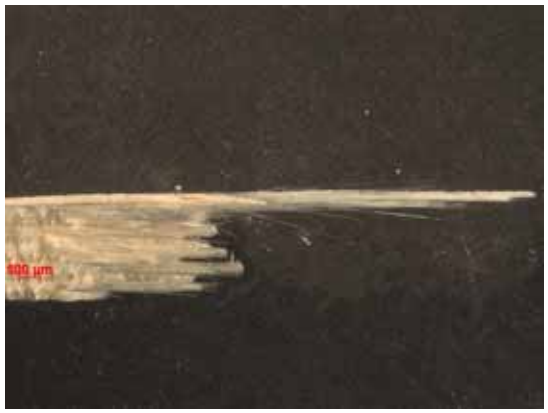

Figure B.61: Fracture surface of the N610/$LaPO_4$/Al_2O_3 specimen with 10ply 0°/90° uni-tape lay-up subjected to creep test at 85 MPa in air at 1100 °C (t_f = 16.2 h).

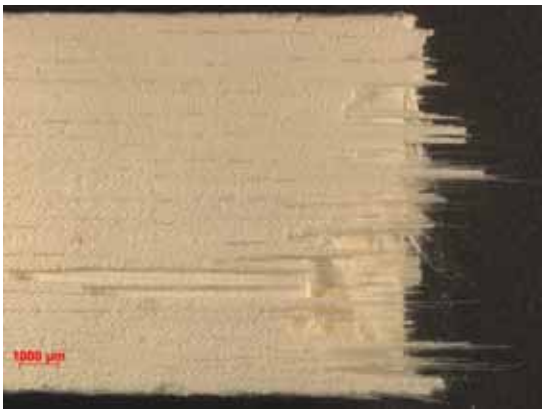

Figure B.62: Fracture surface of the N610/$LaPO_4$/Al_2O_3 specimen with 10ply 0°/90° uni-tape lay-up subjected to creep test at 85 MPa in air at 1100 °C (t_f = 16.2 h).

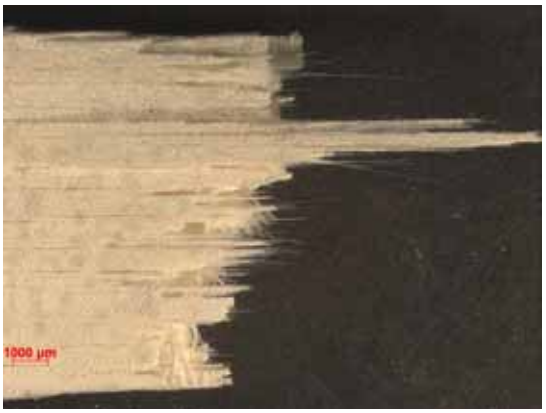

Figure B.63: Fracture surface of the N610/$LaPO_4$/Al_2O_3 specimen with 10ply 0°/90° uni-tape lay-up subjected to creep test at 85 MPa in air at 1100 °C (t_f = 16.2 h).

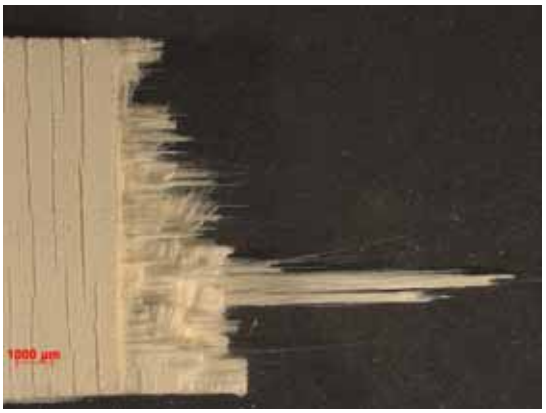

Figure B.64: Fracture surface of the N610/$LaPO_4$/Al_2O_3 specimen with 10ply 0°/90° uni-tape lay-up subjected to creep test at 85 MPa in air at 1100 °C (t_f = 16.2 h).

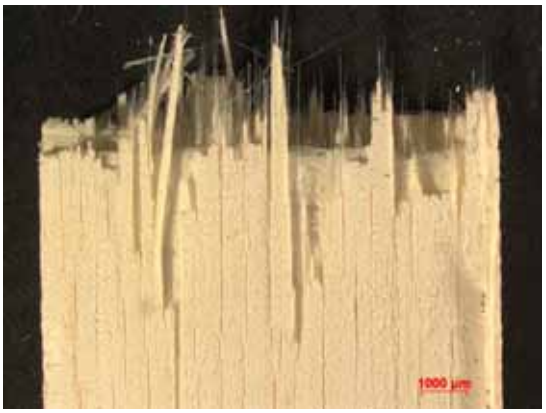

Figure B.65: Fracture surface of the N610/$LaPO_4$/Al_2O_3 specimen with 10ply 0°/90° uni-tape lay-up subjected to creep test at 85 MPa in steam at 1100 °C (t_f = 8.18 h).

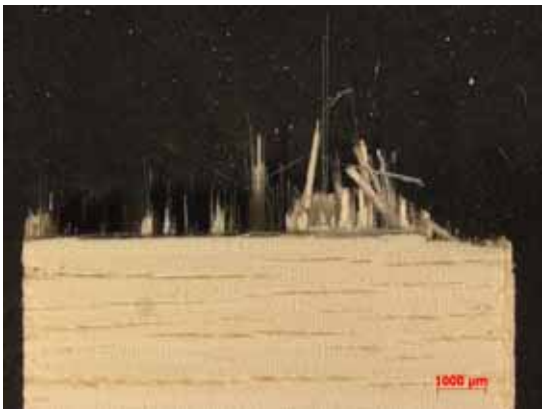

Figure B.66: Fracture surface of the N610/$LaPO_4$/Al_2O_3 specimen with 10ply 0°/90° uni-tape lay-up subjected to creep test at 85 MPa in steam at 1100 °C (t_f = 8.18 h).

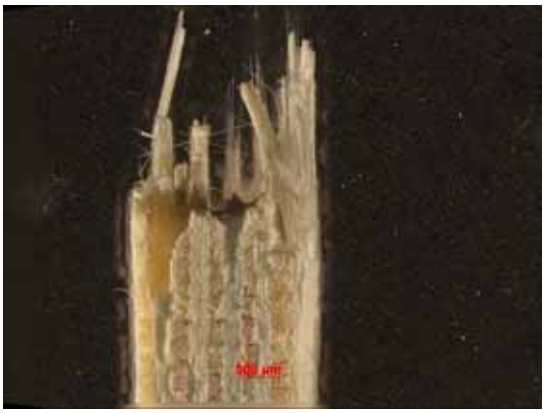

Figure B.67: Fracture surface of the N610/$LaPO_4$/Al_2O_3 specimen with 10ply 0°/90° uni-tape lay-up subjected to creep test at 85 MPa in steam at 1100 °C (t_f = 8.18 h).

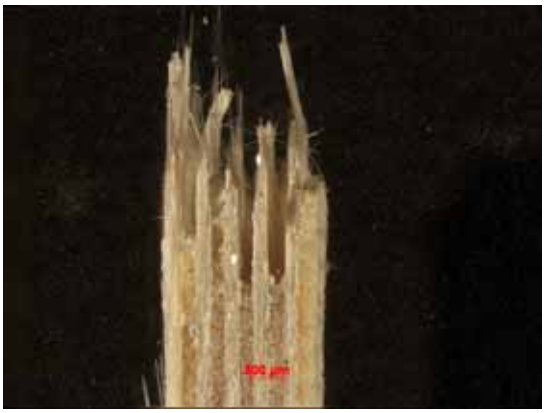

Figure B.68: Fracture surface of the N610/$LaPO_4$/Al_2O_3 specimen with 10ply 0°/90° uni-tape lay-up subjected to creep test at 85 MPa in steam at 1100 °C (t_f = 8.18 h).

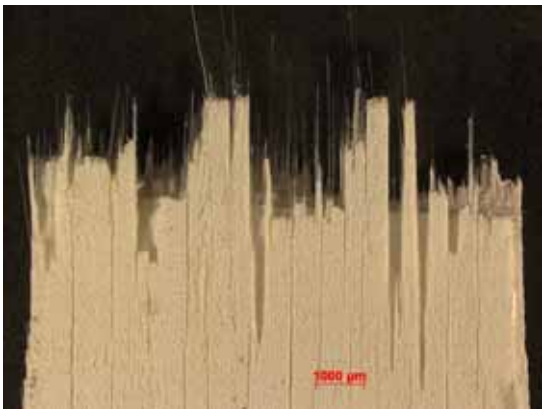

Figure B.69: Fracture surface of the N610/$LaPO_4$/Al_2O_3 specimen with 10ply 0°/90° uni-tape lay-up subjected to creep test at 85 MPa in steam at 1100 °C (t_f = 8.18 h).

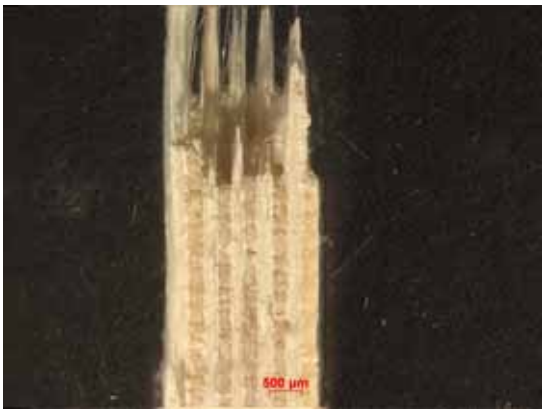

Figure B.70: Fracture surface of the N610/$LaPO_4$/Al_2O_3 specimen with 10ply 0°/90° uni-tape lay-up subjected to creep test at 85 MPa in steam at 1100 °C (t_f = 8.18 h).

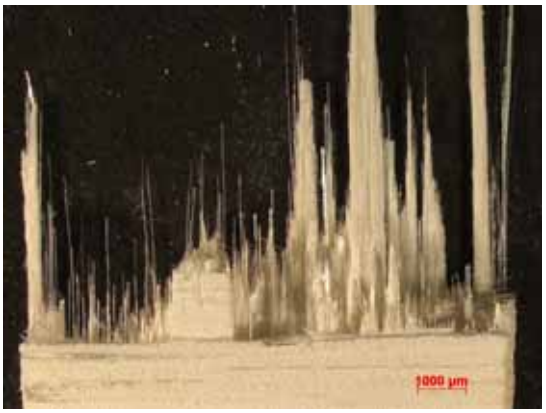

Figure B.71: Fracture surface of the N610/$LaPO_4$/Al_2O_3 specimen with 10ply 0°/90° uni-tape lay-up subjected to creep test at 110 MPa in steam at 1100 °C (t_f = 0.35 h).

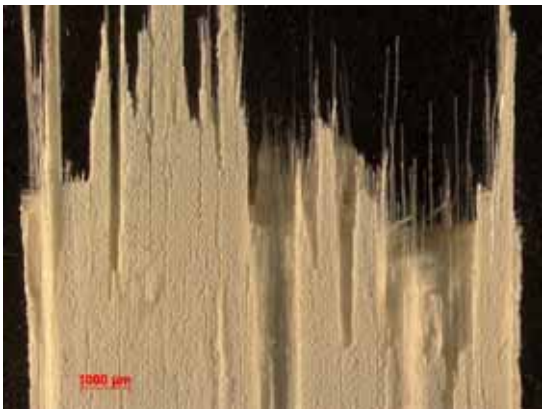

Figure B.72: Fracture surface of the N610/$LaPO_4$/Al_2O_3 specimen with 10ply 0°/90° uni-tape lay-up subjected to creep test at 110 MPa in steam at 1100 °C (t_f = 0.35 h).

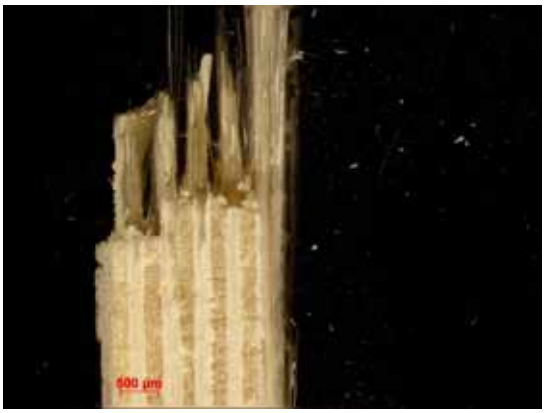

Figure B.73: Fracture surface of the N610/$LaPO_4$/Al_2O_3 specimen with 10ply 0°/90° uni-tape lay-up subjected to creep test at 110 MPa in steam at 1100 °C (t_f = 0.35 h).

Figure B.74: Fracture surface of the N610/$LaPO_4$/Al_2O_3 specimen with 10ply 0°/90° uni-tape lay-up subjected to creep test at 110 MPa in steam at 1100 °C (t_f = 0.35 h).

Figure B.75: Fracture surface of the N610/$LaPO_4$/Al_2O_3 specimen with 10ply 0°/90° uni-tape lay-up subjected to creep test at 110 MPa in steam at 1100 °C (t_f = 0.35 h).

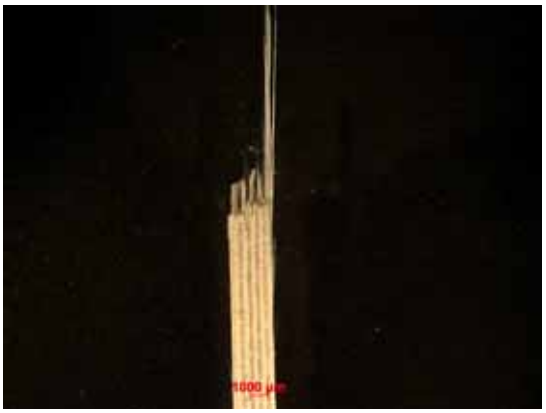

Figure B.76: Fracture surface of the N610/$LaPO_4$/Al_2O_3 specimen with 10ply 0°/90° uni-tape lay-up subjected to creep test at 110 MPa in steam at 1100 °C (t_f = 0.35 h).

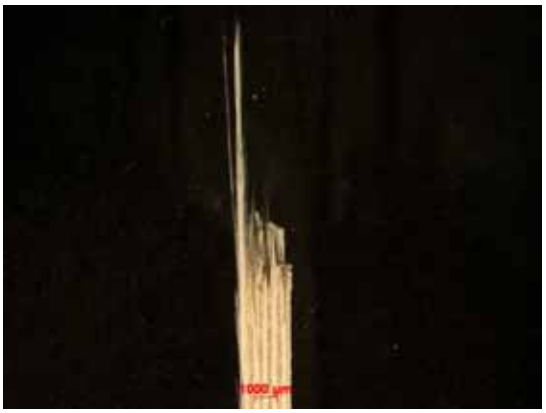

Figure B.77: Fracture surface of the N610/$LaPO_4$/Al_2O_3 specimen with 10ply 0°/90° uni-tape lay-up subjected to creep test at 110 MPa in steam at 1100 °C (t_f = 0.35 h).

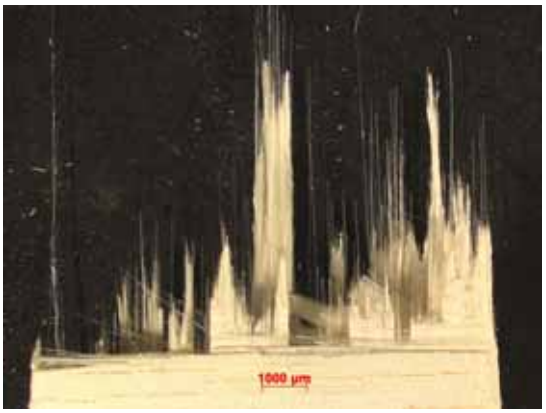

Figure B.78: Fracture surface of the N610/$LaPO_4$/Al_2O_3 specimen with 10ply 0°/90° uni-tape lay-up subjected to creep test at 110 MPa in steam at 1100 °C (t_f = 0.35 h).

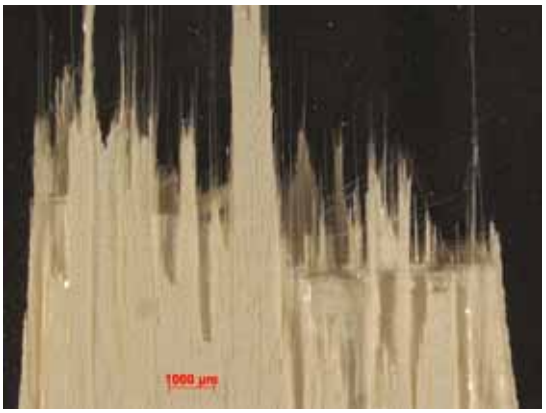

Figure B.79: Fracture surface of the N610/$LaPO_4$/Al_2O_3 specimen with 10ply 0°/90° uni-tape lay-up subjected to creep test at 110 MPa in steam at 1100 °C (t_f = 0.35 h).

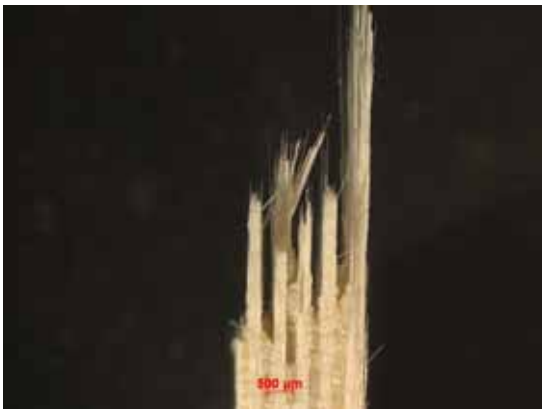

Figure B.80: Fracture surface of the N610/$LaPO_4$/Al_2O_3 specimen with 10ply 0°/90° uni-tape lay-up subjected to creep test at 110 MPa in steam at 1100 °C (t_f = 0.35 h).

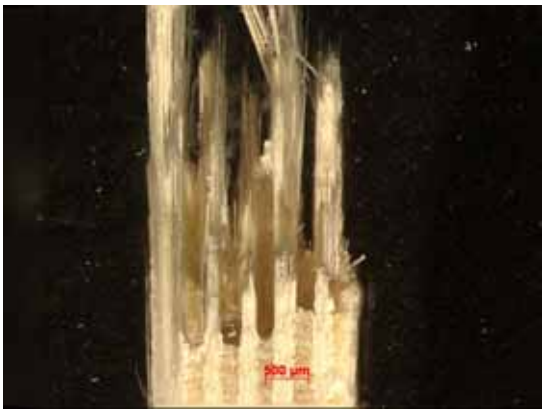

Figure B.81: Fracture surface of the N610/$LaPO_4$/Al_2O_3 specimen with 10ply 0°/90° uni-tape lay-up subjected to creep test at 110 MPa in steam at 1100 °C (t_f = 0.35 h).

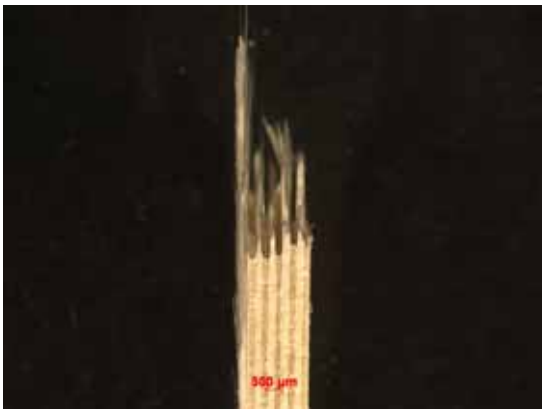

Figure B.82: Fracture surface of the N610/$LaPO_4$/Al_2O_3 specimen with 10ply 0°/90° uni-tape lay-up subjected to creep test at 110 MPa in steam at 1100 °C (t_f = 0.35 h).

Figure B.83: Fracture surface of the N610/$LaPO_4$/Al_2O_3 specimen with 10ply 0°/90° uni-tape lay-up subjected to creep test at 120 MPa in air at 1100 °C (t_f = 0.74 h).

Figure B.84: Fracture surface of the N610/$LaPO_4$/Al_2O_3 specimen with 10ply 0°/90° uni-tape lay-up subjected to creep test at 120 MPa in air at 1100 °C (t_f = 0.74 h).

Figure B.85: Fracture surface of the N610/$LaPO_4$/Al_2O_3 specimen with 10ply 0°/90° uni-tape lay-up subjected to creep test at 120 MPa in air at 1100 °C (t_f = 0.74 h).

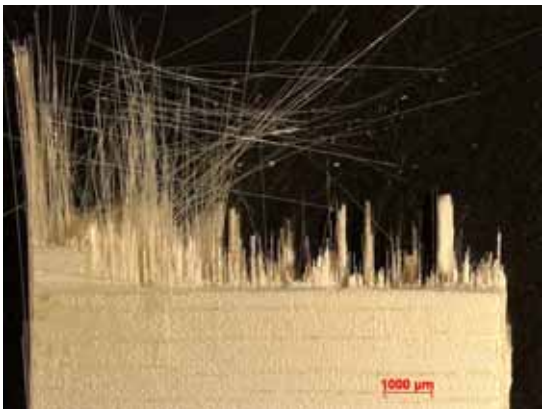

Figure B.86: Fracture surface of the N610/$LaPO_4$/Al_2O_3 specimen with 10ply 0°/90° uni-tape lay-up subjected to creep test at 120 MPa in air at 1100 °C (t_f = 0.74 h).

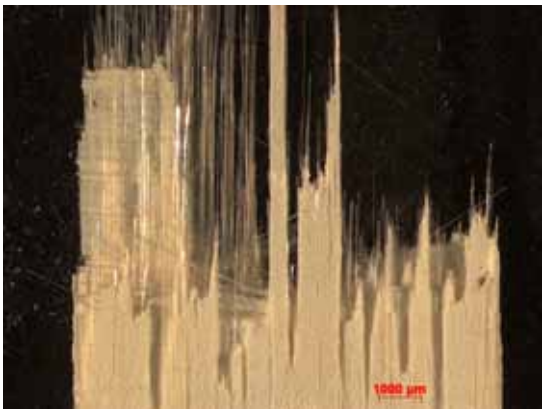

Figure B.87: Fracture surface of the N610/$LaPO_4$/Al_2O_3 specimen with 10ply 0°/90° uni-tape lay-up subjected to creep test at 120 MPa in air at 1100 °C (t_f = 0.74 h).

Figure B.88: Fracture surface of the N610/$LaPO_4$/Al_2O_3 specimen with 10ply 0°/90° uni-tape lay-up subjected to creep test at 120 MPa in air at 1100 °C (t_f = 0.74 h).

Figure B.89: Fracture surface of the N610/$LaPO_4$/Al_2O_3 specimen with 10ply 0°/90° uni-tape lay-up subjected to creep test at 120 MPa in air at 1100 °C (t_f = 0.74 h).

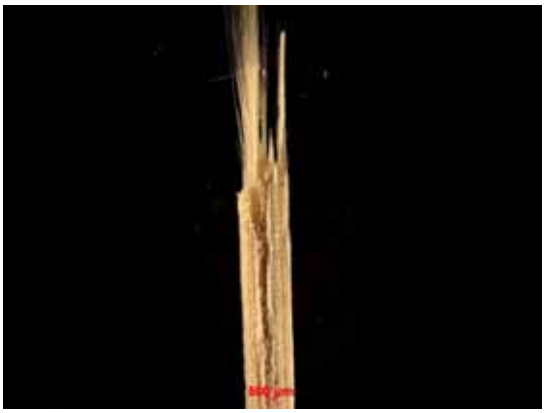

Figure B.90: Fracture surface of the N610/$LaPO_4$/Al_2O_3 specimen with 10ply 0°/90° uni-tape lay-up subjected to creep test at 120 MPa in air at 1100 °C (t_f = 0.74 h).

Figure B.91: Fracture surface of the N610/$LaPO_4$/Al_2O_3 specimen with 10ply 0°/90° uni-tape lay-up subjected to creep test at 120 MPa in steam at 1100 °C (t_f = 0.03 h).

Figure B.92: Fracture surface of the N610/$LaPO_4$/Al_2O_3 specimen with 10ply 0°/90° uni-tape lay-up subjected to creep test at 120 MPa in steam at 1100 °C (t_f = 0.03 h).

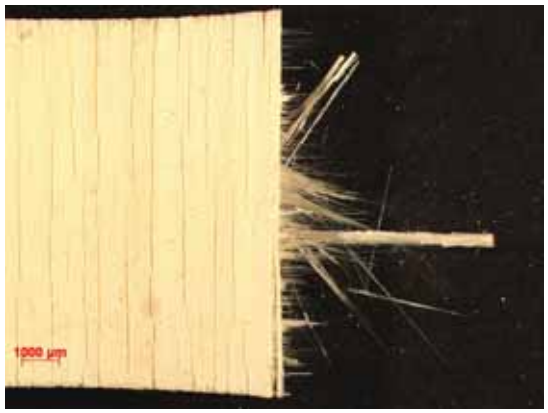

Figure B.93: Fracture surface of the N610/$LaPO_4$/Al_2O_3 specimen with 10ply 0°/90° uni-tape lay-up subjected to creep test at 120 MPa in steam at 1100 °C (t_f = 0.03 h).

Figure B.94: Fracture surface of the N610/$LaPO_4$/Al_2O_3 specimen with 10ply 0°/90° uni-tape lay-up subjected to creep test at 120 MPa in steam at 1100 °C (t_f = 0.03 h).

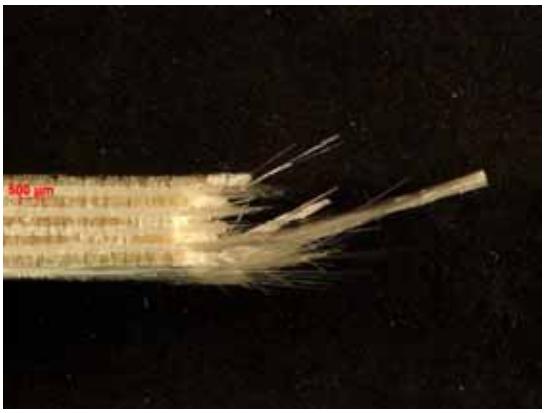

Figure B.95: Fracture surface of the N610/$LaPO_4$/Al_2O_3 specimen with 10ply 0°/90° uni-tape lay-up subjected to creep test at 120 MPa in steam at 1100 °C (t_f = 0.03 h).

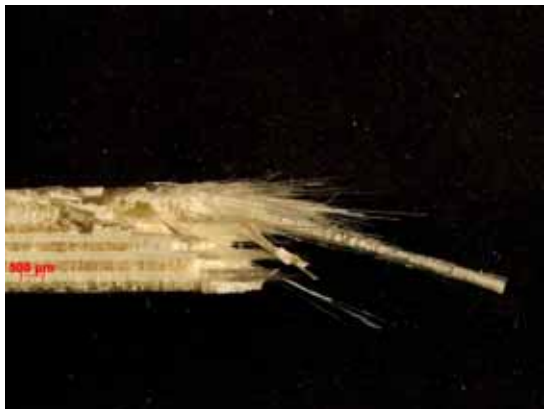

Figure B.96: Fracture surface of the N610/$LaPO_4$/Al_2O_3 specimen with 10ply 0°/90° uni-tape lay-up subjected to creep test at 120 MPa in steam at 1100 °C (t_f = 0.03 h).

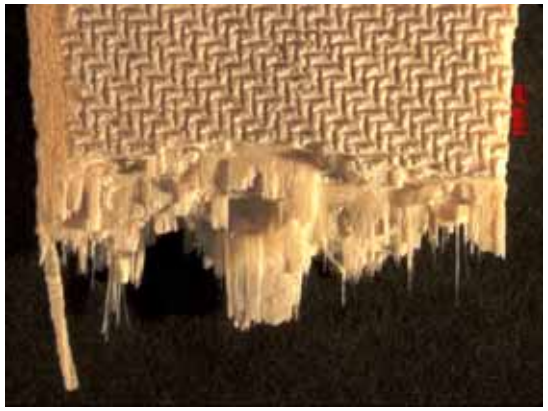

Figure B.97: Fracture surface of the N610/$LaPO_4$/Al_2O_3 specimen with 8ply HSW subjected tension to failure in laboratory air at 1100 °C.

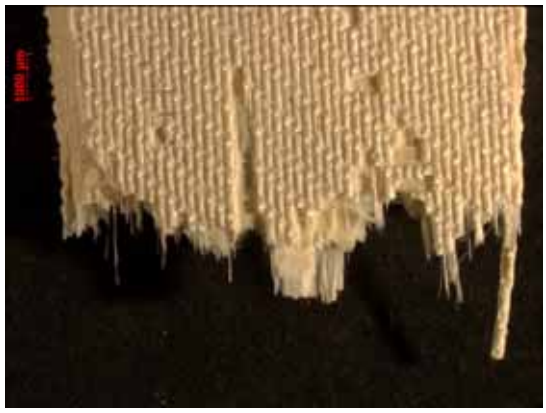

Figure B.98: Fracture surface of the N610/$LaPO_4$/Al_2O_3 specimen with 8ply HSW subjected tension to failure in laboratory air at 1100 °C.

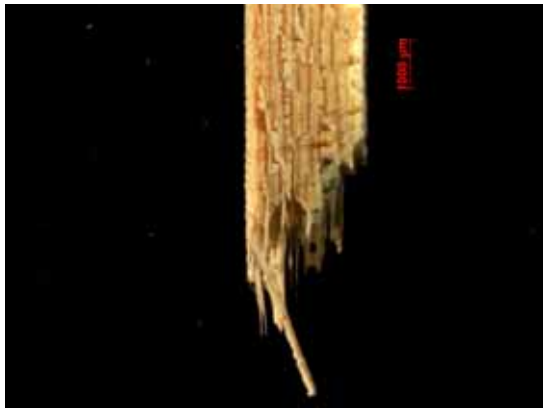

Figure B.99: Fracture surface of the N610/$LaPO_4$/Al_2O_3 specimen with 8ply HSW subjected tension to failure in laboratory air at 1100 °C.

Figure B.100: Fracture surface of the N610/$LaPO_4$/Al_2O_3 specimen with 8ply HSW subjected tension to failure in laboratory air at 1100 °C.

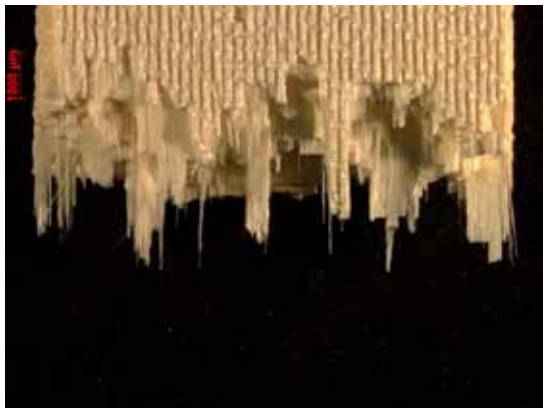

Figure B.101: Fracture surface of the N610/$LaPO_4$/Al_2O_3 specimen with 8ply HSW subjected tension to failure in laboratory air at 1100 °C.

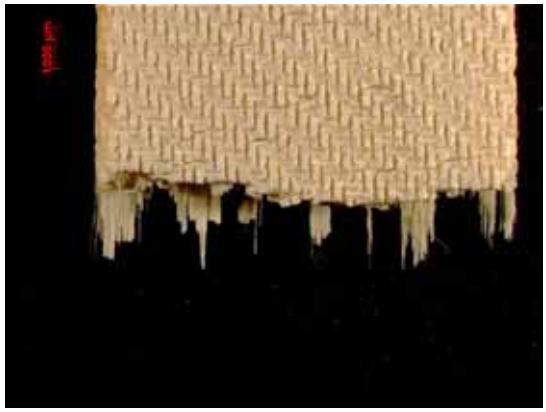

Figure B.102: Fracture surface of the N610/$LaPO_4$/Al_2O_3 specimen with 8ply HSW subjected tension to failure in laboratory air at 1100 °C.

Figure B.103: Fracture surface of the N610/$LaPO_4$/Al_2O_3 specimen with 8ply HSW subjected tension to failure in laboratory air at 1100 °C.

Figure B.104: Fracture surface of the N610/$LaPO_4$/Al_2O_3 specimen with 8ply HSW subjected tension to failure in laboratory air at 1100 °C.

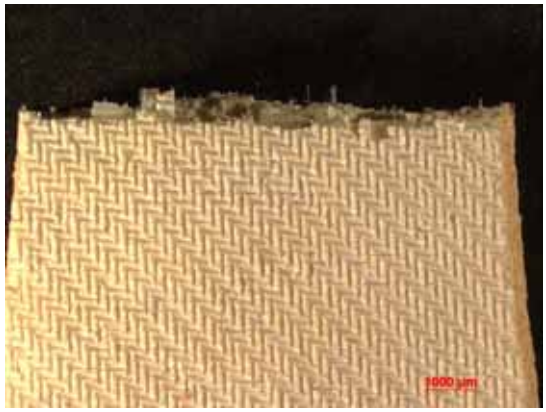

Figure B.105: Fracture surface of the N610/$LaPO_4$/Al_2O_3 specimen with 8ply HSW subjected tension to failure in laboratory air at 1100 °C.

Figure B.106: Fracture surface of the N610/$LaPO_4$/Al_2O_3 specimen with 8ply HSW subjected tension to failure in laboratory air at 1100 °C.

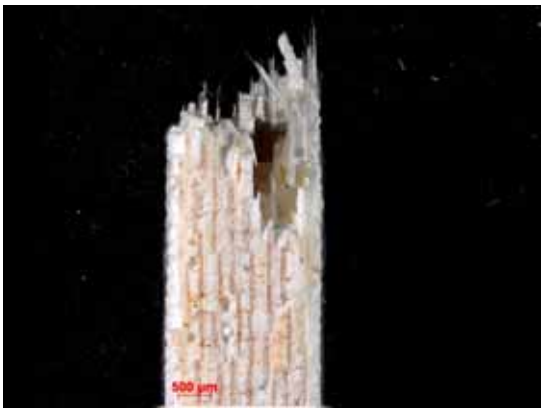

Figure B.107: Fracture surface of the N610/$LaPO_4$/Al_2O_3 specimen with 8ply HSW subjected tension to failure in laboratory air at 1100 °C.

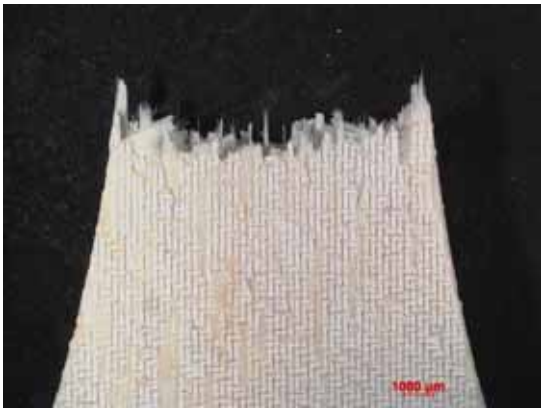

Figure B.108: Fracture surface of the N610/$LaPO_4$/Al_2O_3 specimen with 8ply HSW subjected tension to failure in laboratory air at 1100 °C.

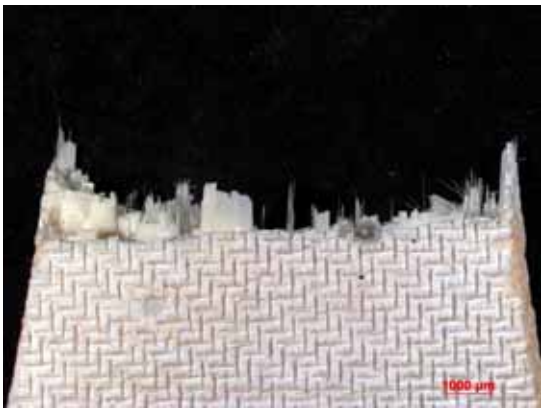

Figure B.109: Fracture surface of the N610/$LaPO_4$/Al_2O_3 specimen with 8ply HSW subjected tension to failure in laboratory air at 1100 °C.

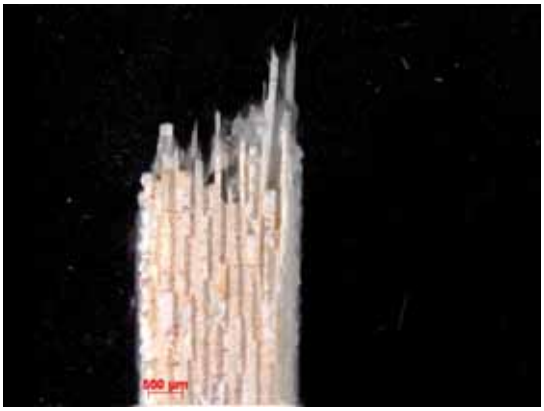

Figure B.110: Fracture surface of the N610/$LaPO_4$/Al_2O_3 specimen with 8ply HSW subjected tension to failure in laboratory air at 1100 °C.

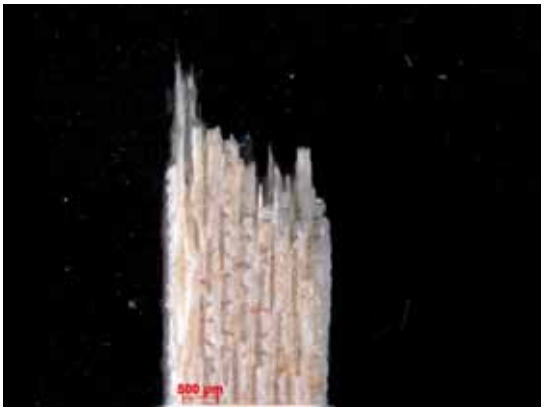

Figure B.111: Fracture surface of the N610/$LaPO_4$/Al_2O_3 specimen with 8ply HSW subjected tension to failure in laboratory air at 1100 °C.

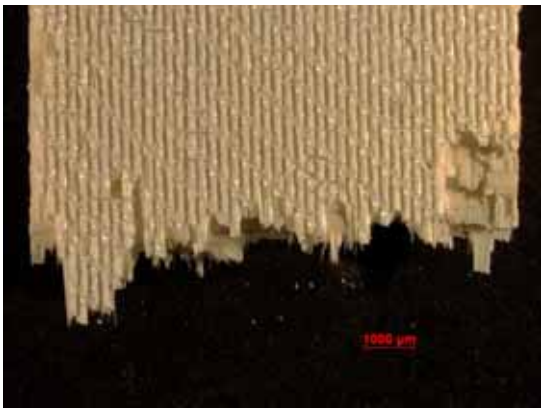

Figure B.112: Fracture surface of the N610/$LaPO_4$/Al_2O_3 specimen with 8ply HSW subjected subjected to creep test at 32 MPa in air at 1100 °C ($t_f > 100$ h).

Figure B.113: Fracture surface of the N610/$LaPO_4$/Al_2O_3 specimen with 8ply HSW subjected subjected to creep test at 32 MPa in air at 1100 °C ($t_f > 100$ h).

Figure B.114: Fracture surface of the N610/$LaPO_4$/Al_2O_3 specimen with 8ply HSW subjected subjected to creep test at 32 MPa in air at 1100 °C ($t_f > 100$ h).

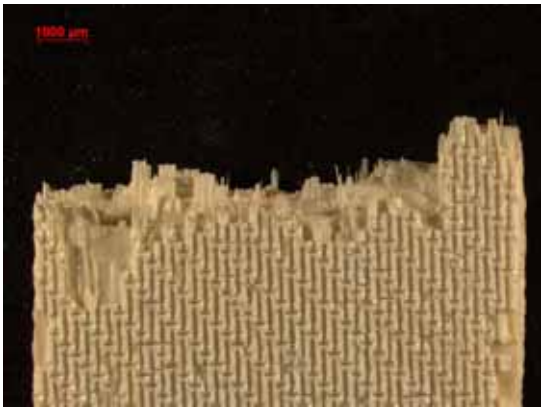

Figure B.115: Fracture surface of the N610/$LaPO_4$/Al_2O_3 specimen with 8ply HSW subjected subjected to creep test at 32 MPa in air at 1100 °C ($t_f > 100$ h).

Figure B.116: Fracture surface of the N610/$LaPO_4$/Al_2O_3 specimen with 8ply HSW subjected subjected to creep test at 32 MPa in air at 1100 °C ($t_f > 100$ h).

Figure B.117: Fracture surface of the N610/$LaPO_4$/Al_2O_3 specimen with 8ply HSW subjected subjected to creep test at 32 MPa in air at 1100 °C ($t_f > 100$ h).

Figure B.118: Fracture surface of the N610/$LaPO_4$/Al_2O_3 specimen with 8ply HSW subjected subjected to creep test at 32 MPa in steam at 1100 °C ($t_f = 51.9$ h).

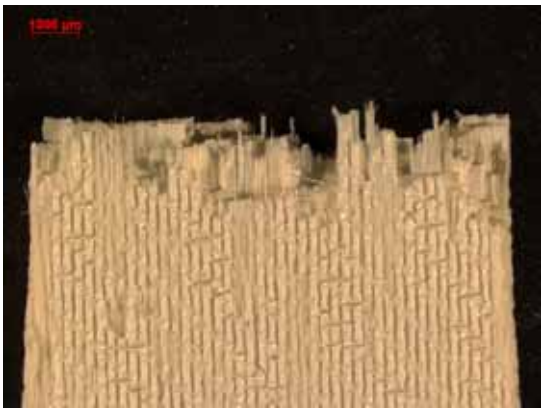

Figure B.119: Fracture surface of the N610/$LaPO_4$/Al_2O_3 specimen with 8ply HSW subjected subjected to creep test at 32 MPa in steam at 1100 °C (t_f = 51.9 h).

Figure B.120: Fracture surface of the N610/$LaPO_4$/Al_2O_3 specimen with 8ply HSW subjected subjected to creep test at 32 MPa in steam at 1100 °C (t_f = 51.9 h).

Figure B.121: Fracture surface of the N610/$LaPO_4$/Al_2O_3 specimen with 8ply HSW subjected subjected to creep test at 32 MPa in steam at 1100 °C (t_f = 51.9 h).

Figure B.122: Fracture surface of the N610/$LaPO_4$/Al_2O_3 specimen with 8ply HSW subjected subjected to creep test at 32 MPa in steam at 1100 °C (t_f = 51.9 h).

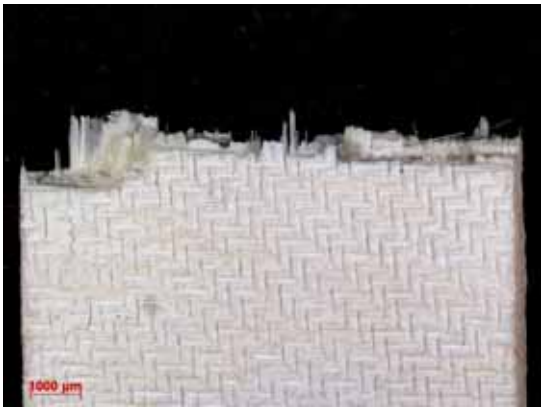

Figure B.123: Fracture surface of the N610/$LaPO_4$/Al_2O_3 specimen with 8ply HSW subjected subjected to creep test at 64 MPa in air at 1100 °C (t_f > 100 h).

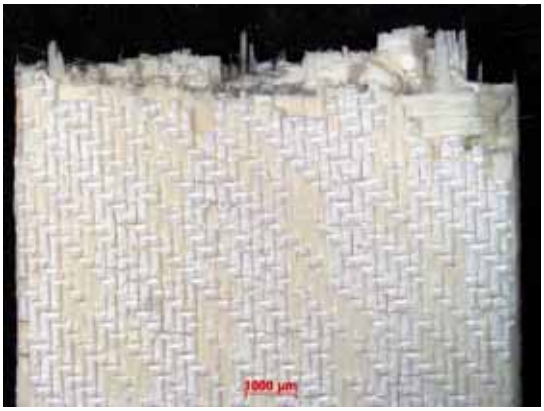

Figure B.124: Fracture surface of the N610/$LaPO_4$/Al_2O_3 specimen with 8ply HSW subjected subjected to creep test at 64 MPa in air at 1100 °C (t_f > 100 h).

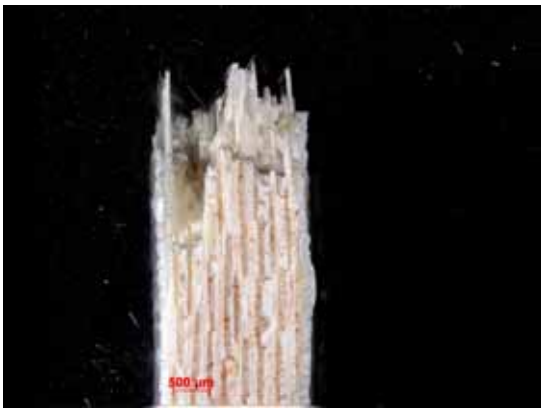

Figure B.125: Fracture surface of the N610/$LaPO_4$/Al_2O_3 specimen with 8ply HSW subjected subjected to creep test at 64 MPa in air at 1100 °C ($t_f > 100$ h).

Figure B.126: Fracture surface of the N610/$LaPO_4$/Al_2O_3 specimen with 8ply HSW subjected subjected to creep test at 64 MPa in air at 1100 °C ($t_f > 100$ h).

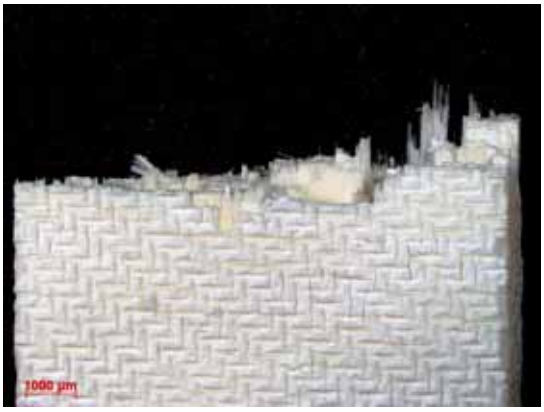

Figure B.127: Fracture surface of the N610/$LaPO_4$/Al_2O_3 specimen with 8ply HSW subjected subjected to creep test at 64 MPa in air at 1100 °C ($t_f > 100$ h).

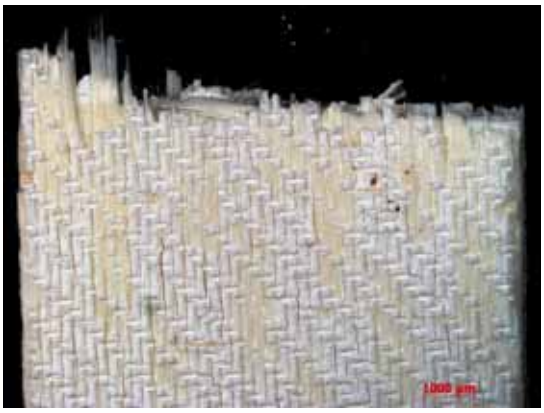

Figure B.128: Fracture surface of the N610/$LaPO_4$/Al_2O_3 specimen with 8ply HSW subjected subjected to creep test at 64 MPa in air at 1100 °C ($t_f > 100$ h).

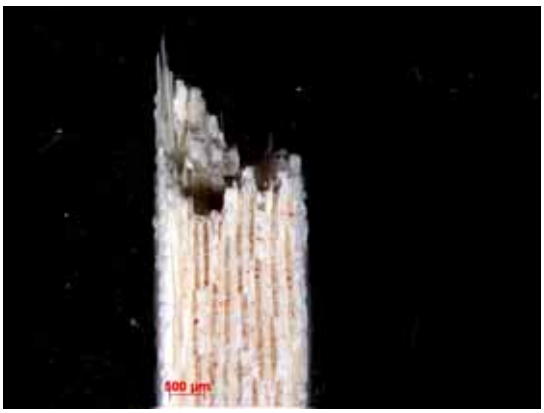

Figure B.129: Fracture surface of the N610/$LaPO_4$/Al_2O_3 specimen with 8ply HSW subjected subjected to creep test at 64 MPa in air at 1100 °C ($t_f > 100$ h).

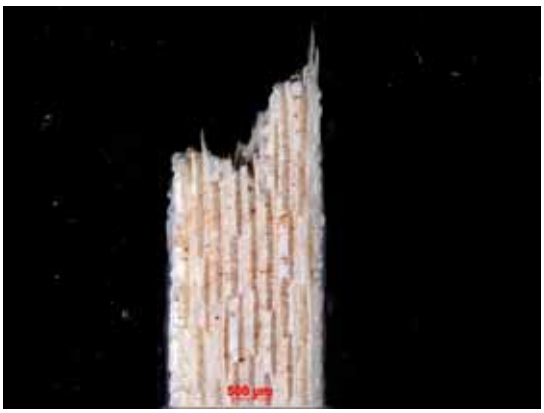

Figure B.130: Fracture surface of the N610/$LaPO_4$/Al_2O_3 specimen with 8ply HSW subjected subjected to creep test at 64 MPa in air at 1100 °C ($t_f > 100$ h).

Figure B.131: Fracture surface of the N610/$LaPO_4$/Al_2O_3 specimen with 8ply HSW subjected subjected to creep test at 48 MPa in steam at 1100 °C (t_f = 7.58 h).

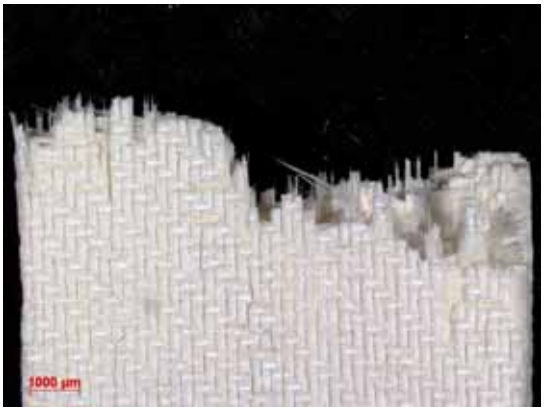

Figure B.132: Fracture surface of the N610/$LaPO_4$/Al_2O_3 specimen with 8ply HSW subjected subjected to creep test at 48 MPa in steam at 1100 °C (t_f = 7.58 h).

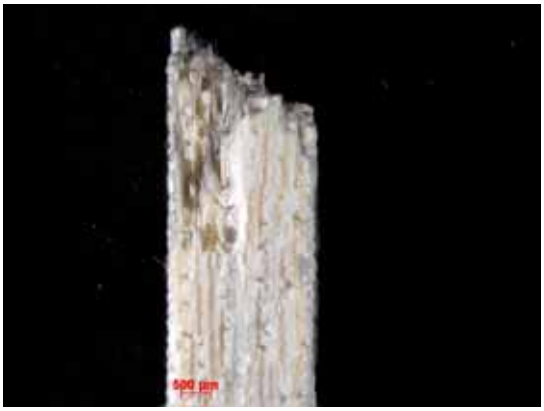

Figure B.133: Fracture surface of the N610/$LaPO_4$/Al_2O_3 specimen with 8ply HSW subjected subjected to creep test at 48 MPa in steam at 1100 °C (t_f = 7.58 h).

Figure B.134: Fracture surface of the N610/$LaPO_4$/Al_2O_3 specimen with 8ply HSW subjected subjected to creep test at 48 MPa in steam at 1100 °C (t_f = 7.58 h).

Figure B.135: Fracture surface of the N610/$LaPO_4$/Al_2O_3 specimen with 8ply HSW subjected subjected to creep test at 48 MPa in steam at 1100 °C (t_f = 7.58 h).

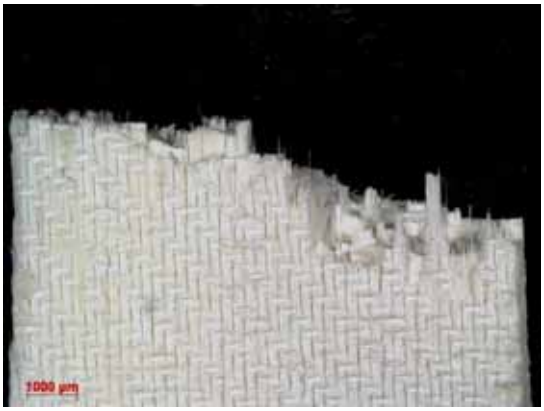

Figure B.136: Fracture surface of the N610/$LaPO_4$/Al_2O_3 specimen with 8ply HSW subjected subjected to creep test at 48 MPa in steam at 1100 °C (t_f = 7.58 h).

Figure B.137: Fracture surface of the N610/$LaPO_4$/Al_2O_3 specimen with 8ply HSW subjected subjected to creep test at 48 MPa in steam at 1100 °C (t_f = 7.58 h).

Figure B.138: Fracture surface of the N610/$LaPO_4$/Al_2O_3 specimen with 8ply HSW subjected subjected to creep test at 48 MPa in steam at 1100 °C (t_f = 7.58 h).

Figure B.139: Fracture surface of the N610/$LaPO_4$/Al_2O_3 specimen with 8ply HSW subjected subjected to creep test at 64 MPa in steam at 1100 °C (t_f = 2.38 h).

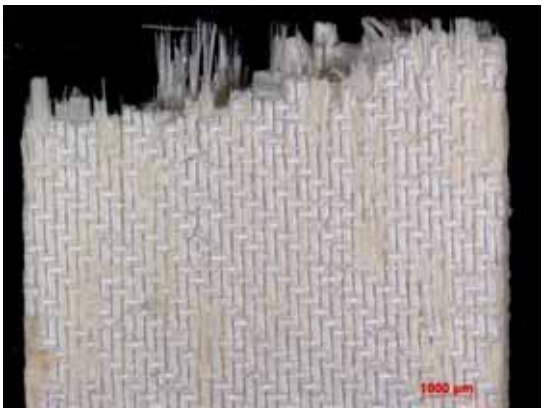

Figure B.140: Fracture surface of the N610/$LaPO_4$/Al_2O_3 specimen with 8ply HSW subjected subjected to creep test at 64 MPa in steam at 1100 °C (t_f = 2.38 h).

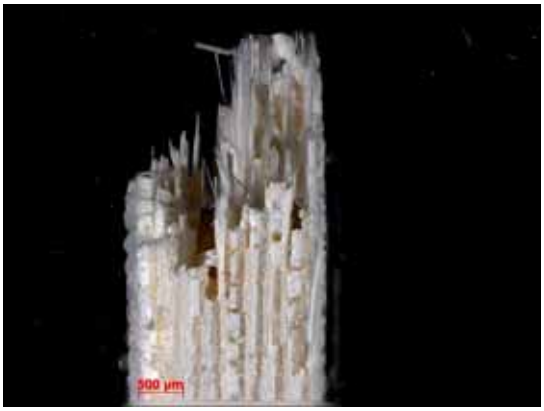

Figure B.141: Fracture surface of the N610/$LaPO_4$/Al_2O_3 specimen with 8ply HSW subjected subjected to creep test at 64 MPa in steam at 1100 °C (t_f = 2.38 h).

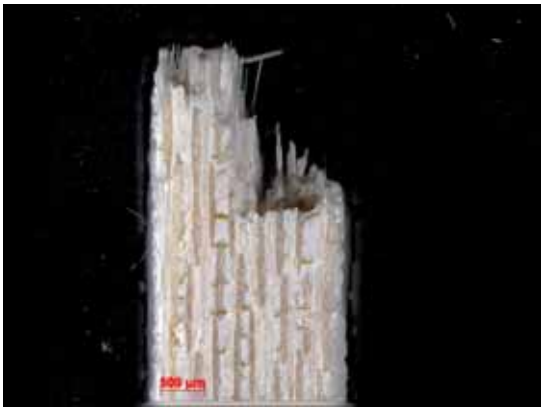

Figure B.142: Fracture surface of the N610/$LaPO_4$/Al_2O_3 specimen with 8ply HSW subjected subjected to creep test at 64 MPa in steam at 1100 °C (t_f = 2.38 h).

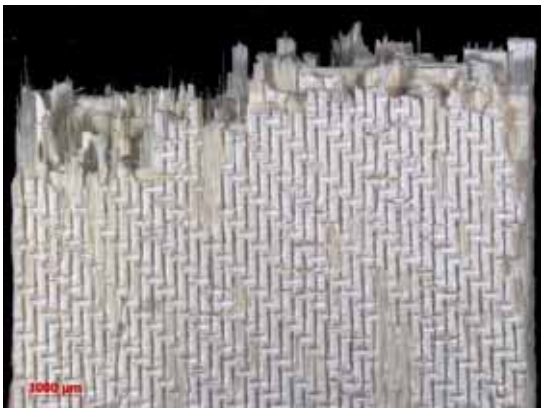

Figure B.143: Fracture surface of the N610/$LaPO_4$/Al_2O_3 specimen with 8ply HSW subjected subjected to creep test at 64 MPa in steam at 1100 °C (t_f = 2.38 h).

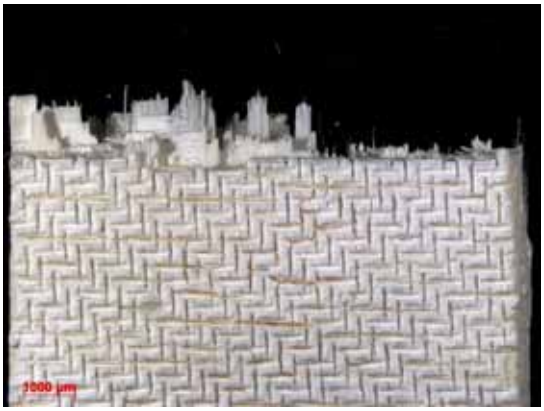

Figure B.144: Fracture surface of the N610/$LaPO_4$/Al_2O_3 specimen with 8ply HSW subjected subjected to creep test at 64 MPa in steam at 1100 °C (t_f = 2.38 h).

Figure B.145: Fracture surface of the N610/$LaPO_4$/Al_2O_3 specimen with 8ply HSW subjected subjected to creep test at 64 MPa in steam at 1100 °C (t_f = 2.38 h).

Figure B.146: Fracture surface of the N610/$LaPO_4$/Al_2O_3 specimen with 8ply HSW subjected subjected to creep test at 64 MPa in steam at 1100 °C (t_f = 2.38 h).

Figure B.147: Fracture surface of the N610/$LaPO_4$/Al_2O_3 specimen with 8ply HSW subjected subjected to creep test at 72 MPa in air at 1100 °C (t_f > 100 h).

Figure B.148: Fracture surface of the N610/$LaPO_4$/Al_2O_3 specimen with 8ply HSW subjected subjected to creep test at 72 MPa in air at 1100 °C (t_f > 100 h).

Figure B.149: Fracture surface of the N610/$LaPO_4$/Al_2O_3 specimen with 8ply HSW subjected subjected to creep test at 72 MPa in air at 1100 °C ($t_f > 100$ h).

Figure B.150: Fracture surface of the N610/$LaPO_4$/Al_2O_3 specimen with 8ply HSW subjected subjected to creep test at 72 MPa in air at 1100 °C ($t_f > 100$ h).

Figure B.151: Fracture surface of the N610/$LaPO_4$/Al_2O_3 specimen with 8ply HSW subjected subjected to creep test at 72 MPa in air at 1100 °C ($t_f > 100$ h).

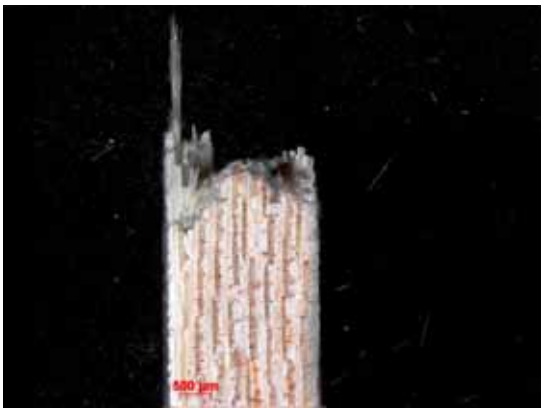

Figure B.152: Fracture surface of the N610/$LaPO_4$/Al_2O_3 specimen with 8ply HSW subjected subjected to creep test at 72 MPa in air at 1100 °C ($t_f > 100$ h).

Figure B.153: Fracture surface of the N610/$LaPO_4$/Al_2O_3 specimen with 8ply HSW subjected subjected to creep test at 72 MPa in steam at 1100 °C ($t_f = 2.24$ h).

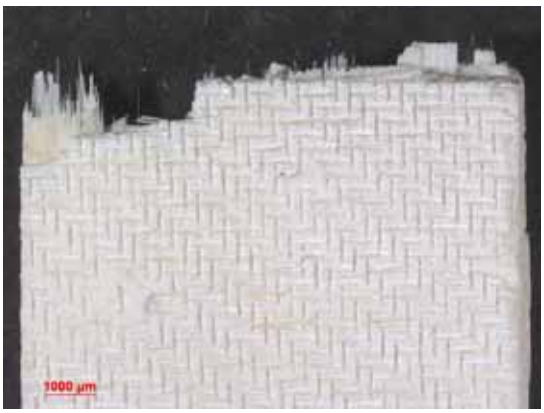

Figure B.154: Fracture surface of the N610/$LaPO_4$/Al_2O_3 specimen with 8ply HSW subjected subjected to creep test at 72 MPa in steam at 1100 °C ($t_f = 2.24$ h).

Figure B.155: Fracture surface of the N610/$LaPO_4$/Al_2O_3 specimen with 8ply HSW subjected subjected to creep test at 72 MPa in steam at 1100 °C (t_f = 2.24 h).

Figure B.156: Fracture surface of the N610/$LaPO_4$/Al_2O_3 specimen with 8ply HSW subjected subjected to creep test at 72 MPa in steam at 1100 °C (t_f = 2.24 h).

Figure B.157: Fracture surface of the N610/$LaPO_4$/Al_2O_3 specimen with 8ply HSW subjected subjected to creep test at 72 MPa in steam at 1100 °C (t_f = 2.24 h).

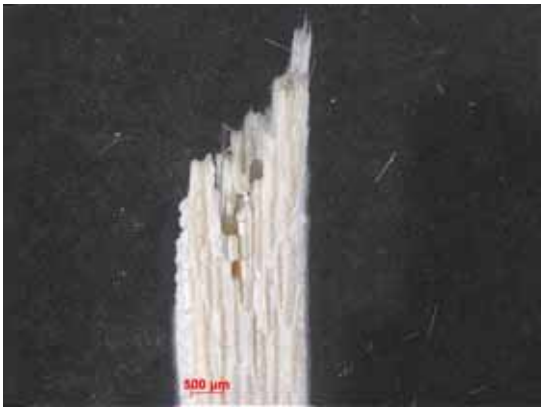

Figure B.158: Fracture surface of the N610/$LaPO_4$/Al_2O_3 specimen with 8ply HSW subjected subjected to creep test at 72 MPa in steam at 1100 °C (t_f = 2.24 h).

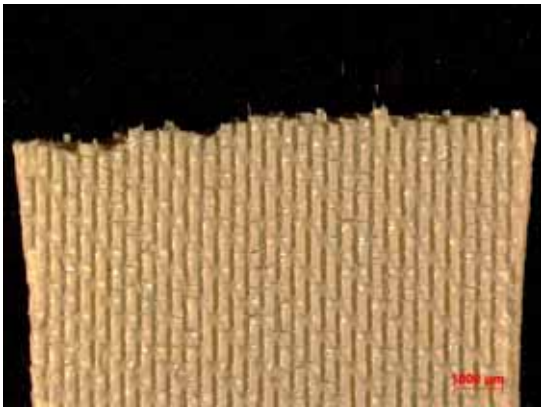

Figure B.159: Fracture surface of the N610/Al_2O_3 specimen with 8ply HSW subjected tension to failure in laboratory air at 1100 °C.

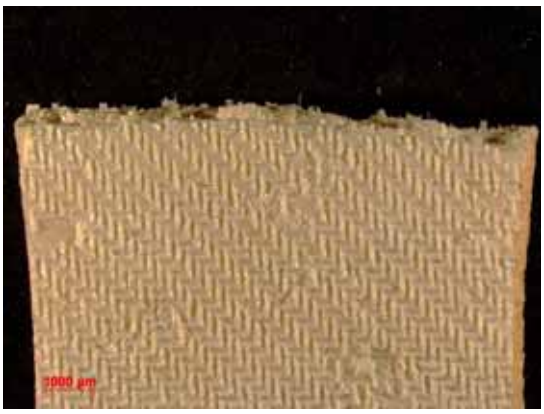

Figure B.160: Fracture surface of the N610/Al_2O_3 specimen with 8ply HSW subjected tension to failure in laboratory air at 1100 °C.

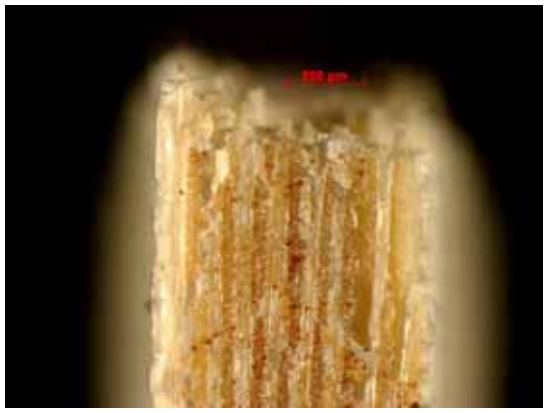

Figure B.161: Fracture surface of the N610/Al_2O_3 specimen with 8ply HSW subjected tension to failure in laboratory air at 1100 °C.

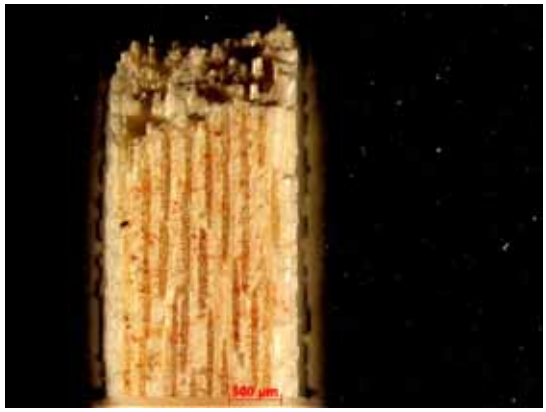

Figure B.162: Fracture surface of the N610/Al_2O_3 specimen with 8ply HSW subjected tension to failure in laboratory air at 1100 °C.

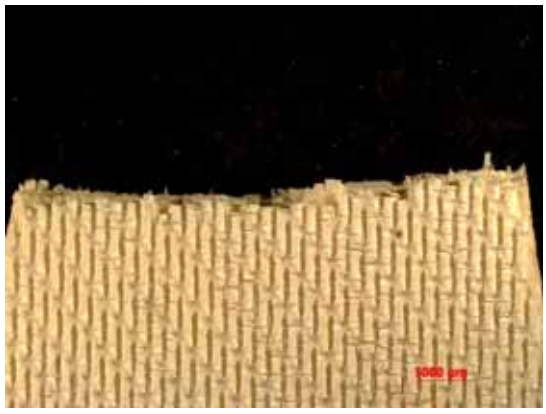

Figure B.163: Fracture surface of the N610/Al_2O_3 specimen with 8ply HSW subjected tension to failure in laboratory air at 1100 °C.

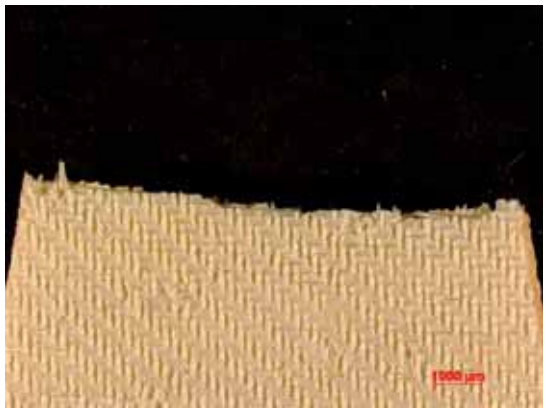

Figure B.164: Fracture surface of the N610/Al_2O_3 specimen with 8ply HSW subjected tension to failure in laboratory air at 1100 °C.

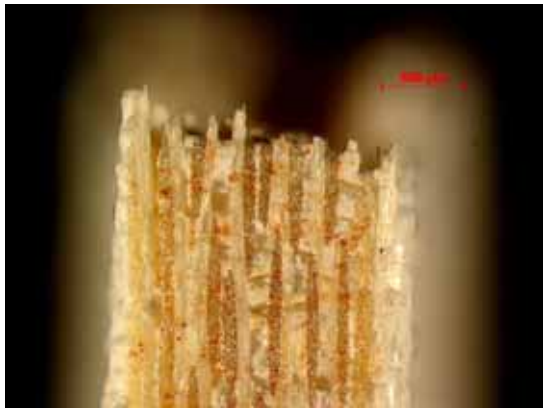

Figure B.165: Fracture surface of the N610/Al_2O_3 specimen with 8ply HSW subjected tension to failure in laboratory air at 1100 °C.

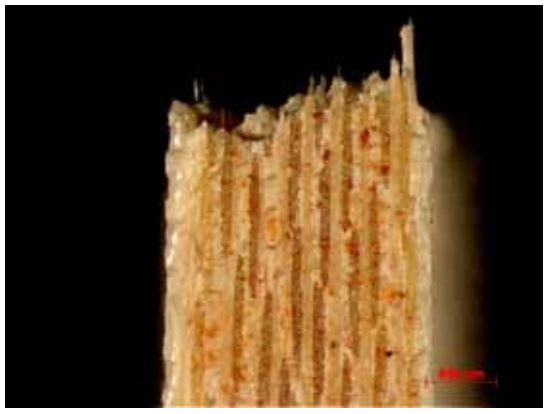

Figure B.166: Fracture surface of the N610/Al_2O_3 specimen with 8ply HSW subjected tension to failure in laboratory air at 1100 °C.

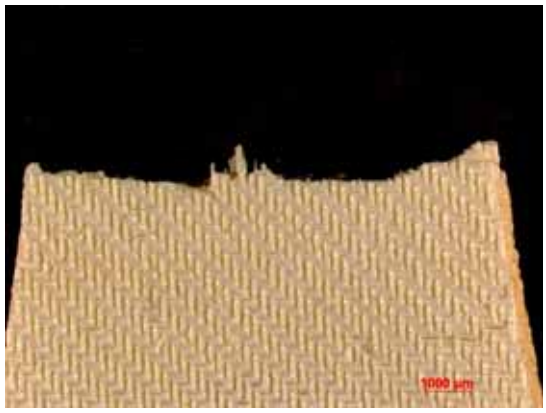

Figure B.167: Fracture surface of the N610/Al_2O_3 specimen with 8ply HSW subjected tension to failure in laboratory air at 1100 °C.

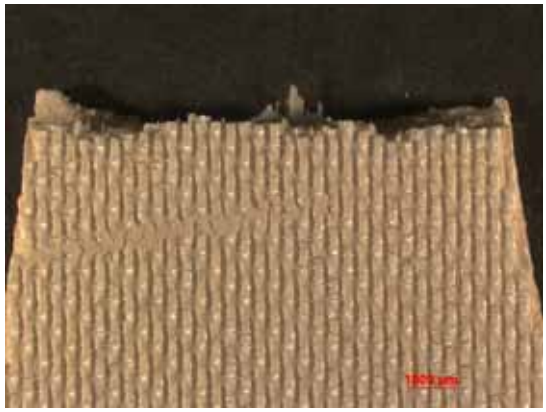

Figure B.168: Fracture surface of the N610/Al_2O_3 specimen with 8ply HSW subjected tension to failure in laboratory air at 1100 °C.

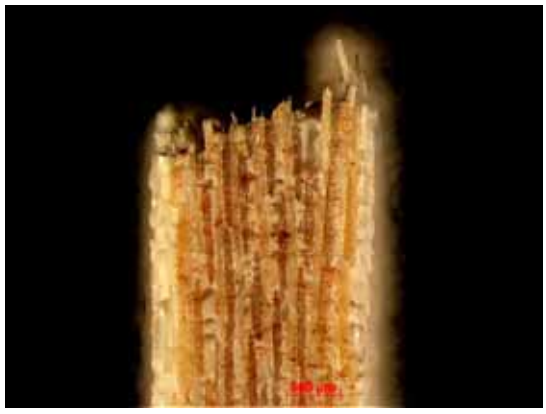

Figure B.169: Fracture surface of the N610/Al_2O_3 specimen with 8ply HSW subjected tension to failure in laboratory air at 1100 °C.

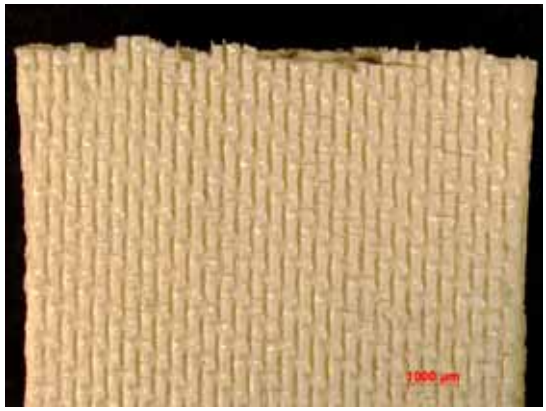

Figure B.170: Fracture surface of the N610/Al_2O_3 specimen with 8ply HSW subjected tension to failure in laboratory air at 1100 °C.

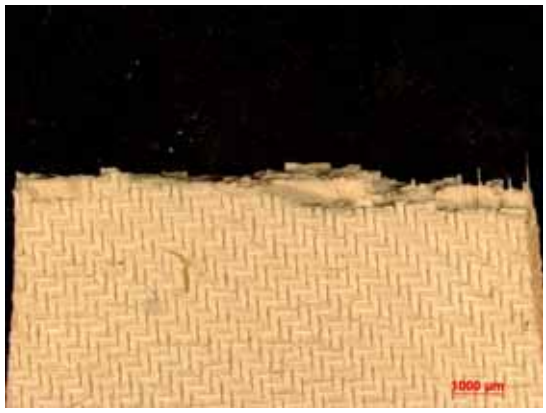

Figure B.171: Fracture surface of the N610/$LaPO_4$/Al_2O_3 specimen with 8ply HSW subjected subjected to creep test at 20 MPa in steam at 1100 °C (t_f = 3.53 h).

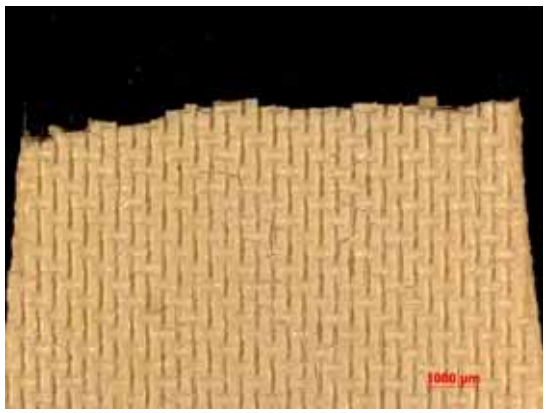

Figure B.172: Fracture surface of the N610/$LaPO_4$/Al_2O_3 specimen with 8ply HSW subjected subjected to creep test at 20 MPa in steam at 1100 °C (t_f = 3.53 h).

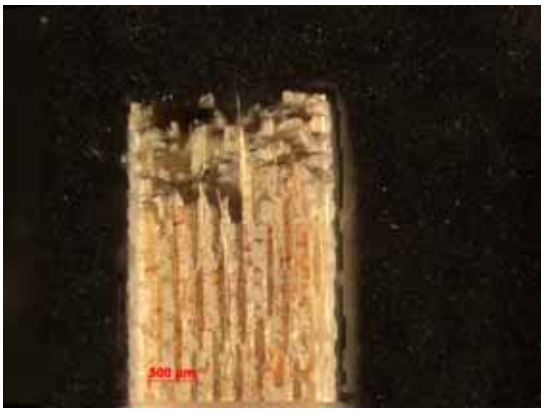

Figure B.173: Fracture surface of the N610/$LaPO_4$/Al_2O_3 specimen with 8ply HSW subjected subjected to creep test at 20 MPa in steam at 1100 °C (t_f = 3.53 h).

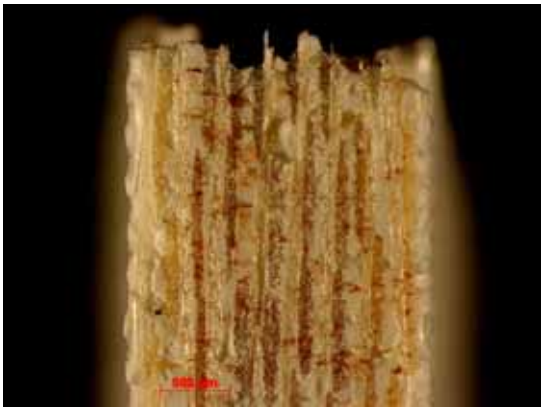

Figure B.174: Fracture surface of the N610/$LaPO_4$/Al_2O_3 specimen with 8ply HSW subjected subjected to creep test at 20 MPa in steam at 1100 °C (t_f = 3.53 h).

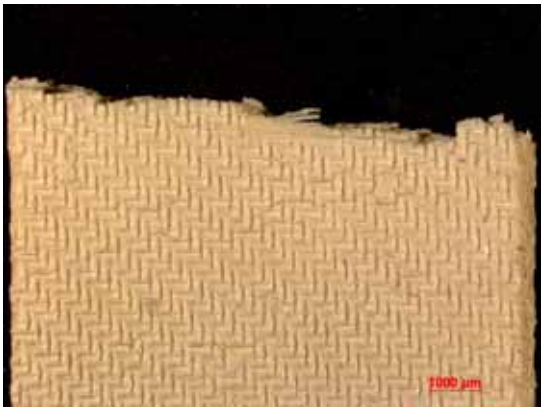

Figure B.175: Fracture surface of the N610/$LaPO_4$/Al_2O_3 specimen with 8ply HSW subjected subjected to creep test at 20 MPa in steam at 1100 °C (t_f = 3.53 h).

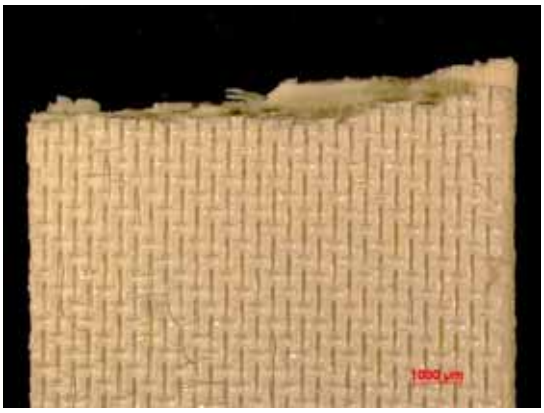

Figure B.176: Fracture surface of the N610/$LaPO_4$/Al_2O_3 specimen with 8ply HSW subjected subjected to creep test at 20 MPa in steam at 1100 °C (t_f = 3.53 h).

Figure B.177: Fracture surface of the N610/$LaPO_4$/Al_2O_3 specimen with 8ply HSW subjected subjected to creep test at 20 MPa in steam at 1100 °C (t_f = 3.53 h).

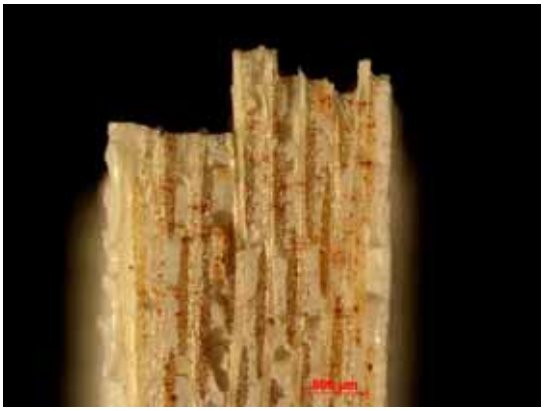

Figure B.178: Fracture surface of the N610/$LaPO_4$/Al_2O_3 specimen with 8ply HSW subjected subjected to creep test at 20 MPa in steam at 1100 °C (t_f = 3.53 h).

Figure B.179: Fracture surface of the N610/$LaPO_4$/Al_2O_3 specimen with 8ply HSW subjected subjected to creep test at 30 MPa in steam at 1100 °C (t_f = 16.1 h).

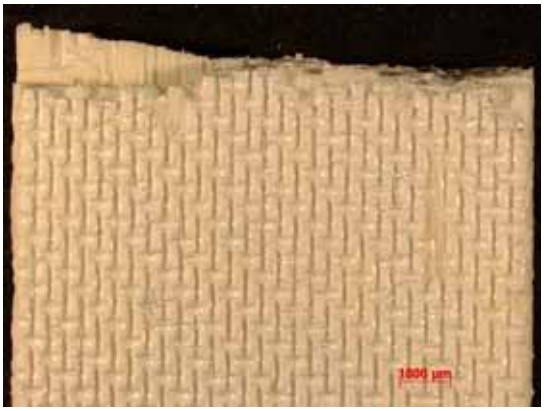

Figure B.180: Fracture surface of the N610/$LaPO_4$/Al_2O_3 specimen with 8ply HSW subjected subjected to creep test at 30 MPa in steam at 1100 °C (t_f = 16.1 h).

Figure B.181: Fracture surface of the N610/$LaPO_4$/Al_2O_3 specimen with 8ply HSW subjected subjected to creep test at 30 MPa in steam at 1100 °C (t_f = 16.1 h).

Figure B.182: Fracture surface of the N610/$LaPO_4$/Al_2O_3 specimen with 8ply HSW subjected subjected to creep test at 30 MPa in steam at 1100 °C (t_f = 16.1 h).

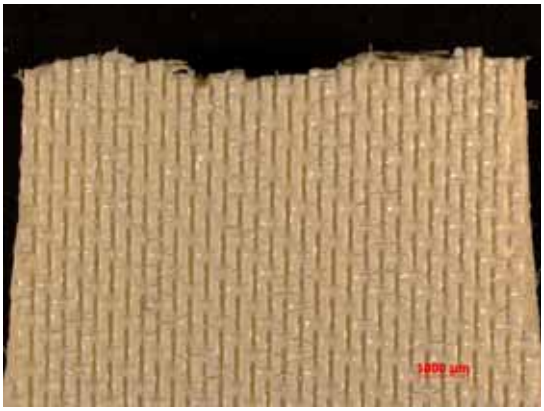

Figure B.183: Fracture surface of the N610/$LaPO_4$/Al_2O_3 specimen with 8ply HSW subjected subjected to creep test at 30 MPa in steam at 1100 °C (t_f = 16.1 h).

Figure B.184: Fracture surface of the N610/$LaPO_4$/Al_2O_3 specimen with 8ply HSW subjected subjected to creep test at 30 MPa in steam at 1100 °C (t_f = 16.1 h).

Figure B.185: Fracture surface of the N610/$LaPO_4$/Al_2O_3 specimen with 8ply HSW subjected subjected to creep test at 40.5 MPa in air at 1100 °C (t_f = 3.34 h).

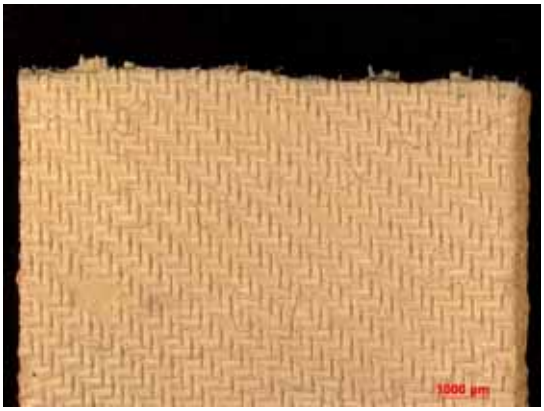

Figure B.186: Fracture surface of the N610/$LaPO_4$/Al_2O_3 specimen with 8ply HSW subjected subjected to creep test at 40.5 MPa in air at 1100 °C (t_f = 3.34 h).

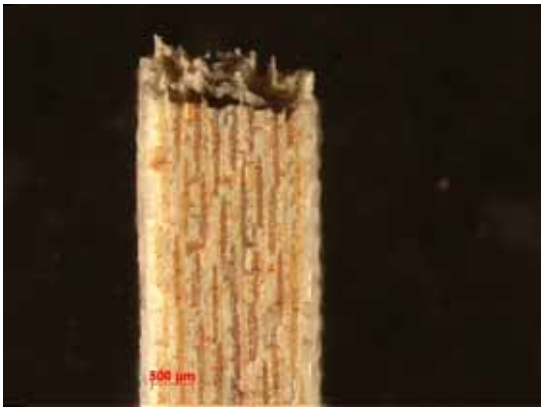

Figure B.187: Fracture surface of the N610/$LaPO_4$/Al_2O_3 specimen with 8ply HSW subjected subjected to creep test at 40.5 MPa in air at 1100 °C (t_f = 3.34 h).

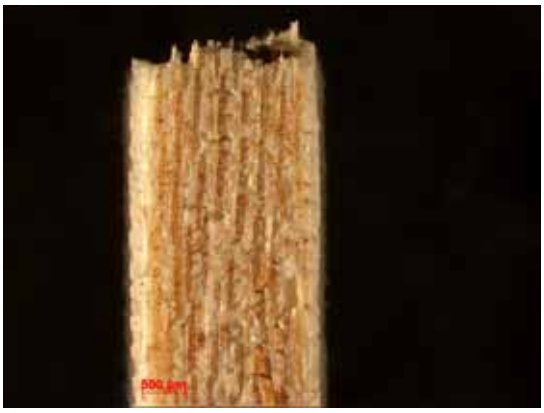

Figure B.188: Fracture surface of the N610/$LaPO_4$/Al_2O_3 specimen with 8ply HSW subjected subjected to creep test at 40.5 MPa in air at 1100 °C (t_f = 3.34 h).

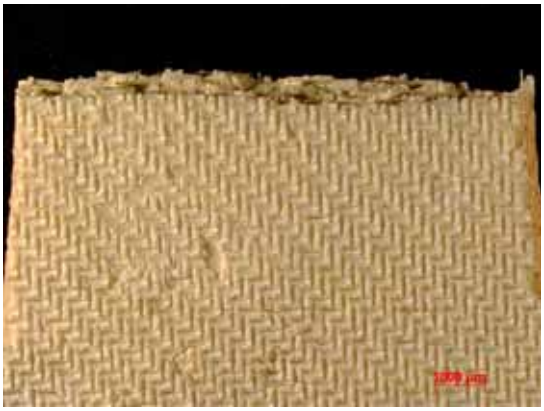

Figure B.189: Fracture surface of the N610/$LaPO_4$/Al_2O_3 specimen with 8ply HSW subjected subjected to creep test at 40.5 MPa in air at 1100 °C (t_f = 3.34 h).

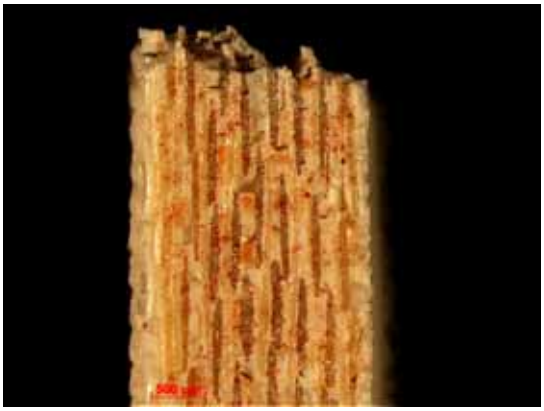

Figure B.190: Fracture surface of the N610/$LaPO_4$/Al_2O_3 specimen with 8ply HSW subjected subjected to creep test at 40.5 MPa in air at 1100 °C (t_f = 3.34 h).

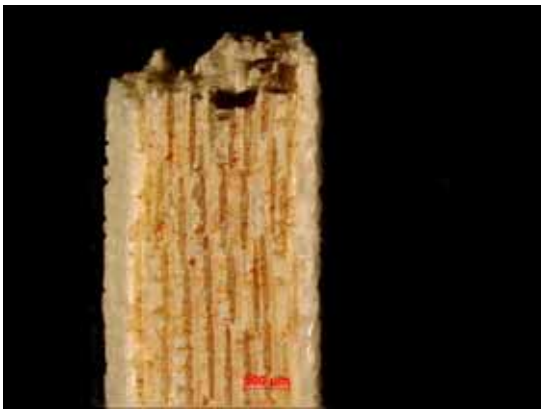

Figure B.191: Fracture surface of the N610/$LaPO_4$/Al_2O_3 specimen with 8ply HSW subjected subjected to creep test at 40.5 MPa in air at 1100 °C (t_f = 3.34 h).

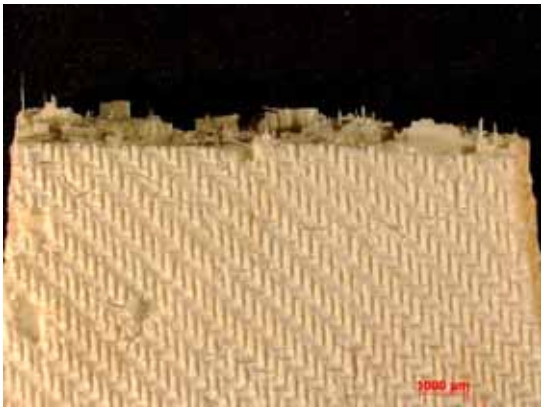

Figure B.192: Fracture surface of the N610/$LaPO_4$/Al_2O_3 specimen with 8ply HSW subjected subjected to creep test at 40.5 MPa in steam at 1100 °C (t_f = 0.01 h).

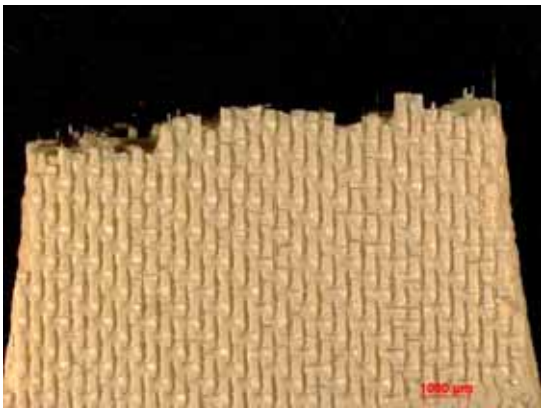

Figure B.193: Fracture surface of the N610/$LaPO_4$/Al_2O_3 specimen with 8ply HSW subjected subjected to creep test at 40.5 MPa in steam at 1100 °C (t_f = 0.01 h).

Figure B.194: Fracture surface of the N610/$LaPO_4$/Al_2O_3 specimen with 8ply HSW subjected subjected to creep test at 40.5 MPa in steam at 1100 °C (t_f = 0.01 h).

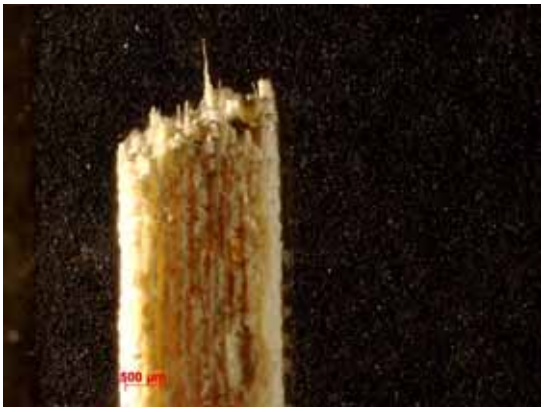

Figure B.195: Fracture surface of the N610/$LaPO_4$/Al_2O_3 specimen with 8ply HSW subjected subjected to creep test at 40.5 MPa in steam at 1100 °C (t_f = 0.01 h).

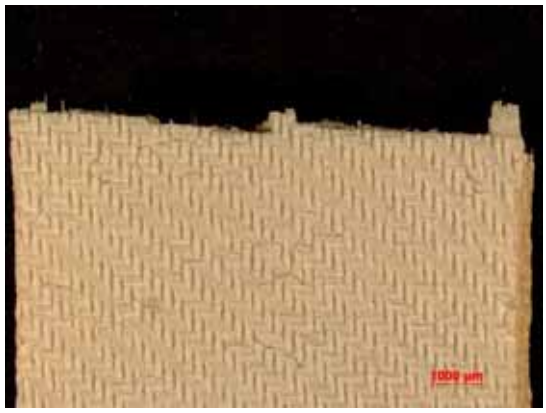

Figure B.196: Fracture surface of the N610/$LaPO_4$/Al_2O_3 specimen with 8ply HSW subjected subjected to creep test at 40.5 MPa in steam at 1100 °C (t_f = 0.01 h).

Figure B.197: Fracture surface of the N610/$LaPO_4$/Al_2O_3 specimen with 8ply HSW subjected subjected to creep test at 40.5 MPa in steam at 1100 °C (t_f = 0.01 h).

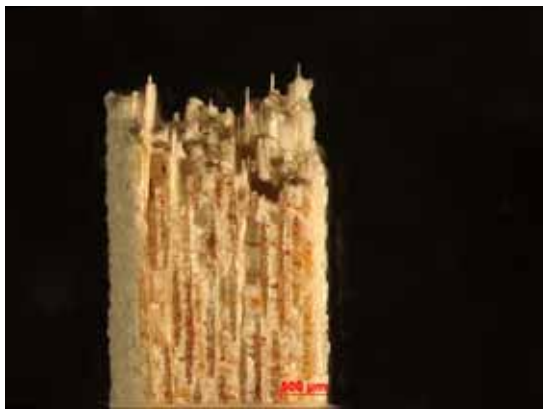

Figure B.198: Fracture surface of the N610/$LaPO_4$/Al_2O_3 specimen with 8ply HSW subjected subjected to creep test at 40.5 MPa in steam at 1100 °C (t_f = 0.01 h).

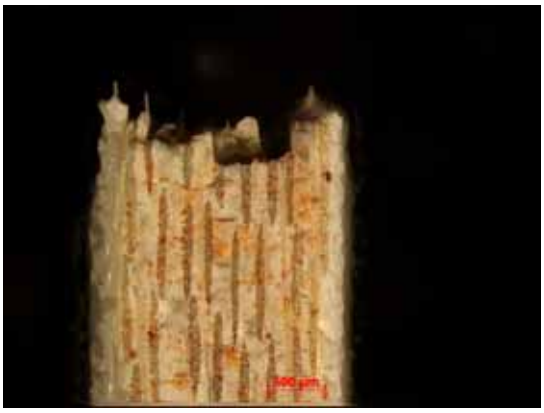

Figure B.199: Fracture surface of the N610/$LaPO_4$/Al_2O_3 specimen with 8ply HSW subjected subjected to creep test at 40.5 MPa in steam at 1100 °C (t_f = 0.01 h).

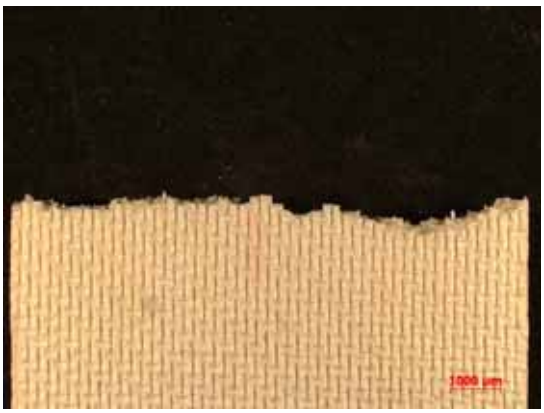

Figure B.200: Fracture surface of the N610/$LaPO_4$/Al_2O_3 specimen with 8ply HSW subjected subjected to creep test at 61 MPa in air at 1100 °C (t_f = 3.42 h).

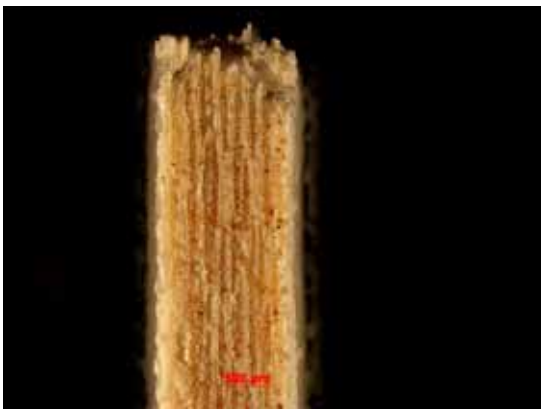

Figure B.201: Fracture surface of the N610/$LaPO_4$/Al_2O_3 specimen with 8ply HSW subjected subjected to creep test at 61 MPa in air at 1100 °C (t_f = 3.42 h).

Figure B.202: Side view of the virgin N610/$LaPO_4$/Al_2O_3-AlOCl specimen with 8ply HSW.

Figure B.203: Side view of the virgin N610/$LaPO_4$/Al_2O_3-AlOCl specimen with 8ply HSW.

Figure B.204: Side view of the virgin N610/$LaPO_4$/Al_2O_3-AlOCl specimen with 8ply HSW.

Figure B.205: Side view of the virgin N610/$LaPO_4$/Al_2O_3-AlOCl specimen with 8ply HSW.

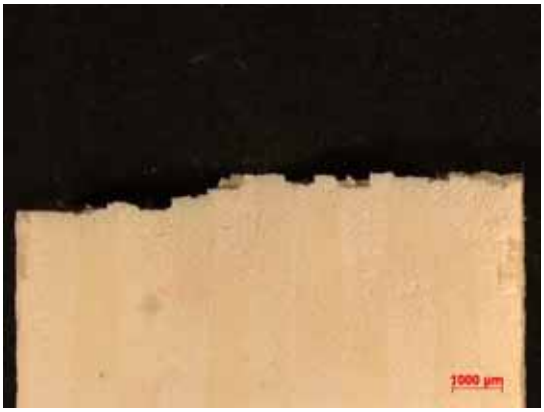

Figure B.206: Fracture surface of the N610/$LaPO_4$/Al_2O_3-AlOCl specimen with 8ply HSW subjected tension to failure in laboratory air at 1100 °C.

Figure B.207: Fracture surface of the N610/$LaPO_4$/Al_2O_3-AlOCl specimen with 8ply HSW subjected tension to failure in laboratory air at 1100 °C.

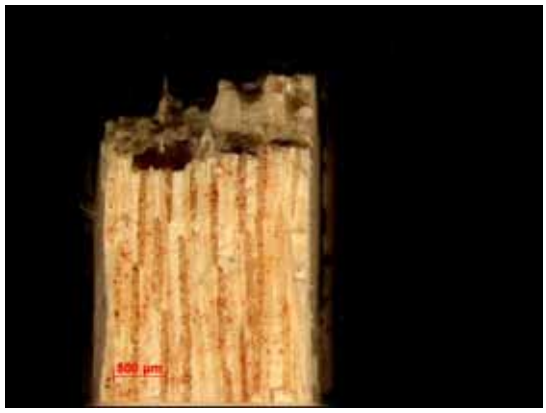

Figure B.208: Fracture surface of the N610/$LaPO_4$/Al_2O_3-AlOCl specimen with 8ply HSW subjected tension to failure in laboratory air at 1100 °C.

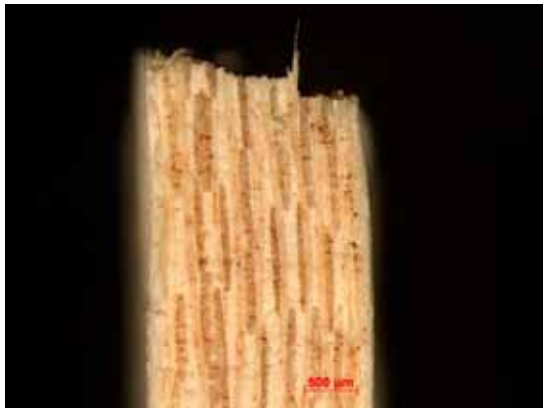

Figure B.209: Fracture surface of the N610/$LaPO_4$/Al_2O_3-AlOCl specimen with 8ply HSW subjected tension to failure in laboratory air at 1100 °C.

Figure B.210: Fracture surface of the N610/$LaPO_4$/Al_2O_3-AlOCl specimen with 8ply HSW subjected tension to failure in laboratory air at 1100 °C.

Figure B.211: Fracture surface of the N610/$LaPO_4$/Al_2O_3-AlOCl specimen with 8ply HSW subjected tension to failure in laboratory air at 1100 °C.

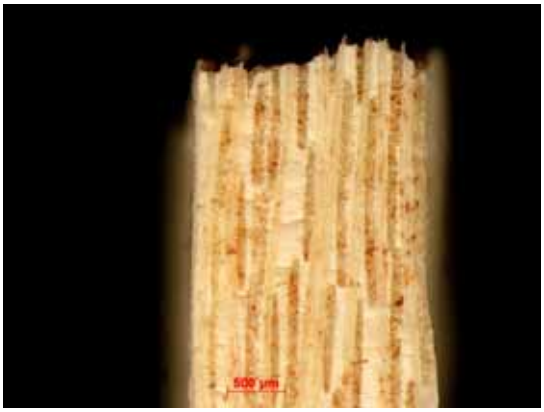

Figure B.212: Fracture surface of the N610/$LaPO_4$/Al_2O_3-AlOCl specimen with 8ply HSW subjected tension to failure in laboratory air at 1100 °C.

Figure B.213: Fracture surface of the N610/$LaPO_4$/Al_2O_3-AlOCl specimen with 8ply HSW subjected tension to failure in laboratory air at 1100 °C.

Figure B.214: Fracture surface of the N610/$LaPO_4$/Al_2O_3-AlOCl specimen with 8ply HSW subjected subjected to creep test at 32 MPa in air at 1100 °C ($t_f > 100$ h).

Figure B.215: Fracture surface of the N610/$LaPO_4$/Al_2O_3-AlOCl specimen with 8ply HSW subjected subjected to creep test at 32 MPa in air at 1100 °C ($t_f > 100$ h).

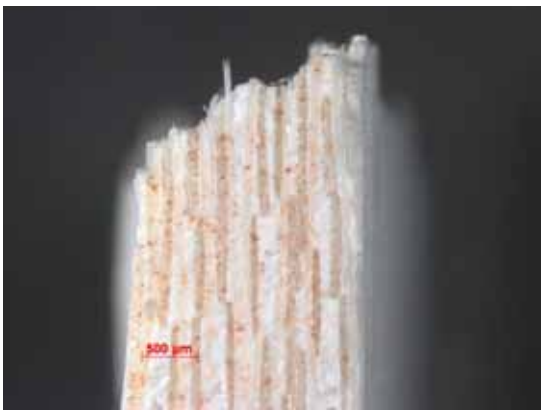

Figure B.216: Fracture surface of the N610/$LaPO_4$/Al_2O_3-AlOCl specimen with 8ply HSW subjected subjected to creep test at 32 MPa in air at 1100 °C ($t_f > 100$ h).

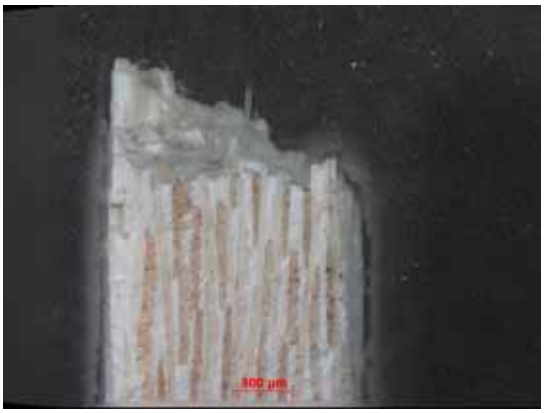

Figure B.217: Fracture surface of the N610/$LaPO_4$/Al_2O_3-AlOCl specimen with 8ply HSW subjected subjected to creep test at 32 MPa in air at 1100 °C ($t_f > 100$ h).

Figure B.218: Fracture surface of the N610/$LaPO_4$/Al_2O_3-AlOCl specimen with 8ply HSW subjected subjected to creep test at 32 MPa in air at 1100 °C ($t_f > 100$ h).

Figure B.219: Fracture surface of the N610/$LaPO_4$/Al_2O_3-AlOCl specimen with 8ply HSW subjected subjected to creep test at 32 MPa in air at 1100 °C ($t_f > 100$ h).

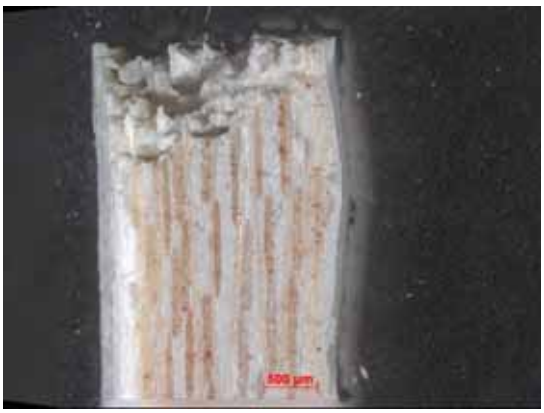

Figure B.220: Fracture surface of the N610/$LaPO_4$/Al_2O_3-AlOCl specimen with 8ply HSW subjected subjected to creep test at 32 MPa in air at 1100 °C ($t_f > 100$ h).

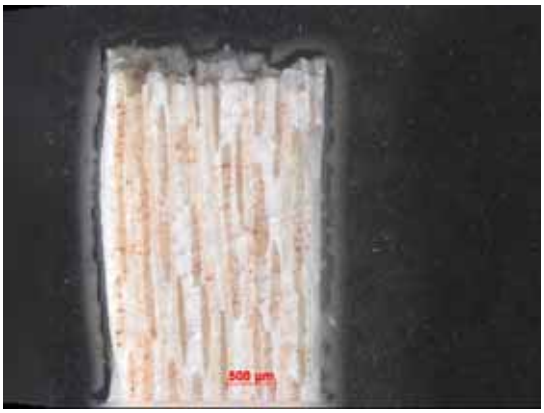

Figure B.221: Fracture surface of the N610/$LaPO_4$/Al_2O_3-AlOCl specimen with 8ply HSW subjected subjected to creep test at 32 MPa in air at 1100 °C ($t_f > 100$ h).

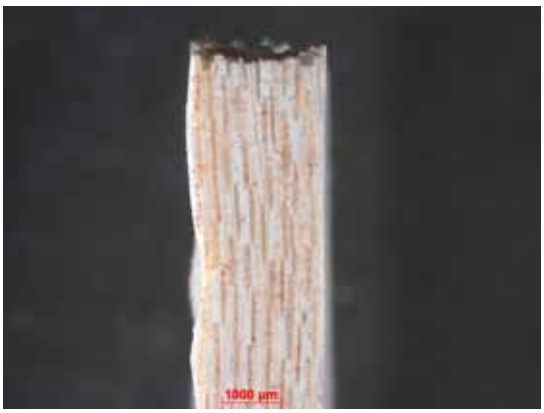

Figure B.222: Fracture surface of the N610/$LaPO_4$/Al_2O_3-AlOCl specimen with 8ply HSW subjected subjected to creep test at 32 MPa in air at 1100 °C ($t_f > 100$ h).

Figure B.223: Fracture surface of the N610/$LaPO_4$/Al_2O_3-AlOCl specimen with 8ply HSW subjected subjected to creep test at 32 MPa in steam at 1100 °C (t_f = 3.47 h).

Figure B.224: Fracture surface of the N610/$LaPO_4$/Al_2O_3-AlOCl specimen with 8ply HSW subjected subjected to creep test at 32 MPa in steam at 1100 °C (t_f = 3.47 h).

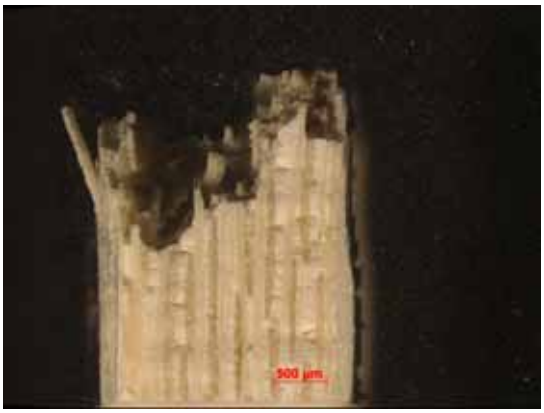

Figure B.225: Fracture surface of the N610/$LaPO_4$/Al_2O_3-AlOCl specimen with 8ply HSW subjected subjected to creep test at 32 MPa in steam at 1100 °C (t_f = 3.47 h).

Figure B.226: Fracture surface of the N610/$LaPO_4$/Al_2O_3-AlOCl specimen with 8ply HSW subjected subjected to creep test at 32 MPa in steam at 1100 °C (t_f = 3.47 h).

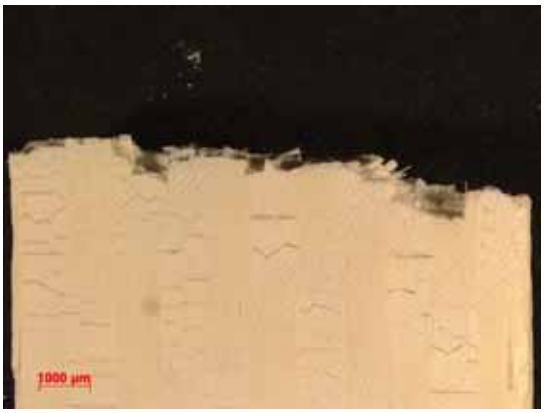

Figure B.227: Fracture surface of the N610/$LaPO_4$/Al_2O_3-AlOCl specimen with 8ply HSW subjected subjected to creep test at 32 MPa in steam at 1100 °C (t_f = 3.47 h).

Figure B.228: Fracture surface of the N610/$LaPO_4$/Al_2O_3-AlOCl specimen with 8ply HSW subjected subjected to creep test at 32 MPa in steam at 1100 °C (t_f = 3.47 h).

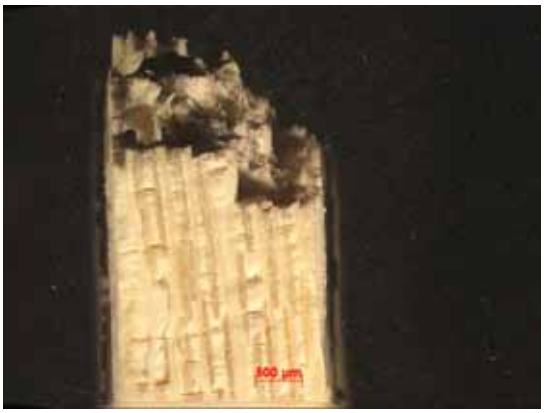

Figure B.229: Fracture surface of the N610/$LaPO_4$/Al_2O_3-AlOCl specimen with 8ply HSW subjected subjected to creep test at 32 MPa in steam at 1100 °C (t_f = 3.47 h).

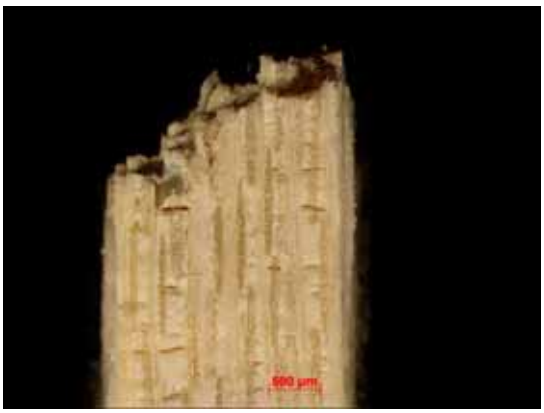

Figure B.230: Fracture surface of the N610/$LaPO_4$/Al_2O_3-AlOCl specimen with 8ply HSW subjected subjected to creep test at 32 MPa in steam at 1100 °C (t_f = 3.47 h).

Figure B.231: Fracture surface of the N610/$LaPO_4$/Al_2O_3-AlOCl specimen with 8ply HSW subjected subjected to creep test at 48 MPa in steam at 1100 °C (t_f = 2.06 h).

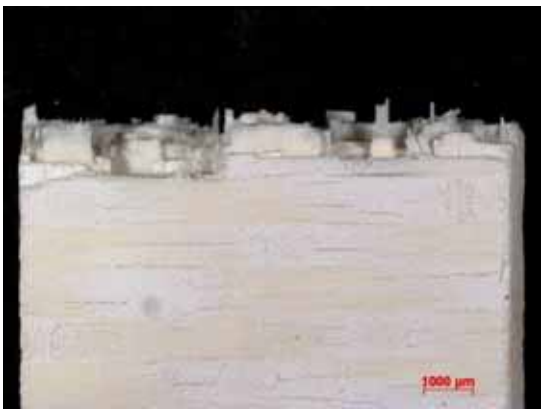

Figure B.232: Fracture surface of the N610/$LaPO_4$/Al_2O_3-AlOCl specimen with 8ply HSW subjected subjected to creep test at 48 MPa in steam at 1100 °C (t_f = 2.06 h).

Figure B.233: Fracture surface of the N610/$LaPO_4$/Al_2O_3-AlOCl specimen with 8ply HSW subjected subjected to creep test at 48 MPa in steam at 1100 °C (t_f = 2.06 h).

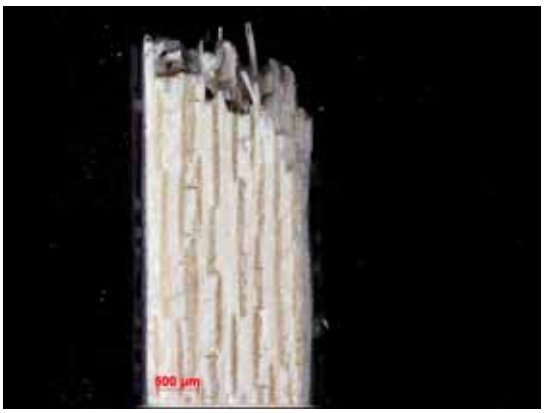

Figure B.234: Fracture surface of the N610/$LaPO_4$/Al_2O_3-AlOCl specimen with 8ply HSW subjected subjected to creep test at 48 MPa in steam at 1100 °C (t_f = 2.06 h).

Figure B.235: Fracture surface of the N610/$LaPO_4$/Al_2O_3-AlOCl specimen with 8ply HSW subjected subjected to creep test at 48 MPa in steam at 1100 °C (t_f = 2.06 h).

Figure B.236: Fracture surface of the N610/$LaPO_4$/Al_2O_3-AlOCl specimen with 8ply HSW subjected subjected to creep test at 48 MPa in steam at 1100 °C (t_f = 2.06 h).

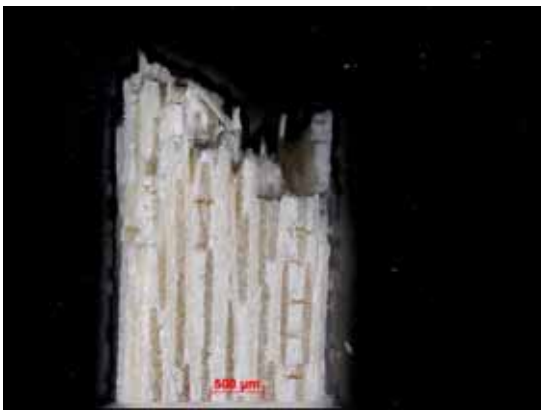

Figure B.237: Fracture surface of the N610/$LaPO_4$/Al_2O_3-AlOCl specimen with 8ply HSW subjected subjected to creep test at 48 MPa in steam at 1100 °C (t_f = 2.06 h).

Bibliography

1. "Report of the Committee on the Definition of the Term Ceramics". *Journal of the American Ceramic Society*, 4:526–542, 1920.

2. B., Harlan Lee. *Creep-Rupture Behavior of an Oxide/Oxide Ceramic Matrix Composite at Elevated Temperatures in Air and Steam Environments*. Master's thesis, Graduate School of Engineering, Air Force Institute of Technology (AETC), Wright-Patterson AFB OH, March 2005. AFIT/GAE/ENY/05-M05.

3. Boakye, M.D. Petry R.S. Hay, E.E. and L.M. Douglas. "Monazite Coatings on Nextel 720, 610, and Tyranno-SA Fiber Tows: Effects of Precursers on Fiber Strength". *Ceramic Engineering Society Proceedings*, 21:229–236, 2000.

4. Boakye, R.S. Hay P. Mogilevsky, E.E. and L.M. Douglas. "Monazite Coatings on Fibers: II, Coating without Strength Degradation". *Journal of the American Ceramic Society*, 84:2793–2801, 2001.

5. Cazzato A., D. Daws-J. Davis P. Morgan J. Porter S Butner, M. Colby and B. Jurf. "Monazite Interface Coatings in Polymer and Sol-Gel Derived CeramicMatrix Composites". 18(3):269–278, 1997.

6. Chawla K.K., J. Janczak-Rusch, H. Liu and S. Sambasivan. "Microstructure and Properties of Monazite (LaPO4) Coated Saphikon Fiber/Alumina Matrix Composites". *Journal of the European Ceramic Society*, 20:551–559, 2000.

7. David, Lewis III. "Continuous Fiber-Reinforced Ceramic Matrix Composites: "A Historical Overview"". 1995.

8. Davis, D.B. Marshall, J.B. and P.E.D. Morgan. "Monazite-Containing Oxide/Oxide Composites". *Journal of the European Ceramic Society*, 20:583–587, 2000.

9. Davis, D.B. Marshall R.M. Housely, J.B. and P. E. D. Morgan. "Machinable Ceramics Containing Rare Earth Phosphates". *Journal of the European Ceramic Society*, 81:2169–2175, 1998.

10. DiCarlo, James A. and Sunil Dutta. "Continuous Ceramic Fibers for Ceramic Matrix Composites," in Handbook on Continuous Fiber-Reinforced Ceramic Matrix Composites". 1995.

11. EJ, Opila. "Variation of the Oxidation Rate of Silicon Carbide with Water Vapor Pressure". *Journal of the American Ceramic Society*, 82:625–636, 1999.

12. Fair Geoff E., Emmanuel E. Boakye, Randall S. Hay. "Precipitation coating of monazite on woven ceramic fibers. I. feasibility". *Journal of the American Ceramic Society*, 90(2):448–455, 2007.

13. Fair Geoff E., Emmanuel E. Boakye, Randall S. Hay. "Precipitation Coating of Monazite on Woven Ceramic Fibers: II. Effect of Processing Conditions on Coating Morphology and Strength Retention of Nextel 610 and 720 Fibers". *Journal of the American Ceramic Society*, 91(5):1508–1516, May 2008.

14. Ferber MK Lin HT, Keiser JR. "Oxidation Behavior of Non-Oxide Ceramics in a High-Pressure, High-Temperature Steam Environment". *Mechanical, Thermal, and Environmental Testing and Performance of Ceramic Composites and Components. ASTM STP 1392*, 210–215, 2000.

15. Hermes EE, Kerans RJ. "Degradation of Non-Oxide Reinforcement and Oxide Matrix Composites". *Symposium Proceedings*, 125:73–78, 1988.

16. J. M. Mehrman, S. S. Baek, M. B. Ruggles-Wrenn. "Influence of Hold Times on the Elevated-Temperature Fatigue Behavior of an Oxide-Oxide Ceramic Composite in Air and in Steam Environment". *Composites Science and Technology*, 67:1425–1438, 2007.

17. Kanazawa, S.M. Johnson, C. and J.R. Porter. "Monazite Coating Promotes Fiber Pullout". *Journal of the American Ceramic Society*, 80:Backcover, 1997.

18. Keller K.A., T.A. Parthasarathy-E.E. Boakye P. Mogilevsky, T. Mah and M. Cinibulk. "Effectiveness of Monazite Coatings in Oxide/Oxide Composites after Long-Term Exposure at High Temperature". *25th Annual Conference on Composites,Advanced Ceramics,Materials,and Structures:A*, 325–332. The American Ceramic Society, The American Ceramic Society, Westerville,OH, January 2003.

19. Kerans, Parthasarathy T.A., R.J. "Crack deflection in ceramic composites and fiber coating design criteria". *Composites: Part A*, 30:521–524, 1999.

20. K.K., Chawla. *Ceramic MAtrix Composites*. Chapman and Hall, London, 1 edition, 1993.

21. K.K., Chawla. *Composite Materials Science and Engineering*. Kluwer Academic Publishers, Boston, 2 edition, 2003.

22. Kuo, Waltraud M. Kriven, Dong-Hau and Thomas J. Mackin. "Control of Interfacial Properties Through Fiber Coatings: Monazite Coatings in Oxide-Oxide Composites". *Journal of the American Ceramic Society*, 80:2987–2996, 1997.

23. Lange F.F., A.G. Evans, W.C. Tu. "Processing of damage-tolerant, oxidation resistant ceramic matrix composites by a precursor infiltration and pyrolysis method". 195:145–150, 1995.

24. LaRochelle, K.J. *Tensile Stress Rupture Behavior of a Woven Ceramic Matrix Composite in Humid Environments at Intermediate Temperatures*. Ph.D. dissertation, School of Engineering and Management, Air Force Institute of Technology (AU), Wright-Patterson AFB OH, March 2005. AFIT/DS/ENG/05-01.

25. Levi Carlos G., Brian J. Dalgleish Frank W. Zok, James Y. Yang and Anthony G. Evans. "Processing and Performance of an All-Oxide Ceramic Composite". *Journal of the American Ceramic Society*, 81:2077–2086, October 1998.

26. Lewis MH, Doleman P Razzell AG Gent J, Cain MG. "Development of Interfaces in Oxide and Silicate Matrix Composites.In: Evans AG, and Naslain RG, editors. High-Temperature Ceramic-Matrix Composites II: Manufacturing and Materials Development". *Journal of the American Ceramic Society*, 41–52, 1995.

27. Lunderberg R, Eckerbom L. "Design and Processing of All-Oxide Composites. In: Evans AG, and Naslain RG, editors. High-Temperature Ceramic-Matrix Composites II: Manufacturing and Materials Development." *Journal of the American Ceramic Society*, 22:95–104, 1995.

28. M. B. Ruggles-Wrenn, C. A. Eber L. B. Harlan, S. Mall. "Effects of Steam Environment on High-Temperature Mechanical Behavior of NextelTM720/ Alumina (N720/A) Continuous Fiber Ceramic Composite". *Composites Part A: Applied Science and Manufacturing*, 37:2029–2040, 2006.

29. M. B. Ruggles-Wrenn, S. Mall K. A. Keller, S. S. Musil. "Creep-Rupture Behavior of NextelTM610/ Monazite/Alumina Composite at Elevated Temperatures". *Composites Science and Technology*, 66:2089–2099, 2006.

30. Mah T, McCullum DE Hoenigman JR Kim HM Katz AP Lipsitt HA, Hecht NL. "Thermal Stability of SiC Fibres (Nicalon)." *Journal of the Material Science*, 19:1191–1201, 1984.

31. Moore EH, Mah T and Keller KA. "3D Composite Fabrication Through Matrix Slurry Pressure Infiltration". *Ceram Eng Sci Proceedings*, 15:113–120, 1999.

32. More KL, Ferber MK Keiser JR, Tortorelli PF. "Observations of Accelerated Silicon Carbide Recession by Oxidation at High Water-Vapor Pressures." *Journal of the American Ceramic Society*, 83:211–213, 2000.

33. Morgan, P.E.D. and D.B. Marshall. "Functional Interfaces for Oxide/Oxide Composites, Material Science and Engineering". *Journal of the American Ceramic Society*, 162:15–25, 1993.

34. Morgan, P.E.D. and D.B. Marshall. "Ceramic Composites of Monazite and Alumina". *Journal of the American Ceramic Society*, 78:1553–1563, 1995.

35. Morgan PED, Marshall DB. "Ceramic Composites of Monazite and Alumina". *Journal of the American Ceramic Society*, 78:1553–1563, 1995.

36. Mouchon E, Colomban P. "Oxide Ceramic Matrix/Oxide Fiber Woven Fabric Composites Exhibiting Dissipative Fracture Behavior". *Journal of Composites*, 26:175–182, 1995.

37. Musikant, S. *What Every Engineer Should Know About Ceramics*. Marcel Dekker, New York, NY, first edition, 1991.

38. Notebook., 3M Nextel Textile. "3M Fiber Selection Guide". Product Brochure., july 2008.

39. Ohnabe H, Onozuka M Miyahara K Sasa T., Masaki S. "Potential Application of Ceramic Matrix Composites to Aero-Engine Components." *Composites*, Part A:489–496, 1999.

40. P. R. Jackson, S. S. Baek K. A. Keller, M. B. Ruggles-Wrenn. "Compressive Creep Behavior of an Oxide-Oxide Ceramic Composite with Monazite Fiber Coating at Elevated Temperatures". *Materials Science and Engineering A*, 454-455:590–601, 2007.

41. Prewo KM, Batt JA. "The Oxidative Stability of Carbon Fibre Reinforced Glass-Matrix Composites". *Journal of the Material Science*, 23:523–527, 1988.

42. Ramulu, Prasad N.E. Malakondaiah G., M. and Z Guo. "Secondary Processing Effects and Damage Mechanisms in Continuous-Fiber Ceramic Composites". *Thermal and Mechanical Test Methods and Behavior of Continuous-Fiber Ceramic Composites, ASTM STP 1309*, 1997.

43. Schmidt S., H. Knabe H. Immich R. Meistring, S. Beyer and A. Gessler. "Advanced Ceramic Matrix composite materials for Current and Future Propulsion Technology Applications". 55(2004AcAau..55..409S):409–420, August 2004.

44. Schwartz, S.C. Lee, C. and P.V. Mosher. *Properties of Silicon Carbide Fiber Reinforced Carbon Composites in Damage and Oxidation Protection in High Temperature Composites: Volume 1.* The American Society of Mechanical Engineers, New York, 1991.

45. Sim SM, Kerans RJ. "Slurry Infiltration and 3-D Woven Composites". *Ceram Eng Sci Proceedings*, 13:632–641, 1992.

46. Szweda A, Harrison MG, Millard ML. "Fiber-Reinforced Ceramic-Matrix Composite Member and Method for Making", 1997. . S. Pat. No. 5 601 674.

47. Tressler, R.E. "Recent developments in fibers and interphases for high temperature ceramic matrix composites,". *Composites: Part A*, 30:429–437, 1999.

48. Tu WC, Evans AG, Lange FF. "Concept for a Damage-Tolerant Ceramic Composite with Strong Interfaces". *Journal of the American Ceramic Society*, 79:417–424, 1996.

49. W., Johnson David et al. *Ceramic Fibers and Coatings: Advanced Materials for the Twenty-First Century.* The National Academy of Sciences, Washington D.C., 1 edition, 1998.

50. www.boeing.com. "Boeing 787 Family". website, july 2008.

51. www.ga.com. "General Atomics website". website, july 2008.

52. Zawada LP, Steel S., Staehler J. "Consequence of Intermittent Exposure to Moisture and Salt Fog on the High-Temperature Fatigue Durability of Several Ceramic-Matrix Composites." *Journal of the American Ceramic Society*, 86:1282–1291, 2003.

53. Zok, Levi C.G., F.W. "Mechanical Properties of Porous-Matrix Ceramic Composites". *Advanced Engineering Materials*, 3:15–23, 2001.

Vita

1st Lt. Tufan YELESER is an officer in Turkish Air Force. He graduated from Maltepe Military High School in 1997. In same year he attended Turkish Air Force Academy and graduated as a 2nd Lt. with a Bachelor of Science degree in Aeronautical Engineering in 2001. He attended pilot training school at 2nd Main Jet Base in Cigli, Izmir. He graduated as a jet pilot in 2003. He was trained with F/NF-5 jet aircraft at 3rd Main Jet Base. Following that he took F-16 Jet Training Course at Oncel Training Squadron, 4th Main Jet Base, Ankara. He graduted as a war-ready fighter pilot at 2004. He was stationed to 162nd Fighter Squadron (Harpoons) where he flew for almost two years as a wingman before attending Graduate School of Engineering and Management, AFIT for master's degree program. After the graduation Lt. YELESER will, again, be stationed to 162nd fighter squadron in Bandirma.

Permanent address: 2950 Hobson Way
Air Force Institute of Technology
Wright-Patterson AFB, OH 45433

REPORT DOCUMENTATION PAGE

Form Approved
OMB No. 0704–0188

The public reporting burden for this collection of information is estimated to average 1 hour per response, including the time for reviewing instructions, searching existing data sources, gathering and maintaining the data needed, and completing and reviewing the collection of information. Send comments regarding this burden estimate or any other aspect of this collection of information, including suggestions for reducing this burden to Department of Defense, Washington Headquarters Services, Directorate for Information Operations and Reports (0704–0188), 1215 Jefferson Davis Highway, Suite 1204, Arlington, VA 22202–4302. Respondents should be aware that notwithstanding any other provision of law, no person shall be subject to any penalty for failing to comply with a collection of information if it does not display a currently valid OMB control number. **PLEASE DO NOT RETURN YOUR FORM TO THE ABOVE ADDRESS.**

1. REPORT DATE *(DD–MM–YYYY)*	2. REPORT TYPE	3. DATES COVERED *(From — To)*
4–08–2008	Master's Thesis	Sep 2006 — Sep 2008

4. TITLE AND SUBTITLE

CREEP BEHAVIOR OF OXIDE/OXIDE COMPOSITES WITH MONAZITE FIBER COATING AT 1100 °C IN AIR AND IN STEAM ENVIRONMENTS

5a. CONTRACT NUMBER

5b. GRANT NUMBER

5c. PROGRAM ELEMENT NUMBER

6. AUTHOR(S)

Tufan Yeleser AFIT, 1st Lt.,TUAF

5d. PROJECT NUMBER

2008-009

5e. TASK NUMBER

5f. WORK UNIT NUMBER

7. PERFORMING ORGANIZATION NAME(S) AND ADDRESS(ES)

Air Force Institute of Technology
Graduate School of Engineering and Management (AFIT/ENY)
2950 Hobson Way
WPAFB OH 45433-7765

8. PERFORMING ORGANIZATION REPORT NUMBER

AFIT/GA/ENY/08-S01

9. SPONSORING / MONITORING AGENCY NAME(S) AND ADDRESS(ES)

AFRL/RXLN (Geoff E. Fair)
2230 Tenth Street, Bldg 655
WPAFB OH 45433-7817

10. SPONSOR/MONITOR'S ACRONYM(S)

11. SPONSOR/MONITOR'S REPORT NUMBER(S)

12. DISTRIBUTION / AVAILABILITY STATEMENT

Approval for public release; distribution is unlimited.

13. SUPPLEMENTARY NOTES

14. ABSTRACT

The creep behavior of six oxide-oxide ceramic-matrix composites (CMCs) was investigated at 1100 °C in air and in steam. The six CMC systems had an alumina matrix reinforced with Nextel^{TM}610 fibers. The CMC systems C1, C2 and C3 were reinforced with 10 uni-directional fiber layers in a symmetric cross-ply orientation while C4, C5,and C6 were reinforced with 8 plies of fiber fabric woven. Composites C2, C3, C4, and C6 had monazite fiber coating. The tensile properties of the six CMC systems were investigated. Different methods used to apply the monazite coating to the uni-tape cross-ply composites, and the woven composites were the likely cause of reduced strength of the woven CMCs. Creep performance of all six CMC systems was noticeably degraded in steam. Creep run-out was achieved for only composites C4 and C6 in air. Results reveal that for a given fiber architecture and fiber coating method, the use of the monazite coating resulted in considerable improvement in creep resistance. Composite microstructure, as well as damage and failure mechanisms were investigated.

15. SUBJECT TERMS

Ceramic Matrix Composite (CMC), Oxide-Oxide, Nextel 610, Creep, Air, Steam

16. SECURITY CLASSIFICATION OF:			17. LIMITATION OF ABSTRACT	18. NUMBER OF PAGES	19a. NAME OF RESPONSIBLE PERSON
a. REPORT	b. ABSTRACT	c. THIS PAGE			Prof. Marina B. Ruggles-Wrenn
U	U	U	UU	344	19b. TELEPHONE NUMBER *(include area code)* (937)255-3636,ext4641;marina.ruggles-wrennafit.edu